UNIVERSITA' DEGLI STUDI DI PAVIA

Dipartimento di Biologia e Biotecnologie "L. Spallanzani"

Istituto di Genetica Molecolare IGM-CNR

DNA damage tolerance by specialized DNA polymerases in humans and plants

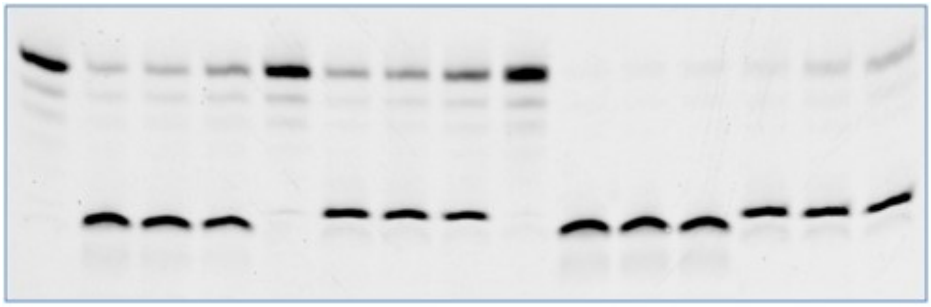

Elisa Mentegari

Dottorato di Ricerca in
Genetica, Biologia Molecolare e Cellulare
Ciclo XXXI – A.A. 2015-2018

UNIVERSITA' DEGLI STUDI DI PAVIA

Dipartimento di Biologia e Biotecnologie "L. Spallanzani"

Istituto di Genetica Molecolare IGM-CNR

DNA damage tolerance by specialized DNA polymerases in humans and plants

Elisa Mentegari

Supervised by Prof. Rino Cella

Co-supervised by Prof. Giovanni Maga

Dottorato di Ricerca in
Genetica, Biologia Molecolare e Cellulare
Ciclo XXXI – A.A. 2015-2018

Abstract

Misincorporated ribonucleotides (rNMPs) are the most common lesions into the genome. Their chemical instability represents a source of genomic instability, impairing replication fork progression and recognition of DNA binding factors. Consequently, cells evolved specific mechanisms to repair such damages. The most relevant is Ribonucleotide Excision Repair (RER), in which RNase H2 initiates the repair process nicking the DNA/RNA hybrid at the junction with the embedded rNMP. rNMPs can be inserted in the genome during replication as well as during repair pathways and translesion synthesis (TLS). X-family repair polymerases (Pols) λ and β have essential functions in performing TLS of oxidative lesions, in particular 7,8-dihydro-8-oxoguanine (8-oxo-G), the most abundant oxidative DNA damage present in our cells. Pol η, a member of Y-family Pols, is essential for TLS over cyclobutane pyrimidine dimers (CPDs) sites, 8-oxo-G, abasic (AP) sites, as well as over the intrastrand crosslinks between two adjacent guanines caused by the anticancer drug cisplatin (Cis-PtGG).

Information regarding the impact of rNTPs misincorporation opposite DNA lesions by TLS activity, as well as the effects of such mispairs on RER efficiency, was missing. Therefore, we investigated the ability of recombinant human Pols λ, β and η to misincorporate rNMPs specifically opposite oxidative lesions (8-oxo-G, 8-methyl-2'-deoxyguanosine (8-met-G), 3-methyl deoxycytidine (3-met-C)), AP site and Cis-PtGG. Furthermore, we characterized the nicking ability of the human RNase H2 on damaged-DNA/RNA hybrid substrates.

Our results suggest that Pol β, rather than Pol λ, can be a source of rNMPs incorporation into genomic DNA, both during BER opposite normal DNA bases and during bypass of 8-oxo-G. Indeed, having a lower selectivity for rNMPs, Pol β can bypass 8-oxo-G lesion also inserting rCMP (wrong sugar/right base), but at least excluding in most cases rAMP (wrong sugar/wrong base). This could be relevant since the presence of rAMP opposite 8-oxo-G strongly inhibits MutYH-initiated BER, while incorporation of rCMP would result in a 8-oxo-G:rC base pair, which is still processed by Ogg1 glycosylase.

Moreover, we found that human Pol η efficiently incorporates and extends rNMPs opposite 8-oxo-G and 8-met-G, while it is not able to insert a rNMP opposite other lesions. In particular, while Pol η efficiently bypasses Cis-Pt adducts using dNTPs, it is able to incorporate only one rCMP toward the 3'G of the Cis-PtGG lesion.

Our experiments indicated that human RNase H2 shows a different preference in the removal of rCMP opposite DNA lesions. rCMP opposite 8-met-G is processed with the same efficiency as opposite a normal guanine, while a substantial drop in reaction efficiency is observed when rCMP paired 8–oxo-G or cis-PtGG lesion. This suggests that insertion of rNMPs opposite different lesions can reduce the efficiency of RNase H2, thus effectively impairing RER.

It has been suggested that *A. thaliana* Polλ (AtPOLL), as its human homolog, exerts an essential role in oxidative DNA-damage tolerance pathways. In mammals, Ogg1 is responsible for the excision of the damaged base pairing with C, thus initiating a canonical Short Patch (SP)-BER, leading to restoration of the correct C:G base pair. If replication occurs before Ogg1 action, replicative Pols likely insert the incorrect dAMP opposite the lesion. MutYH glycosylase is devoted to recognition of A:8-oxoG mispair and removal of incorrect A. Both glycosylases have been identified in *A. thaliana* too. However, the mechanism of SP-BER in plants has not been fully elucidated yet, and the activities of the enzymes involved in such pathway have not been fully characterized. Therefore, we aimed to express and purify recombinant AtMutYH in order to better characterize BER pathway. In our laboratory, we previously succeeded in expressing AtOgg1 in *E. Coli* system. On the contrary, we were not able to purify AtMutYH because its expression in a bacterial system resulted too toxic. The project included also the investigation of plant cells behaviour under stressful conditions, specifically in a cellular background deficient for AtOgg1 or for AtMutYH, and with the concomitant silencing of AtPOLL.

Acknowledgements

I'd like to express my gratitude to professors Rino Cella and Giovanni Maga for giving me the opportunity to work in their laboratories during my PhD. They have always been very kind and helpful. I had the opportunity to work on interesting projects and to learn a lot about science.

I would like to thank very much Dr. Emmanuele Crespan, my supervisor since my master's degree. Thank you for all the advices and teaching. In this lab I have learned to work and I grew up.

I want to thank a lot all "Lab 500" ,"Cella's Lab" and PhD course mates for these years. In particular I'd like to thank Dr. Laura Bavagnoli and Dr. Matteo Faè from whom I learned a lot. And also my mates and friends Nadia, Jorge, Ale, Ambra, Solvia, Dome, Bart, Silvietta and Marco. We shared a lot together. Whenever I needed help or advice, I have always found open arms. And thanks also to Claudia and Davide, always helpful.

A special thank goes to all my family. For my entire life you have always supported me until reaching this new goal. In particular thanks to mum, dad, sister, my lovely grandparents and to my future husband Marco. Without you I wouldn't have been who I am. And thanks also to Bassano, Antonia, Luca, Laura, my little niece Gioia, uncle Silvan, my little cousin Egle and Federico for your presence in these years.

Abbreviations

AGS	Aicardi-Goutières syndrome
A-EJ	Alternative end-joining
amiRNA	Artificial microRNA
AOA1	Oculomotor apraxia
AP	Abasic
APTX	Aprataxin
At	Arabidopsis thaliana
APX	Ascorbate peroxidase
BAP	6-benzylaminopurine
BER	Base Excision Repair
BRCT	Breast cancer carboxy-terminal
BSA	Bovine serum albumin
CAT	Catalase
CI	Callus Induction
CisPt	Cisplatin
dNMPs	Deoxynucleoside monophosphates
dNTPs	Deoxynucleoside triphosphates
ds	Double-stranded
DSBs	Double-strand breaks
DTT	Dithiotreitol
EDTA	Ethylenediaminetetraacetic acid
FAM	Carboxyfluorescin
FapyGua	2,6-diamino-4-hydroxy-5-formamido-pyrimidine
FEN	Flap endonuclease
GR	Glutathione reductase
GSH	Glutathione
GST	Glutathione-*S*- transferase
HD	Huntington disease
HRP	Horseradish peroxidase
Hyg^R	Hygromycin resistance
IFN-α	Interpheron alpha
IR	Ionizing radiation
LB	Left Border
LF	Little finger
MEFs	Mouse embryonic fibroblasts
MMEJ	Microhomology-mediated end joining
MMR	Mismatch repair

MS	Murashige – Skoog
MutYH	MutY DNA glycosylase
NAA	Naphthaleneacetic acid
NHEJ	Non-Homologous End Joining
Ni-NTA	Nickel-nitrilotriacetic acid
nt	Nucleotide
Ogg1	8-Oxoguanine glycosylase
PA	Polyacrylamide
PAD	Polymerase-associated domain
PCNA	Proliferating Cell Nuclear Antigen
PIP	PCNA-Interacting peptide
PolDIP2	DNA Polymerase Delta Interacting Protein 2
Pol	Polymerase
p/t	Primer/ template
RB	Right Border
RER	Ribonucleotide Excision Repair
RIR	Rev1 interacting region
RNase	Ribonuclease
rNMPs	Ribonucleoside monoposphates
rNTPs	Ribonucleoside triposphates
ROS	Reactive oxygen species
SSBs	Single strand breaks
SOD	Superoxide dismutase
TLS	Translesion synthesis
TNR	Trinucleotides repeat
Top	Topoisomerase
UBZ	Ubiquitinbinding zinc domain
UV	Ultraviolet
WCE	Whole cell extract
WT	Wild-type
XP	*Xeroderma pigmentosum*
3-met-C	3-methyl deoxycytidine
8-met-G	8-methyl-2'-deoxyguanosine
8-oxo-G	7,8-dihydro-8-oxoguanine

Contents

1. Introduction

1.1 DNA damages in living organisms

Endogenous and exogenous stress constantly attack cells, causing DNA damages. Endogenous agents include metabolic products and by-products, such as reactive oxygen species (ROS) and alkylating agents, while exogenous or environmental stresses include physical, chemical and biological agents such as ultraviolet (UV) light, ionizing radiation (IR), heavy metals, air pollutants, chemotherapeutic drugs and inflammation. Moreover, DNA itself possesses an intrinsic chemical instability, undergoing hydrolytic deamination and depurination. Up to 10^5 DNA lesions can occur per mammalian cell per day. Among them, oxidized bases and single strand breaks (SSBs) are particularly frequent (~10^4 per day). Other types of DNA damages include double-strand breaks (DSBs), abasic (AP) sites, intra- and inter- strand crosslinks and protein-DNA adducts. The effects of DNA damages persistence are various and sometimes deleterious. Indeed, DNA lesions can induce mutagenesis, such as base substitutions, insertions, deletions. Mutations may be a threat for both replicative and repair DNA polymerases (Pols). DNA damages, and DBSs in particular, can also lead to chromosomal aberrations. These consequences, in turn, can potentially activate oncogenes or inactivate tumor suppressor genes, thus increasing cancer risk. Therefore, the maintenance of genome integrity through efficient and accurate removal of DNA damage is of paramount importance for cells survival (Iyama and Wilson 2013; Marteijn et al. 2014).

1.1.1 Ribonucleotides in the genome

Pols are specialized enzymes that synthesize polymers of nucleic acids. They are divided into DNA and RNA Pols, based on their substrate specificity. DNA Pols, essential to DNA replication, selectively use deoxynucleoside triphosphates (dNTPs) as building blocks for the synthesis of DNA, while RNA Pols produce RNA chains using ribonucleoside triphosphates (rNTPs). rNTPs are normally introduced as ribonucleoside monophosphates (rNMPs) in place of the corresponding deoxynucleoside monophosphates (dNMPs), in eukaryotic nuclear genome during replication: Pol α/ primase, associated to initiation complex at DNA origin, synthesizes short RNA/DNA hybrids that are then elongated by the more

processive Pols ε and δ, on the leading and on the lagging strand, respectively. Since direction of synthesis of Pols is 5'→3', replication on the lagging strand occurs through synthesis of short tracts of DNA called Okazaki fragments, with initiation events repeated at the beginning of each Okazaki fragment (Hübscher et al. 2002). Ribonucleases (RNases) H and flap endonucleases (FEN1) remove RNA primers which are replaced with DNA. Finally, ligase I joins the DNA fragments. The short stretches of RNA used as primers are about 10 nt long; as their synthesis occurs at multiple replication origins at about 200-bp intervals on the lagging strand, this means that about 5% of the genome is initially synthesized as chains of consecutive rNMPs (Clausen et al. 2013).

RNA is more prone to cleavage than DNA due to the presence of the 2'-OH on its ribose ring. For this reason, cells need to remove RNA primers in order to maintain genome integrity. Most DNA Pols have therefore evolved to exclude rNMPs during DNA synthesis, since they can potentially lead to strand breaks (Yao et al. 2013).

Ability of Pols to exclude rNMPs during DNA synthesis is based on the presence of a "steric gate", where a side chain residue collides with the 2'-OH of the incoming ribonucleotide, sterically hindering its binding (Joyce 1997). Selectivity of incorporation of dNMPs spans from 10-fold to 10^6-fold more than rNMPs incorporation, depending on the identity of the polymerase, on the base examined and on rNTP:dNTP ratio (Nick McElhinny et al. 2010a). When Pols, occasionally, insert a wrong dNMP into correctly aligned primer-templates, generating a mismatch, the incorrect nucleotide can be excised by Pols' 3′ to 5′ exonuclease activity. The rare mismatches that escape this proofreading mechanism can be corrected by mismatch repair (MMR) pathway. These processes of correction of errors, together with selectivity of Pols, ensure high fidelity during DNA replication, thus allowing eukaryotic nuclear genome stability over many generations (Williams et al. 2012).

However, in spite of their specificity, replicative Pols discriminate dNMPs imperfectly and so they can frequently incorporate rNMPs during DNA replication; this is due to the fact that in mammalian cells, as well as in yeast cells, rNTPs concentration is 10-100 fold higher than dNTPs concentration (Clausen et al. 2013; Yao et al. 2013). Studies performed in *Saccharomyces cerevisiae* revealed that dNTPs concentration *in vivo* ranges from 12 to 30 μM, while rNTPs concentration ranges from 500 to 3000 μM, resulting 36- to 190-fold molar excess over their corresponding dNTPs (e.g. rCTP:dCTP ratio is 36:1 and rATP:dATP ratio is 190:1) (Clausen et al. 2013). Being

rNTPs present physiologically in such high concentrations, it is of great interest to understand how frequently they are incorporated into DNA by replicative DNA Pols α, δ and ε, which synthesize the majority of DNA in eukaryotic cells. In this perspective, McElhinny and co-workers performed a series of DNA synthesis reactions using those recombinant Pols. These *in vitro* experiments were performed using physiological concentrations of both rNTPs and dNTPs. The results suggested that rNMPs incorporation varies according to the Pols, the type of template base and the sequence context, predicting that thousands of rNMPs would be incorporated in *S. cerevisiae* genome during each round of replication (Nick McElhinny et al. 2010b). Actually, insertions of rNMPs into *S. cerevisiae* genome were proven to take place also *in vivo* (Nick McElhinny et al. 2010a). As mammalian nuclear genome is approximately 500 times bigger than yeast nuclear genome, mammalian Pols would introduce millions of rNMPs every round of DNA replication, probably making misincorporated rNMPs the most common lesion in the genome.

The 3'→ 5' exonuclease proofreading activity of replicative Pols can also remove incorporated rNMPs, but with low efficiency (Caldecott 2014). For example, *S. cerevisiae* Pol ε, which is the main Pol involved in synthesis of the leading strand during DNA replication, has the potential to proofread rNMPs; *in vitro* reactions show that about one third of rNMPs can be removed, with the following efficiency: rU > rA > rC = rG (Williams et al. 2012). Due to limits of proofreading rNMPs by Pols, other more efficient mechanisms have evolved to face the problem of rNMPs incorporation (See 1.1.1.4 section).

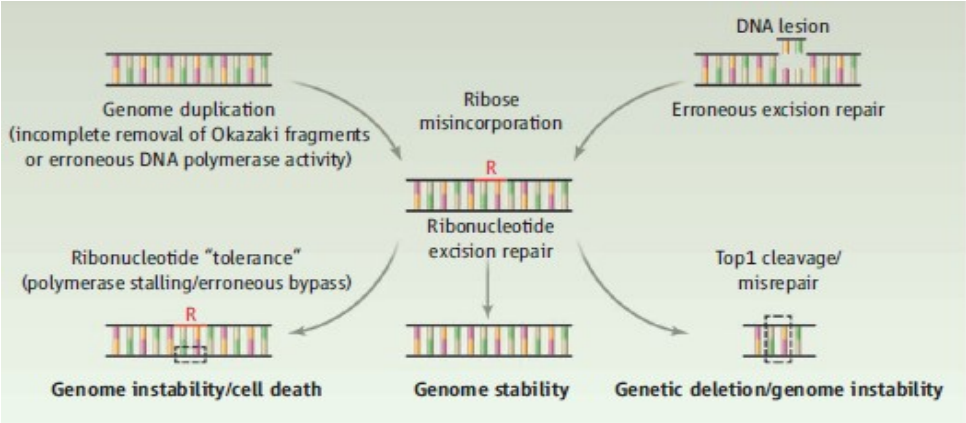

Fig. 1: RNA contamination in DNA. Routes of ribonucleotide (R) misincorporation into DNA are shown in the upper part of the figure. Mechanisms of ribonucleotide removal or tolerance are shown in the lower part of the figure (Caldecott 2014).

rNMPs can be inserted in the genome by Pols also during repair pathways. Family X includes specialized, monomeric Pols, conserved in most organisms from bacteria to humans (Bebenek et al. 2014), that are required in several DNA repair pathways. The family members are Pols β, λ, μ and terminal deoxynucleotidyl transferase (TdT). They are able to insert rNMPs during synthesis in presence of undamaged DNA but with varying sugar selectivity. For high-fidelity Pols the range of sugar selectivity is 500-4,400,000 while, for repair low-fidelity Pols, values span from 1.3 to 50,000. This difference is probably to be ascribed to the overall flexibility and arrangement of repair Pols active sites (Brown and Suo 2011). In particular, Pol μ basically has both DNA and RNA polymerase activities, showing a selectivity for dNMPs incorporation over rNMPs that spans from 1 to 10-fold (Nick McElhinny and Ramsden 2003), in sharp contrast with the majority of DNA-dependent DNA polymerases which have an efficiency of discrimination of more than 1000 fold (Ruiz et al. 2003). As already mentioned, most Pols rely, indeed, on a nucleotide selection mechanism based on a steric exclusion system, that is the presence of a residue in the active site which collides with the hydroxyl group of rNTPs. Differently from Pols β and λ, that possess Tyr or Phe residues at the "steric gate" position, Pol μ possesses a Gly residue that is responsible for its low sugar selectivity (Martin et al. 2013; Brown and Suo 2011). Thus, both the active site architecture and the particular mechanism of sugar selection may account for the very diverse range of selectivities measured for the different

Pols.

1.1.1.1 Physiological roles of ribonucleotides in the genome

The incorporation of rNMPs in the genome can also have a physiological relevance. Some roles have been described, while some others have only been suggested:

- In *Schizosaccharomyces pombe,* mating occurs between two different types of haploid cells (*a* and α mating types) in order to produce diploid cells, which can then undergo mitosis and produce haploid spores. Haploid yeasts are capable of switching mating type; this switching occurs by a molecular mechanism that relies on asymmetry of DNA replication and it depends on the specific imprint at mat1 locus (Vengrova and Dalgaard 2006). Studies revealed that such imprint consists of two consecutive ribonucleotides in the genome, introduced into the lagging strand DNA template during S phase; so lagging strand replication is a possible origin for ribonucleotide imprinting, probably involving RNA primase or rNMPs incorporation by Pol α, the more prone among yeast Pols in inserting rNMPs (Nick McElhinny et al. 2010b).

- In *Schizosaccharomyces pombe,* cdc22 and tds1 genes, encode, respectively, the large subunit of ribonucleotide reductase and a putative thymidylate synthase; mutations in these genes are associated with spreading of silencing in the mating-type switching region. As these two genes regulate dNTP pool, mutations may affect dNTP:rNTP ratio so that more rNMPs may be incorporated into DNA. This has been proposed as an epigenetic mechanisms regulating gene silencing (Nick McElhinny et al. 2010b).

- rNMPs transiently embedded in DNA before being substituted with dNMPs have the potential to cause B- to A- conformation transition (Meroni et al. 2017). Such geometrical properties might have signalling function. It was demonstrated that the presence of one rNMP every 125 bp of DNA reduces nucleosome formation while DNA containing more than 5% ribonucleotide cannot form nucleosomes at all (Hovatter and Martinson 1987). Other signalling functions include gene silencing and chromatin remodelling

involving a non-catalytic subunit of Pol ε (Nick McElhinny et al. 2010b).

- It has been suggested that rNMPs incorporation during DNA replication may help recognition of the newly synthesized strand by MMR. MMR is targeted onto the nascent DNA strand by specific strand-discrimination signals: in gram-negative bacteria the signal is constituted of a nick generated by mismatch-activated endonucleases at level of transiently unmethylated adenines at d(GATC) sites. Differently, gram-positive bacteria and eukaryotes do not rely on methylation for strand discrimination; however, also initiation of eukaryotic MMR *in vitro* requires the presence of pre-existing strand discontinuities. Based on these observations, it was suggested that gaps between Okazaki fragments on the lagging strand could be a signal for eukaryotic MMR *in vivo*. On the other hand, the situation is less clear for the leading strand, since it is replicated in a more continuous manner. Different observations suggest that, in *S. cerevisiae*, rNMPs incorporated into the genome during leading strand replication by Pol ε function as signals that can direct MMR onto the leading strand to correct errors. The idea is that the subsequent processing of rNMPs through specialized repair, functions as strand discrimination signal. Interestingly, the non-catalytic subunit of RNase H2 contains a putative Proliferating Cell Nuclear Antigen (PCNA) binding motif; so RNase H2 may also aid in delivering PCNA onto the nascent leading strand, where it contributes to strand discrimination, participating in signalling for MMR (Ghodgaonkar et al. 2013; Lujan et al. 2013).

1.1.1.2 Damages caused by ribonucleotides

rNMPs inserted in the genome, both during initiation of replication or erroneously misincorporated by Pols, are not always removed, provoking deleterious consequences (Caldecott 2014). As already mentioned, the presence of the 2'-OH in their ribose ring renders DNA chemically unstable, more susceptible to strand breakage. Moreover, crystallographic and NMR studies revealed that the presence of rNMPs in double-stranded DNA can alter the double helix geometry, both increasing the rate of mutagenesis and decreasing the rate of DNA replication (Nick McElhinny et al. 2010b).
Studies conducted reconstituting *Escherichia coli* replisome demonstrated that rNTPs/dNTPs pool imbalance slows fork progression. Indeed, rNTPs present in high amount compete with dNTPs at the active site of Pol III replicase, at a step preceding base pairing of dNTPs to the template base, causing a slower progression of the replisome from two- to three- fold. Among the four rNTPs, rUTP is the one causing less problems to replisome progression, probably because it is the only one having a difference in the nucleotide base compared to dTTP. Interestingly, on a template strand containing rNMPs the replisome pauses 4-30 fold, depending on the number and on the nature of rNMPs embedded in the template strand, suggesting that rNMPs not removed from a strand before the successive round of replication could also slow down replication fork progression and favour genomic instability (Yao et al. 2013). In particular, Pol ε is about 3 folds less efficient than Pol δ at bypassing two consecutive rNMPs. If the rNMPs to bypass are three, Pol ε bypass efficiency drops to 10 compared to Pol δ, while it is completely unable to bypass four consecutive rNMPs (Clausen et al. 2013).
It has been shown that yeast cells defective in RNase H1 and RNase H2, the enzymes involved in removing incorporated rNMPs, show characteristics typical of replicative stress. In particular, these cells showed high rates of deletion of 2-5 nucleotides from repetitive DNA sequences due to the action of topoisomerase I, slower progression through S phase, accumulation of PCNA and sensitivity to hydroxyurea, an inhibitor of replication that reduces dNTPs pools, thus altering dNTPs : rNTPs ratio (Clausen et al. 2013).
Recently Meroni *et al*. confirmed, by means of atomic force microscopy, that the incorporation of rNMPs into the DNA double-helix causes structural and conformational changes. In particular, their presence causes a systematic shortening of DNA molecules. The hydroxyl group present at the

2' of the ribose ring is responsible for such compaction of DNA backbone. Intrusion of rNMPs into DNA molecules also leads to a decrease of double helix flexibility. Moreover, compared to control DNA molecules that retain their native B conformation, a fraction (between 20 and 60%) of rNMPs-containing DNA molecules showed B- to A- conformation transition, thus suggesting that conformational changes may occur also *in vivo* (Meroni et al. 2017). The DNA conformational transition caused by a 3'- terminal ribose may render more difficult the extension of the primer terminus (Nick McElhinny et al. 2010b).
Therefore, rNMPs embedded into DNA represent an issue for the cell, potentially leading to stalling of replication fork to DNA strand breakage. Since millions of rNMPs can potentially be introduced into mammalian nuclear genome, these non canonical substrates of Pols can be considered as one of the most relevant lesions present in DNA.

1.1.1.3 Ribonuclease H2 (RNase H2)

RNases H are enzymes present in all living organisms that nick RNA/DNA hybrids at the 5' of embedded rNMPs in a sequence aspecific manner. They are, therefore, fundamental for the maintenance of genome integrity. In most cases, organisms possess two types of RNases: RNase H1 and RNase H2, which belong to different classes according to amino acid sequence similarities. In particular, eukaryotic RNases H1 and H2 have different biochemical properties and substrate specificity: RNase H1 is a monomeric, processive enzyme, acting when four or more consecutive rNMPs are present in a DNA strand. It does not show any activity on a DNA substrate containing a single rNMP. On the other hand, RNase H2, can process the same substrates recognized by RNase H1, but it is also able to incise a single rNMP embedded within double stranded DNA. Furthermore, RNase H2 is the predominant source of RNase activity in eukaryotic cells. When RNase H2 encoding gene is deleted in in *Saccharomyces cerevisiae*, a 70% reduction in RNase H activity in crude extracts is observed (Jeong et al. 2004; Sparks et al. 2012; Clausen et al. 2013; Chon et al. 2009; Cerritelli and Crouch 2009).
Eukariotic RNase H2 is an heterotrimeric enzyme composed of subunits A, B and C (Chon et al. 2009). The three subunits are arranged so that the C subunit is in the middle while B and A subunits are on its sides (see Fig. 2) (Figiel et al. 2011). Subunit A is the catalytic one and it interacts almost exclusively with subunit C, that, together with subunit B, possesses a

structural role in supporting the activity of A subunit. Indeed, it seems that these accessory subunits form a scaffold on which the catalytic one can assume the appropriate conformation. They may also be relevant for RNase H2 processivity. Moreover, they are involved in interactions with other proteins. Interactions with *S. cerevisiae* yeast *SGS1, RAD27* and *ESC2* have been found. The three genes encode, respectively, a DNA helicase, the Fen1 protein involved in the removal of RNA primers, and a protein that has effects on recombination frequencies. Such interactions suggest a role of RNase H2 in the processing of Okazaki fragments. Impairment of RNase H2 in combination with defects in DNA2 or RAD27 (FEN1) results in lethal or sickness phenotypes, supporting a functional role of RNase H2 in Okazaki fragments processing. Furthermore, a PCNA-Interacting-peptide box (PIP-box) has been found at the C-terminus of human RNase H2 B subunit, thus suggesting RNase H2 involvement in replication and repair. (Chon et al. 2009).

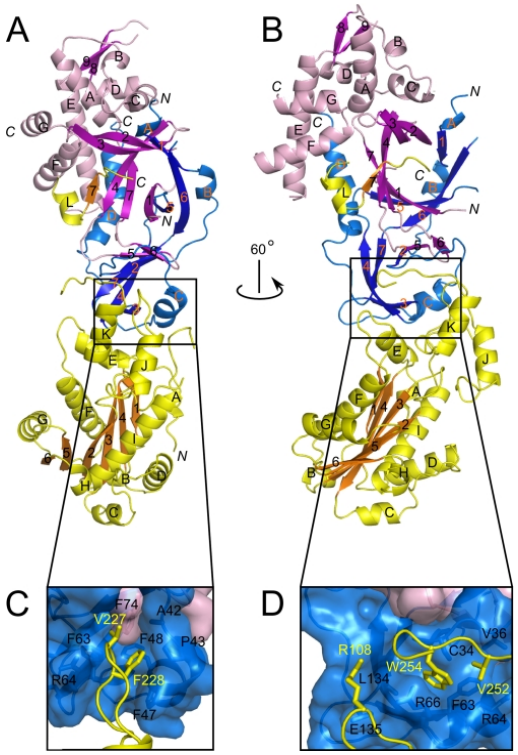

Fig. 2: Overall structure of human RNase H2. *A* and *B*, shown is the structure of the RNase H2 complex colored by subunits (*yellow*, A; *magenta*, B; *blue*, C). β-Strands are indicated with darker shades of the respective colors. C and D, shown is a close-up view of

the interface between subunit A and the B/C dimer. The residues forming the interface are shown as sticks and labeled (Figiel et al. 2011).

1.1.1.4 Ribonucleotide Excision Repair (RER)

Ribonucleotide Excision Repair (RER) is the main pathway responsible for the removal of misincorporated rNMPs (Sparks et al. 2012).

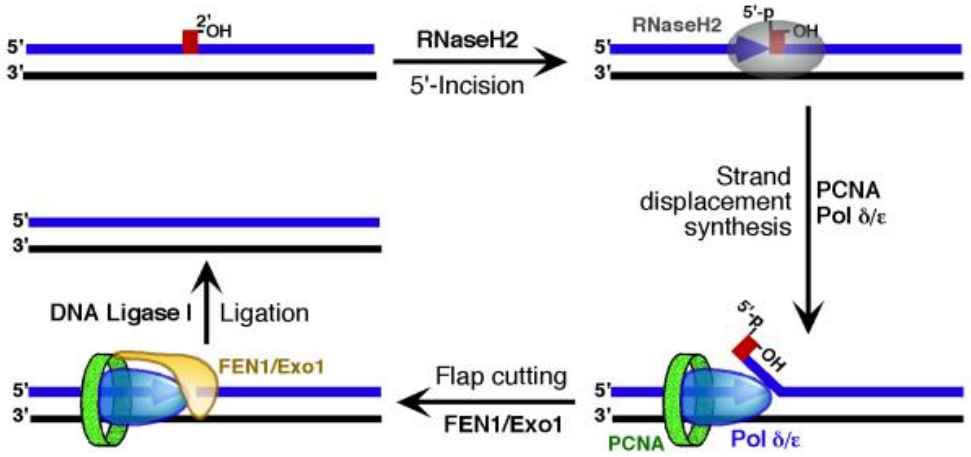

Fig. 3: Model for Ribonucleotide Excision Repair. Redundant functions of Fen1 with Exo1 and Pol δ with Pol ε are indicated (Sparks et al. 2012).

RNase H2 starts RER cutting DNA at the 5' of the incorporated rNMP, generating 3'-OH and 5'-P ends. The clamp loader RF-C loads onto DNA the sliding clamp PCNA, an homotrimeric protein which encircles DNA and takes contacts with Pol δ and Pol ε, thus allowing processive DNA synthesis (Hübscher et al. 2002). The 3' hydroxyl resulting from RNase H2 incision, is used by DNA Pols δ/ε to elongate the strand, causing the displacement of the downstream strand. At this point FEN1 cuts the flap, leaving a nick substrate for DNA ligase I, which seals the DNA backbone (Sparks et al. 2012).
The crucial role of RNase H2 in RER is supported by the observation that it cannot be substituted by RNase H1(Sparks et al. 2012). Moreover, in experiments performed in budding yeast, where a mutant replicative polymerase with low selectivity for dNMPs vs. rNMP incorporation was expressed, it was found that rNMPs incorporation was abundant only when the gene for RNase H2 was silenced (Reijns et al. 2012).

An alternative pathway for excision of incorporated rNMPs relies on topoisomerase I (TopI) type B, an eukaryotic enzyme that relaxes supercoiled helix by nicking reversibly dsDNA (Vaisman and Woodgate 2015). Differently from RNase H2, TopI cuts the DNA backbone on the 3' side of the rNMP; a tyrosine residue present in the active site of the enzyme reacts with the phosphodiester DNA backbone, generating a 3'-phospho-tyrosyl intermediate. At this point, the 2'-OH of the ribose ring, with a nucleophilic addition, causes the formation of a 2'-3'-cyclic phosphate, with concomitant release of TopI. In this way, a single-strand break is generated (Sparks et al. 2012; Caldecott 2014). Currently, it is believed that the Sgs2 helicase and the Exo1 nuclease proteins are recruited to excise the rNMP and to process the 5'-OH and cyclic 2'-3'phosphate ends (Williams et al. 2013). Anyway, genetic analysis conducted in yeasts suggest that this is a minor pathway and unlikely to be favoured, as it seems to promote deletions in DNA (Caldecott 2014).

1.1.1.5 Removal of ribonucleotides in mammals

Removal of rNMPs from DNA, a process in which RNase H2 plays a fundamental role, seems to be an essential requirement also in mammals. In mice, rNMPs removal is necessary for embryonic development since RNase H2-knockout results in embryonic lethality in null mice. Lethality emerges knocking out any of the genes encoding the three subunits of RNase H2. In the genome of RNase H2-null embryos fibroblasts, more than a million of single and/or di-rNMPs are present, making them the most common lesion in the entire genome. Moreover, such fibroblasts show also a number of chromosomal aberrations and strand breaks. These DNA lesions, and the consequent genome instability, might be the consequence of undegraded RNA primers, misincorporation of rNMPs by DNA Pols, transcriptionally induced R-loops and/or consequence of TopI action (Clausen et al. 2013; Reijns et al. 2012). These embryos are also characterized by reduced cell proliferation during gastrulation; the growth arrest is the consequence of a p53-dependent DNA damage response due to accumulation of rNMPs in the genome (Reijns et al. 2012).
Removal of misincorporated rNMPs is extremely important also in humans. Mutations in RNH201A/B/C genes, encoding the three subunits of RNase H2, are associated to the autosomal recessive Aicardi-Goutières syndrome (AGS). This is a rare early-onset neuroinflammatory condition, resembling (and hence often misdiagnosed as) a congenital viral infection since both are

characterized by an increased production of interferon alpha (IFN-α). It also shows similarities to the autoimmune disease systemic lupus erythematosus, where altered IFN-α homeostasis is altered (Reijns et al. 2012; Rice et al. 2009).
The rNMPs in DNA can be a threat not only for actively replicating cells, but also for post-mitotic cells, such as neurons. In these cells, rNMPs incorporation can be relevant because, even if nuclear genome does not duplicate, their mitochondrial genome does. Moreover, when other DNA lesions are present, induced, for example, by oxidative stress, short stretches of nucleotides are excised and replaced. Since rNMPs can be introduced also by repair Pols, DNA repair reactions are potentially a source of rNMPs incorporation in post-mitotic cells. This can be particularly relevant because, in brain tissue, the oxidative stress, due to extensive consumption of oxygen, is rather high (about 20% of inhaled oxygen is consumed by brain) (Caldecott 2014).
Interestingly, defective SSBs repair has been associated to a faster neurodegeneration: when rNMPs are repaired through RER pathway, SSBs intermediates seem to be a preferred substrate for aprataxin (APTX), which is a SSB-repair protein that, if mutated, contributes to progressive neurodegeneration (Caldecott 2014).

1.1.2 Translesion synthesis pathway (TLS)

DNA integrity is a fundamental requirement for the transmission of proper and complete genetic information. As already underlined, cells are not only subjected to exogenous attacks as ionizing radiations, UV light and chemical agents, but also face endogenous reactive metabolites generated during normal cellular metabolism. Therefore, cells have evolved different repair mechanisms, mainly acting during the G_0/G_1 phases. However, lesions that escape such repair pathways can impair DNA replication blocking the progression of the replication fork. Indeed, replicative Pols possess a tight active site that does not allow the efficient bypass of damages encountered during the replication. To face these threatening DNA damages, cells have evolved other mechanisms to tolerate DNA lesions without actually repair them. DNA damage tolerance processes are important in promoting cell survival and, in some cases, contribute to generation of mutations (Waters et al. 2009; Chou et al. 2011; Hübscher and Maga 2011; Yang 2014). The number of Pols devoted to damage tolerance

systems underlines the importance of this essential task. In humans, 12 out of 17 DNA Pols are involved in TLS or DNA breaks repair (Yang 2014).

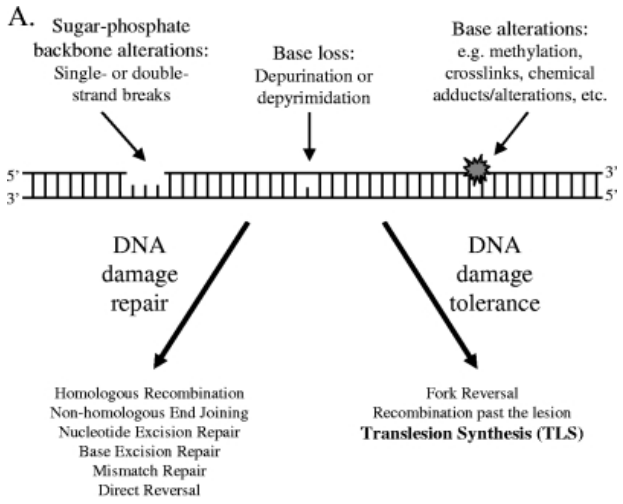

Fig. 4: DNA damage repair and bypass mechanisms. DNA damage results in breakage of the sugar-phosphate backbone, DNA base loss (indicated by a gap in the DNA), or base alterations (as indicated by the gray star). This damage can be repaired/removed from the DNA strand or tolerated, in which case the DNA lesion remains but cellular processes continue (Adapted from Waters et al. 2009).

In translesion synthesis (TLS), specialized Pols are recruited at the stalled fork where they temporarily act instead of replicative ones (Bebenek et al. 2014). TLS Pols are able to use damaged DNA bases as template and to insert nucleotides opposite them. TLS Pols are present in all three domains of life and they mainly belong to the Y family of DNA polymerases, but also some A- and X- family members play a role in TLS (Waters et al. 2009).
A common feature of TLS Pols is the lack of intrinsic 3' → 5' exonuclease activity to proofread replication of the new strand. For this reason, these Pols display a significant lower accuracy in inserting nucleotides opposite to an undamaged DNA template with respect to replicative ones, with frequencies of erroneously incorporated bases ranging from 10^{-1} to 10^{-4}. On the other hand, due to a wide active site, TLS Pols fulfil the important role of bypassing specific lesions with reasonable accuracy. Given the broad variety of DNA lesions, each TLS Pol has evolved the ability to bypass in a quite accurate way a particular damage, referred to as cognate lesion. TLS

Pols recognize physico-chemical features of the damaged base reading it "correctly". For example, while the majority of replicative Pols insert an A in front of 7,8-dihydro-8-oxoguanine (8-oxo-G) lesion, TLS Pols recognize it as a G, inserting the right C base opposite the lesion. This ability is not based on a diverse mechanism of action, but on special structural features, some of which are generally conserved in all Y-family enzymes (such as a wider active site), as well as specific for each particular enzyme (such as the "wrist" subdomain of Pol κ) (Hübscher and Maga 2011; Waters et al. 2009). Other important features of TLS Pols are their low catalytic efficiency and low processivity, compared to replicative Pols. These properties allows a rapid displacement of TLS Pols after lesion bypass, with their replacement with replicative ones. (Yang 2014). Two possible mechanisms, not mutually exclusive, for lesion bypass by TLS Pols have been proposed: the polymerase-switching model and the gap-filling model (See Fig. 5) (Waters et al. 2009).

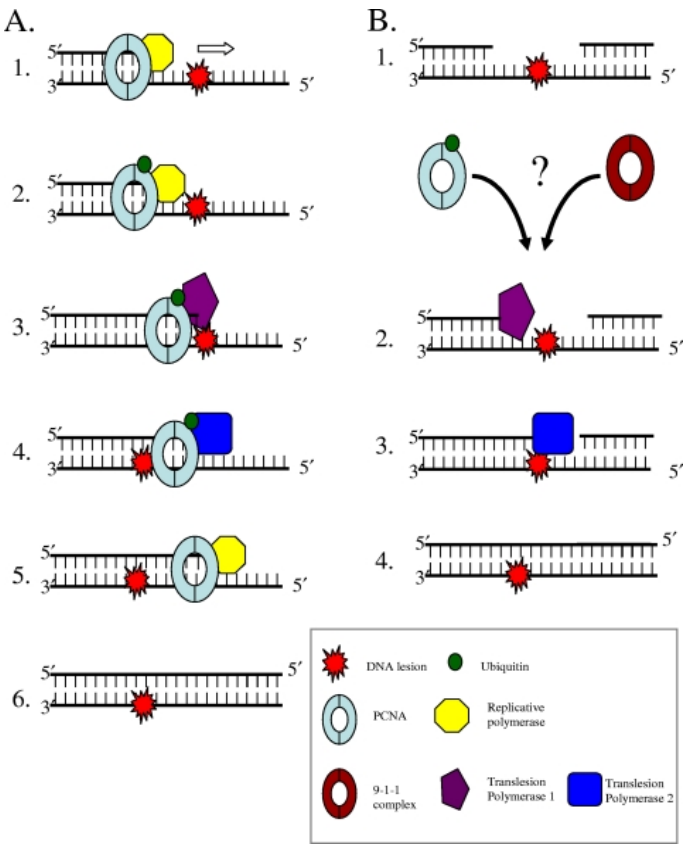

Fig. 5: Two non exclusive models for TLS: the polymerase-switching model (A) and the gap-filling model (B) (Waters et al. 2009).

In the polymerase-switching model, protein-protein interactions favour the switch between replication and TLS Pols when the replication fork encounters a lesion, and a further switch after the damage bypass occurs. On the other hand, the gap-filling model has been proposed for TLS occurring outside replication forks. In this situation, the replication machinery leaves a ssDNA gap in front of a DNA lesion due to repriming events that take place downstream, leaving to TLS Pols the role of gap filling (Hübscher and Maga 2011; Waters et al. 2009).

1.1.2.1 DNA polymerase η

Pol η belongs to Y-family. It is a monomeric protein of about 78kDa encoded by *POLH* gene (also known as *RAD30* gene or *XP-V* gene). Differently from replicative Pols, Y-family Pols catalytic core presents a preformed active site, with the finger domain in the closed conformation also in the absence of DNA, dNTP substrate, or both substrates. Moreover, the active site is also larger than the one of replicative Pols and solvent-exposed. These features are important to confer the low fidelity, the low catalytic efficiency and the low processivity of DNA synthesis typical of TLS Pols (Yang 2014). Other than palm, thumb and finger subdomains, typical of all Pols, Pol η presents the additional "little finger" (LF) domain, also called polymerase-associated domain (PAD), that is peculiar of Y-family Pols. Structural data indicates that the rotation of this domain gives rise to a "relaxed" active site, thus allowing accommodation of the bulky lesions present in the DNA template and the incoming nucleotides (Chou et al. 2011). Moreover, it possesses a PCNA interacting peptide (PIP), a Rev1 interacting region (RIR) and a ubiquitin binding zinc domain (UBZ). Upon DNA damage, PCNA undergoes ubiquitination, allowing interaction with Pol η via PIP and UBZ domains (see 1.1.2.3 section for Pol η interaction with PCNA). Furthermore, Pol η itself can be ubiquitinated on a Lys residue present within the nuclear localization signal (NLS) segment (Yang 2014).

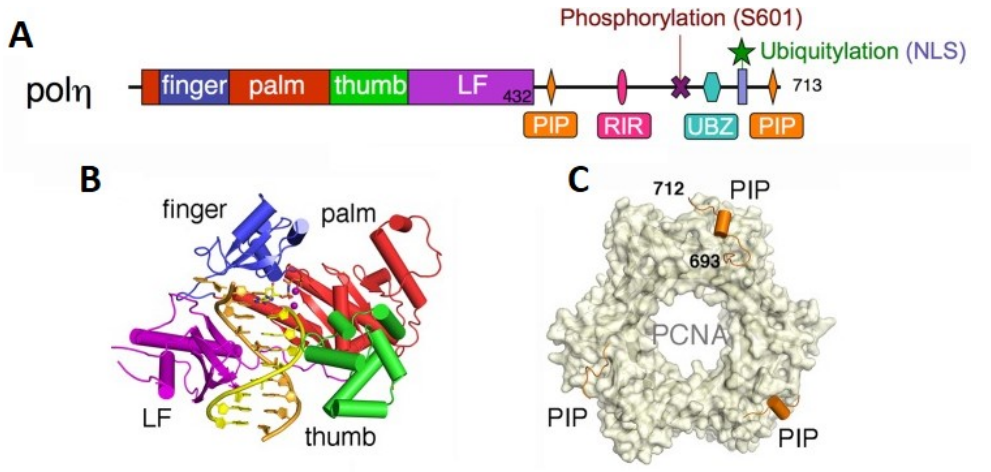

Fig. 6: Structural domains in human Pol η. (A) Diagram of the linear arrangement of functional domains in human Pol η. Domains are colorcoded. (B) Crystal structure of the catalytic region (amino acids 1−432) in a complex with DNA and dNTP (PDB entry 3MR2). (C) Crystal structure of human PCNA complexed with the Pol η PIP (PDB entry 2ZVK). All parts of human Pol η are shown as ribbon diagrams, and their interacting partners are shown as a molecular surface. The α-helices of pol η are shown as cylinders in panels B and C (Adapted from Yang 2014).

1.1.2.2 DNA polymerase η and cancer

Pol η has always raised great interest since it is the only Pol known to be directly correlated with a human genetic disease. Indeed, inactivation of XP-V gene in humans is responsible for the genetic disease known as the variant form of xeroderma pigmentosum (XP-V). Patients show extreme UV sensitivity, skin cancer predisposition and; in some cases, signs of neurodegeneration. Among XP patients, about 20% are XP-V. Pol η is the solely Pol able to perform error-free TLS at UV-light induced cyclobutane pyrimidine dimers (CPDs) sites, a four-member ring structure resulting from saturation of the pyrimidine 5,6 double-bond. Differently from the other Pols, Pol η is able to insert correctly two adenines in front of the two crosslinked thymines of CPDs lesions because of the more relaxed active site generated by rotation of PAD domain (see 1.1.2.1 section). This event allows the formation of hydrogen bonds and van der Waals forces between the two lesioned bases and the incoming two adenines. On the contrary, in case of undamaged DNA template these interactions do not form, thus

explaining Pol η higher fidelity during TLS past CPDs sites (Su et al. 2016; Chou et al. 2011).

Other than CPDs, Pol η is involved in the bypass of other lesions, such as 8-oxo-G, AP sites and CisPt-GG (Su et al. 2016; Chou et al. 2011). *cis*-diamminedichloroplatinum(II) (cisplatin) (Fig. 7) and its analogues are chemotherapeutic agents used to treat specific tumors including ovarian and testicular ones. These compounds can inhibit the DNA elongation step by inducing DNA alterations. For example, cisplatin causes the formation of intrastrand crosslinks between two adjacent guanines, resulting in local distortions of the DNA double helix. This hampers DNA replication by interfering with Pols progression thus killing the fastest proliferating cells, which are supposed to be tumorigenic (Vaisman et al. 2000; Chou et al. 2011). One of the limitations in the use of these compounds is the onset of drug resistance. Nucleotide Excision Repair (NER) pathway has been found to be most proficient in removing cisplatin adducts, but Pol η exerts an important function bypassing such lesion during TLS. Significantly, Pol η displays an higher efficiency and fidelity in bypassing Cis-PtGG compared to other TLS Pols. The crystal structure of yeast Pol η in complex with a DNA substrate containing a Cis-PtGG crosslink revealed that Pol η is able to insert the correct dCTP opposite both Gs of the lesion. Moreover, experiments performed with fibroblasts deriving from XP-V patients, showed a 2-3 fold increase in cisplatin-induced mutation frequency, compared to XP-V fibroblasts complemented with Pol η or WT fibroblasts (Chou et al. 2011). *In vitro* results indicated that Pol η, after the bypass of CisPt-GG lesion, does not efficiently extend the primer. B-family Pol ζ is thought to perform the extension, until its switch with a high-fidelity polymerases (Gregory et al. 2014).

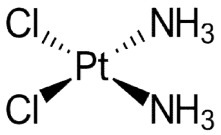

Fig. 7: Structure of the anticancer agent cisplatin. Adapted from (Chou et al. 2011).

1.1.2.3 PCNA

DNA replication is a fundamental and highly regulated step during the cell cycle. Other than replicative Pols, various accessory proteins are required during this process, in order to face all possible obstacles and to ensure a correct duplication of the genome. Proliferating cell nuclear antigen (PCNA) is an accessory protein acting during DNA replication, recombination and repair. Eukaryotic PCNA (Pol30 in *S. cerevisiae*) is a ring-shaped DNA slinding clamp that encircles DNA (Fig. 8). The PCNA homotrimer is loaded onto the 3'-end of primer/template junction by the clamp loader RF-C, a step that requires ATP hydrolysis. RF-C binds to the "C-side" of PCNA that is the protruding C-terminus of PCNA monomer. Also replicative Pols bind to the C-side of PCNA, ensuring their right orientation toward the growing primer end. Once PCNA is loaded onto DNA, it brings replicative Pols and other factors necessary for Okazaki fragment processing at the replication fork (Moldovan et al. 2007; Chon et al. 2009).

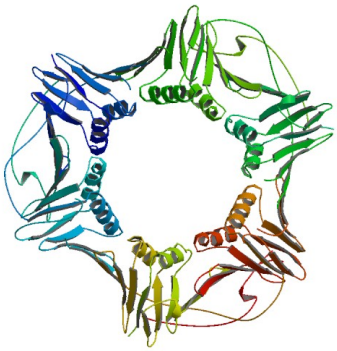

Fig. 8: Human PCNA. [https://www.rcsb.org/structure/1AXC]

In vitro experiments demonstrated that PCNA greatly enhances Pols processivity. Being PCNA an homotrimer, it may bind more than one protein containing a PIP box. Examples of proteins presenting a PIP box are FEN I and DNA ligase I, that are part of the replication complex on the lagging strand. Also two subunits of Pol ε and the p12 and p66 small subunits of Pol δ contain PIP boxes (Moldovan et al. 2007).
PCNA has an important role in promoting the switch from replicative to TLS Pols. Indeed, upon DNA damage and/or stalled replication forks, PCNA undergoes mono- or poly-ubiquitination at the lysine 164, with

monoubiquitination that triggers TLS pathway (Moldovan et al. 2007). Human Pol η physically and functionally interacts with PCNA. Haracksa et al. reported that the addition of PCNA, RF-C and Replication Protein A (RP-A) in *in vitro* reactions, enhanced hPol η synthetic activity of about 12-fold. However, differently from Pol δ, such association is not correlated to an increased processivity of Pol η. Indeed, being Pol η able to misincorporate nucleotides more frequently than Pol δ, a stronger processivity would have resulted in an higher mutagenic potential (Haracska et al. 2001).
PCNA is also involved in Base Excision Repair (BER) pathway where it acts before the step of DNA repair synthesis. Some glycosylases, such as Uracil-DNA glycosylase 2 (UNG2), or AP endonucleases, as human APE2, and the repair cofactor XRCC1 have been found to interact with PCNA through a PIP box (Moldovan et al. 2007).
Moreover, as already mentioned in 1.1.1.3 section, PCNA interacts with the B subunit of RNase H2. However, Chon *et al*. did not observe any significant effect on RNase H2 activity upon addition of PCNA in *in vitro* assays, but is rather possible a role of PCNA in loading RNase H2 at least on some DNA contexts (Chon et al. 2009).

1.1.2.4 PolDIP2

DNA Polymerase Delta Interacting Protein 2 (PolDIP2), also known as PDIP38 or mitogenin 1, is an ubiquitously expressed, multifunctional, 368aa protein. PolDIP2 has been initially discovered as a protein interacting with the p50 subunit of Pol δ and with PCNA. Subsequently, PolDIP2 has been associated to a variety of tasks, including regulation of nuclear redox environment, assembly of the mitotic spindle, pre-mRNA processing, cytoskeletal reorganization and cell cycle checkpoint regulation. Moreover, PolDIP2 is involved not only in DNA replication but also in DNA repair processes. (Brown et al. 2014; Paredes et al. 2018; Guilliam et al. 2016). It also stimulates the processivity of Prim-Pol (Guilliam et al. 2016).

1.1.2.5 DNA polymerases β and λ

DNA Pol β is the smallest Pol of the X family: it is a monomeric enzyme with a molecular mass of 39 kDa, constituted of a 31-kDa carboxyl-terminal polymerase domain (about 250 residues) connected by a short hinge region

to an 8-kDa amino-terminal lyase domain (about 90 residues). (Fig. 9) (Beard and Wilson 2006; Beard and Wilson 2000).

Pol β is ubiquitously expressed in all vertebrates species. The high degree of sequence conservation of Pol β among mammalian species suggests its fundamental role in cells survival; this is demonstrated by embryonic lethality of mice in which Pol β homologous gene was knocked-out (Beard and Wilson 2006).

Pol β is the major Pol involved in BER. Since the majority of enzymes acting in BER prefer double-stranded DNA substrates, this pathway is likely to operate in G1 phase of the cell cycle, during which it ensures error-free transcription, removing eventual DNA lesions from strands that has to be replicated (Dianov and Hübscher 2013).

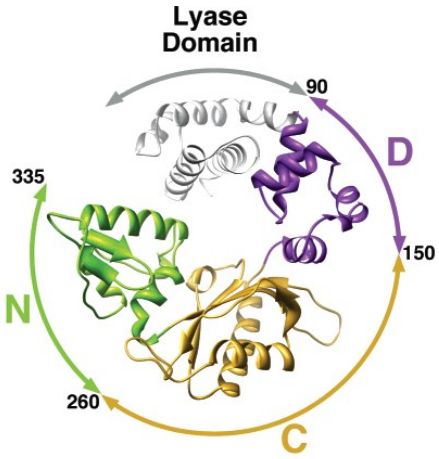

Fig. 9: Domain and subdomain organization of DNA polymerase β. DNA polymerase β is composed of a polymerase (colored) and an amino-terminal lyase domain (gray). The polymerase domain is composed of three subdomains: D- (purple), C- (gold), and N- (green) subdomains (Beard and Wilson 2006).

It has been demonstrated that an excess of Pol β results in high number of DNA breaks and that its overexpression can perturb the function of replicative DNA Pols, lowering their fidelity. This mutagenic potential is due to the intrinsic low fidelity of Pol β in replicating DNA and to a poor ability in discriminating damaged nucleotides. A possible mechanism through which this enzyme increases the genetic instability is the misincorporation of rNMPs. *In vitro* experiments demonstrated that Pol β is able to incorporate eight successive rNMPs in a DNA primer/template

chain, thus acting, even if inefficiently, as an RNA-synthetizing enzyme. Moreover, competition experiments showed that the presence of rNMPs in an *in vitro* reaction affects the ability of Pol β to incorporate dNMPs, especially when the concentration of the two pools are equal or unbalanced in favour of rNTPs. These results suggest that rNMPs incorporation into DNA by Pol β can occur and may be biologically relevant (Bergoglio et al. 2003). Moreover, Pol β can bypass in an error-prone manner CPDs site *in vitro*. It can also misincorporate all four rNMPs opposite to the two bases of CPD, reducing the efficiency of replicative Pols to further elongate the growing strand (Bergoglio et al. 2003).
About 30% of tumors, among which colorectal, gastric and prostate cancer, express Pol β variants (Iwanaga et al. 1999; Starcevic et al. 2004; Albertella et al. 2005). These variants can differently affect Pol β activities, leading to genome instability (Lang et al. 2004). On a total of 152 tumor samples analyzed, Albertella *et al.* found that Pol β was overexpressed by two fold or more in about one third of them. In particular, Pol β was frequently overexpressed in uterus, breast, ovary, stomach and skin tumors. This overexpression can lead to increased mutation rate and to chromosomal instability (Albertella et al. 2005).
It is also interesting to notice that many studies associate defects in BER to trinucleotides repeat (TNR) expansion. Such expansion, leading to genome instability, is typical of neurodegenerative diseases, among which Huntington disease (HD). There are evidences supporting a possible involvement of Pol β in somatic TNR expansion, an important field that deserves further investigations (Crespan et al. 2015).

With its 575 amino acids and a molecular mass of 65k-Da, Pol λ is the largest human polymerase of the X family. It has an N-terminal breast cancer carboxy-terminal (BRCT) domain, separated from the catalytic core by a serine-proline-rich domain. The catalytic core contains an N-terminal 8-kDa domain and a C-terminal polymerase domain. The amino acid sequence of its catalytic core is 30% identical to the one of Pol β (Bebenek et al. 2014).

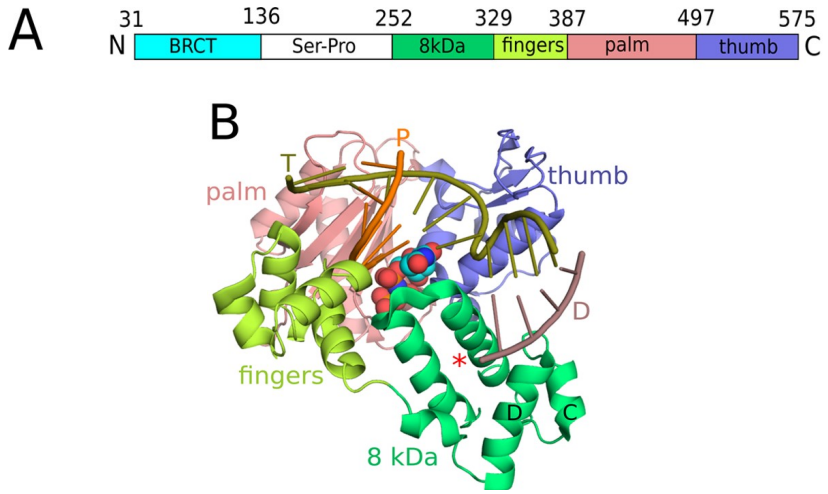

Fig. 10: Domain organization of Pol λ. (A) Schematic representation of domains in Pol λ. (B) Crystal structure of the ternary complex of the catalytic domains of polymerase λ with bound one-nucleotide gapped DNA and an incoming nucleotide (PDB entry 2PFO). The 8 kDa dRP lyase domain, fingers, palm, and thumb subdomains are colored lime green, lemon, salmon, and slate, respectively. The DNA templating strand (T) is colored olive, the primer strand (P) orange, and the downstream strand (D) violet. The position of the 5′-phosphate is marked with a red asterisk. A space-filling model of the incoming nucleotide is colored cyan (C) (Bebenek et al. 2014).

Pol λ is the most ancient member of the eukaryotic X family, since it is conserved across the biological kingdoms, which likely renders it the Pol most similar to the common ancestor from which members of the family evolved (Bebenek et al. 2014).

Pol λ is a multifunctional enzyme. Like Pol β, the 8-kDa domain of Pol λ possesses an intrinsic dRP lyase activity (Moon et al. 2007). Moreover, through the 8-kDa domain, Pol λ binds the 5'-phoshate residue of the downstream strand in DNA gapped substrates, an event that stimulates its gap filling efficiency. It shows a high affinity for dNTPs, which can allow its activity of synthesis when the concentration of dNTPs pool in the cell is low. Pol λ, compared to the other Pols, shows a different catalytic mechanism for incorporation of nucleotides. Indeed, it does not undergo the typical open-to-close transition in response to dNTP binding, which induces generally a relocation of fingers and thumb subdomains. Pol λ catalytic domain remains in a close conformation throughout the catalytic cycle; the binding of the dNTP causes a shift of the template strand so that the

template nucleotide is brought at level of the active site (Bebenek et al. 2014).
Other than BER, Pol λ plays a fundamental role during Non Homologous End-Joining (NHEJ), which is the principal DSBs repair system in higher organisms, active throughout the cell cycle. Pol λ seems to be involved also in microhomology-mediated end joining (MMEJ), a mechanism through which a pathway alternative to the classical NHEJ (called "alternative end-joining" (A-EJ) pathway) can act (Frit et al. 2014; Lieber 2010; Crespan et al. 2012). BER and NHEJ occur during G0-G1 transition and in G1 phase, when dNTPs pools are particularly low (Brown and Suo 2011). Like Pol β, during its gap-filling activity, Pol λ may incorporate rNMPs. However, among Pols associated with NHEJ, it has been shown that Pol λ does not incorporate efficiently rNMPs, displaying higher affinity for dNMPs compared to the other X-family enzyme Pol μ which, on the other hand, preferentially incorporate rNMPs during NHEJ (Pryor et al. 2018; Ramsden 2011). Experiments demonstrated that Pol λ has a relatively high sugar selectivity (3,000 – 50,000) varying depending on the base (rUTP < rCTP < rGTP < rATP). Its binding affinity and rate of incorporation of rNMPs are on average 53-fold lower and 117-fold slower with respect to the correct dNMPs. However, due to the high ratio of rNTPs concentration over dNTPs, and since the fidelity of rNMP incorporation (from 10^{-4} to 10^{-5}) is similar to values of dNMPs misincorporation, is likely that rNMPs insertion during DNA repair *in vivo* is more common than erroneous introduction of dNMPs by Pol λ (Brown and Suo 2011).
Other than Pol β, Albertella *et al.* also found Pol λ deregulated in a number of tumor specimens. In particular, in 24% of the tumor analysed Pol λ was overexpressed. This suggests that deregulation of specialized Pols may have a role in tumorigenesis (Albertella et al. 2005).

1.1.3 Oxidative DNA lesions

Reactive oxygen species (ROS) formed during normal cellular metabolism cause oxidative lesions, one the most frequent kind of DNA damage. ROS are mainly generated in mitochondria during electron transfer reactions, by the cytocrome P450 system, in microsomes, peroxisomes and by different cellular oxidases. (Amoroso et al. 2008; Markkanen 2017). Also ionizing or ultraviolet radiations may cause ROS production (COOKE et al. 2003). The major ROS in living cells are peroxyl radicals, such as the hydroxyl radical

(•OH) and the superoxide anion ($O^{2\bullet-}$). They are responsible for diverse types of additions to DNA bases, causing stable modifications to DNA (Amoroso et al. 2008). About 10^5 oxidative damages occur in every cell each day, including 8-oxoguanine (8-oxo-G) (see 1.1.3.1 section), 2,6-diamino-4-hydroxy-5-formamido-pyrimidine (FapyGua), and the oxidised pyrimidines cytosine glycol and thymine glycol. Chronic oxidative stress, in particular in the presence of chronic inflammation, has been linked to carcinogenesis (Bridge et al. 2014).

Due to their high mutagenic potential, several DNA repair pathways, often overlapping, have evolved to repair oxidative DNA lesions. Basically, two main pathways allow to remove these kind of lesions: BER and NER, that differ regarding the size of the damages handled. BER deals with single or few damaged nucleotides while NER deals with large DNA-distorting lesions (e.g. intra-strand crosslinks, tandem lesions, bulky adducts) (Bridge et al. 2014; Cooke et al. 2003). In eukaryotes BER is divided into Short-Patch (SP) BER, to replace single lesioned nucleotides, and Long Patch (LP) BER, for two or more lesioned nucleotides (Fig. 11). The only Pol acting during SP BER is Pol β. On the other hand, during LP BER Pol β is responsible for the incorporation of the first nucleotide while replicative Pols act during the elongation step (Fortini and Dogliotti 2007). In both SP and LP BER, a DNA glycosylase hydrolizes the N-glycosidic bond thus removing the base from the sugar-phosphate backbone. Subsequently, the main 5' AP endonuclease in humans (APE1) can nick the sugar-phosphate backbone of the resulting AP site. In particular, APE1 cleaves the phosphodiester bond 5' to the AP site, generating a 5'dRP and a 3'-OH. At this point, Pol β removes the 5'dRP through its intrinsic dRP-lyase activity, leaving a phosphate at 5'-end. Then Pol β fills the gap and ligase III, in complex with its accessory protein XRCC1, ligates the nicked DNA (Fortini et al. 2007; Beard and Wilson 2006). In LP BER 2-11 nucleobases can be synthesized via strand displacement of the downstream DNA strand. This synthesis is performed by the replicative Pols δ or ε (or by chance also by Pol β) in association with PCNA and RF-C. FEN1 then cuts the flap and DNA ligase I ligates the gap (Hübscher and Maga 2011). Like Pol β, also Pol λ is involved in BER: while Pol β is the main enzyme for BER occurring in nuclear DNA, Pol λ involvement in BER is supported by the observation that, it can substitute Pol β in BER reactions *in vitro*. Moreover, chicken cells and mouse fibroblasts in which genes encoding for both Pol λ and β were deleted, are more exposed to oxidizing DNA-damaging

agents than cells and fibroblasts in which only Pol β gene was knocked out (Bebenek et al. 2014).

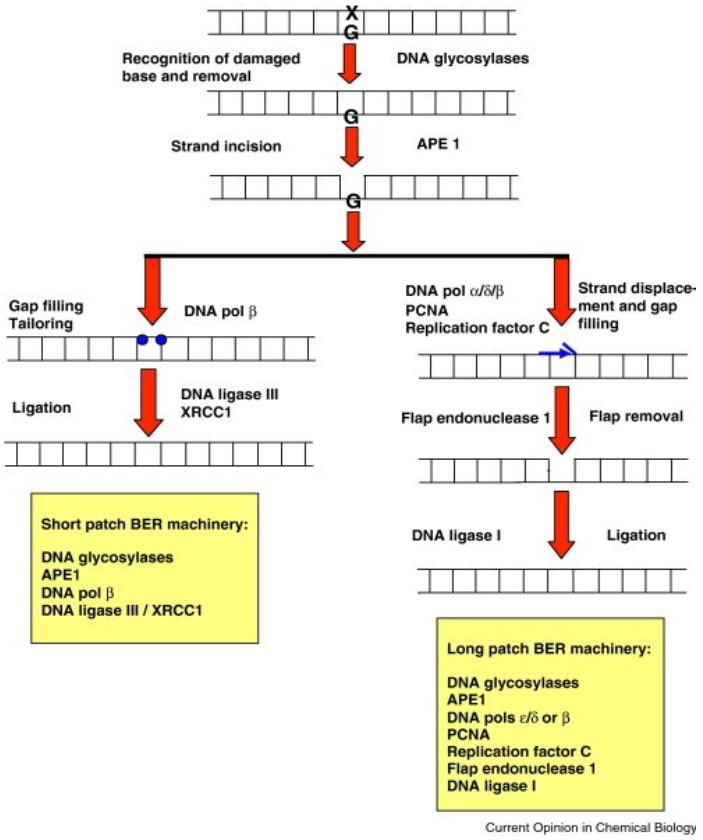

Fig. 11: Short patch BER and long patch BER. The short patch BER machinery contains DNA glycosylases, APE1, DNA Pol β, DNA ligase III/XRCC1; the long patch BER machinery consists of DNA glycosylases, APE1, DNA polymerases α/δ or β, PCNA, replication factor C, flap endonuclease 1 and DNA ligase I (Hübscher and Maga 2011).

1.1.3.1 8-oxo-G lesion

Purines often react with •OH, whose addition to C4-, C5- and C8- positions generates modified bases, threatening for DNA integrity (Roldán-Arjona and Ariza 2009). Among the most relevant and investigated oxidative lesions there are the C8-OH adducts of guanine, such as 7-hydro-8-hydroxyguanine and 8-oxo-G, and the C2-OH adduct of adenine (Amoroso et al. 2008). In particular, 8-oxo-G is an abundant and threatening lesion. It

is estimated that at least 10^4 8-oxo-G damaged bases are generated spontaneously in cells every day (Maga et al. 2008). Due to its abundance, 8-oxo-G is frequently used as cellular biomarker for oxidative stress (David et al. 2007). This lesion is potentially mutagenic in bacteria and mammals since it possesses the capability to pair with an A assuming a syn conformation (Hoogsteen base pair). This miscoding lesion, if not repaired before the beginning of replication, can cause G:C to T:A transversions (David et al. 2007). Indeed, replicative Pols α, δ and ε bypass 8-oxo-G lesion mainly in an error-prone manner, incorporating an A instead of a C (Hübscher and Maga 2011).8-oxo-G lesions accumulate with age, especially in the mitochondrial genome. They have also been correlated with different types of tumors, such as breast, colorectal, gastric and lung cancer and neurodegenerative diseases (e.g. Parkinson and Alzheimer diseases) (Bridge et al. 2014; Amoroso et al. 2008).

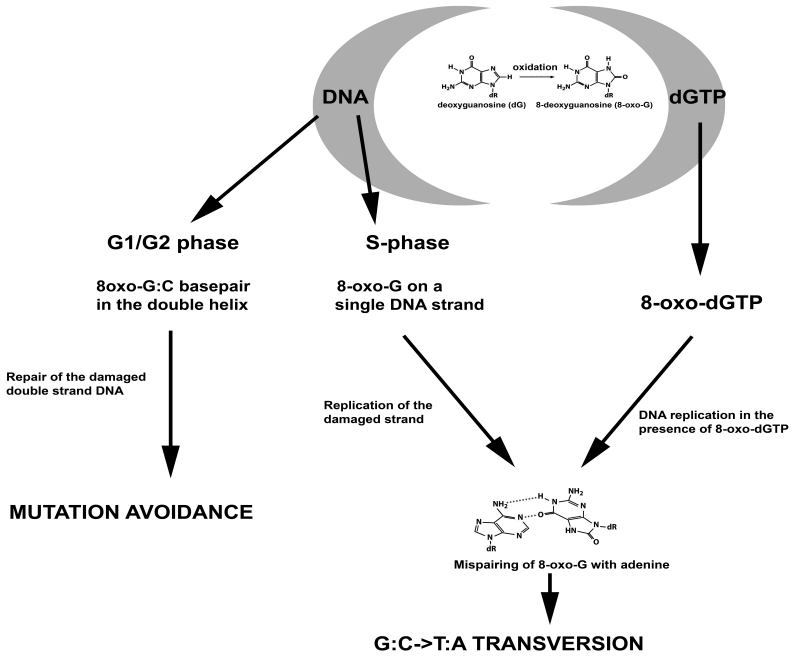

Fig. 12: Schematic drawing of the mutagenic consequences of the 8-oxo-G lesion. (Amoroso et al. 2008).

To avoid occurrence of mutations caused by the presence of 8-oxo-G lesions, a specific 8-oxo-G repair pathway exists in prokaryotic and eukaryotic cells, named guanine oxide or "GO" system. It relies on 8-oxo-G

DNA glycosylase 1 (Ogg1) and on MUTHY glycosylase (Fig. 13) (Amoroso et al. 2008; David et al. 2007). In all tissues Ogg1 starts the SP BER through recognition of 8-oxo-G when paired to a C, allowing damaged base removal and damage repair by BER (Amoroso et al. 2008; Hübscher and Maga 2011).
On the other hand, if the 8-oxo-G is not removed through this process, when the replication machinery encounters an 8-oxo-G, it incorporates an A instead of a C in most of the cases. In such situation, MutYH recognize 8-oxo-G:A mispair, removing the A. APE1 then incises the DNA and Pol λ, together with PCNA and RP-A, inserts the correct C opposite the 8-oxo-G still present on the template strand. Frequently Pol λ can incorporate a second nucleotide, thus creating a 1-nt flap. FEN1 can remove the flap and DNA ligase I can then seal DNA. Through this process the C:8-oxo-G pair is restored becoming substrate of the OGG1-dependent SP BER (Hübscher and Maga 2011).

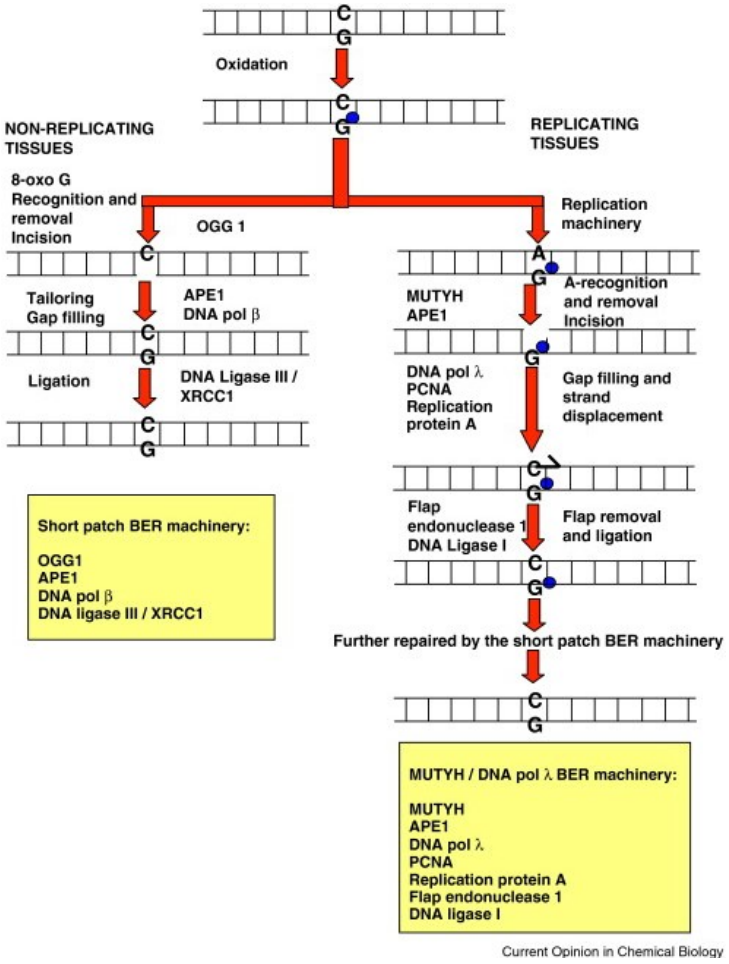

Fig. 13: Faithful BER of an 8-oxo-G lesion in a non-replicating tissue (left) and in a replicating tissue (right). (Hübscher and Maga 2011).

The preferential selection of the Pol in the "GO" system relies on the ability of PCNA and RP-A to recruit Pol λ instead of Pol β on a 8-oxo-G lesion facing a window gap. It has been shown that PCNA and RP-A in association with Pol λ ensure a 750-fold preference for dCTP vs dATP incorporation opposite 8-oxo-G on 1-nt gap. On the other hand, Pol β bypasses the damage with a reduced fidelity, leading to a misincorporation of dAMP in about 20-30% of cases. Pol β is, indeed, 145-fold less efficient than Pol λ in performing error-free TLS past 8-oxo-G damage on 1-nt gap substrate. (Maga et al. 2008; Maga et al. 2007).

1.1.3.2 Oxidative DNA damage tolerance in plants

Oxidative DNA damages caused by exposure to ROS occur also in plants. As already mentioned, ROS are the result of endogenous and exogenous factors. The endogenous stresses include respiration and photosynthesis. For example, the singlet oxygen ($^1O_2$) and the superoxide radical ($O^{2\bullet-}$) are two byproducts of photosynthesis while hydrogen peroxide (H_2O_2), together with O^{2-}, originates from peroxisomes. O^{2-} is also the main result of the electron transport chain in mitochondria (Roldán-Arjona and Ariza 2009). Moreover, plants are sessile organisms continuously exposed to different environmental (exogenous) stresses like UV, IR, salinity, drought, pathogens that cause alteration of cellular homeostasis and, as consequence, higher ROS production. At high concentrations, ROS are very dangerous for plant cells. In particular, 8-oxo-G lesion is very dangerous not only for mammals but also for plants (for details on 8-oxo-G lesion see 1.1.3.1 section) (Roldán-Arjona and Ariza 2009; Amoroso et al. 2008).
Studies have demonstrated that plants have evolved a variety of mechanisms to face oxidative damages, some peculiar while others similar to those evolved by other eukaryotes. Plants are endowed with a lot of different antioxidant molecules, that can be enzymatic (e.g. superoxide dismutase (SOD), catalase (CAT), ascorbate peroxidase (APX); glutathione reductase (GR),glutathione-*S*- transferase (GST)) or non enzymatic (e.g. L-ascorbic acid (Vitamin C); glutathione (GSH); phenolic compounds, alkaloids, non-protein amino acids, α-tocopherols (Vitamin E), carotenoids) (Gill and Tuteja 2010; Roldán-Arjona and Ariza 2009). In particular, Glutathione (GSH) has a vital role in controlling oxidative stress. It participates in different metabolic processes, detoxifying ROS, modulating antioxidant enzymes and regulating the expression of stress defense genes (Hasanuzzaman et al. 2017).
Many DNA repair pathways present in higher eukaryotes are conserved in plants, including BER and TLS. Plants mainly rely on BER to remove oxidized DNA bases. However, they lack Pol β and DNA ligase III, thus suggesting that some differences between plant and mammalian repair mechanisms do exist. On the other hand, plants possess multiple copies of other genes encoding for proteins involved in DNA repair. PCNA is present in two copies (PCNA1 and PCNA2) in *A. thaliana* genome (Amoroso et al. 2011; Strzalka and Aggarwal 2013). BER is initiated by N-glycosilases, that leave an AP site (for details see 1.1.3 section). Generally, DNA glycosilases are classified into two groups: monofunctional and bifunctional

glycosilases. The monofunctional only catalyse the hydrolysis of the glycosylic bond between damaged base and sugar-phosphate backbone, while the glycosilases/lyases (bifunctional) are also able to incise the DNA backbone after base removal. Most of the glycosilases identified in prokaryotes and eukaryotes acting on oxidized bases are bifunctional. Ogg1 homolog in *A. thaliana* (AtOgg1) is a bifunctional, purine-specific enzyme. As for its mammals countrepart, AtOgg1 allows the release of 8-oxo-G and the cleavage of DNA backbone at the resulting abasic site. Moreover, plants possess also a MutYH enzyme (AtMutYH), which is supposed to remove A paired to 8-oxo-G. However, AtMutYH has not been fully functionally characterized yet (Roldán-Arjona and Ariza 2009).

In humans, Pol λ interacts with PCNA and RPA allowing high-fidelity TLS of 8-oxo-G lesion. In higher plants, family X of DNA polymerases includes only POLL, which shares 30% of homology with its human homologue (Amoroso et al. 2011). Results obtained from Amoroso *et. al* indicated a functional cooperation between AtPOLL and PCNA2 in presence of AtRPA *in vitro*, but not between AtPOLL and PCNA1. The physical interaction between the two proteins was also confirmed *in vivo*. Plants overexpressing AtPOLL showed a delayed growth and treatment with UV-B irradiation, that contribute to ROS production, caused increasing in AtPOLL transcripts, both in seeds and leaves. Overall, the results suggested that *A. thaliana* possesses a TLS pathway in which, similarly to humans, AtPOLL interacts with AtPCNA2 and AtRPA, thus supporting the essential role of Pol λ in oxidative DNA-damage tolerance pathway in all eukaryotes (Amoroso et al. 2011).

2. Aims of the research

All living organisms need to preserve the integrity of their genome to properly store and transmit genetic informations. However, DNA is subjected to a variety of damages that, if not removed, can have dangerous effects. Misincorporated rNMPs are the most abundant lesions in the genome (Potenski and Klein 2014). Their permanence in the DNA has been linked to genome instability and replication stress (McElhinny et al. 2010a; Meroni et al. 2017). Indeed, other than spontaneous SSBs, unrepaired rNMPs lead to geometrical distortion of double helix, impairing DNA binding protein activities and progression of the replication fork. It is known that RER activity, initiated by RNase H2, is essential for the removal of rNMPs and for the survival of all life forms. However, it was not known if rNMPs could be misincorporated opposite other DNA lesions by TLS activity and the effects of such mispair on RER. Therefore, we attempted to assess these questions by comparing the ability of the two BER Pols, β and λ, and the Y-family Pol η, to incorporate rNMPs versus dNMPs opposite different types of DNA damages, which are linked to aging, cancer, neurodegenerative diseases. We then evaluated the impact of such rNMPs incorporation on the BER pathway, initiated by the human Ogg1 and MutYH glycosylases, and we characterized the cleavage ability of the human RNase H2 on the damaged-DNA/RNA hybrid substrates.
The same biochemistry was applied to plants, in the attempt to better characterize the mechanism of SP-BER, both *in vitro* and in a cellular context. Some preliminary data are presented in this thesis.

3. Materials and methods

3.1 Chemicals

Deoxynucleotides were purchased from GeneSpin (Milan, Italy). Ribonucleotides were purchased from GE Healthcare (Uppsala, Sweden). The rNTPs stocks were double checked in house by HPLC for dNTPs contamination, which was found to be below the limit of detection (> 99.6% purity). Labelled [γ-32P]ATP was purchased from Hartmann Analytic GmbH (Braunschweig, Germany). Adenosine, guanosine, cytidine and uridine standards were obtained from Sigma (St Louis, MO, USA). All the other reagents were of analytical grade and purchased from Fluka or Merck.

3.2 Oligonucleotides

The 24-mer oligonucleotide containing the cis-PtGG adduct was prepared and purified as described previously (Nilforoushan et al. 2015). All other DNA oligonucleotides were synthesized by Purimex (Grebenstein, Germany) and purified from polyacrylamide denaturing gels. When indicated, oligonucleotides were 5'-labelled with T4 polynucleotide kinase (New England Biolabs) and [γ-32P]ATP, according to the manufacturer's protocol or directly synthesized as 5'-labeled with carboxyfluorescin (FAM) group. Each labelled primer was mixed to the complementary template oligonucleotide at 1:1 (M/M) ratio in the presence of 25mM Tris-HCl pH 8 and 50mM KCl, heated at 75 °C for 10 min and then slowly cooled down at room temperature.

3.3 Oligonucleotide sequences

40-mer template:
3'-ATAGGTGGTTATGATGGGATGCTATGATAGAGGTGAGTTG-5' .

The sequence underlined corresponds to the four templating bases at position +1, generated on annealing of the template to the 18-merA, 19-merT, 20-merG and 21-merC primers, respectively.

18-merA primer:
5'-TATCCACCAATACTACCC-3'

19-merT primer:
5'-TATCCACCAATACTACCCT-3'

20-merG primer:
5'-TATCCACCAATACTACCCTA-3'

21-merC primer:
5'-TATCCACCAATACTACCCTAC-3'

For the generation of the 1 nt-gap template, the 100mer was annealed to the 39-mer primer and to the 60-mer downstream oligo, which has been 5'-phosphorylated with unlabelled ATP by using T4 polynucleotide kinase (NEB).

100 mer template:
3'-ATGTTGGTTCTCGTATGCTGCCGGTCACGGCTTAAGTGTXCCACAACAC
ACAACCAACACCACCACAACACACCAACAACCACAACACACACAACCACAC
-5', where X=G or 8-oxo-G. The sequence underlined is the one complementary to the 39-mer primer.

39-mer primer:
5'-TACAACCAAGAGCATACGACGGCCAGTGCCGAATTCACA-3'

60-mer downstream oligonucleotide:
5'-GGTGTTGTGTGTTGGTTGTGGTGGTGTTGTGTGGTTGTTGGTGTTGTGT
GTGTTGGTGTG-3'

20-merG primer:
5'-TATCCACCAATACTACCCTA-3'

72-mer template:
3′-ATGTTGGTTCTCGTATGCTGCCGGTCACGGCTTAAGTGTXGCGGCCGCG
GGTTGGAGGGCTTATAGATTATG–5'

where X=3-met-C or 8-met-G
24-mer template:
5′-CTAC**GG**CTCACACTATCTCACACT-3′
The bold letters indicate the position of the cis-PtGG crosslink.

40-mer rNMPs templates:

40-mer rC:
5'–ATTGAGTGGAGATAT**C**GTAGGGTAGTATTGGTGGATA–3'

40-mer rG:
5'–ATTGAGTGGAGATATC**G**TAGGGTAGTATTGGTGGATA–3'

40-mer rU:
5'–ATTGAGTGGAGATATCG**U**AGGGTAGTATTGGTGGATA–3'

40-mer rA:
5'–ATTGAGTGGAGATATCGT**A**GGGTAGTATTGGTGGATA–3'

The bold letter corresponds to the single ribonucleotide present in each 40-mer oligonucleotide, which generated, upon annealing to a complementary 40-mer DNA oligonucleotide the 40/40-mer rC, 40/40-mer rG, 40/40-mer rU and 40/40-mer rA, respectively.

3.4 Enzymes and proteins

Human recombinant Pols λ and β (Maga et al. 2007) and human recombinant glycosylases MutYH and Ogg1 (van Loon et al. 2009; Simonelli et al. 2013) were used.

Recombinant human PCNA and PolDIP2 were expressed and purified as described (Maga et al. 2013).

The bacterial clone for the expression of human Pol η was a kind gift from R. Woodgate (NIH, USA). Human recombinant Pol η was expressed and purified as described (Frank et al. 2012).
TheMIC1066 *E. coli* strain and the plasmid for the simultaneous expression of the three subunits of human RNase H2 were a kind gift of R. J. Crouch (National Institute of Child Health and Human development, Bethesda, MD, USA). The heterotrimeric human recombinant RNase H2 was expressed and purified as described (Chon et al. 2009), with the following modifications: cells were lysed for 30 min on ice in 20 mM KPO4 buffer pH 7.4, 300 mM NaCl, 30 mM Imidazole, 10 mg ml^{-1} lysozyme, 0.05%

phenylmethylsulfonyl fluoride and protease inhibitors. The lysate was sonicated and cleared by ultracentrifugation at 38000 rpm in a Ti70 Beckman rotor. The cleared lysatewas loaded onto a FPLC-NiNTAcolumn (G&E Healthcare) equilibrated in 20 mM KPO4 buffer pH 7.4, 300mM NaCl, 30mM imidazole, 5% glycerol. The protein was eluted with a 30–500 mM linear gradient of imidazole in the equilibration buffer. The fractions containing the enzyme in 20% glycerol were stored separately in liquid nitrogen.

3.5 Enzymatic assays

All reactions were in a 10 μl final volume.
Reactions with Pols λ and β were incubated for 10 min at 37 °C in the presence of 5'-labelled p/t at the concentrations stated in the figure legends. Pol λ, β reaction buffer: 50mM Tris pH 7.5, 1mM DTT, 0.2 mg ml1 BSA. Mg^{++} was included for all Pols at 5 mM, unless otherwise stated in the figures or figure legends. When crude extracts were used, the reaction mixture was supplemented with 0.1 mg ml^{-1} aphidicolin and 1 μM of a 49mer single-stranded DNA oligonucleotide with a non-complementary sequence to the DNA substrate, to inhibit exonuclease degradation. Crude whole cell extracts were prepared as described in ref. (Furrer and van Loon 2014). Proteins, Mg^{++}, Mn^{++} and nucleotides were in the concentration specified in the figures and figure legends.
Pol η reaction buffer: 40 mM Tris pH 8, 1 mM dithiotreitol, 0.25 mg/ml bovine serum albumin (BSA). Mg^{++} was included at 5 mM, unless otherwise stated in the figures or figure legends.
RNase H2 reaction buffer: 50mMTris-HCl pH8.5, 25mM NaCl, 50 μg ml^{-1} BSA, 1mM 2-mercaptoethanol, 1% glycerol, 5mM Mg^{++}. Enzymes and DNA substrates concentrations are indicated in the figures or figure legends. Reactions were incubated at 37◦C for 5 min, unless otherwise stated in the figures or figure legends.
For denaturing gel analysis of the DNA products, the reaction mixtures were stopped by addition of standard denaturing gel loading buffer (95% formamide, 10mM EDTA, xylene cyanol and bromophenol blue), heated at 95 ° C for 5min and loaded on a 7-M urea 12% polyacrylamide (PA) gel. The reaction products were analysed by using Molecular Dynamics Phosphoimager (Typhoon Trio, GE Healthcare) and quantified by the program Image Quant.

3.6 DNA glycosylase assays

hOgg1 was incubated with 5'-labelled ds 100-mer DNA with 8-oxo-G:dC or 8-oxo-G:rC mispairs. On incubation, the reaction products were treated with NaOH (2M), heated for 15 min at 75 °C and reactions analysed on a 7-M urea 10% polyacrylamide gel. The reactions were performed at 37 °C in final volume of 10 µl containing 20 fmol 5'-labelled ds 100-mer DNA with 8-oxo-G:dC or 8-oxo-G:rC, 20mM Tris-HCl (pH 8), 1mM DTT, 1mM EDTA and 0.1 mg ml^{-1} BSA. hOGG1 concentration and incubation times varied and are indicated in figures. On incubation hOGG1 reaction products were treated with 1 ml NaOH (2M), heated for 15 min at 75 _C and reactions stopped by the addition of denaturing gel loading buffer and heating at 95 _C for 5min. The samples were separated on 7M urea 10% PA gel, analysed by Phosphoimager and quantified by GelEval 1.35 scientific imaging software (FrogDance Software, UK).

MutYH assay (van Loon and Hübscher 2009) was performed in 10 µl reactions containing 25mM Hepes–KOH pH 6.8, 5mM EDTA, 1.5% glycerol, 50 µM ZnCl2, 50mM NaCl, 7.5mM MgCl2, 20fmol 5'-labelled ds 100-mer DNA with dA:8-oxo-G or rA:8-oxo-G, 200nM MutYH and varying amounts of APE1.Reactions were stopped by the addition of denaturing gelloading buffer, heating at 95°C for 5min and separated on 7-M urea 10% PA gel. The products were detected by Phosphoimager and quantified by GelEval 1.35 scientific imaging software (FrogDance Software, UK).

3.7 Kinetic analysis

Due to the highly distributive nature of the reaction and the relatively low efficiency of rNTPs incorporation, the enzymes and the DNA substrate were used at similar concentrations. This implies that, at equilibrium, the concentration of the binary enzyme–DNA complex does not approximate the total enzyme concentration, but there is always a fraction of enzyme not bound to the DNA substrate, that does not participate in catalysis. Thus, to account for the fraction of enzyme not bound to the DNA substrate at equilibrium, the variation of the nucleotide incorporation rates (v) as a function of the nucleotide substrate concentration was fitted to the modified Briggs–Haldane equation:

(1) $v = \frac{kca \quad {}_0S}{(S \cdot a)+(K_m \cdot b)}$

where *kcat* is the apparent catalytic rate, E_0 is the input enzyme concentration, S is the variable nucleotide substrate concentration, K_m is the apparent equilibrium dissociation constant of the nucleotide substrate from the catalytically active ternary complex, *a* and *b* are two constants, whose values were kept fixed during the computer fitting and were calculated from the expressions:

(2) $a = \frac{1}{\left(1+\frac{Km}{K'}\right)}$

(3) $b = \frac{1}{\left(1+\frac{K'}{S'}\right)}$

where K_m is the same as in Eq. (1), K' is the apparent dissociation constant for binding to the DNA substrate and S' is the concentration of DNA used in each experiment. The values of K' used for the fitting process were: Pol β = 22 nM (Batra et al. 2012); Pol λ = 29 nM (Cavanaugh et al. 2011); Pol η 1.1 nM (Washington et al. 2001). Under conditions of forced termination (single nucleotide incorporation), $K_m = K_s(k_{off}/(k_{pol}+k_{off}))$ and $k_{cat} = k_{pol}(k_{off}/(k_{pol}+k_{off}))$. Where K_s is the Michaelis constant for nucleotide binding, k_{off} is the dissociation rate of the enzyme from the DNA substrate and k_{pol} is the polymerization rate. Hence $k_{cat}/K_m = k_{pol}/K_s$.
In the case of RNase H2, the apparent initial velocities were plotted as a function of the DNA substrate concentrations and fitted to the Michaelis-Menten equation:

(4) $v = \frac{k\text{cat}E_0S}{K_M + S}$

Here *kcat* is the apparent catalytic rate, E_0 is the input enzyme concentration, *S* is the variable DNA substrate concentration, K_M is the apparent Michaelis constant. Fitting was obtained with the GraphPad Prism 5.0 computer program.

3.8 Electronic image manipulation

Linear transformations have been applied in some instance to the whole

images using the exposure/brightness filters of Adobe Photoshop CS6 with the sole purpose of reducing excessive background. No masking/enhancement was applied to any specific feature of the images. Solid lines identify different portions of the same gel brought next for clarity of presentation.

3.9 Cell lines and culturing conditions

Immortalized Pol λ+/+, Pol λ-/-, Pol β+/+ and Pol β-/- MEFs (Bertocci et al. 2006),(Sobol et al. 1996) were grown in a humidified 5% CO2 atmosphere in Dulbecco's modified Eagle's medium containing GlutaMAX-I supplemented with 10% fetal bovine serum and 100U ml^{-1} penicillin–streptomycin (all obtained from Gibco, Invitrogen). XP-V patient-derived XP30R0 fibroblast cells transformed with simian virus 40 were a gift from Alan Lehman (University of Sussex, Brighton, UK). XP-V cells were grown in a humidified 5% CO2 atmosphere in Dulbecco's modified Eagle's medium containing GlutaMAX-I supplemented with 10% fetal bovine serum and 100 U/ml penicillin– streptomycin (all obtained from Gibco, Invitrogen). To complement XP-V cells, human Polη mammalian expression vector pJRM56 (kindly provided by Roger Woodgate, NIH, USA) was used. pJRM56 or empty pcDNA 3.1 (Invitrogen) constructs were transiently transfected into XPV cells using lipofectamine (Invitrogen) according to manufacturers protocol. Alternatively XP30RO cells stably expressing eGFP-Polη were used (Kannouche et al. 2001; Bienko et al. 2010). Cells were harvested 48 h respectively after transfection or seeding and wholecell extract (WCE) were prepared. Cells were harvested 48 h after the transfection and WCE prepared.

3.10 Cell extracts and western blot

Cell extracts were prepared as described (Furrer and van Loon 2014). Proteins were separated on 10% Bis-Tris poly-acrylamide gels and transferred to Immobilon-FL membrane (Millipore) for immunoblotting analysis. Primary antibodies against Pol η (Abcam), Pol β (custom made antibody) and Tubulin (Sigma) were detected using infrared dye-conjugated secondary antibodies (LI-COR Biosciences). For signal visualization the Odyssey Scanner (LI-COR Biosciences) was used.

3.11 AtMUTYH expression in bacterial strains

pTrcHisA vector expressing N-terminal His-tagged *Arabidopsis thaliana MutYH* (at4g12740) gene was from Genscript. C43(DE3) (Lucigen) and BL21(DE3)pLysS (Promega) competent cells were transformed with pTrcHisA vector. Plates containing 50μg/ml ampicillin or 50μg/ml ampicillin and 34μg/ml chloramphenicol were used to identify ampicillin-resistant or ampicillin/ chloramphenicol-resistant colonies that were picked and grown overnight at 37°C. DNA purified from bacterial cultures using PureYield™ PlasmidMiniprep System (Promega) was digested to confirm the presence of the gene expressing MutYH. Bacterial glycerol stocks were made and used to inoculate 20ml starter cultures. After overnight growth at 37°C, each starter culture was put in 200ml of LB medium (containing 50μg/ml ampicillin or 50μg/ml ampicillin and 34μg/ml chloramphenicol). Bacterial cultures were grown until Optical Density $(OD)_{600}$ of 0.4 or 1.0. Isopropil-β-D-1-tiogalattopiranoside (IPTG) 0.1 or 0.3 or 0.6 mM was added. Cells were grown for 4 hour at 37°C or O/N at 15°C, harvested by centrifugation and pellets frozen at -80°C. Each pellet was resuspended in lysis buffer (0.1M KPO_4 pH7.4, Nonidet P-40 0.01%), 1X lysozime (Eurobio, Courtaboeuf, France), 1X ethylenediaminetetraacetic acid [EDTA]-free protease inhibitor (SIGMAFAST™ Protease Inhibitor Cocktail Tablets, Sigma-Aldrich), 1mM phenylmethane sulfonyl fluoride [PMSF] and lysed through sonication. After centrifugation at 20,000g at 4°C for 20minutes, the supernatant or soluble fraction was collected. The remaining pellets were resuspended in water and lysed through sonication. Laemmli buffer 1X was added, samples were heated for 8 minutes at 95°C, centrifuged 20,000g at 4°C for 20minutes and the supernatant, representing the insoluble fraction, was collected. Samples were resolved on 10% SDS-PAGE gels that were either stained with Coomassie Brilliant Blue dye or used for immunoblotting analysis. Primary anti-His6 (1:500) rabbit IgG antibody (Cell Signaling) and HRP-conjugated anti-rabbit secondary antibody (Jackson ImmunoResearch) were used. Detection was performed by using chemiluminescence reagents (Pierce Thermo Scientific). The signal was visualized through Chemidoc Imaging System (Bio-Rad).

3.12 *AtMutYH* sequence

AtMutYH coding sequence cloned between BamHI and EcoRI sites in pTrcHisA:

5'-GATCCATGGCTTGTCTTCTCCGCGTGGCTCTAAACCCTACATTCGAAAG
ATCAACGGTCGCTTCACAGAGACAAAATCCAAAGACCATTCTAAGTTTTCA
TTGCAAAGTTTCGAGCTTTAAGACCAAAACGATGTCCCAATCTTTTGCTCC
TCGCGAGAAACTCATGAGAAAGTGTCGAGAGAAAAAAGAAGCAGAACGAGA
AGCAGAACGAGAAGCAAACGAGAAGCAGAAGAAGAAGAAAAAGCAGAAGAA
GCAGAAGCAGAAGCAGACAAAGAAGAAGCAGAAGAAGAATCAGAAGAAGAG
AAGAAGAAGAAGAAGAAGAAGCAGAAGCAGAAGAAGAAGCGCTTGGAGGAG
ATATAGAGGATCTCTTTAGTGAAAATGAAACTCAGAAAATCAGAATGGGTT
TGCTTGATTGGTACGATGTGAATAAGAGAGATCTTCCATGGAGGAACAGAA
GAAGTGAAAGTGAAAAGGAGAGAAGAGCTTATGAGGTTTGGGTATCGGAGA
TTATGCTTCAGCAAACTAGGGTTCAGACTGTAATGAAGTATTATAAACGTT
GGATGCAGAAATGGCCAACCATTTATGACCTTGGTCAAGCTTCTCTTGAGA
ATCTTATCGTTAGTAGATCAAGAGAGCTTTCTTTTCTTAGGGGGAATGAGA
AAAAAGAGGTAAACGAAATGTGGGCAGGTTTGGGATACTATCGGCGGGCAC
GTTTTCTTTTAGAGGGTGCAAAGATGGTTGTTGCAGGGACGGAGGGTTTCC
CTAATCAAGCGTCTAGCTTGATGAAAGTTAAAGGAATAGGACAGTACACAG
CCGGAGCAATTGCCTCAATTGCTTTCAATGAGGCAGTACCTGTTGTTGATG
GAAATGTGATAAGAGTGCTTGCTAGATTAAAAGCCATCTCAGCTAATCCAA
AAGACCGACTTACGGCCAGGAATTTCTGGAAACTAGCTGCTCAGCTAGTGG
ATCCTTCACGCCCTGGAGATTTCAACCAATCTCTGATGGAGCTTGGTGCTA
CACTATGCACTGTATCAAAGCCAAGTTGCTCTTCTTGTCCTGTTTCCAGCC
AATGTCGTGCATTTTCACTTTCCGAGGAAAACAGAACGATTTCCGTGACAG
ATTATCCTACAAAAGTAATCAAGGCCAAGCCAAGGCACGACTTTTGTTGCG
TTTGTGTTTTGGAGATACATAATCTGGAGAGGAACCAATCAGGAGGTAGAT
TTGTTCTTGTAAAAAGACCCGAACAAGGTCTGCTTGCTGGTCTTTGGGAGT
TCCCATCTGTTATATTAAATGAGGAAGCTGATTCGGCAACAAGGAGGAACG
CAATAAACGTCTACCTTAAGGAAGCATTTCGTTTTCATGTAGAACTCAAGA
AAGCATGCACTATAGTTTCAAGAGAAGAACTCGGAGAATTCGTCCACATAT
TCACTCACATTCGTCGAAAAGTTTATGTGGAGCTATTAGTTGTACAACTTA
CAGGCGGAACCGAAGATCTGTTCAAAGGTCAGGCAAAGGACACTCTAACAT
GGAAGTGTGTGAGCAGTGATGTTCTTTCTACCTTGGGACTGACATCAGCTG
TTAGAAAGGTACCTCCTTTTCGTCTTCAACATATTAAAAGACTATCCTTGG
ATGTGATGGTTGAGAAGGAACAAATTTTGGAGTGCAGGTGTATTCAATGGT
TGAAGCACACAAGCAAGGCTTATCTGTTTCTCATGTCTCATCAAATAGAAC
AGCCATATCGAGGAAACGAAAATTCTCATGATCTCCTTCTCACACTTTTCT
TCATGTTGCTTAGCTTCTATAGTTCTTGTCTAGCATTGGGAATCAAATTTG
GTGATCTTGGTTTGAAATTGAACAGCTTAGTTTCTACTGAGAAAAGTGACG
GTGATGTGTGAGAATTC-3'

3.13 Cloning *AtMutYH* in pET30a vector

Primers (Invitrogen, Thermo Fisher Scientific) to PCR-amplify the gene encoding AtMutYH protein were designed to facilitate incorporation into the pET-30a(+) expression vector (Novagen). The forward and reverse primers are listed in Table 1, with NdeI and NotI restriction sites underlined. PCR amplification was carried out using *Pfu* DNA polymerase (Promega). Following amplification, the *AtMutYH* DNA was cleaned using the ISOLATE II PCR and Gel Kit (Bioline). The pET-30a (+) vector and amplified AtMUTYH DNA were double-digested using NdeI and NotI restriction enzymes in buffer D (Promega). After digestion, all DNA fragments were cleaned using the ISOLATE II PCR and Gel Kit (Bioline) and the fragments were ligated at 15 °C overnight using T4 DNA ligase (Promega). The ligation product was transformed into DH5α competent cells (Thermo Fisher Scientific) for DNA amplification. The DNA was used for PCR amplification, carried out using the forward and reverse primers of Table 1 and *Pfu* DNA polymerase. PCR products were separated by electrophoresis.

3.13.1 Primers

PCR primer	Sequence (5′–3′)
Frw_AtMutYHpET	TAGGCCTA**CATATG**ATGGCTTGTCTTCTCCGCGT
Rev_AtMutYHpET	TATA**GCGGCCGC**TCACACATCACCGTCACTTTTCTC

DNA oligomers used for cloning.

3.14 *Agrobacterium*-mediated stable transformation of *A. thaliana* cells

3.14.1 Arabidopsis thaliana genotypes

Three genotypes of *Arabidopsis thaliana* were used: wild-type Columbia (Col-8, N60000), Ogg1$^{-/-}$ (N53545) and MutYH$^{-/-}$ (N657044) homozygous mutants (NASC, The European Arabidopsis Stock Centre). The two mutant lines were obtained through T-DNA insertion inside *MutYH* coding sequence or inside *Ogg1* promoter, thus preventing proper transcript expression. Both alleles are knockout.
MutYH , TAIR: AT1G21710, polymorphism SALK_053545.54.75.x
Ogg1, TAIR: AT4G12740.1**,** polymorphism SALK_140362.26.50.n

3.14.2 .Murashige – Skoog (MS) Medium (Murashige and Skoog 1962)

Component	Concentration (mg/l)
NH_4NO_3	1650
$CaCl_2 \cdot 2H_2O$	440
$MgSO_4 \cdot 7H_2O$	370
KH_2PO_4	170
KNO_3	1900
H_3BO_3	6.2
$CoCl_2 \cdot 6H_2O$	0.025
$CuSO_4 \cdot 5H_2O$	0.025
$FeSO_4 \cdot 7H_2O$	27.8
$MnSO_4 \cdot 4H_2O$	22.3
KI	0.83
$Na_2MoO_4 \cdot 2H_2O$	0.25
$ZnSO_4 \cdot 7H_2O$	8.6
Mio-inositolo	100
Niacina	0.5
Piridossina · HCl	0.5
Tiamina · HCl	0.1
$Na_2EDTA \cdot 2H_2O$	37.2
Glicina	2000
Etilendiammina	1000

Agar 8 g/l was also added in the case of semi-solid MS Medium.

3.14.3 Callus Induction Medium (Gamborg et al. 1968)

Component	Concentration
Gamborg's B-5 salts	3051,98 mg/l
Glucose	2% w/v
Agar	0,8% w/v
MES	0,5 g/l
2,4-Dichlorophenoxyacetic acid (2,4-D)	0,5 mg/l
Kinetin	0,05 mg/l

3.14.4 Cell suspension cultures from calli

A. thaliana seeds WT, Ogg1$^{-/-}$ and MutYH$^{-/-}$ were sterilized using bleach (Lindsey et al. 2017) and germinated on plates containing MS Medium without hormones. Leaf pieces were put on plates containing Callus Induction Medium. The dishes were stored at 25°C in the dark until calli formation was observed, usually after 2 or 3 weeks. Calli were then grown on liquid MS medium, gently shaking at 25°C in the dark. For the mutants, kanamycin 50µg/ml (Duchefa Biochemie) was added.

3.14.5 Bacterial strain and plasmid

Agrobacterium tumefaciens EHA105 strain (Lifescience) was used. pGWB5kdPOLL plasmid used to engineer *A.tumefaciens* was previously obtained in our laboratory. The plasmid contains the cassette expressing an artificial microRNA (amiRNA) to silence AtPolλ and the gene for resistance to Hygromycin (Hyg^{R}).

3.14.6 Co-cultivation

Agrobacterium-mediated transformation of *A. thaliana* cell suspension cultures was performed following a protocol obtained from VIB (Flanders, Belgium). *A. thaliana* WT, Ogg1$^{-/-}$ and MutYH$^{-/-}$ cell suspension cultures were diluted 1:5. 2ml of *Agrobacterium* culture was grown in LB (Luria-Bertani) broth at 28°C o/n with shaking and then transferred in 20ml MS medium. The day after, the bacterial culture was washed twice with 40ml of MS (4500g 20', discard supernatant, add 40ml MS, repeat the steps). 660µl of bacterial culture at $(OD)_{600}$ of 1.0 was used to perform each co-

cultivation with 10ml of 2-days old *A. thaliana* cell suspension cultures in presence of 20µl of Acetosyringone 100mM. Three days after, 5ml of MS medium, supplied with appropriate antibiotics, was added to each co-cultivation. Co-cultivations were propagated weekly, for about three months.

3.15 Protein extraction and western blot

Proteins were extracted from co-cultivations or from leaves according to (Tsugama et al. 2011) with the following modification: 0.1% SDS in lysis buffer. Proteins were separated on 10% Bis-Tris poly-acrylamide and used for immunoblotting analysis. Primary anti-human rabbit Pol λ antibody (1:2,000) (Bethyl Laboratories) and HRP-conjugated anti-rabbit secondary antibody (Jackson ImmunoResearch) were used. Detection was performed by using chemiluminescence reagents (Pierce Thermo Scientific). The signal was visualized through Chemidoc Imaging System (Bio-Rad).

3.16 Stable transformation by floral dipping

Stable transformation by floral dipping of *A. thaliana* MutYH$^{-/-}$ plants was performed by Dr. Raynaud Cécile, Institute of Plant Sciences Paris Saclay, Equipe Chromosome Dynamics as described in (Clough and Bent 2008). pGWB5kdPOLL plasmid was used. Seeds were harvested from transformed plants. For each T2 line, 40 seeds were sterilized using bleach (Lindsey et al. 2017) and put on solid MS medium with hygromycin 15µg/ml. Seeds were grown at 25°C in long-day conditions (17hours light, 7hours dark) for three weeks. Only dishes showing the appropriate 3:1 ratio were selected. Seedlings were transferred into jiffy pots and put in growth chamber in short-day conditions (Amoroso et al. 2011).

3.17 DNA extraction from leaves

Healthy leaves (0.035 – 0.045 g) were collected from each plant and grinded using a porcelain mortar and pestle in liquid nitrogen. The homogenates were transferred into microcentrifuge tubes. DNA was extracted modifying the protocol described in (Doyle 1990). 800µl of DNA extraction buffer (1% CTAB, 1.4 M NaCl, 75 mM TrisHCl pH8, 100 mM EDTA) and 2% β-mercaptoethanol were added to the tubes. Afer 30 min at 60°C, 2µl of RNase A Solution (Promega) were added. Tubes were put 30 min at 37°C

and 660µl of P-C-I (Phenol-Chloroform-Isoamyl alcohol) 25:24:1 were added. Tubes were spinned at 15500g for 10 min, supernatant was collected, 0.56Volumes of cold isopropanol were added. Tubes were put at -20°C for 1hour and then spinned at 17000g for 10 min at 4°C. Supernatant was discarded, 100µl of cold ethanol were added to the tubes that were then spinned at 17000g for 10 min at 4°C. Ethanol was removed, DNA was dryed and resuspended in 100 µl of RNAse-free water.

3.17.1 PCR

PCR amplification of DNA extracted from leaves was carried out using the following conditions: 1X Green GoTaq® Flexi Buffer, 1.25U GoTaq® Flexi G2 DNA Polymerase (Promega), 2.5mM $MgCl_2$, 3% DMSO, 200µM dNTPs, 0.5µM primers, 100ng DNA. The PCR reaction was performed in a thermal cycler (Mastercycler epGradient 5341, Eppendorf) using an initial 94 °C denaturing step for 2 min followed by 30 cycles at 94 °C for 1 min, annealing for 1 min at the primer's annealing temperature, extension at 72 °C for 5 min 15 s and a final extension at 72 °C for 5 min.

3.17.2 Primers

PCR primer	Sequence (5'- 3')
LBb1.3	ATTTTGCCGATTTCGGAAC
LPMUT	ACCAGGCAGTACCTGTTGTTG
RPMUT	CACCAAATTTGATTCCCAATG
LPOGG	TTAGGGCTTGTGCTACAATGG
RPOGG	ACGTCATCCATTTCTTCGTTG
Frw_AtpPolL	TAAGGGATGACGCACAAT
Rev_AtpPolL	ACAAGAAAGCTGGGTCATG

3.18 UV-B irradiation

Healthy leaves were sterilized using bleach (Lindsey et al. 2017), cut and put on plates containing MS Medium including 0.5 mg/L naphthaleneacetic acid, 0.05 mg/L kinetin, 3% (w/v) sucrose, pH adjusted to 5.8 using 1 N KOH (*MS Medium + NAA*)(May and Leaver 1993) and MS Medium including vitamins 3% sucrose, 0.5 µg/ml 2,4-dichlorophenoxyacetic acid (2,4-d), 0.25 µg/ml 6-benzylaminopurine (BAP), 0.8% plant agar, pH 5.5(Sello et al. 2017) (*MS Medium + BAP*). The dishes were stored at 25°C

in the dark overnight and then UV-B irradiated for 27 minutes at 216nm. After the irradiation, plates were stored again at 25°C in the dark for about one month.

4. Results

4.1 Metal-dependent rNMPs incorporation by Pol β and λ

All Pols require for their catalytic activity a divalent metal cation, Mg^{++} or Mn^{++}, whose identity can deeply influence both Pols fidelity and activity. (Steitz 1999). Two metal ions are generally coordinated by acidic amino acids in the active site of the polymerase, facilitating the contact between the enzyme and the terminal phosphoryl group of the substrate, thus acting as activator cofactor (Frank and Woodgate 2007). The levels of Mg^{++} and Mn^{++} are finely regulated in the cells and their physiological range of concentrations is quite different depending on the cell type and cell cycle phase. Intracellular concentrations of Mg^{++} range from 1 to 20 mM (Romani 2007) while Mn^{++} is usually found between 0.01 and 0.2 mM (Aschner and Aschner 2005; Roth 2006). Different studies have demonstrated that Pols β (Cavanaugh et al. 2010) and λ (Gosavi et al. 2012) can incorporate rNMPs *in vitro*. However, in many experiments only one cation was used as metal activatort and at a fixed concentration. Therefore, to compare the influence of Mg^{++} and Mn^{++} on the ability of Pols β and λ to incorporate rNMPs, DNA polymerization assays were performed on a 20/40mer primer/template (p/t) oligonucleotide, in the presence of different concentrations of the two metal activators, with values remaining in their physiological ranges. Similarly, dNTPs and rNTPs concentrations were non-equimolar and chosen according to previously published cellular concentrations (Traut 1994; Ferraro et al. 2010). Pols β and λ show different optimal Mg^{++} and Mn^{++} conditions for incorporation of rNMPs on undamaged DNA. As shown in Fig. 14 A andB, Pols β and λ were able to incorporate rNMPs at physiological (1–5mM) Mg^{++} concentrations, while significant rNMPs incorporation in the presence of Mn^{++} occurred only at 0.5–1 mM concentrations, higher than those normally measured in the cell. Therefore, it seems that the main physiological activator for rNMPs incorporation by Pols β and λ is Mg^{++}, even if it is possible to find higher Mn^{++} concentration in certain cell types. Therefore, we decided to perform subsequent experiments using Mg^{++}.

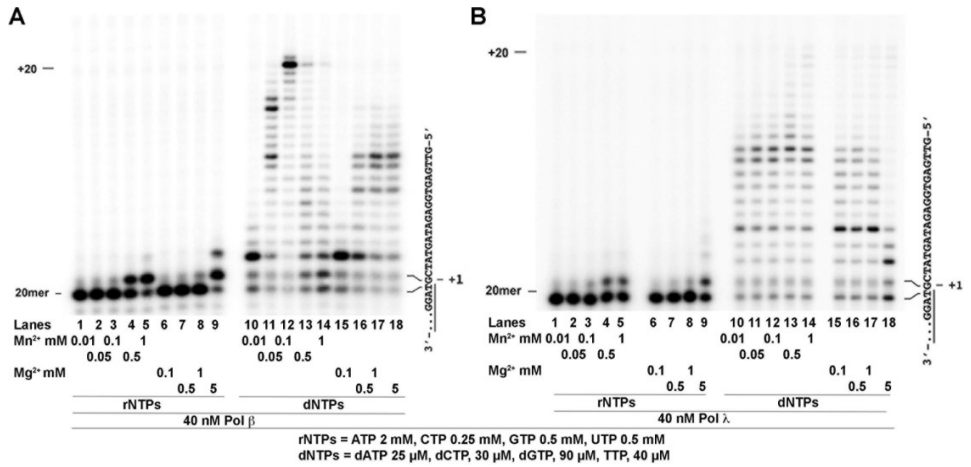

Fig. 14: Nucleotide incorporation by Pols β and λ under different Mg^{++} and Mn^{++}conditions. Pol β (**A**) and λ (**B**) activity was assayed in the presence of a 5'-labelled 20/40mer p/t oligonucleotide, at increasing Mg^{++} or Mn^{++}concentrations and with all four rNMPs or dNMPs at fixed concentrations in their physiological range. The sequence of the template strand of the 5'- labelled 20G/40mer p/t is shown on the right side of each panel. The rNMPs and dNMPs concentrations used are indicated at the bottom of each panel.

The fidelity of rNMPs incorporation was investigated for all the sixteen possible base pairs in the presence of Mg^{++}. Primer/template substrates used are reported in Fig 15. Commercial rNTPs stocks often contain small (<1%) amounts of contaminating dNTPs, that could be incorporated by Pols. However, the products resulting from rNMPs incorporation could be distinguished since they migrate slower on the sequencing gels compared to products arising from dNMPs incorporation. As shown in Fig. 15A, Pol λ was able to insert the correct rNMP opposite to the complementary template base (lanes 5, 9, 19, 25). Pol λ is quite faithful in inserting rNMPs. The rGMP incorporation with the 20merG/40mer primer template leading to a +2 product observed in lane 17, is likely the result of incorporation of dCMP (contaminating the rGMP preparation), followed by incorporation of rGMP opposite the C at template position +2. On the other hand, Pol β was able to incorporate rCMP opposite G and, to a lower extent, rGMP opposite C (Fig 15B lanes 19 and 27), while rUMP and rAMP incorporation opposite their complementary bases was minimal (lanes 7 and 11). The product detected in lane 5 (rCMP) with the 18merA/40mer p/t runs with the same mobility of the dTMP control (lane 3), hence it is likely due to misincorporation of contaminating dTMP present in the rCMP preparation.

Overall, these data revealed that Pols β and λ incorporate rNMPs opposite undamaged bases with different efficiency and fidelity.

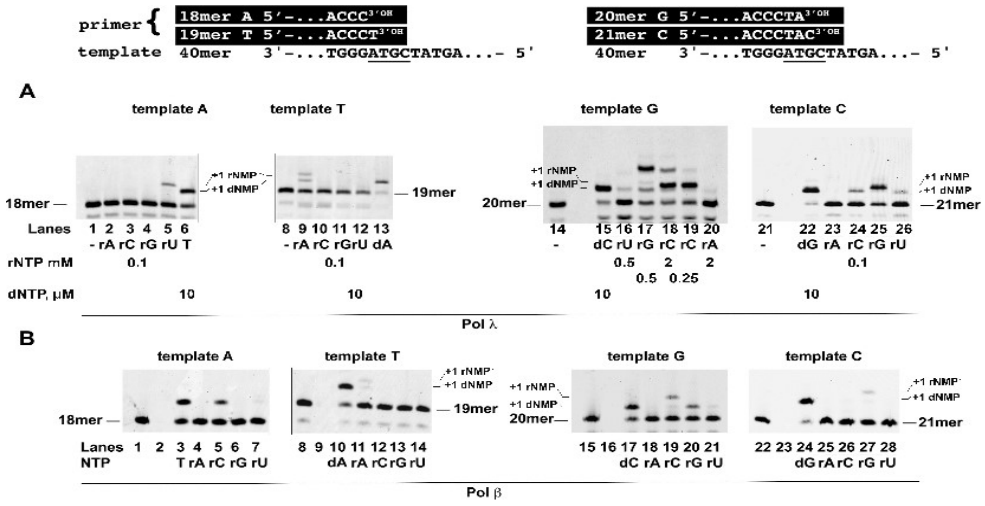

Fig. 15: A. Pol λ (20 nM) was incubated in the presence of 10 nM of the 5'-labelled 18A/40mer p/t (lanes 1-6), 19T/40mer p/t (lanes 8-13), 20G/40mer p/t (lanes 14-20), 21C/40mer p/t (lanes 21-26), in the presence of different combinations of rNMPs and dNMPs, as indicated. Lanes 1, 8, 14, 21, control reactions in the absence of nucleotides. **B**. As in panel A, but in the presence of 50 nM Pol β and 100 nM templates. Lanes 1, 8, 15, 22, control reactions in the absence of nucleotides. Solid lines indicate different parts of the same gel.

4.2 rNMPs incorporation opposite 8-oxo-G by Pol λ

Repair Pols could potentially incorporate rNMPs also opposite damaged DNA bases. Among the various DNA damages, we chose 8-oxo-G as relevant example. 8-oxo-G is a common oxidized base that can be correctly bypassed by Pol λ using dCTP (Maga et al. 2007). To test if Pol λ is able to bypass 8-oxo-G lesion inserting a rNMP, DNA polymerases assays were performed in the presence of eacha rNTPs on a 39/100mer p/t or using a single nucleotide (1 nt)-gap template, which resembles a BER intermediate. Both substrates beared at the +1 position either 8-oxo-G or G. On both substrates, Pol λ significantly incorporated only rCMP opposite a normal G (Fig. 16A, lane 4; Fig. 16C, lane 10), while it incorporated both rCMP and rAMP opposite an 8-oxo-G (Fig. 16B,C, lanes 5 and 6). On both substrates, low level of rGTP incorporation can be observed opposite a normal G or 8-

oxo-G (Fig. 16A, lane 2; Fig. 16B, lane 3; Fig. 16C, lanes 3 and 8). However, as indicated by the faster electrophoretic mobility of the resulting +1 product, such events were due to contaminating dNTPs in the commercial rGTP stock. Only minimal rGMP incorporation was observed opposite 8-oxo-G on the 1 nt-gap template (Fig. 16C, lane 3).

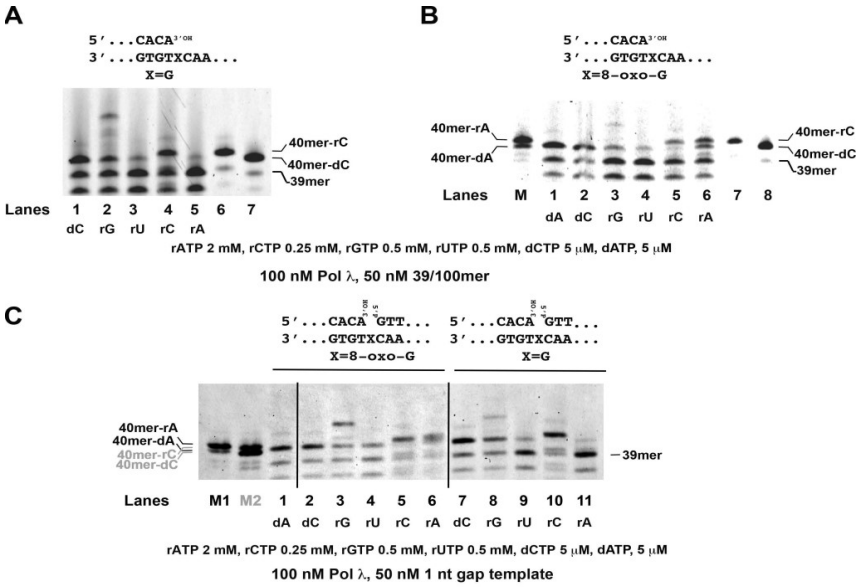

Fig. 16: Enzyme, substrate and nucleotide concentrations are indicated at the bottom of each panel. Solid lines indicate that different portions of the same gel were brought next to each other for better clarity. **A** Pol λ activity was measured on the undamaged 5'-labelled 39/100mer p/t, in the presence of each of the four rNTPs. Lane 6, 40mer rCMP-terminated oligonucleotide marker. Lane 7, dCMP-terminated 40mer oligonucleotide marker. **B**. As in panel A, but in the presence of the 5'-labelled 39/100mer p/t containing 8-oxo-G. Lane M, a mixture of 5'-labelled 40mer oligonucleotides bearing either dCMP or rCMP as the terminal nucleotide, as markers. **C**. Pol λ activity was tested in the presence of the 5'-labelled 39/60/100mer 1-nt gap template either bearing 8-oxo-G (lanes 1 – 6) or undamaged (lanes 7 – 11), in the presence of each of the four rNTPs. Lane M1, a mixture of 5'-labelled 40mer oligonucleotides bearing either dAMP or rAMP as the terminal nucleotide, as markers. Lane M2, a mixture of 5'-labelled 40mer oligonucleotides bearing either dCMP or rCMP as the terminal nucleotide, as markers.

Incorporation was monitored as a function of dCTP, rCTP, dATP or rATP concentrations (Fig.17) on both substrates. Kinetic parameters of the reactions and sugar selectivity are reported in Table 1. According to previously published data (Brown and Suo 2011), Pol λ showed a 7,500-

fold selectivity for dCMP over rCMP when the template base was a G in a 1-nt gap template. However, this selectivity increased to 14,000-fold when incorporation occured opposite an 8-oxo-G. On this template Pol λ also strongly preferred to misincorporate dAMP rather than rAMP, with a selectivity toward dATP of 17,840-fold. Interestingly, Pol λ maintains a relative fidelity also in the case of rNMPs insertion since it clearly incorporates rCMP better than rAMP opposite 8-oxo-G, at a similar rate observed in the case of dCMP over dAMP insertion (5,5 fold and 4,5 fold respectively). Using p/t substrates, the preference of incorporation of dCMP with respect to rCMP opposite G was of 5,140 fold. When the template contained 8-oxo-G lesion this preference increased to 9,500 fold. In the case of p/t substrates containing 8-oxo-G lesion, Pol λ shows a decreased fidelity and selectivity with respect to 1-nt gap substrates bearing the lesion. In fact, it showed 3,000 fold preference for dAMP incorporation vs rAMP and a preference for rCMP over rAMP of only 0.9, suggesting that both rNTPs may be used in a similar way to bypass 8-oxo-G on this type of template.
Taken together, these data clearly indicated that fidelity and sugar selectivity of Pol λ during 8-oxo-G bypass in the presence of rNMPs is influenced by the structure of the DNA substrate. On its preferred 1-nt gap BER-mimicking template containing an 8-oxo-G, Pol λ increases its preference for dCMP incorporation relative to rCMP incorporation. Since Pol λ acts in the specialized MutYH-dependent BER of A:8-oxo-G mismatches (Maga et al. 2007; van Loon and Hubscher 2009), our results suggest that Pol λ not only incorporates the correct dCMP over the incorrect dAMP (Maga et al. 2007) but that it also minimizes the chances of incorporating rNMPs opposite this lesion.

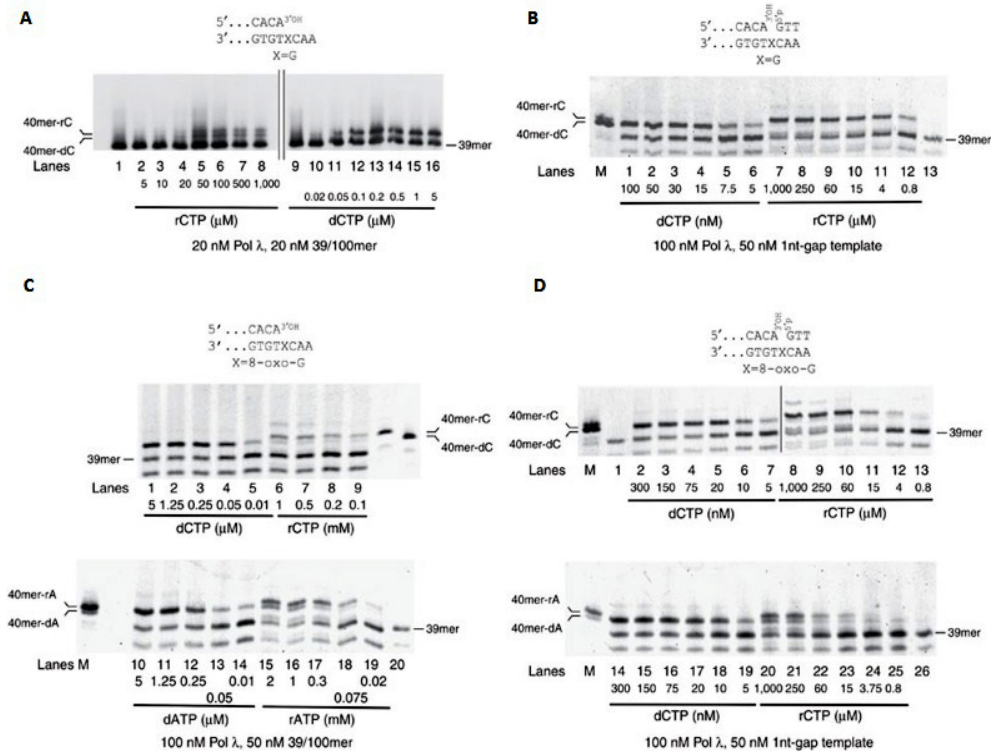

Fig. 17. The fidelity of 8-oxo-G bypass by DNA polymerase λ in the presence of rNTPs is influenced by the structure of the DNA template. (**A**) Pol λ activity was measured on the undamaged 5'-labelled 39/100mer p/t, in the presence of increasing concentrations of rCTP or dCTP. Lane 1, control reaction in the absence of nucleotides. (**B**) As in A, but in the presence of the undamaged 5'-labelled 39/60/100mer 1 nt-gap template. M, a mixture of 5'-labelled 40mer oligonucleotides bearing either dCMP or rCMP as the terminal nucleotide, as markers. Lane 13, control reaction in the absence of nucleotides. (**C**) Pol λ activity was measured on the 50-labelled 39/100mer p/t containing 8-oxo-G, in the presence of different concentrations of dCTP and rCTP (top panel), or dATP and rATP (bottom panel). 5'-Labelled 40mer oligonucleotides bearing either dCMP, rCMP, dAMP or rAMP as the terminal nucleotide, were used as markers. Lane 20, control reaction without nucleotides. (**D**) As in C, but in the presence of the 5'-labelled 39/60/100mer 1 nt-gap 8-oxo-G template. Lane M, 5'-labelled 40mer oligonucleotides bearing either dCMP, rCMP, dAMP or rAMP as the terminal nucleotide, were used as markers.

	K_m[a], µM	k_{cat}[a] (min^{-1})	k_{cat}/K_m[a] (M^{-1} s^{-1})	f_{inc}[b] dNTP/rNTP	f_{inc} rNTP/dNTP	f_{inc} C vs A
1nt gap control						
Pol λ						
rCTP	83±4	0.024±0.003	4.8		1.3×10^{-4}	n.a.
dCTP	0.018±0.004	0.039±0.002	3.6×10^{4}	7,500		n.a.
1nt gap 8-oxo-G						
Pol λ						
rCTP	50±10	0.06±0.003	20		7.1×10^{-5}	5.5
rATP	185±20	0.04±0.01	3.6		5.8×10^{-5}	
dCTP	0.007±0.001	0.12±0.01	28×10^{4}	14,000		4.5
dATP	0.015±0.001	0.056±0.01	6.2×10^{4}	17,840		
39/100mer control						
Pol λ						
rCTP	38±0.5	0.008±0.0003	3.5		1.9×10^{-4}	n.a.
dCTP	0.03±0.005	0.032±0.007	18×10^{3}	5,140		n.a.
39/100mer 8-oxo-G						
Pol λ						
rCTP	155±18	0.02±0.004	2.1		1×10^{-4}	0.9
dCTP	0.05±0.004	0.08±0.008	20×10^{3}	9,500		4
rATP	200±5	0.027±0.009	2.2		3.3×10^{-4}	
dATP	0.15±0.004	0.06±0.01	6.6×10^{3}	3,000		

Table 1: **Kinetic parameters for rNTPs incorporation by DNA polymerase λ** . The meaning of the kinetic parameters K_m, k_{cat} and k_{cat}/K_m and their calculations are described in Materials and Methods. Values are the means of two independent estimates ± S.D. b. f_{inc}, relative incorporation frequencies for the different nucleotide pairs, defined as the ratio of the respective k_{cat}/K_m values.

4.3 Fidelity of rNMPs incorporation opposite 8-oxo-G by Pol β

Previous experiments demonstrated that Pol β can bypass 8-oxo-G lesion in a less accurate way than Pol λ, often misincorporating dAMP opposite it (Maga et al. 2007). As shown in Fig. 18, with the 1-nt gap BER-mimicking template, Pol β incorporated both rCMP and rAMP opposite 8-oxo-G (lanes 1 and 2), while only rCMP was inserted opposite a normal G (lane 9). As already noticed above, with rUTP and rGTP, only incorporation of contaminating dNTPs was detected.

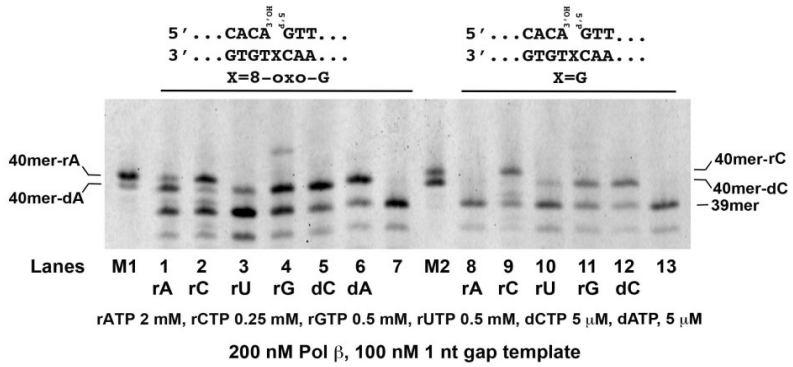

Fig. 18: Pol β activity was tested in the presence of the 5'-labelled 39/60/100mer 1nt-gap template either bearing 8-oxo-G (lanes 1 – 6) or undamaged (lanes 7 – 11), in the presence of each of the four rNTPs. Enzyme, substrate and nucleotide concentrations are indicated at the bottom of the panel. Lane M1, a mixture of 5'-labelled 40mer oligonucleotides bearing either dAMP or rAMP as the terminal nucleotide, as markers. Lane M2, a mixture of 5'-labelled 40mer oligonucleotides bearing either dCMP or rCMP as the terminal nucleotide, as markers. Lanes 7 and 13 control reactions in the absence of nucleotides.

Substrate titrations with increasing concentrations of dCTP, rCTP, dATP or rATP were performed on both the 39/100 mer p/t and the 1 nt-gap templates (Fig. 19). The results of the kinetic analysis (Table 2) showed that on the 1-nt gap BER-mimicking template containing the normal G base, Pol β had a sugar selectivity of 3,400 for incorporation of dCMP vs rCMP, in line with previously published data (Brown and Suo 2011; Cavanaugh et al. 2010). On 1-nt gap substrate bearing 8-oxo-G the value remains very similar (3,200), a different behaviour with respect to Pol λ , which increased its selectivity for dCMP insertion in the presence of the lesion. Interestingly, on the same template containing 8-oxo-G, Pol β showed strong discrimination against rAMP incorporation, with selectivity value of 25,600. Incorporation of rCMP opposite 8-oxo-G lesion is 13.4-fold more than rAMP, while the preference of Pol β for dCMP vs dAMP is only of 1.65-fold. On the 39/100 mer p/t containing the undamaged G, the selectivity value for dCMP vs rCMP incorporation was 1,690 while on the same substrate bearing the 8-oxo-G the value was 4,250. On the latter template however, the selectivity for dAMP versus rAMP incorporation opposite the lesion was 1,750. The fidelity was similar, with 2.6-fold and of 2.9-fold respectively for rCTP vs rATP and for dCTP vs dATP usage. These data suggested that Pol β was sensitive to the structure of the DNA template, similarly to Pol λ. In particular, while Pol β showed lower sugar selectivity for rCMP versus

dCMP incorporation than Pol λ on the 1-nt gap BER-mimicking template, its bypass fidelity with rNTPs was higher, since it it shows a relevant preference for rCMP vs rAMP utilization opposite 8-oxo-G lesion.

	K_m[a], μM	k_{cat}[a] (min^{-1})	k_{cat}/K_m[a] (M^{-1} s^{-1})	f_{inc}[b] dNTP/rNTP	f_{inc} rNTP/dNTP	f_{inc} CvsA
1nt gap control						
Pol β						
rCTP	47±3	0.034±0.002	12		2.9×10^{-4}	n.a
dCTP	0.03±0.004	0.074±0.002	4.1×10^{4}	3,400		n.a
1nt gap 8-oxo-G						
Pol β						
rCTP	29±1	0.018±0.002	10.3		3.1×10^{-4}	13.4
dCTP	0.01±0.01	0.02±0.001	3.3×10^{4}	3,200		1.65
rATP	367±30	0.017±0.003	0.77		3.9×10^{-5}	
dATP	0.017±0.002	0.021±0.002	2×10^{4}	25,600		
39/100mer control						
Pol β						
rCTP	64±7	0.015±0.003	3.9		6×10^{-4}	
dCTP	0.05±0.01	0.02±0.002	6.6×10^{3}	1,690		
39/100mer 8-oxo-G						
Pol β						
rCTP	73±13	0.007±0.002	1.6		2.3×10^{-4}	2.6
dCTP	0.04±0.01	0.018±0.002	6.8×10^{3}	4,250		2.9
rATP	150±15	0.007±0.003	0.8		5.7×10^{-4}	
dATP	0.25±0.02	0.021±0.003	1.4×10^{3}	1,750		

Table 2: Kinetic parameters for rNTPs incorporation by DNA polymerase β. The meaning of the kinetic parameters K_m, k_{cat} and k_{cat}/K_m and their calculations are described in the Experimental Procedures section. Values are the means of two independent estimates ± S.D. b. f_{inc}, relative incorporation frequencies for the different nucleotide pairs, defined as the ratio of the respective k_{cat}/K_m values

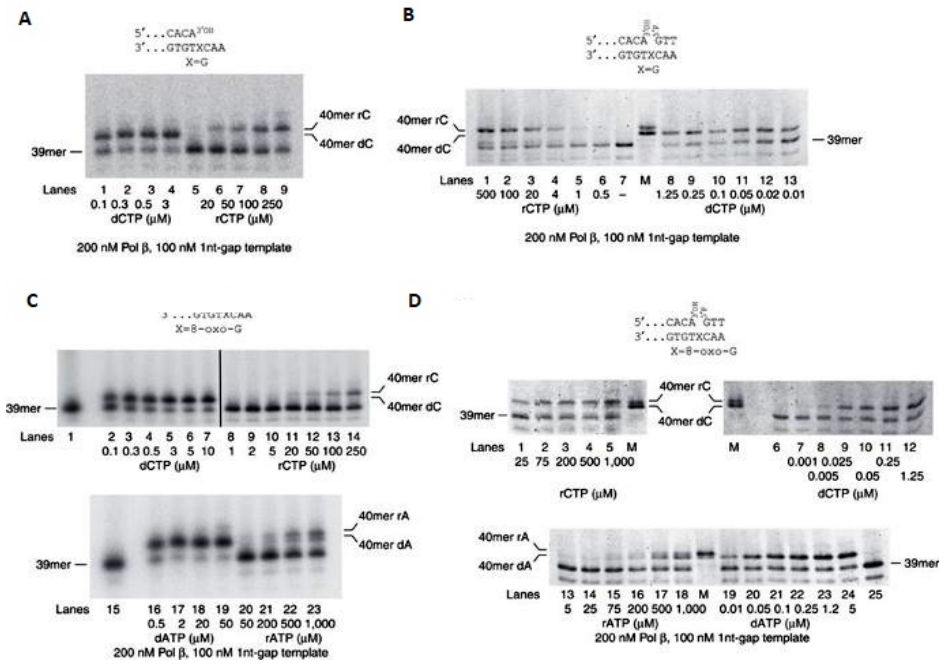

Fig. 19: DNA polymerase β bypasses 8-oxo-G more faithfully in the presences of rNTPs than dNTPs. (**A**) Pol β activity was measured on the undamaged 5'-labelled 39/100mer p/t, in the presence of increasing concentrations of rCMP or dCMP. (**B**) As in A, but in the presence of the undamaged 5'-labelled 39/60/100mer 1 nt-gap template. M, a mixture of 5'-labelled 40mer oligonucleotides bearing either dCMP or rCMP as the terminal nucleotide, as markers. Lane 7, control reaction in the absence of nucleotides. (**C**) Pol β activity was measured on the 5'-labelled 39/100mer p/t containing 8-oxo-G, in the presence of different concentrations of dCMP and rCMP (top panel), or dAMP and rAMP (bottom panel). 50-Labelled 40mer oligonucleotides bearing either dCMP, rCMP, dAMP or rAMP as the terminal nucleotide, were used as markers. Lanes 1 and 15, control reactions without nucleotides. (**D**) As in C, but in the presence of the 5'-labelled 39/60/100mer 1 nt-gap 8-oxo-G template. Lanes M, 5'-labelled 40mer oligonucleotides bearing either dCMP, rCMP, dAMP or rAMP as the terminal nucleotide, were used as markers. Lane 25, control reaction in the absence of nucleotides.

To directly visualize simultaneous incorporation of rCMP or dCMP opposite 8-oxo-G, competition experiments were performed on the 1 nt-gap template (Fig. 20). As in the other gels,the products coming from the incorporation of either rCMP or dCMP could be distinguished, as they differ in electrophoretic mobility. By titrating increasing amounts of one nucleotide (either dCTP or rCTP), in the presence of a fixed amount of the other competing nucleotide, both Pol λ (lanes 1–11) and Pol β (lanes 12–16)

showed a dose-dependent increase in the band corresponding to the nucleotide titrated into the reaction, while the band corresponding to the incorporation of the nucleotide at a fixed concentration, decreased. These experiments confirmed that rCTP and dCTP compete as substrates for incorporation opposite 8-oxo-G by both Pols.

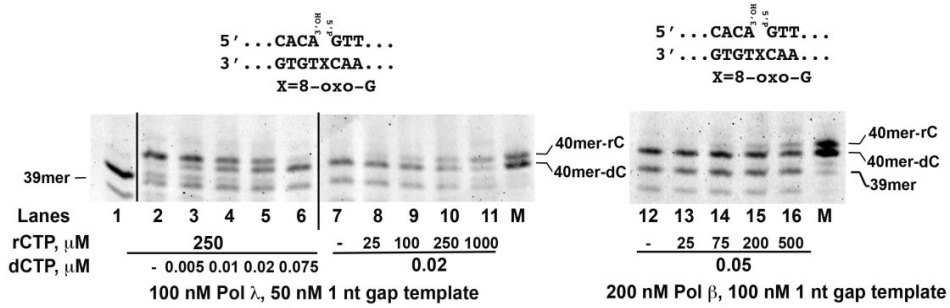

Fig. 20: Pol λ (lanes 2 – 11) or Pol β (lanes 12 – 16) activity was tested in the presence of fixed concentrations of rCTP (lanes 2 – 6) or dCTP (lanes (7 – 16), alone (lanes 2, 7, 12) or in combination with increasing concentrations of rCTP (lanes 8 -11, 13 – 16) or dCTP (lanes 3 – 6). Lanes M, a mixture of 5'-labelled 40mer oligonucleotides bearing either dCMP or rCMP as the terminal nucleotide, as markers. Lane 1, 39mer primer alone.

4.4 rNMPs opposite 8-oxo-G impair repair by hOgg1 and MutYH

The BER glycosylase Ogg1 is responsible for the removal of 8-oxo-G paired to dC in double-stranded (ds) DNA (van Loon et al. 2010). From our data clearly emerged that rCMP could be incorporated opposite 8-oxo-G by the specialized repair Pols β and λ. Therefore, to investigate whether this fundamental glycosylase reaction was affected by the pairing of a rC base to an 8-oxo-G, a glycosylase assay was performed, with hOgg1 and a ds DNA oligonucleotide bearing either a dC:8-oxo-G or a rC:8- oxo-G base pair. Interestingly, hOgg1 was able to remove the 8-oxo-G incorporated opposite rCMP, even if at a 4-folds slower rate (Fig. 21A; Fig. 22A). Besides rC:8-oxo-G pair, both Pols β and λ may also generate rA:8-oxo-G mispairs (Figs 17 and 19). The removal of dA erroneously paired with 8-oxo- G is mainly accomplished by the BER glycosylase MutYH (van Loon and Hübscher 2009). To address wether MutYH is also able to act on rA:8-oxo-G mispair, a glycosylase assay was performed using ds DNA oligonucleotide substrate bearing either a dA:8-oxo-G or a rA:8-oxo-G mismatch. MutYH very efficiently removed dA opposite 8-oxo-G, on the contrary its activity on a

rA:8-oxo-G mismatch was severely impaired (Fig. 21B; Fig. 22B). Taken together, these results suggest that incorporation of rNMPs opposite 8-oxo-G may impair repair of the damaged base by the BER pathway, potentially posing a threat to genomic stability.

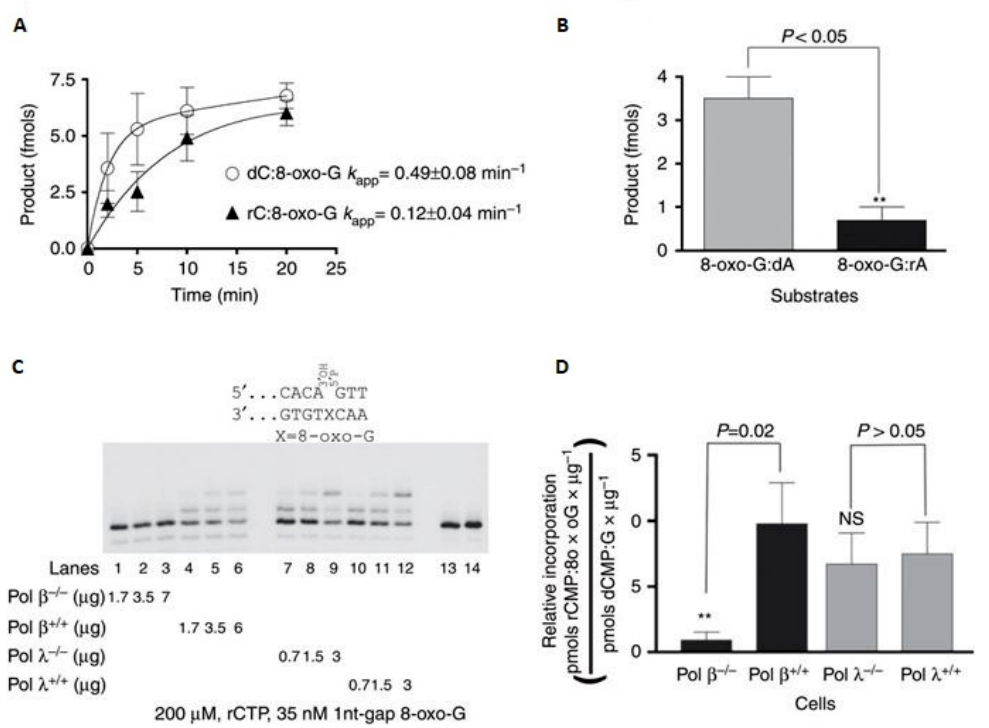

Fig. 21: Incorporation of rNMPs opposite 8-oxo-G inhibits DNA repair and is reduced in the absence of DNA polymerase β. (**A**) Time course of the excision products accumulation generated by hOgg1 in the presence of a 8-oxo-G:dC (empty circles) or 8 oxo-G:rC (filled triangles) base pairs. The k_{app} values refer to the apparent rates for the exponential phase. Values are the mean of three independent replicates, error bars represent ±s.d. A representative experiment is shown in Fig. 22A. (**B**) Quantification of the excision products generated by MutYH in the presence of a 8-oxo- G:dA (grey bars) or 8-oxo-G:rA (black bars) mismatch. Values are the mean of three independent replicates as the one presented in Fig. 22B, error bars represent ±s.d. The P values were calculated by two-tailed Student's t-test. (**C**) Increasing amounts of the different cell extracts were titrated in the presence of the 1 nt-gap template bearing an 8-oxo-G and 200 mM rCTP. Lanes 13 and 14, control reactions in the absence of extracts. (**D**) The rCMP incorporation activity (expressed as pmols of rCTP incorporated opposite 8-oxo-G per μg of proteins of each extract) was normalized to the total DNA polymerase activity (expressed as pmols of dCMP incorporated opposite undamaged dG per μg of proteins of each extract). Values are the mean of three independent replicates like the one shown in c, error bars represent ±s.d. The

P values were calculated by two-tailed Student's t-test.

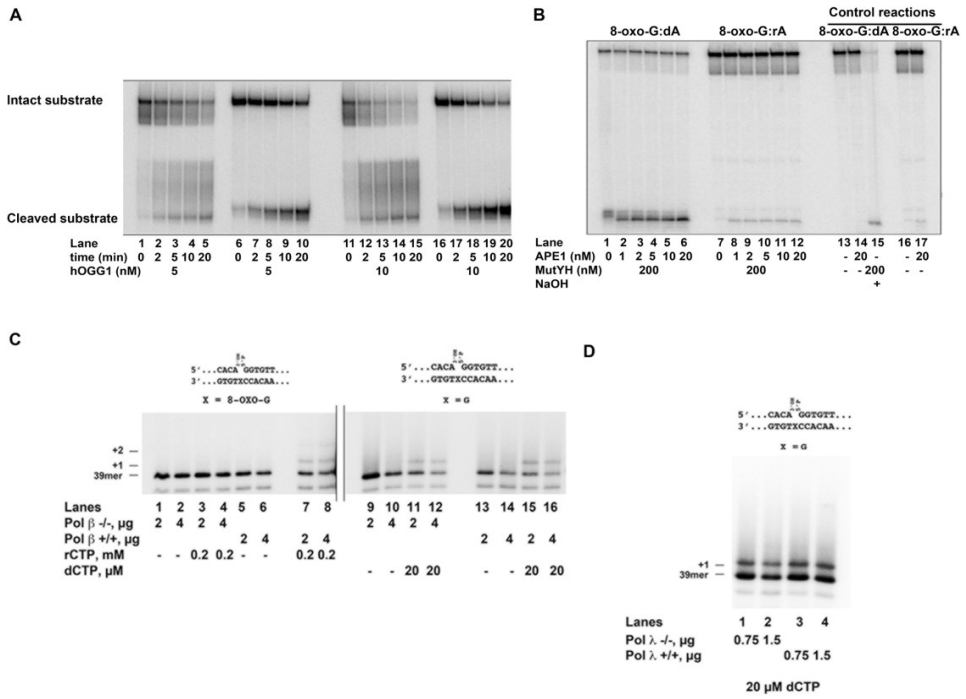

Fig. 22: (**A**) Time course of the reaction catalyzed by hOgg1 at 5nM (lanes 1- 10) or 10nM (lanes 11-20) on the ds100mer substrate containing a 8-oxo-G:dC (lanes 1 – 5; 11 – 15) or a 8-oxo-G:rC (lanes 6 – 10; 16 - -20) mispair. (**B**) Titration of APE1 in the presence of MutYH on the ds100mer substrate containing a 8-oxo-G:dA (lanes 1 – 6) or a 8-oxo-G:rA (lanes 7 – 12) mispair. Lanes 13 – 17, various control reactions for the 8-oxo-G:dA (lanes 13 – 15) or a 8-oxo-G:rA (lanes 16 – 17) templates. The conditions are specified at the bottom of each lane. (**C**) Increasing amounts of extracts from Polβ$^{-/-}$ (lanes 1 – 4; 9 – 12) or Polβ$^{+/+}$ (lanes 2 – 8; 13 – 16) cells, were titrated with the 1-nt gap template containing an 8-oxo-G (lanes 1 – 8) or undamages (lanes 9 – 16), in the absence (lanes 1, 2, 5, 6, 9, 10, 13, 14) or in the presence of rCTP (lanes 3, 4, 7, 8) or dCTP (lanes 11, 12, 15, 16). Solid lanes indicate that lanes 1 – 8 and 9 – 16 represent different portions of the same gel. (**D**) Increasing amounts of extracts from Polλ$^{-/-}$ (lanes 1, 2) or Polλ$^{+/+}$ (3, 4) cells were titrated with the undamaged 1-nt gap template in the presence of dCTP.

4.5 rCMP incorporation opposite 8-oxo-G in cell extracts

Our results indicated that both Pols β and λ bypass an 8-oxo-G lesion utilizing rCTP as a substrate, thus generating a rC:8-oxo-G base pair, on which hOgg1 acted less efficiently. To better understand to which extent

Pols β and λ contribute to this potentially harmful event, the incorporation opposite 8-oxo-G on a BER mimicking 1 nt-gap template was measured in extracts from mouse embryonic fibroblasts (MEFs) either proficient or deficient for Pol β or λ. Many other specialized Pols present in the cell, such as Pols μ, ν, η, ι, θ or κ, can efficiently fill 1-nt gaps. As Pols β and λ, they are all resistant to the inhibitor aphidicolin. On the contrary, replicative Pols α, δ and ε are sensitive to this inhibitor. The specialized Pol ζ is also aphidicolin sensitive, but its contribution to rNMPs incorporation in the cell was proposed to be minimal (Makarova et al. 2014). Therefore, aphidicolin was added to the reactions, thus blocking the incorporation by family B Pols α, δ, ε and ζ. The specific incorporation frequency (expressed as pmols of rCMP incorporated opposite 8-oxo-G per μg of proteins of the extract) was calculated in each extract and normalized to the normal DNA synthesis (pmols of dCMP opposite guanine per μg of proteins of the extract). As shown in Fig. 21C on the 1-nt gap on BER-mimicking template, Pol $\beta^{-/-}$ MEFs displayed severely reduced rCMP incorporation opposite 8-oxo-G, with respect to Pol $\beta^{+/+}$, as well as to Pol $\lambda^{+/+}$and Pol $\lambda^{-/-}$ MEFs (compare lanes 1–3 with 4–12). In contrast, incorporation of dCMP opposite normal G was almost equal between Pol $\beta^{-/-}$ and Pol $\beta^{+/+}$ MEFs (Fig. 22C, compare lanes 11 and 12 with lanes 15 and 16) and comparable with Pol λ extracts (Fig. 22C,D). Overall these results suggest that, among the aphidicolin-resistant Pols, Pol β seems to be the main responsible for the incorporation of rCMP opposite 8-oxo-G in the extracts. On the other hand, no statistically significant differences were found between Pol λ proficient and deficient cells (Fig. 21D).

These results are part of a paper published on Nature Communications. in 2016. The original paper is attached.

4.6 Incorporation of ribonucleotides by human Pol η

Human Pol η was incubated in the presence of a mixture of the four rNTPs or dNTPs, each present at its average intracellular concentration. Incorporation was measured as a function of increasing concentrations of Mg^{2+} or Mn^{2+} cofactors. As shown in Fig. 23A, Pol η incorporated multiple rNMPs in the presence of physiological concentration (5 mM) of Mg^{2+} (Fig. 23A, lane 9), but also at Mn^{2+} concentrations as low as 0.1 mM, even displaying more robust activity than with Mg^{2+}, at relatively high Mn^{2+} concentrations (0.5 - 1 mM) (Fig. 23A, lanes 4, 5). The 5 mM Mg^{2+} concentration was then used for all subsequent experiments. Pol η showed remarkable fidelity, being able to significantly incorporate rCMP only opposite an undamaged guanine (Fig. 23B). When dCTP or rCTP were titrated into the reaction, robust incorporation of both nucleotides was observed opposite the template G, along with some misincorporation events leading to a +2 product (Fig. 23C, lanes 4 – 7 and 12 – 15). The kinetic parameters for rCMP vs. dCMP incorporation opposite a normal G are summarized in Table 3. On this template, the discrimination factor for deoxy- vs. ribonucleotide incorporation by Pol η was 400. Since the products arising from rCMP incorporation had a different electrophoretic mobility with respect to those due to dCMP incorporation, it was possible to simultaneously visualize both incorporation events in the same reaction. Indeed, titrating rCTP in the reaction, in the presence of fixed amounts of dCTP, led to the accumulation of the +1 rCMP product with concomitant reduction of the +1 dCMP product (Fig. 23D, lanes 3 – 8). The same pattern was observed in the reciprocal experiment, i.e. titrating dCTP while keeping rCTP fixed (Fig. 23D, lanes 9 – 13). These results confirmed that dCTP and rCTP can compete for incorporation opposite G. Comparable amounts of either products were observed at a rCTP/dCTP (M/M) ratio between 500 (Fig. 23D, lane 8) and 300 (Fig. 23D, lane 11), in agreement with the selectivity value derived from the kinetic analysis.

4.7 Pol η can synthesize hybrid DNA/RNA chains

Next, different combinations of the four deoxy- or riboncleotides were tested, according to the template sequence. As shown in Fig. 23E, after rCMP incorporation at position +1, Pol η was able to efficiently elongate by incorporating either deoxy- (Fig. 23E, lane 3) or ribo-GMP (lane 5) opposite

C at position +2. Similarly, efficient elongation was observed starting from a dCMP-terminated primer, with either deoxy- or ribo-GMP (Fig. 23E, lanes 4 and 6). Long products were synthesized by Pol η when provided with all four rNTPs at equimolar (Fig. 23E, lane 7) or physiological (lane 10) concentration ratios. Comparable products were observed when rCTP was provided in combination with the three remaining dNTPs (Fig. 23E, lane 8). These products, however, were shorter than those synthesized in the presence of dNTPs only (Fig. 23E, lanes 9 and 11). Overall, these results indicated that Pol η can efficiently elongate rNMP-terminated primers, synthesizing both RNA and RNA/DNA polynucleotide chains. Physiologically, this RNA-synthetic activity may potentially be a threat for the replicative Pols δ and ε, that cannot bypass more than few consecutive rNMPs (Clausen et al. 2013).

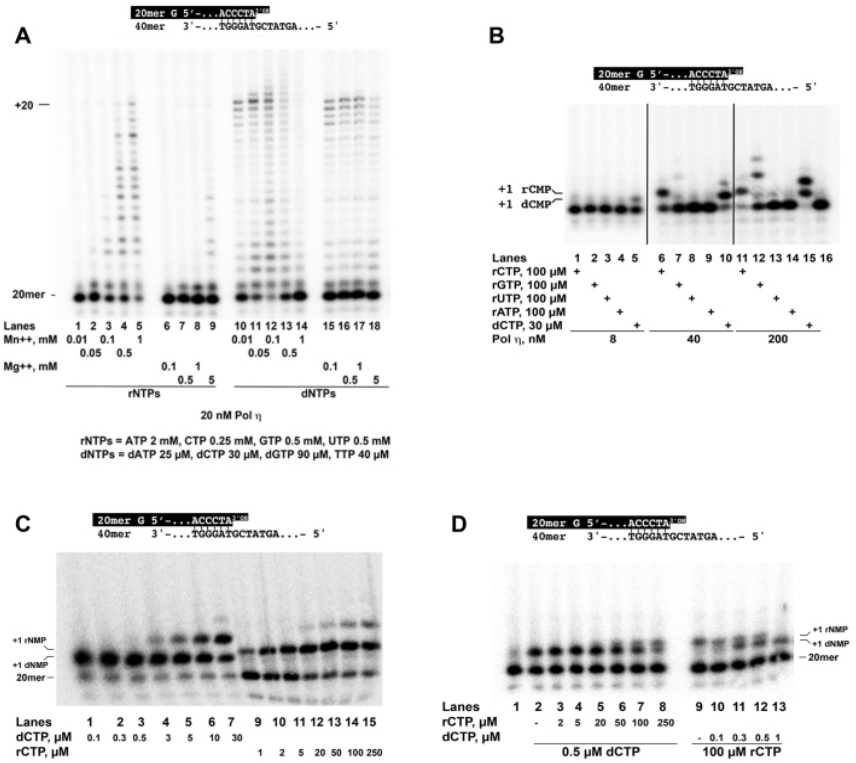

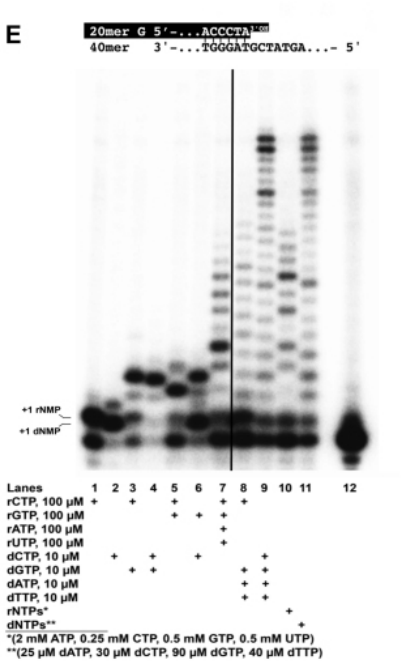

Fig. 23: Incorporation and elongation of ribonucleotides by human Pol η. The sequence of the 5' ^{32}P-labelled 20/40mer substrate (50 nM) used in all the experiments is indicated on top of each panel. (**A**) Pol η (20 nM) was incubated in the presence of non-equimolar mixtures of rNTPs (lanes 1 – 9) or dNTPs (lanes 10 – 18) and different amounts of Mn^{2+} (lanes 1 – 5; 10 – 14) or Mg^{2+} (lanes 6 – 9; 15 – 18). The final concentrations of the individual rNTPs and dNTPs are indicated on the bottom of the panel. (**B**) Increasing amounts of Pol η were titrated in the presence of fixed concentrations of each individual rNTP (lanes 1 – 4; 6 – 9; 11 – 14) or dCTP (lanes 5, 10, 15). Lane 16, control reaction in the absence of nucleotides. (**C**) Pol η (40 nM) was tested in the presence increasing concentrations of dCTP (lanes 1 – 7) or rCTP (lanes 9 – 15). (**D**) Pol η (20 nM) was tested in the presence of a fixed dose of dCTP and increasing concentrations of rCTP (lanes 2 – 8) or a fixed dose of rCTP and increasing concentrations of dCTP (lanes 9 – 13). Lane 1, control reaction in the absence of nucleotides. (**E**) Pol η (40 nM) was tested in the presence of various combinations of dNTPs or rNTPs. Lane 12, control reaction in the absence of nucleotides.

4.8 Translesion synthesis of 8-oxo-G by Pol η with ribonucleotides

Pol η can perform faithful bypass of 8-oxo-G, inserting dCMP. In line with the experiments performed with Pols λ and β, we wanted to test if and to what extent Pol η is capable to perform TLS past 8-oxo-G lesion using rNTPs. When rCTP was provided in the reaction, robust incorporation opposite 8-oxo-G was observed for both a 1-nt gapped (Fig. 24A, lanes 1 - 6) or an open primer/template (Fig. 24B, lanes 1 - 5). The kinetic parameters for rCMP and dCMP incorporation opposite 8-oxo-G are summarized in Table 3. The selectivity of Pol η for dCMP vs. rCMP incorporation opposite the lesion was increased 3.5-fold, with respect to a normal G, showing a value of 1428. Pol η could also incorporate both dAMP and rAMP, opposite the lesion (Fig. 24C). The selectivity for dAMP vs. rAMP was in the order of 3800, while the preference for dCMP vs. rAMP incorporation was 12700 (Table 3). Interestingly, the fidelity of lesion bypass was increased with rNTPs relative to dNTPs, with a 3.3-fold preference for dCMP vs. dAMP incorporation and an 8.9-fold preference for rCMP vs. rAMP incorporation, respectively (Table 3). These values were also in agreement with those reported in a recent study (Su et al. 2016). When all four dNTPs or rNTPs were provided, Pol η could perform efficient TLS (Fig. 24D, compare lane 1 with lane 5). The products synthesized in the presence of rNTPs were sensitive to RNase treatment (Fig. 24D, lane 3), confirming that they were authentic RNA chains. These results indicated that Pol η can synthesize RNA chains as a result of TLS past an 8-oxo-G lesion.

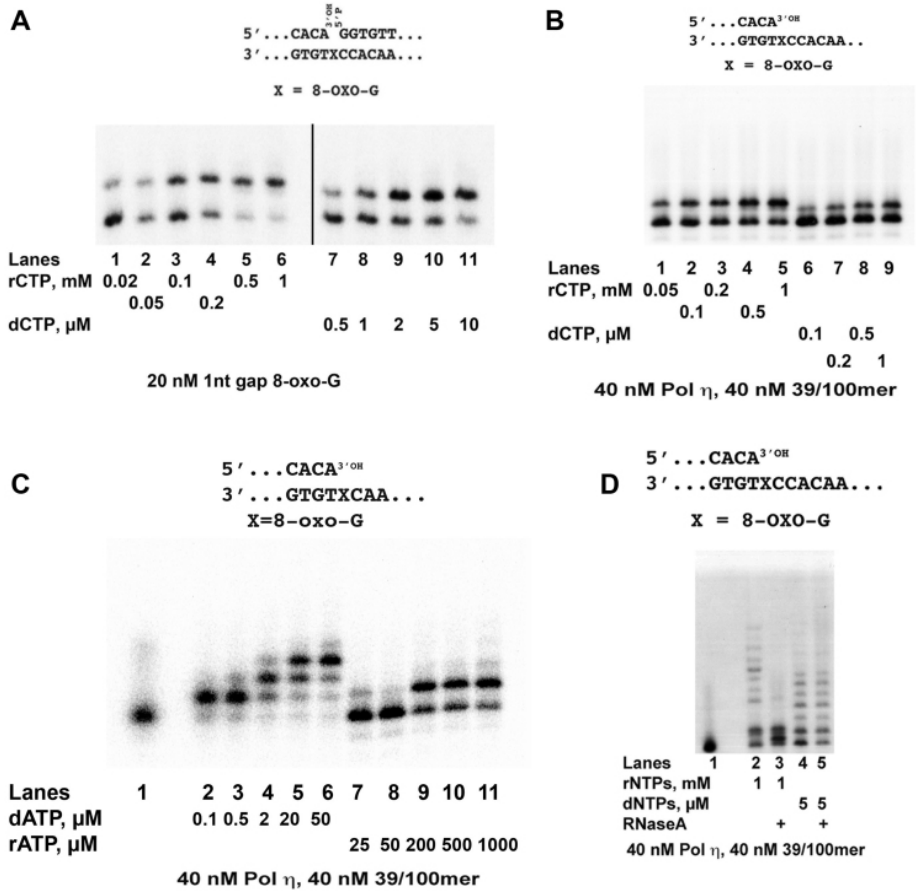

Fig. 24: Translesion synthesis of 8-oxo-G by Pol η with ribonucleotides. The sequences of the 5' ^{32}P-labelled DNA substrates used are indicated on top of each panel. (**A**) Pol η (40 nM) was incubated with the 1-nt gapped 8-oxo-G template, in the presence of increasing concentrations of rCTP (lanes 1 – 6) or dCTP (lanes 7 – 11). (**B**) Pol η was incubated with the 39/100-mer 8-oxo-G template, in the presence of increasing concentrations of rCTP (lanes 1 – 5) or dCTP (lanes 6 – 9).(**C**) Pol η was incubated with the 39/100-mer 8-oxo-G template, in the presence of increasing concentrations of dATP (lanes 2– 6) or rATP (lanes 7 – 11). Lane 1, control reaction in the absence of nucleotides. (**D**) Pol η was incubated with the 39/100-mer 8-oxo-G template, in the presence of all four rNTPs (lanes 2, 3) (1 mM each, final concentration) or dNTPs (lanes 4, 5) (5 µM each, final concentration). 2 Units of RNaseA (lanes 3, 5) or buffer (lanes 2, 4) were added after 10 min and the incubation continued for additional 5 min. Lane 1, control reaction in the absence of nucleotides.

Nucleotide	K_M, μM[a]	k_{cat}, min^{-1}	k_{cat}/K_M M^{-1} s^{-1}	f_{rel}[b](dCTP/ rCTP)	f_{rel} (dCTP/ dATP)	f_{rel} (dCTP/ rATP)	f_{rel} (rCTP/ dATP)	f_{rel} (rCTP/ rATP)
39/100 mer G								
dCTP	0.20±0.05	1.9±0.05	1.60×10^5	400	n.a.	n.a.	n.a.	n.a.
rCTP	15±0.3	0.40±0.1	0.40×10^3					
39/100mer 8oxoG								
dCTP	0.50±0.02	1.8±0.01	0.60×10^5	1428	3.30	12765		
rCTP	117±4	0.30±0.01	42				2.30×10^{-3}	8.90
dATP	0.30±0.01	0.32±0.01	0.18×10^5					
rATP	247±5	0.07±0.02	4.70					
39/72mer 8metG								
dCTP	2.70±0.1	1.10±0.02	6.80×10^3	693	n.a.	n.a.	n.a.	n.a.
rCTP	187±3	0.11±0.03	9.80					
rCTP + PolDIP2	100±2	0.37±0.04	61	111				
18/24mer								
dCTP	0.30±0. 3	2.50±0.2	1.40×10^5	546	n.a.	n.a.	n.a.	n.a.
rCTP	26±0.5	0.40±0.2	256					
18/24mer cis-Pt								
dCTP	1.50±1	1.20±0.1	1.30×10^4	1212	n.a.	n.a.	n.a.	n.a.
rCTP	113±5	0.07±0.01	11					

Table 3: a. Kinetic parameters were calclulated as indicated in the Methods section. Values are the means of three independent experiments ±S.D. b. Relative incorporation frequency f_{rel} was calculated as the ratio between the k_{cat}/K_M values for the indicated nucleotide pairs.

4.9 Ribonucleotide-mediated lesion bypass in XP-V cell extracts

In humans, defective Pol η causes a variant form of the genetic disease Xeroderma pigmentosum (XP-V). We decided to evaluate the rCMP incorporation opposite 8-oxo-G in extracts from XP-V cells lacking Pol η, in comparison with the same XP-V cell line complemented with ectopic expression of human Pol η (XP-V/η). As shown in Fig. 25A, TLS of 8-oxo-G with rCMP was detected in both XP-V and XP-V/η extracts (lanes 1 - 3). When this activity was normalized to the total Pol activity (measured as incorporation of dCMP opposite a normal G, Fig. 25B), rCMP incorporation was reduced by about 25% in the absence of Pol η (Fig. 25C). We have found that the majority of rCMP incorporation opposite 8-oxo-G is carried out by Pol β. Western blot analysis of the extracts confirmed that both Pol β and Pol η were present in the extracts (Fig. 25D). Thus, the apparently modest contribution of Pol η to rCMP incorporation opposite 8-oxo-G, could be explained by the competition of Pol β. On the other hand, when the extracts were tested with the cis-PtGG template, bypass was observed only in XP-V/η cells, with either dCMP or rCMP (Fig. 25E), in agreement with the notion that Pol η contributes most to TLS past this lesion. Collectively, these data suggest that the frequency of rNMP incorporation opposite a certain lesion is a function of *(i)* the type of TLS pols potentially acting on that lesion, *(ii)* their sugar selectivity and *(*iii) their relative affinity for the lesion.

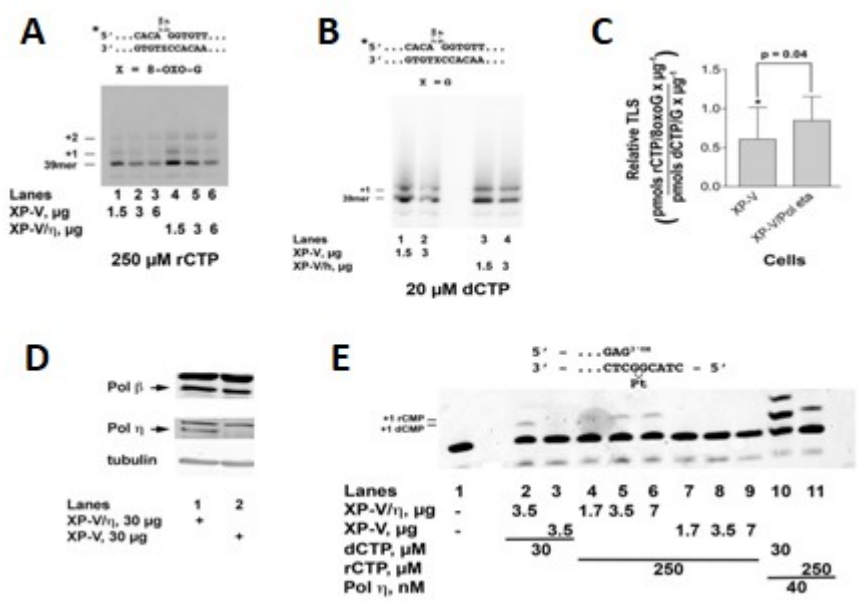

Fig 25. : (**A**) XP-V (lanes 1- 3) or XP-V/η (lanes 4 - 6) extracts were incubated with the 1 nt-gapped 8-oxo-G template in the presence of rCTP. (**B**) XP-V (lanes 1- 2) or XP-V/η (lanes 3 - 4) extracts were incubated with the 1 nt-gapped undamaged template in the presence of dCTP. (**C**) The TLS activity in the XP-V (grey bar) or XP-V/η (black bar) extracts, expressed as pmols of rCMP incorporated opposite 8-oxo-G x μg^{-1} of proteins, was normalized to the total polymerase activity, expressed as pmols of dCMP incorporated opposite undamaged guanine x μg^{-1} of proteins. Values are the means of two independent estimates, error bars indicate S.D. The *p* values were calculated with Student's *t* test. (**D**) Western blot analysis for Pols β and η in the XP-V/η (lane 1) or XP-V (lane 2) extracts. Tubulin was used as internal control. (**E**) XP-V (lanes 3, 7 - 9) or XP-V/η (lanes 2, 4 - 6) extracts, or purified human Pol η (lanes 10, 11) were incubated with the cis-PtGG template in the presence of dCTP (lanes 2, 3, 10) or rCTP (lanes 4- 9, 11). Lane 1, control reaction in the absence of extracts.

4.10 Pol η bypasses 8-met-G, but not 3-met-C with ribonucleotides

We extended our investigation of Pol η bypass to the 3-met-C and 8-met-G alkylation lesions. Pol η incorporated all four dNMPs opposite 3-met-C or 8-met-G (Fig. 26A, lanes 2 – 5; 11 – 14). On the contrary, while none of the rNMPs was incorporated opposite 3-met-C (Fig. 26A, lanes 1 – 9), robust rCMP incorporation was observed opposite 8-met-G (lane 16). Titration of dCTP or rCTP in the reaction revealed the accumulation of the expected +2 product (Fig. 26B), indicating efficient translesion synthesis by Pol η with

both deoxy- and ribonucleotides. The kinetic parameters for 8-met-G bypass are summarized in Table 3. The selectivity for dCMP vs. rCMP incorporation by Pol η opposite 8-met-G was 693, which is only slightly higher than the selectivity measured opposite a normal G. To the best of our knowledge, this is the first report of bypass of the 8-met-G lesion by a human pol with rNTPs.

Next, the effect of the auxiliary proteins PCNA and PolDIP2 was tested. PCNA did not stimulate rCMP incorporation opposite 8-met-G by Pol η (Fig. 26C, compare lanes 1 – 4 with lanes 7 – 10). On the other hand, a significant stimulation was observed in the presence of PolDIP2 (Fig 26C, lanes 11 – 14). Kinetic analysis showed that PolDIP2 increased the apparent catalytic efficiency (k_{cat}/K_M) for rCMP incorporation by 6- fold, lowering the selectivity value of Pol η for dCMP vs. rCMP incorporation to 111 (Table 3). PolDIP2 stimulated translesion synthesis by Pol η past 8-met-G also when all four dNTPs or rNTPs were provided to the reaction at their average physiological concentrations (Fig. 26D). However, the length of the RNA chains synthesized were limited to about 5 nucleotides (Fig. 26D, lanes 5 – 8), while full length products were detected with dNTPs (Fig. 26D, lanes 1 – 4). When PCNA was added in the reaction in a molar excess with respect to PolDIP2, TLS by Pol η with rNTPs was partially inhibited (Fig. 27A, lane 4). However, this effect was abolished when the PolDIP2 concentration was increased (lane 8), suggesting a possible competition between PCNA and Pol η for binding to PolDIP2.

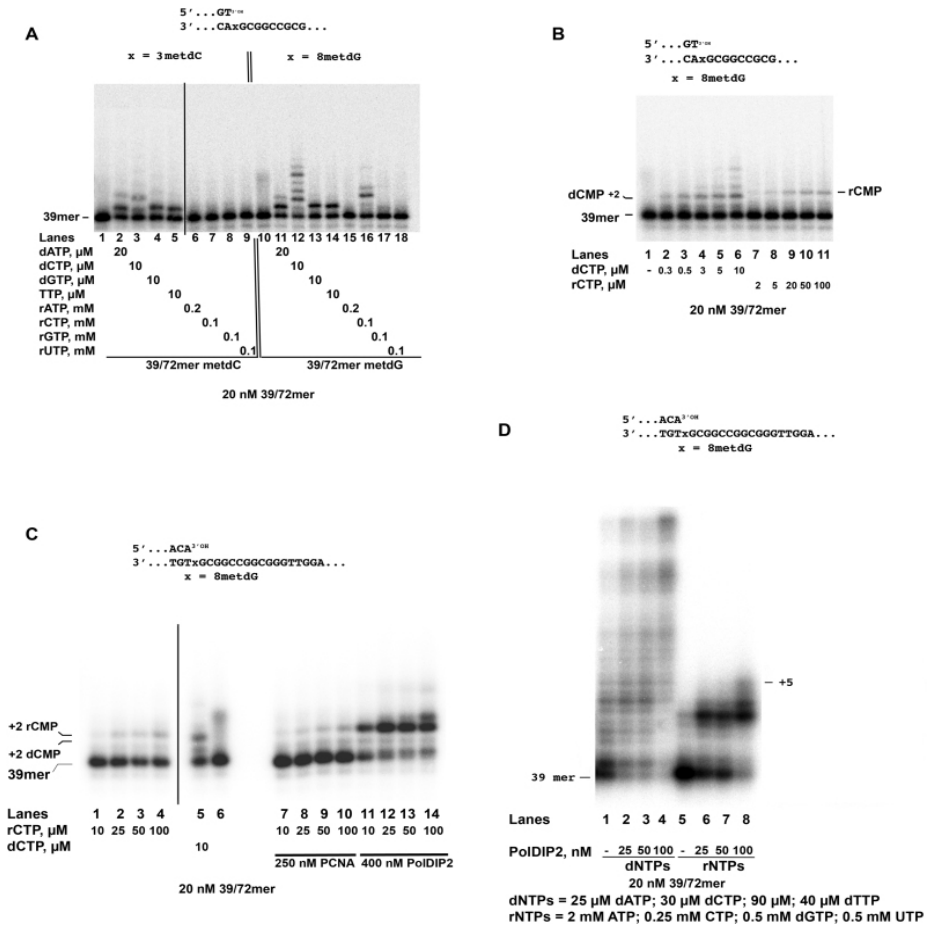

Fig. 26: Pol η bypass of 8-met-G and 3-met-C with ribonucleotides. The sequences of the 5' ^{32}P-labelled DNA substrates used are indicated on top of each panel. (**A**) 20 nM Pol η was incubated in the presence of the 3-met-C (lanes 1 – 9) or 8-met-G (lanes 10 – 18) 39/72mer substrates and a fixed concentration of each dNTP (lanes 2 – 5; 11 - 14) or rNTP (lanes 6 – 9; 15 – 18). Lanes 1 and 10, control reactions without nucleotides. (**B**) 20 nM Pol η was incubated with the 8-met-G substrate, in the presence of increasing concentrations of dCTP (lanes 2 – 6) or rCTP (lanes 7 – 11). Lane 1, control reaction in the absence of nucleotides. (**C**) 20 nM Pol η was incubated with the 8-met-G substrate, in the presence of rCTP (lanes 1 – 4; 7 – 14) or dCTP (lane 5) and in the absence (lanes 1 – 5) or in the presence of PCNA (lanes 7 – 10) or PolDIP2 (lanes 11 – 14). Lane 6, control reaction in the absence of nucleotides. (**D**) 20 nM Pol η was incubated with the 8-met-G substrate, in the presence of non-equimolar mixtures of dNTPs (lanes 1 – 4) or rNTPs (lanes 5 – 8) and in the absence (lanes 1, 5) or in the presence of increasing concentrations of PolDIP2 (lanes 2 – 4; 6 – 8). The final concentrations of the individual rNTPs and dNTPs are indicated on the bottom of the panel.

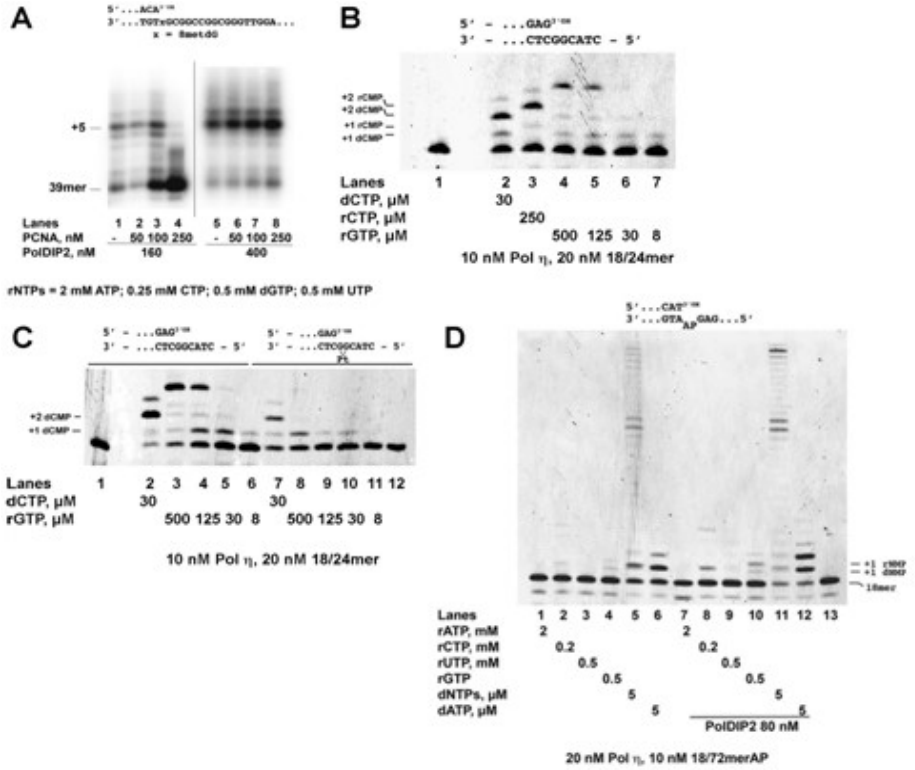

Fig. 27: (**A**) Pol η (20 nM), was tested on the 8-met-G containing primer/template, in the presence of all four rNTPs in the non-equimolar concentrations indicated at the bottom of the panel, and in the presence of PolDIP2 alone (lanes 1, 5) or in combination with PCNA (lanes 2 - 4; 6 - 8). (**B**) Pol η was tested on the 18/24 control template (lanes 1 - 6) or the 18/24 cisPt-GG template (lanes 7 - 12) in the presence of dCTP (lanes 2, 7), or rGTP (lanes 3 - 6; 8 - 11). Lanes 1, 12, control reactions in the absence of nucleotides. (**C**) Pol η was tested on the 18/24 control template in the presence of dCTP (lane 2), rCTP (lane 3) or rGTP (lanes 4 - 7). Lane 1, control reaction in the absence of nucleotides.(**D**) Pol η was incubated with AP containing template, in the presence of each single rNTP (lanes 1 – 4), all four dNTPs (lanes 5, 11) or dATP (lanes 6, 12) and in the absence (lanes 1 – 6) or in the presence (lanes 7 – 12) of PolDIP2. Lane 13, control reaction without nucleotides.

4.11 Pol η bypasses cis-PtGG but not an abasic site with ribonucleotides

Pol η is the main enzyme involved in the bypass of the intrastrand guanine crosslinks (cisPt-GG) caused by the anticancer drug cisplatin (Vaisman et al. 2000). Such crosslinks hamper DNA replication by interfering with replication fork progression, thus requiring the intervention of a specialized TLS Pol. Pol η is thought to be the main Pol responsible for Cis-Pt tolerance

since it can bypass the lesion *in vitro* and cells lacking this Pol are hypersensitive to Cis-Pt treatment (Albertella et al. 2005; Chen et al. 2006). In cancer cells, Pol η overexpression is induced by cis-Pt treatment and its levels correlate with chemoresistance and poor clinical outcomes of several tumors, such as non-small-lung or ovarian cancers (Chen et al. 2006, Srivastava et al. 2015). We were then interested in understanding if Pol η was able to insert ribonucleotides opposite Cis-PtGG lesion.

When tested in the presence of each of the four rNTPs, Pol η was capable of incorporating rCMP opposite the lesion (Fig. 28A, lane 10). The products observed with rGTP and rUTP as substrates resulted from the incorporation of dNTPs contaminating the commercial preparation used, as judged by their electrophoretic mobility, which was similar to those of products obtained with dCTP as substrate (Fig. 28A, compare lanes 8, 9 with lane 7; Fig. 27B and 1 C). Interestingly, the incorporation of rCMP was largely limited to the +1 product (Fig. 28A, lane 10), corresponding to incorporation opposite the first guanine (termed 3'-G, according to the template strand orientation) of the adduct, similar to what has been observed for the insertion of non-canonical dNTPs opposite Pt-GG by Pol η, while dCMP was correctly incorporated opposite both guanines, yielding the expected +2 product (Fig. 28A, lane 2). Titration of dCTP (Fig. 28B) or rCTP (Fig. 28C) into the reaction confirmed that rCMP incorporation was limited to opposite the 3'-G of cisPt-GG (Fig. 28C, lanes 9 – 14). PolDIP2 stimulated rCMP (Fig. 28D) and dCMP (Fig. 28E) incorporation by Pol η opposite cis-PtGG, but even in the presence of PolDIP2, rCMP incorporation was limited to the first position (Fig. 28D, lanes 5 – 13). When a primer/template bearing a rCMP opposite the 3'-G of the lesion was tested, only dCMP, but not rCMP, was incorporated opposite the 5'-G (Fig. 28F). Interestingly, when a primer/template with a dCMP opposite the 3'-G was used, no incorporation of rCMP was observed either (Fig. 28G). Overall, these results indicated that bypass of a cis-PtGG adduct by Pol η can lead to incorporation of rCMP opposite the first guanine (3'-G) only. The bypass, however, can be subsequently completed by incorporating dCMP opposite the 5'-G. The selectivity for dCMP vs. rCMP incorporation opposite the two guanines on the undamaged template was 546, similar to the one observed on the template with a single guanine (Table 3). This selectivity was increased to about 1200, opposite the 3'-G of cisPt-GG, a value similar to the one observed for 8-oxo-G (Table 3).

In a competition experiment, dCTP was titrated in the presence of the cisPt-GG template and fixed amounts of rCTP, resulting to the accumulation of

the +1 dCMP product with concomitant reduction of the +1 rCMP product (Fig. 28H, lanes 2 – 6). The same pattern was observed in the reciprocal experiment, i.e. titrating rCTP while keeping dCTP fixed (Fig. 28H, lanes 7 – 10). These results confirmed that dCTP and rCTP can compete for incorporation opposite the 3'-G of a cisPt-GG adduct. Comparable amounts of either products were observed at a rCTP/dCTP (M/M) ratio of 1/1000 (Fig. 28H, lanes 4 and 10), in agreement with the selectivity value derived from the kinetic analysis (Table 3). Simultaneous incorporation of rCMP and dCMP opposite the lesion was also observed in a similar competition experiment carried out with XP-V/η extracts (Fig. 28I, lane 6), suggesting that rCMP incorporation opposite the cisPt-GG lesion by Pol η can also occur in a cellular context.

Finally, when tested in the presence of an AP site, Pol η was unable to significantly incorporate rNMPs opposite the lesion (Fig. 27D, lanes 1 – 4), even in the presence of PolDIP2 (lanes 7 – 10), with the exception of a very weak incorporation of rCMP (Fig. 27F, lane 10), while it efficiently bypassed the lesion with either dATP or all four dNTPs (Fig. 27D, lanes 5, 6, 11, 12).

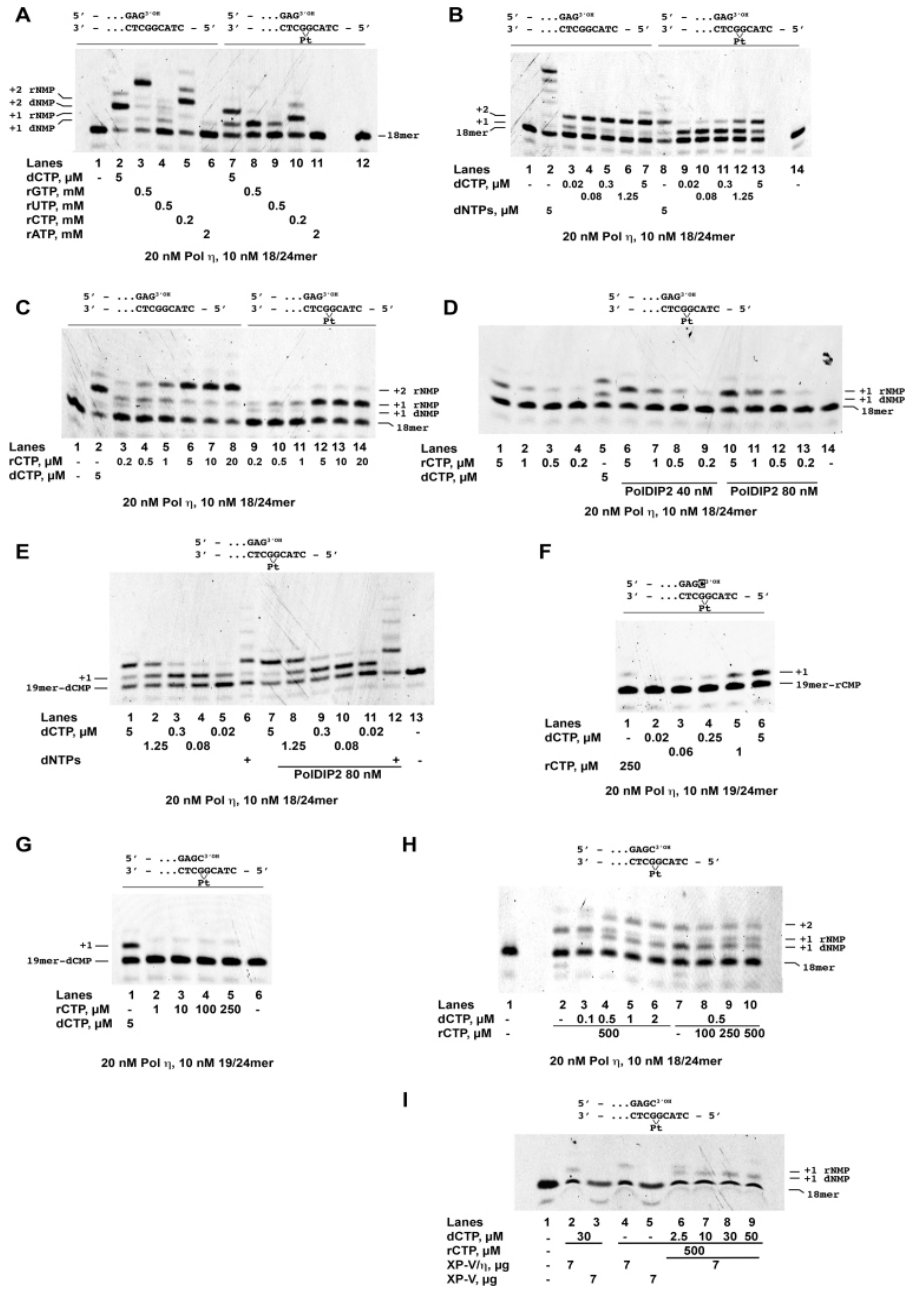

Fig. 28: Pol η bypass of cis-PtGG and abasic site with ribonucleotides. The 5' FAM-labelled DNA substrates used are indicated on top of each panel. (**A**) Pol η was incubated with the undamaged (lanes 1 – 6) or the cis-PtGG (lanes 7 – 12) templates, with dCTP

(lanes 5, 7) or each rNTP (lanes 3 – 6; 8 – 11). Lanes 1, 12, control reactions without nucleotides. (**B**) Pol η was incubated with the undamaged (lanes 1 – 7) or the cis-PtGG (lanes 8 – 14) templates, in the presence of dNTPs (lanes 2, 8) or dCTP (lanes 3 – 7; 9 – 13). Lanes 1, 14, control reactions without nucleotides. (**C**) Pol η was incubated with the undamaged (lanes 1 – 8) or the cis-PtGG (lanes 9 – 14) templates, in the presence of rCTP (lanes 3 - 14). Lane 1, control reaction without nucleotides. Lane 2, control reaction with dCTP. (**D**) Pol η was incubated with the cis-PtGG template in the presence of rCTP (lanes 1- 4; 6 – 13) and in the absence (lanes 1 – 4) or in the presence of PolDIP2 (lanes 6 – 13). Lane 5, control reaction with dCTP. Lane 14, control reaction without nucleotides. (**E**) Pol η was incubated with the cis-PtGG template in the presence of dNTPs (lanes 6, 12) or dCTP (lanes 1 – 5; 7 – 11) and in the absence (lanes 1 – 6) or in the presence of PolDIP2 (lanes 7 – 12). Lane 13, control reaction without nucleotides. (**F**) Pol η was incubated with the cis-PtGG template bearing a rCMP opposite the 3'-G of the lesion, in the presence of rCTP (lane 1) or dCTP (lanes 2 – 6). (**G**) Pol η was incubated with the cis-PtGG template bearing a dCMP opposite the 3'-G of the lesion, in the presence of dCTP (lane 1) or rCTP (lanes 2 – 5). Lane 6, control reaction without nucleotides. (**H**) Pol η (20 nM) was tested in the presence of a fixed dose of rCTP and increasing concentrations of dCTP (lanes 2 – 6) or a fixed dose of dCTP and increasing concentrations of rCTP (lanes 7 – 10). Lane 1, control reaction in the absence of nucleotides. (**I**) XP-V (lanes 3, 5) or XP-V/η (lanes 2, 4, 6 - 9) extracts, were incubated with the cis-PtGG template in the presence of dCTP alone (lanes 2, 3), rCTP alone (lanes 4, 5), or both nucleotides at different M/M ratios (lanes 6 - 9). Lane 1, control reaction in the absence of extracts.

4.12 Cleavage of rCMP opposite normal or damaged guanines by human RNase H2

In a 1993 report of the first purification from mammalian cells of the enzyme later identified as RNase H2, Eder *et al*. showed that the efficiency of the enzyme depended on the identity of the base pair being cleaved (Eder et al. 1993). To verify this property, we expressed and purified the recombinant human trimeric RNase H2 (Fig. 30A) and tested it with all four ribo-to-deoxynucleotide base pairs. Time course experiments were performed with increasing amounts of the 40/40mer ds DNA oligonucleotide substrates, bearing either a rC:dG, rG:dC, rA:dT or rU:dA pair at a specific position. The strand containing the single rNMPs was 5'-labelled so that after cleavage by RNase H2, products of a defined length were generated and resolved by sequencing gel electrophoresis. Representative experiments are shown in Fig. 29A – D, while the kinetic parameters are summarized in Table 4. Human RNase H2 had a strong preference for rA:dT cleavage, followed by rU:dA. Interestingly, rC:dG and rG:dC pairs were cleaved with a 6-fold and 15-fold reduced efficiency with respect to rA:dT. RNase H2 subunit H2B contains a PCNA-binding domain

and PCNA has been shown to interact with RNase H2 and direct it to the DNA substrate. We therefore tested whether PCNA could rescue the reduced catalytic activity of human RNase H2 with rC- or rG-containing substrates. As shown in Fig. 30 B and C, however, PCNA did not stimulate rC:dG or rG:dC cleavage by RNase H2. Next, we evaluated whether rCMP paired to a damaged guanine may affect RNase H2 cleavage. RNase H2 showed a 3.4-fold reduced efficiency in removing rCMP when it was opposite 8-oxo-G vs. G (Fig. 31A and B). On the other hand, no differences were seen in cleavage efficiency between rC:dG and rC:8metG pairs (Fig. 31C and D). RNase H2 exhibited reduced cleavage efficiency of rCMP opposite both the 3'-G and 5'-G of cis-PtGG relative to the controls (Fig. 29D). Since rCMP incorporation by Pol η can occur only opposite the 3'-G (see Fig. 28), we better characterized RNase H2 cleavage at this position (Fig. 31E). Quantification of the results indicated a 3.8-fold reduced cleavage efficiency by RNase H2 when rCMP was opposite the 3'-G of a cis-PtGG lesion, relative to it being opposite an undamaged guanine at the same position (Fig. 31F). Overall, these results indicated that rCMP opposite an undamaged guanine is already less efficiently cleaved by RNase H2 and incorporation of rCMP as a result of TLS can further reduce the efficiency of its removal by RNase H2.

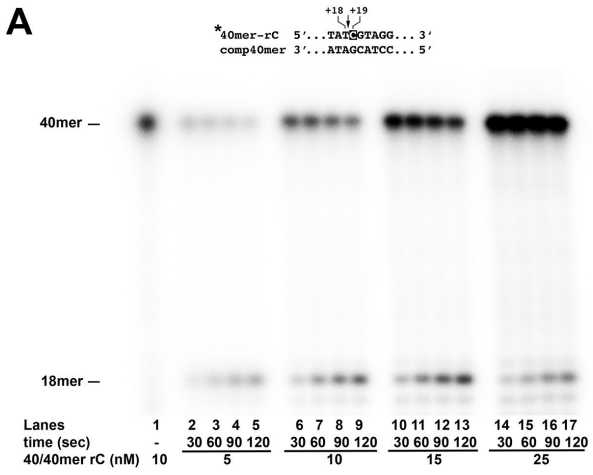

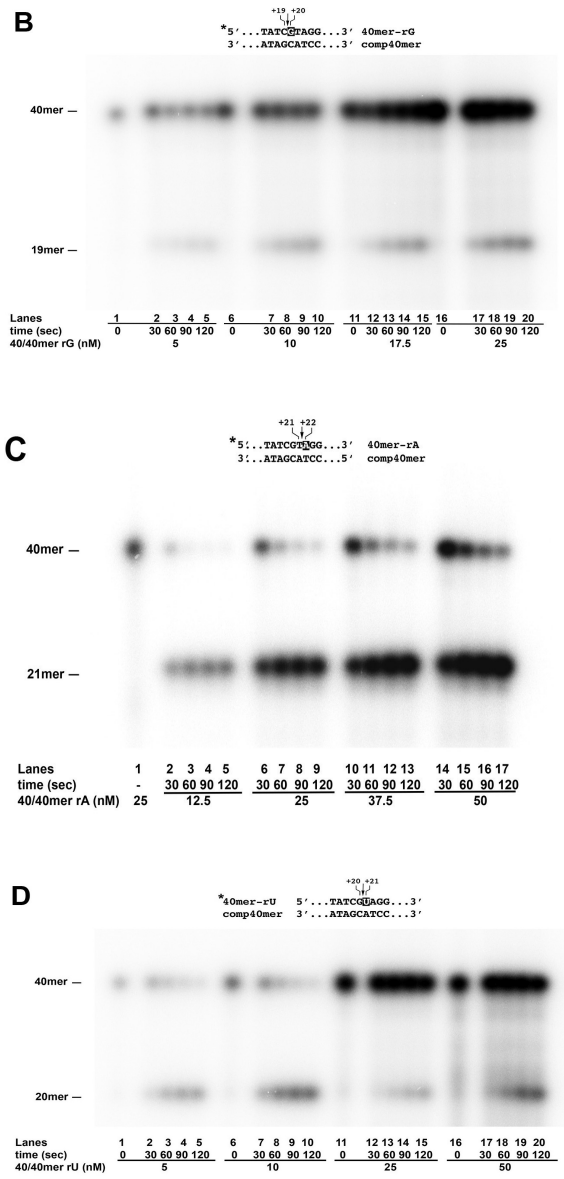

Fig. 29: Time course of the reaction of recombinant human RNase H2 (2.8 nM) with increasing concentrations of the the 5'-32P labeled 40/40mer containing a single rCMP (**A**), rGMP (**B**), rAMP (**C**) or rUMP (**D**). The position of the single rNMP in each substrate is indicated on top of each panel, along with the position of the RNase H2 cleavage (arrows). Asterisk indicates the labeled strand.

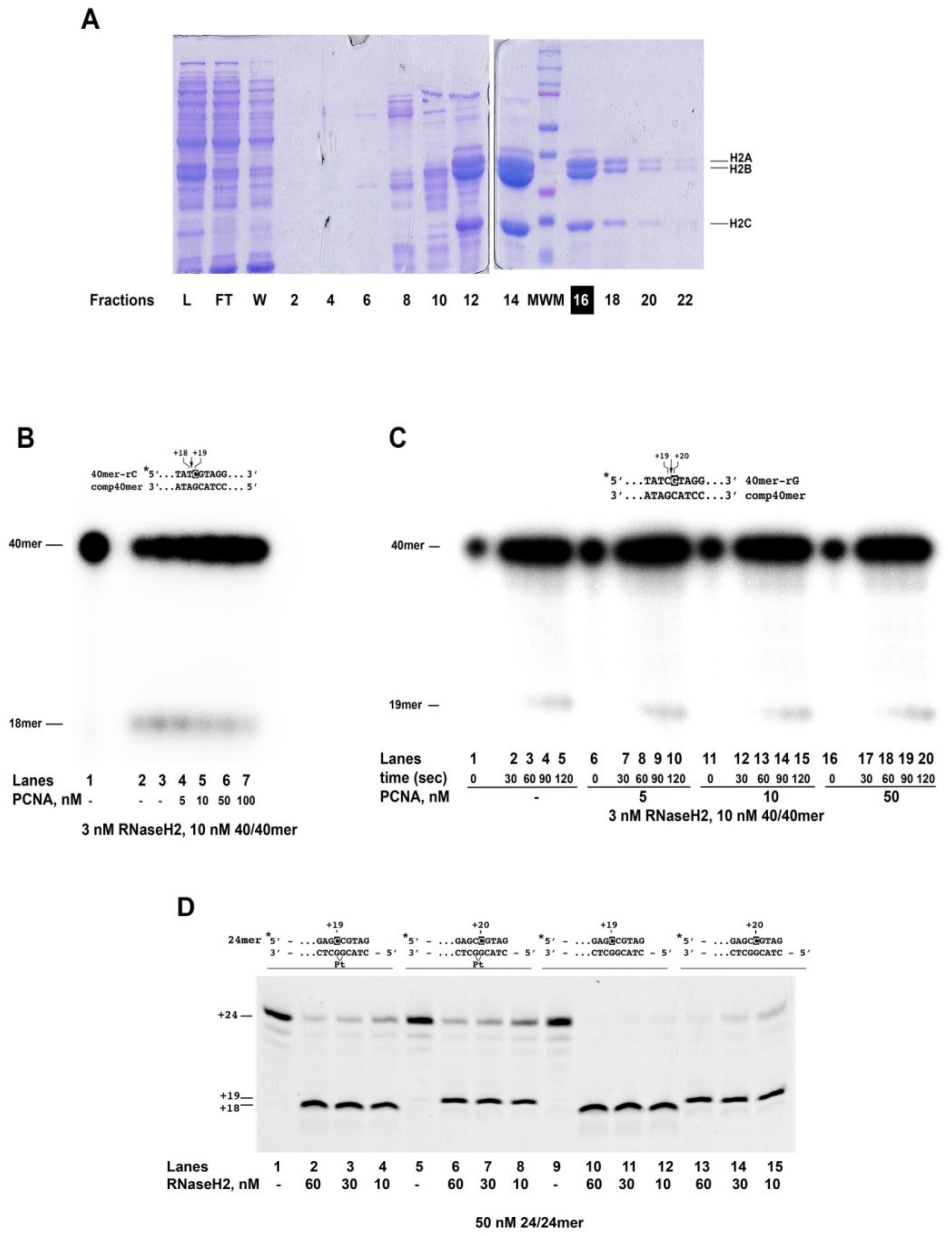

Fig. 30: (**A**). Coomassie stained SDS gel of the fractions from the Rnase H2 purification. L, loading; FT, flow-through; W, wash; MWM, molecular weight markers. The bands corresponding to the subunits H2A, H2B and H2C of the trimeric Rnase H2 complex are indicated. Fraction 16 (4.8 mg ml^{-1}; 56 µM) was used for all the experiments. (**B**) RNase H2 was tested in the absence (lanes 2, 3) or in the presence (lanes 4 - 7) of PCNA on the 5'-

32P labeled 40/40mer substrate containing a single rCMP. Lane 1, control reaction without RNase H2 or PCNA. (**C**) Time course of RNase H2 digestion of the 40/40mer bearing a single rGMP, in the absence (lanes 1 - 5) or in the presence of PCNA (lanes 6 - 20). Asterisk indicates the labeled strand.(**D**) RNase H2 was titrated in the presence of the 5'-FAM labelled 24/24mer substrate bearing a single rCMP opposite the 3'-G (lanes 2 - 4) or the 5'-G (lanes 6 - 8) of a cis-PtGG adduct, or the corresponding control templates (lanes 10 - 15). Lanes 1, 9, control reactions without RNase H2. Asterisk indicates the labeled strand.

Basepair	**K_M (nM)[a]**	**k_{cat} (min^{-1})**	**k_{cat}/K_M (M^{-1}, s^{-1})**	**efficiency (-fold)**
rA:dT	**10±3**	**6.7±0.2**	**11 x 10^6**	**6.1**
rU:dA	**12±2**	**3.1±0.5**	**4.3 x 10^6**	**2.4**
rC:dG	**8±2**	**0.9±03**	**1.8 x 10^6**	**1**
rG:dC	**27±5**	**1.2±0.3**	**0.7 x 10^6**	**0.4**

Table 4: Kinetic parameters for RNase H2 cleavage of different ribo-/deoxynucleoside basepairs . Kinetic parameters have been calculated as indicated in the Methods section. Values are the means of four independent experiments ±S.D.

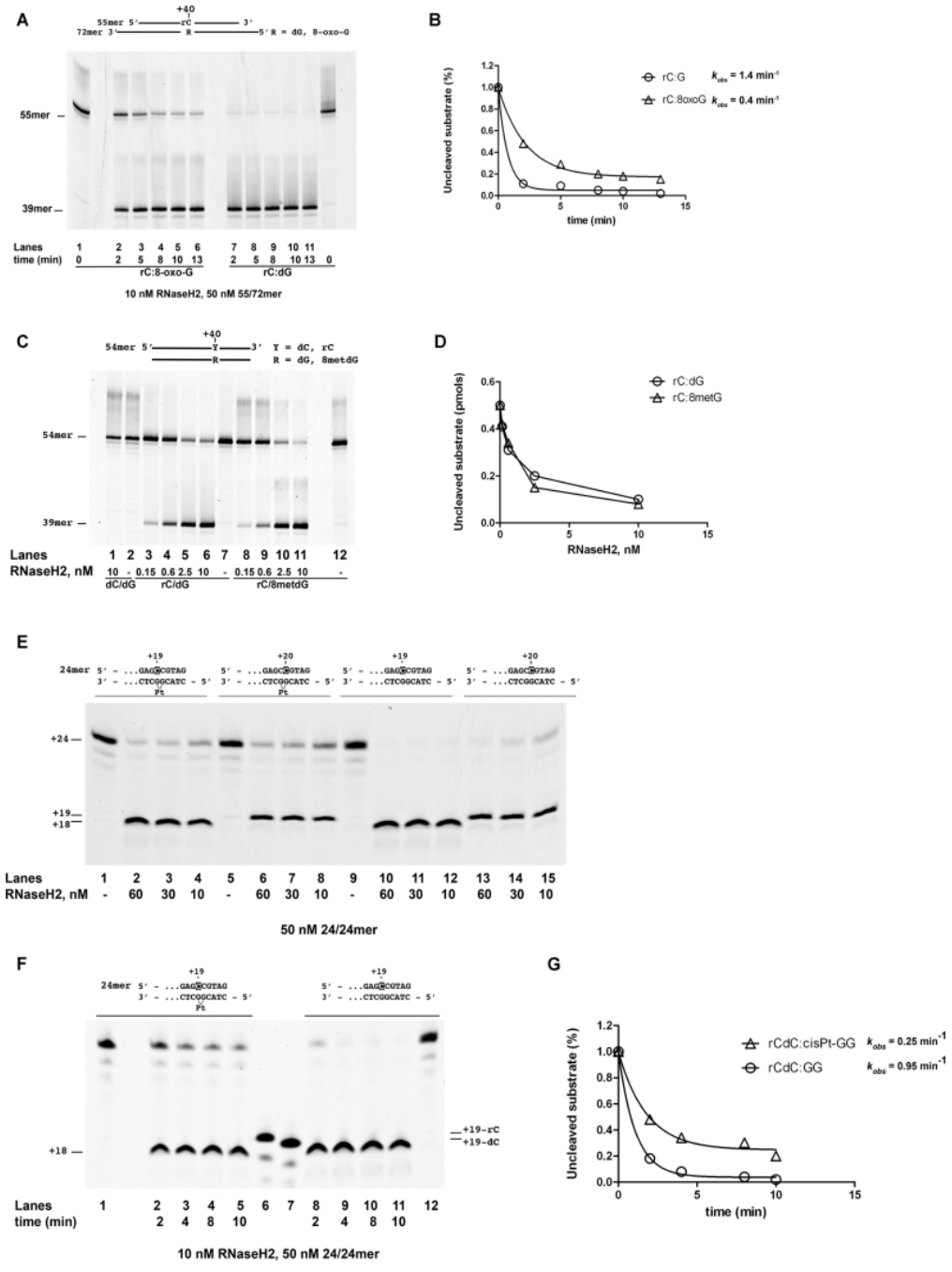

Fig. 31: Cleavage of rCMP opposite normal or damaged guanines by human RNase H2. The 5' FAM-labelled templates used are indicated on top of each panel. Asterisks

indicate the labeled strands. (**A**) Time course of RNase H2 digestion of the DNA substrate containing a single rCMP opposite 8-oxo-G (lanes 1 – 6) or undamaged guanine (lanes 7 – 12). (**B**) Quantification of the experiment shown in panel A. Data points were fitted to the simple exponential ([substrate]/[substrate+ product]) = $e^{-k_{obs}t}$. (**C**) RNase H2 was titrated in the presence of the DNA substrate containing a single rCMP opposite an undamaged guanine (lanes 3 – 6) or opposite a 8-met-G lesion (lanes 8 – 11). Lanes 7, 12, control reactions in the absence of enzyme. Lanes 1, 2, control reactions with the DNA substrate bearing a dCMP opposite guanine with or without enzyme, respectively. (**D**) Quantification of the experiment shown in panel A. No curve fitting was applied. (**E**) RNase H2 was titrated in the presence of the DNA substrate containing a single rCMP opposite either the 3' G (lanes 1 - 4) or the 5' G (lanes 5 - 8) of a cis-PtGG lesion (lanes 1 – 8) or the same guanines in an undamaged template (lanes 9–15). (**F**) Time course of RNase H2 digestion of the DNA substrate containing a single rCMP opposite the 3'-G of a cis-PtGG lesion (lanes 1 – 10) or the same guanine in an undamaged template (lanes 8 – 12) Lanes 6, 7, rCMP- and dCMP-terminated 19mer oligonucleotides, respectively, as markers. (**G**) Quantification of the experiment shown in panel E. Data points were fitted to the simple exponential ([substrate]/[substrate+ product]) = $e^{-k_{obs}t}$.

These results are part of a paper published in Nucleic Acids Res. in 2017. The original paper is attached.

4.13 Attempts of expressing AtMutYH in bacterial strains

We repeatedly attempted to express *Arabidopsis thaliana MutYH* gene in two different strains of *E. coli.* Details of the steps performed are reported in the Materials and methods section. Nonetheless, Western Blot analysis failed to show the presence of any band corresponding to AtMutYH.

4.14 Cloning *AtMutYH* gene

We therefore decided to clone *AtMutYH* gene in pET30a(+) plasmid. Details of the steps performed are reported in the Materials and methods section. The cloning procedure, which was attempted twice, did not succeed.

4.15 Attempts to obtain *A. thaliana* cell lines characterized by silencing of *AtPOLL* in a Ogg1$^{-/-}$ or MutYH$^{-/-}$background.

A. thaliana WT (Col-8), Ogg1$^{-/-}$ and MutYH$^{-/-}$ cell suspension cultures were co-cultivated with a *Agrobacterium tumefaciens* EHA105 strain that was previously engineered with pGWB5kdPOLL (Hyg^{R}) (provided by Camilla Valdesturli and Matteo Faè), a plasmid that contains a cassette expressing an artificial microRNA (amiRNA) necessary to silence *AtPOLL***.** The marker gene present in this cassette confers the resistance to hygromycin. It is worth noting that a hygromycin resistance marker was required since Ogg1$^{-/-}$ and MutYH$^{-/-}$ lines were obtained by insertional mutagenesis using a T-DNA containing a kanamycin-resistance gene. After several months of stunted growth we extracted proteins and separated them by SDS-PAGE. However, Western Blot analysis failed to reveal the presence of any band thus indicating that transformed cells did not proliferate. For details see the Materials and Methods section.

4.16 Transformation of *A. thaliana* mutant plants

To overcome the problems encountered with the co-cultivation of suspension cell lines, *A. thaliana* MutYH$^{-/-}$ plants were transformed by floral dipping using pGWB5kdPOLL plasmid (Hyg^{R}). Seeds of the 32 T2 mutant lines were germinated on Hygromycin-containing medium in order to select them. We expected two phenotypes; growing or non-growing, corresponding, respectively, to plants containing or not containing the Hyg^{R} gene marker. Viable seeds able to germinate on the selective medium,

should contain the recombinant *AtPOL* silencing gene. Resistant plantlets are heterogeneus since they comprise both homozygous and heterozygous genotypes for the Hyg^R gene. Moreover, the ratio between viable and unviable seeds indicates the copy number of transferred T-DNA. To proceed with this analysis 40 seeds of each T2 line were plated on selective dishes in order to visualize *seeds germinated : seeds aborted* ratio. A 3:1 ratio (30 seeds grown : 10 seeds not grown) corresponds to one integration event while a higher ratio means that more than one integration events had occurred. In general, one integration event is preferable (Smith et al. 2001).
The T2 mutant lines in which the ratio was 3:1 were: 1; 2; 3; 4; 30; 31; 32. Some seedlings of these lines were transferred to jiffy pots and grown until we had sufficient material to perform DNA extraction from healthy leaves. As control, we seeded Col-8 (wt) and mutant parental lines. Moreover, we transferred into jiffy pots also some seedlings of the T2 mutant line 29 (which did not show the 3:1 ratio). Results presented here are only a part of the entire work, since we had to perform two rounds of sowing for reasons of space. Analysis of half of the 32 lines are still ongoing. Details of the conditions and of the steps performed are reported in the Materials and methods section.

4.17 Analysis of the genetic background of T2 mutant lines

First of all, we carried out a PCR analysis to be sure that the parental line, transformed by our collaborators with the silencing plasmid, was really $MutYH^{-/-}$. *A. thaliana* $MutYH^{-/-}$ and $Ogg1^{-/-}$ mutants have been obtained through the insertion of a 4000bp T-DNA, flanked by Left Border (LB) and Right Border (RB) sequences, inside *MutYH* coding sequence or inside *Ogg1* promoter. Therefore, primers were previously chosen in our laboratory to reveal the presence or the absence of the T-DNA, to distinguish homozygous mutants, with both alleles knockout or heterozygous mutants, with just one allele knockout or plants with both alleles wt. The five primers (LPMUT, RPMUT, LBb1.3, LPOGG and RPOGG), coupled in different combinations, are able to reveal the bands corresponding to wt or mutant alleles. The LP primers (forward primers) anneal upstream the site of T-DNA insertion while the RP primers (reverse primers) anneal downstream the site of T-DNA insertion. LBb1.3 primer anneals to the LB that flanks the T-DNA. The length of the bands expected is reported in the table below.

MutYH (wt)	LPMUT + RPMUT	1158bp
	LBb1.3 + RPMUT	No band (no insertion)
MutYH-/-	LPMUT + RPMUT	No detectable band (1158+4000)bp
	LBb1.3 + RPMUT	710bp
Ogg1(wt)	LPOGG + RPOGG	1055bp
	LBb1.3 + RPOGG	No band (no insertion)
Ogg1 -/-	LPOGG + RPOGG	No detectable band (1055+4000)bp
	LBb1.3 + RPOGG	830-840bp

Table 5: Length of the fragments expected utilizing the indicated primers. In the PCR reaction with LPMUT and RPMUT primers on DNA extracted from a wt line, a 1158bp band is expected, corresponding to the length of *MutYH* wt allele. Utilizing, instead, RPMUT primer coupled to LBb1.3 one, no band is expected in the case of a wt line, since the insertion of T-DNA is not present and so the LBb1.3 primer can not anneal to the LB.
In tha case of *MutYH*$^{-/-}$ line, the PCR reaction with LPMUT and RPMUT primers should produce a band of 5158bp, corresponding to the length of the wt allele (1158bp) and the length of T-DNA insertion (4000bp). However, in this situation the band expected is too big to be amplified by the Taq Polymerase used in PCR reactions, therefore we should not be able to observe this band. A band of 710bp is expected in the case of *MutYH-/-* line, utilizing LBb1.3 an RPMUT primers. In the case of LPOGG and RPOGG primers used on a wt line, the band expected is of 1055bp, corresponding to the length of *Ogg1* wt . As for LBb1.3 and RPMUT primers, also in the case of LBb1.3 + RPOGG primers no band is expected in the case of a wt line, since the insertion of T-DNA is not present and so the LBb1.3 primer can not anneal to the LB. In the case of *Ogg1*$^{-/-}$ line, the PCR reaction with LPOGG and RPOGG primers should produce a band of 5055bp, corresponding to the length of the wt allele (1055bp) and the length of T-DNA insertion (4000bp). Again, also in this situation the band expected is too big to be amplified by the Taq Polymerase used in PCR reactions, therefore we should not be able to observe this band. Finally, the band obtained by PCR utilizing LBb1.3and RPOGG primers on *Ogg1*$^{-/-}$ line should be of 830-840bp.

As shown in Fig. 32A (Lane 8) and in Fig. 32B (Lane 3), two bands of 710bp and 1055bp were obtained using the parental DNA, thus confirming that the parental line is *MutYH*$^{-/-}$. The same pattern was obtained for T2 mutant line 2, plant n°1 (Lane 11 Fig. 32A and Lane 5 Fig. 32B), indicating that this line is knockout for both *MutYH* alleles and wt for *Ogg1*. On the other hand, we did not observe any band of the expexted 710bp length in the case of T2 mutant line 30, plant n° 1 (Fig. 32A, Lane 10). Moreover, also the band in lane 4 of Fig. 32B was uncertain. Since we could not confirm that this plant is knockout for *MutYH,* we did not consider it for further investigations. As expected Col-8 line is wt for both genes (see Lane 2 Fig. 32B and Lane 2 Fig. 32C).

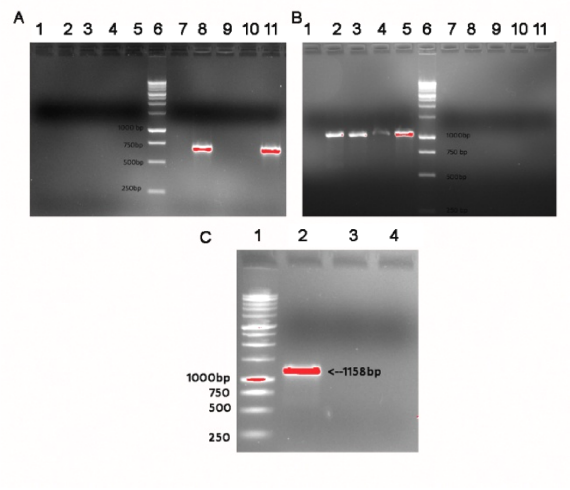

Fig. 32: The parental line that was transformed with pGWB5kdPOLL plasmid is knockout for both *MutYH* alleles and wt for *Ogg1*. PCR reactions were performed utilizing all the different combinations of primers on DNA extracted from parental line, Col-8 wt line,T2 mutant line 30 and T2 mutant line 2. (**A**) Lanes 1 and 7: controls. Lanes 2-5: LPMUT+RPMUT primers and DNA of parental/Col-8/30/2 lines. Lanes 8 – 11: LBb1.3 + RPMUT primers and DNA of parental/Col-8/30/2 lines. (**B**) Lanes 1 and 7: controls. Lanes 2-5: LPOGG + RPOGG primers and DNA of parental/Col-8/30/2 lines. Lanes 8 – 11: LBb1.3 + RPOGG primers and DNA of parental/Col-8/30/2 lines. (**C**) Lanes 2, 3: LPMUT+RPMUT primers and DNA of Col-8 and T2 30 mutant line, plant n°1. Lane 4: control.

In the same way, we performed PCR reactions with the DNA of the other T2 mutant lines (Figs. 33 and 34). All the mutant plants, except T2 mutant line 3 plant n°1, were used for the subsequent experiments.

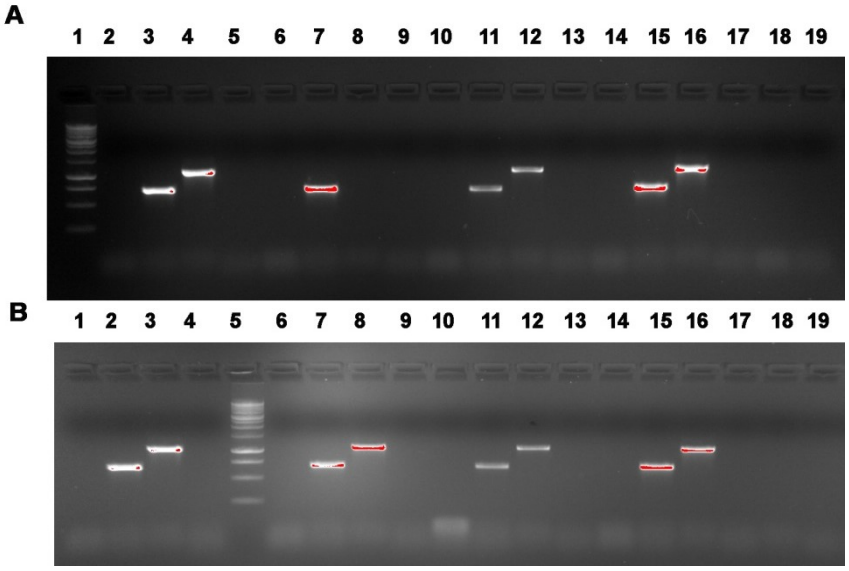

Fig. 33: All the T2 mutant lines tested, except one, are MutYH$^{-/-}$ and Ogg1$^{+/+}$. (**A**) Lanes 2-5: DNA of T2 mutant line 1, plant n°2. Lanes 6-9: DNA of T2 mutant line 3, plant n°1. Lanes 10-13: DNA of T2 mutant line 4, plant n°3. Lanes 14-17: DNA of T2 mutant line 2, plant n°1 (PCR was repeated for this plant, to confirm the previous result). Lanes 2, 6, 10, 14: LPMUT+RPMUT primers. Lanes 3, 7, 11, 15: LBb1.3+RPMUT primers. Band of 710bp, corresponding to *MutYH*$^{-/-}$. Lanes 4, 8, 12, 16: LPOGG+RPOGG primers. Band of 1055bp, corresponding to Ogg1 wt. No band in lane 8. Lanes 5, 9, 13, 17: LBb1.3+RPOGG primers. Lanes 18, 19: controls. (**B**) Lanes 1-4: DNA of T2 mutant line 29, plant n°1. Lanes 6-9: DNA of T2 mutant line 30, plant n°1. Lanes 10-13: DNA of T2 mutant line 31, plant n°2. Lanes 14-17: DNA of T2 mutant line 32, plant n°2. Lanes 1, 6, 10, 14: LPMUT+RPMUT primers. Lanes 2, 7, 11, 15: LBb1.3+RPMUT primers. Band of 710bp, corresponding to *MutYH*$^{-/-}$.Lanes 3, 8, 12, 16: LPOGG+RPOGG primers. Band of 1055bp, corresponding to Ogg1 wt. Lanes 4, 9, 13, 17: LBb1.3+RPOGG primers. Lanes 18, 19: controls.

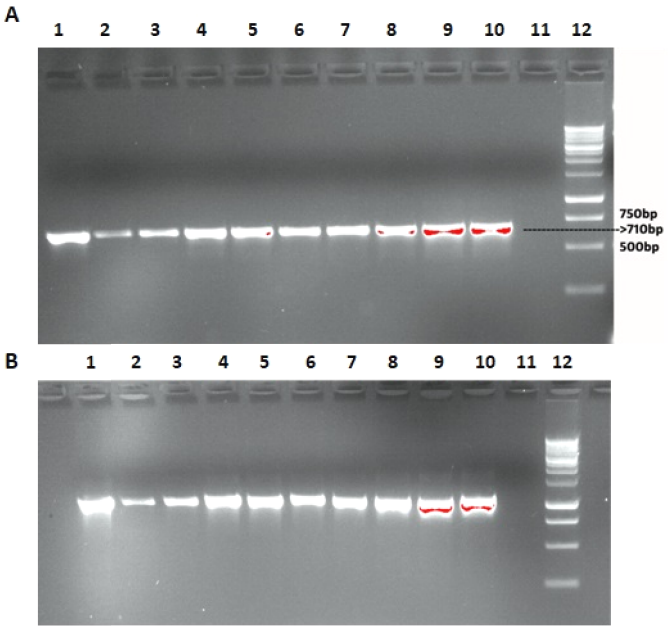

Fig. 34: All the T2 mutant lines tested are MutYH$^{-/-}$ and Ogg1$^{+/+}$. (**A**) LBb1.3+RPMUT primers. Band of 710bp, corresponding to *MutYH*$^{-/-}$. (**B**) LPOGG+RPOGG primers. Band of 1055bp, corresponding to *Ogg1* wt. (**A and B**) Lane1: DNA of T2 mutant line 1, plant n°1. Lane 2: DNA of T2 mutant line 1, plant n°3. Lane 3: DNA of T2 mutant line 2, plant n°2. Lane 4: DNA of T2 mutant line 2, plant n°3. Lane 5: DNA of T2 mutant line 3, plant n°2. Lane 6: DNA of T2 mutant line 3, plant n°3. Lane 7: DNA of T2 mutant line 4, plant n°2. Lane 8: DNA of T2 mutant line 30, plant n°2. Lane 9: DNA of T2 mutant line 31, plant n°1. Lane10: DNA of T2 mutant line 32, plant n°1.

4.18 AtPOLL is silenced in T2 mutant lines

We then extracted proteins from the plants resulted *MutYH*$^{-/-}$ and *Ogg1*$^{+/+}$and from Col-8. Proteins were separated on SDS-PAGE gels and Immunoblotting was performed (see Material and Methods section for details). As expected, bands of around 60kDa, corresponding to AtPOLL, are visible in lanes 1 and 2 of Fig. 35, where proteins extracted from Col-8 and MutYH parental lines were loaded. Bands are also visible in lanes 4 and 5 of Fig. 35, meaning that silencing of AtPOLL was not successful in T2 mutant line 4, plant n°3 and, as expected since the beginning, in T2 mutant line 29, plant n°1. Fig 36, showing the results of Immunoblotting on the other T2 mutant lines, is more uncertain.

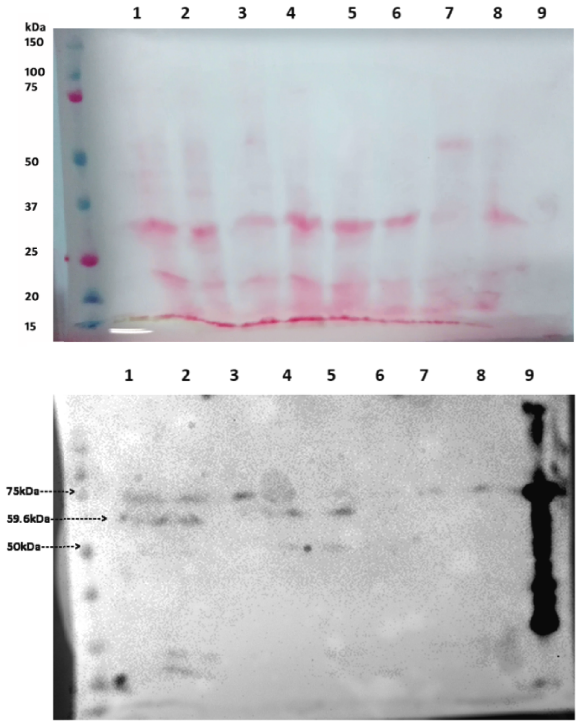

Fig. 35: The *AtPOLL* gene is silenced in four T2 mutant plants. Lane 1: Col-8 (wt) line. Lane 2: Parental (MutYH$^{-/-}$) line. Lane 3: T2 mutant line 1, plant n°2. Lane 4: T2 mutant line 4, plant n°3. Lane 5: T2 mutant line 29, plant n°1. Lane 6: T2 mutant line 30, plant n°1. Lane 7: T2 mutant line 31, plant n°2. Lane 8: T2 mutant line 32, plant n°2. 75µg of each sample were loaded. Lane 9: Control, human recombinant Polλ, 100ng.

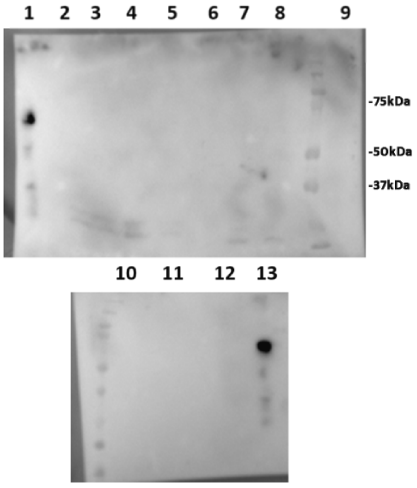

Fig. 36: Western blot analysis shows that AtPOLL is not present in all T2 mutant plants. Lane 1: Control, human recombinant Polλ, 50ng. Lane 2: T2 mutant line 1, plant n°1. Lane 3: T2 mutant line 1, plant n°3. Lane 4: T2 mutant line 2, plant n°1. Lane 5: T2 mutant line 2, plant n°2. Lane 6: T2 mutant line 2, plant n°3. Lane 7: T2 mutant line 3, plant n°2. Lane 8: T2 mutant line 3, plant n°3. Lane 9: T2 mutant line 4, plant n°2. Lane 10: T2 mutant line 32, plant n°1. Lane 11: T2 mutant line 31, plant n°1. Lane 12: T2 mutant line 30, plant n°2. Lane 13: Control, human recombinant Polλ, 50ng. 75µg of each sample were loaded.

Therefore, as further control, we performed PCR reactions to confirm the presence of pGWB5kdPOLL plasmid, by utilizing Frw_AtpPolL and Rev_AtpPolL. The primers anneal to the promoter region of the plasmid and to the amiRNA sequence. As shown in Fig. 37, we observed the expected band of 713bp in all the plants of T2 mutant lines 2, 3, 4, 30 and 32, that were used for next analysis. No bands were observed for the control lines Col-8 and the parental MutYH$^{-/-}$.

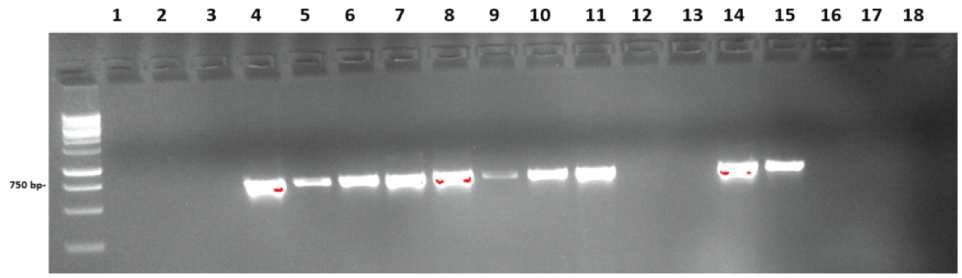

Fig. 37: pGWB5kdPOLL plasmid is present in T2 mutant lines 2, 3, 4, 30 and 32. Lanes 1 – 3 : T2 mutant line 1, plants n°1, 2, 3. Lanes 4 – 6 : T2 mutant line 2, plants n°1, 2, 3. Lanes 7, 8 : T2 mutant line 3, plants n° 2, 3. Lane 9: T2 mutant line 4, plant n°2. Lanes 10 – 11: T2 mutant line 30, plants n° 1, 2. Lanes 12 – 13: T2 mutant line 31, plants n° 1, 2. Lanes 14 – 15: T2 mutant line 32, plants n° 1, 2.Lane 16: Col-8. Lane 17: parental line MutYH$^{-/-}$. Lane 18: Control.

4.19 UV-B irradiation of T2 mutant lines AtPOLL^{Kd}

Healthy leaves were harvested from Col-8, parental MutYH$^{-/-}$ and AtPolλ^{Kd} T2 mutant lines 2 (plants n°1,2,3), 3 (plants n°2,3), 4 (plant n°2), 30 (plants n°1,2), 32 (plants n°1,2) and sterilized. Small pieces (4x4mm) were cut, in sterile conditions, from each leaf and put overnight on plates containing either *MS Medium + NAA* (May and Leaver 1993) or *MS Medium + BAP* (Sello et al. 2017) (see the Materials and methods section for details), to allow calli formation. Each plate was divided into three sections. Two sections always contained pieces of leaves from Col-8, parental MutYH$^{-/-}$, as control. In (Amoroso et al. 2011), plants were UV-B irradiated for 30min at 0.3 mW/cm2, corresponding to 2.9 J/m2/s, at 243 nm of wavelength. Similarly, we irradiated the plates for 27 minutes at 216nm. After the irradiation, plates were stored again at 25°C in the dark for about one month.

5. Discussion

Specialized DNA polymerases are involved in different DNA damage tolerance systems to maintain genome integrity, both in mammalian and plants. We focused our attention on the specialized DNA polymerases λ, β and η that have essential roles in various DNA repair or DNA damage tolerance pathways such as NHEJ, BER and TLS. NHEJ, during which Pol λ acts, allows the repair of DSBs. This pathway is of paramount importance for cells: unrepaired DSBs would result in apoptosis or senescence while mis-processing of DSBs can result in genomic instability and carcinogenesis (Davis and Chen 2013). BER, whose main actor is Pol β, deals with damages that do not distort DNA lesions, such as abasic sites, oxidised, deaminated and alkylated bases and SSBs. BER is important in relation to neurodegeneration, aging and cancer (Krokan and Bjørås, 2013; Jeppesen et al. 2011). TLS is the main DNA damage tolerance system, during which different DNA Pols act, mainly those belonging to Y-family (such as Pol η) but also to X-family (such as Pol λ). Perturbation of TLS polymerase activity may lead to accumulation of mutations in cells exposed to specific carcinogens (Makridakis and Reichardt, 2012). Another source of genomic insability is the persistence of ribonucleotides in the DNA (McElhinny et al. 2010a; Meroni et al. 2017), that can be incorporated both during replication and repair pathways. Moreover, misincorporated ribonucleotides are the most frequent lesions in the genome (Potenski and Klein 2014). Information regarding the ability of Pols λ, β and η to incorporate ribonucleotides opposite the different DNA lesions they deals with during TLS, was missing. Therefore, we performed a series of experiments in order to understand to which extent such Pols may bypass the various lesions by inserting ribonucleotides. In particular, we compared incorporation of ribonucleotides catalysed by these Pols opposite normal or damaged bases, under physiological concentrations of metal activators and nucleotides and in presence of accessory proteins, such as PCNA and PolDIp2. We also evaluated the effect of ribonucleotide incorporation on the subsequent steps of BER (in the case of 8-oxo-G lesion) or on the ability of RNase H2 enzyme to remove ribonucleotides inserted opposite canonical bases as well as opposite the lesions. Moreover, our research was extended to the characterization of BER pathway in plants, using *A. thaliana* as model organism.

One of the major DNA repair pathways is BER, acting both in resting and proliferating cells. Pols λ and β are responsible for gap-filling synthesis in this process. It was previously demonstrated that both Pols also participate in the 8-oxo-G TLS pathway (Maga et al. 2008). However, the contribution of BER to the incorporation of rNMPs into the genome was not fully understood. Therefore, we decided to investigate incorporation of rNMPs catalysed by Pols λ and β opposite normal or damaged bases under physiological concentrations of metal activators and nucleotides. Data obtained from previous studies already shown differences in sugar discrimination ability among these Pols (Brown and Suo 2011) but those experiments were performed in some cases with Mg^{2+} and in some others with Mn^{2+}, as well as using different substrates. So, we started by comparing Pols λ and β under identical conditions (i.e. in the presence of Mg^{2+} and on the same substrates) obtaining results that highlight clear differences in their sugar discrimination ability which agree with the previous studies. Pols λ and β showed, respectively, a sugar selectivity of 5,100–7,500 and of 1,690–3,400 for incorporation of rCMP opposite a G present in the DNA template, depending on the structure of the template itself (Tables 1 and 2). Previous studies revealed that rCMP/dCMP selectivity values were 4,000 and 2,000–8,000 for Pols λ and β, respectively (Nick McElhinny and Ramsden 2003; Brown and Suo 2011; Cavanaugh et al. 2010). While these results suggest that Pols λ and β can incorporate rNMPs opposite canonical DNA bases, it was not known so far whether these Pols could also incorporate rNMPs opposite oxidative DNA damages. We chose 8-oxo-G, a very frequent oxidative DNA lesion, to investigate this issue. Results obtained from Donigan *et al*. (Donigan et al. 2014) showed that Pol ι and, to a much lesser extent, Pol η, can bypass 8-oxo-G by incorporating rNMPs. Interestingly, we observed that the presence of an 8-oxo-G damage on the template strand significantly affected Pol λ selectivity for rNMP/dNMP: when Pol λ activity was tested on 1nt gap template, its preference of dCMP incorporation vs rCMP increased two-fold when 8-oxo-G was present. Its fidelity was, instead, not influenced, since its preference for rCMP incorporation over rAMP was similar to those of dCMP over dAMP. Previous studies showed that Pol λ is mainly used in MUTHY-dependent BER acting on 8-oxo-G:A, because of its higher efficiency in incorporating the correct dCMP instead of the incorrect dAMP opposite the lesion (Maga et al. 2008; Maga et al. 2007; van Loon and Hübscher 2009). Our results suggest that Pol λ also lowers the probability of incorporation of rNMPs opposite the damaged base. On the contrary, Pol β has a lower

selectivity for rCMP incorporation opposite 8-oxo-G than Pol λ (Table 2). Pol β can incorporate dAMP or dCMP opposite the lesion almost with the same efficiency (Maga et al. 2007). We found that when it acts on 1-nt gap template, mimicking a BER intermediate, it shows only 1.6-fold preference for dCMP vs dAMP incorporation, but 13-fold preference for rCMP incorporation than rAMP (Table 2). A possible explanation for this difference comes from crystal structures. In the crystal structure of the ternary complexes of Pol β with a (syn)8-oxo-G:(anti)dATP base pair, the oxidized guanine was accommodated in the enzyme active site in its syn conformation by a hydrogen bond between the 8-O of the guanine and the side chain of Arg283 (Batra et al. 2012). On the other hand, the structure of a ternary complex of Pol β with an incoming rCTP and an undamaged template showed that when a rNTP is accommodated into the enzyme's active site, a displacement of the sugar-phosphate backbone occurs and the 2'-OH of the ribose collides with the backbone carbonyl of Tyr271. Moreover, the hydroxyl group of this Tyr cannot form a hydrogen bond with the primer end base. The barrier could become stronger due structural rearrangements in the enzyme active site that take place to accommodate the 8-oxo-G base, which may exacerbate the unfavourable interactions of Tyr271 with the ribose sugar and the primer end, rendering stronger the steric gate (Cavanaugh et al. 2011). Anyway, crystal structures of Pol β in complex with an 8-oxo-G template and an incoming rNTP are needed to further clarify the molecular basis for this difference.

The experiments performed with extracts from cells defective in either Pol β or λ revealed that, after inhibition of Pols α, δ, ε and ζ by aphidicolin, Pol β was responsible for the majority of rCMP incorporation opposite 8-oxo-G while Pol λ did not contribute significantly to rCMP-mediated bypass of 8-oxo-G. This is in agreement with our kinetic data, showing that Pol λ discriminates against rCMP incorporation much more than Pol β (Tables 1 and 2). In proliferating cells, the majority of rNMPs incorporation occurs during DNA replication. Our *in vitro* data suggest that also DNA synthesis during DNA repair pathways of oxidative damages, among which the main one is BER, may be a source of rNMPs incorporation.

As shown in Table 6, we estimated the theoretical frequency of rCMP versus dCMP incorporation opposite a normal G or 8-oxo-G for three representative mammalian tissues, based on the selectivity values and on the known intracellular nucleotide concentrations (Traut 1994; Ferraro et al. 2010). In agreement with previously published data (Cavanaugh et al. 2010), Pol β may incorporate rCMP opposite a normal G with frequencies

about twofold higher than Pol λ (0.38–5.8% versus 0.23–2.6%, respectively). Moreover, under physiological rCTP/dCTP ratios, Pol β may incorporate rCMP opposite 8-oxo-G fourfold more frequently than Pol λ. Our results indicated that Pol λ could bypass an 8-oxo-G with either rCMP or rAMP, depending on the template. However, its high discrimination against rNMPs incorporation and its preference for dCMP over dAMP, ensures that in most cases dCMP incorporation will occur. Pol β, on the other hand, having a lower selectivity for rNMPs, can bypass 8-oxo-G lesion also inserting rCMP (wrong sugar/right base), but at least excluding in most cases rAMP (wrong sugar/wrong base). This could be relevant since the presence of rAMP opposite 8-oxo-G strongly inhibits MutYH-initiated BER, while incorporation of rCMP would result in a 8-oxo-G:rC base pair, which can be still repaired by the Ogg1 glycosylase, even if with a lower rate (Fig. 21A,B). It has been shown (Cilli et al. 2015) that insertion of rNMPs opposite 8-oxo-G in the context of CAG triplet repeats sequences, can negatively affect its subsequent repair. Moreover, it has been found that *Schizosaccharomyces pombe* RNase H2 can remove rCMP incorporated opposite 8-oxo-G (Albertella et al. 2005), while *E. coli* RNase H2 in the presence of MutYH removed less efficiently rAMP opposite 8-oxo-G (Gasparutto et al. 2002). These results suggest that the RER pathway can face the deleterious effects of rNMPs accumulation during DNA repair mechanisms, but possibly with some loss of efficiency when rNMPs are incorporated opposite an oxidize base.

Another aspect that should be taken into account concerns accumulation of rNMPs in the brain that, together with the increase in the amount of oxidative DNA lesions, have been linked to neurodegeneration (Chen et al. 2006; Srivastava et al. 2015). Since Pol β is the major Pol expressed in post-mitotic neurons, which are cells with a low dNTPs levels and that undergo severe oxidative stress, its ability to misincorporate rNTPs may have a physiological relevance in enhancing the deleterious effects of DNA oxidation in the brain.

Tissue	rCTP/dCTP ratio	Template G *f*(rCTP/dCTP)*x10^{-3}	Template 8-oxo-G *f*(rCTP/dCTP)*x10^{-3}
Polλ			
Skin fibroblasts	18**	2.3	1.3
Lymphocytes	200***	26	14
Liver	13***	1.7	0.9
Polβ			
Skin fibroblasts	18**	5.2	5.6
Lymphocytes	200***	58	62
Liver	13***	3.8	4

Table 6: Estimated misincorporation frequencies of rCTP versus dCTPs opposite 8-oxo-G or a normal G, for DNA polymerases λ and β under physiological dNTPs/rNTPs concentrations.

* Frequencies of incorporation for each ribo-/deoxy-nucleotide substrate pair were calculated according to the Cornish–Bowden relationship: *f*(rCTP/dCTP) = (k_{cat}/K_mrCTP)/(k_{cat}/K_mdCTP)(rCTP)/(dCTP) using the values from Tables 1 and 2 for the 1-nt gap and from refs (Traut 1994; Ferraro et al. 2010).

** The rCTP and dCTP concentrations have been taken from ref. (Ferraro et al. 2010).

*** The rCTP and dCTP concentrations have been taken from ref. (Traut 1994).

In the second part of this work, we focused our attention on human Pol η. We evaluated the possible consequences of insertion of rNMPs opposite five different lesions (8-oxo-G, 8-met-G, 3met-C, cis-PtGG and AP site) and their subsequent cleavage by human RNase H2. Our results indicate that human Pol η behaves differently from Pols β and λ, that are able to incorporate one or two rNMPs, but it behaves similarly to the X-family Pol μ (Nick McElhinny and Ramsden 2003; Martin et al. 2013) or the Y-family Pol ι (Donigan et al. 2014). Indeed, we found that human Pol η has robust DNA-dependent RNA polymerase activity at physiological concentrations of Mg^{2+} and rNMPs both on undamaged DNA or during TLS. The long RNA chains synthesized may be physiologically relevant for the cells since replicative Pols δ and ε are not able to bypass more than few consecutive rNMPs (Clausen et al. 2013). Lazzaro *et al.* demonstrated that accumulation of rNMPs in *S. cerevisiae* genome influences negatively replication and has toxic effects, especially when genes encoding RNase H2 and RNase H1 are inactivated. When the gene encoding yeast Pol η was deleted, cells exhibited less negative effects, even in the absence of RNase H-2 and -1 (Lazzaro et al. 2012). Overall, these findings suggest that Pol η may cause accumulation of RNA chains in cells where RNase H-2 and -1 are not present.

We found that human Pol η has the ability to bypass some of the lesions tested incorporating rNMPs. In particular, Pol η inserts rCMP opposite 8-

oxo-G and 8-met-G. No incorporation was observed against 3-met-C and AP site. Moreover, we observed that sugar selectivity of human Pol η is influenced by the type of damage. While dCMP vs. rCMP preference for incorporation opposite 8-met-G was similar to the one opposite a normal G (693 vs. 400, respectively, Table 3), when it encounters 8-oxo-G lesion, it incorporates more efficiently dCMP than rCMP (about 1400, Table 3). Also the fidelity of 8-oxo-G bypass was increased: the preference for rCMP vs. rAMP incorporation was 8.9, while the one for dCMP vs. dAMP was 3.3 (Table 3). Another study also found a similar increase in fidelity for the bypass of 8-oxo-G with rNMPs by human Pol η (Su et al. 2016).

The other lesion considered was 8-Met-G, a major alkylation product of deoxyguanosine that has miscoding properties (Kohda et al. 1996). Up to now, no human glycosylase able to remove this lesion has been identified (Gasparutto et al. 2002). Thus, cells may rely mainly on the TLS pathway for its tolerance. However, the capability of human Pols to perform TLS over 8-met-G is still mostly unknown. This modification occurs at the C-8 of the purine ring of a guanine, in the same position as in the 8-oxo-G, thus offering an interesting opportunity of comparison of the effects of the two lesions. From our experiments, it emerged that human Pol η bypasses 8-met-G misincorporating diverse dNMPs, or inserting rCMP. Efficient elongation past 8-met-G was observed with both dNMP and rNMP insertion. As far as we know, this is the first indication of a human DNA polymerase that can perform TLS past 8-met-G lesion.

Pol η is also the major Pol involved in the bypass of Cis-Pt adducts (Vaisman et al. 2000) caused by the anticancer drug cisplatin. When we tested the ability of human Pol η to perform TLS on cisPt-GG using rNMPs, we found that it can incorporate rCMP opposite the 3'-G of the lesion and then inserting a dCMP opposite the 5'-G. No rCMP incorporation occurred opposite the 5'-G, either starting from a rCMP- or a dCMP-terminated primer. Crystal structures of Pol η in complex with a cis-PtGG and an incoming dCTP (Alt et al. 2007; Zhao et al. 2012) clearly show that incorporation opposite the 5'-G requires structural rearrangements. The 5'-G of the adduct can adopt either an inactive "open" conformation or a catalytically active "stacked" conformation. It is possible that the presence of a 2'-OH group in the sugar of the incoming nucleotide cannot be accommodated opposite the 5'-G in the stacked conformation.

RNase H2 is the main enzyme that processes rNTPs incorporated into DNA. Since very little is known about the capability of human RNase H2 to remove rNMPs incorporated opposite DNA lesions, we investigated the ability of the human recombinant enzyme to remove rNMPs

misincorporated opposite the five lesions under investigation.
When rNTPs are paired to their complementary undamaged dNTPs, RNase H2 displayed a preference of their removal that follow the order rA>rU>rC>rG. There is not a clear explanation for such behavior. A possible explanation comes from the crystal structure of *Thermotoga maritima* RNase H2 in complex with DNA/RNA substrate (Rychlik et al. 2010), from which it emerges that, at the level of the DNA/RNA junction, cleavage requires structural rearrangement of the sugar-phosphate backbone. Possibly, such local backbone distortion, may be energetically more favored when the rNMP to be cleaved is part of a less stable rA:dT or rU:dA with respect to rC:dG or rG:dC pair. The preferential activity of RNase H2 may contribute to persistence of rNMPs in genome. Moreover, the enzyme exhibited a difference in removing rCMP opposite different type of lesions. E.g. RNase H2 is very efficient in processing rCMP opposite 8-met-G but not when the ribonucleotide pairs 8-oxo-G or the 3'-G of cisPt-GG crosslink. Interestingly, this order of preference is paralleled by Pol η, that prefers to incorporate a rCMP opposite 8-met-G than opposite 8-oxo-G or cisPt-GG. Therefore, a sort of mechanism of compensation between rNMPs incorporated by Polη and their removal by RNase H2 may exist. On the contrary, incorporation of rCMP opposite 8-oxo-G or cis-PtGG may lead to a substantial delay in their processing by RNase H2.
rNMPs incorporation during TLS can also be influenced by auxiliary proteins. It has been demonstrated that PCNA interacts with both Pol η and RNase H2, thus recruiting them at DNA repair foci (Chon et al. 2009) (Bubeck et al. 2011; Kannouche et al. 2004). However, we did not observe any enhancement of rNMP incorporation by Pol η or of rNMP cleavage by RNase H2 in presence of PCNA. We also tested PolDIP2, a recently identified auxiliary factor that stimulates the activity of Pols λ and η (Maga et al. 2013). We found that PolDIp2 significantly stimulated rNMP incorporation by Pol η on both undamaged DNA and during TLS of 8-oxo-G, 8-met-G and cis-PtGG. It has been shown PCNA can functionally interact with both Pol η and PolDIP2 (Maga et al. 2013; Tissier et al. 2010). Therefore, our *in vitro* data suggest that Pol η and PCNA may compete for their binding to PolDIP2 in a mutually exclusive way, a point that requires further investigation.

As all living organisms, also plant cellular metabolism normally generates reactive oxygen species (ROS), including superoxide anion radical (O^{2-}), hydrogen peroxide (H_2O_2) and hydroxyl radical (•OH). ROS are, indeed, byproducts of metabolic reactions taking place at level of plasma membrane

and in different cellular compartments such as peroxisomes, plastids and mitochondria (Foyer and Noctor 2003; Bailey-Serres and Mittler 2006; Sharma et al. 2012). Various types of environmental stress, including UV-B, irradiation, adverse conditions and pathogens can lead to an alteration of cellular homeostasis in plants and, in turn, an increase in ROS production. At high concentrations, ROS are very dangerous for cells (Amoroso et al. 2008). They can cause oxidation of DNA bases, which may result in stalling of Pols at replicative fork or lead to mutations by mispairing if not properly corrected by DNA repair mechanisms. Oxidative DNA lesions, including 8-oxo-G, are mainly repaired trough Base Excision Repair (BER) pathway. In humans, when in the dsDNA 8-oxo-G lesion is present in front of a C, the 8-Oxoguanine glycosylase (Ogg1) is responsible for the excision of the damaged base, thus initiating a canonical Short Patch (SP)-BER, that leads to restoration of the original C:G base pair. If Ogg1 fails to repair all 8-oxo-G lesions before the beginning of replication, A residues will be incorrectly inserted by the majority of DNA Pols. MutYH glycosylase, the homologue of *E. coli* MutY, is devoted to recognition and removal of misincorporated A residues (Markkanen et al. 2013). Different DNA glycosylases have been identified and characterized in *A. thaliana*; including AtOgg1 and AtMutYH. MutYH-dependent BER requires the action of a TLS Pol, able to insert a C residue opposite 8-oxo-G lesion. In humans, Pol λ interacts with PCNA and RPA, and it is considered the TLS Pol devoted to high-fidelity bypass of 8-oxo-G (Amoroso et al. 2011; Crespan et al. 2016). In higher plants, family X of DNA polymerases includes only POLL, which shares 30% of homology with its human homologue. On the other hand, plants possess two genes encoding for two PCNA proteins. (Amoroso et al. 2011). *In vitro* assays showed that AtPOLL and PCNA2 interacts during TLS bypass of 8-oxo-G. The physical interaction between the two proteins was also confirmed *in vivo*. Plants overexpressing or knockdown for AtPOLL were also obtained and the physiological responses investigated. In particular, plants overexpressing AtPOLL showed a delayed growth, while the knockdown plants had early flowering. UV-B irradiation, that is known to contribute to ROS production, caused increasing in AtPOLL transcripts, both in seeds and leaves. Overall, the results suggested that *A. thaliana* possesses a TLS pathway in which, similarly to humans, AtPOLL interacts with AtPCNA2 and AtRPA, thus supporting the essential role of Pol λ in oxidative DNA-damage tolerance pathway in all eukaryotes (Amoroso et al. 2011). However, the mechanism of SP-BER in plants has not been fully elucidated yet and the proteins involved in such pathway have not been fully characterized. We therefore decided to focus our attention on the

glycosylases AtOgg1 and AtMutYH. Recombinant AtOgg1 has been previously expressed in a bacterial system and purified. Glycosylase/lyase assays have been then performed with recombinant AtOgg1, AtPCNA1 and AtPCNA2 on different DNA oligonucleotides substrates. Moreover, various unsuccessful attempts of expressing AtMutYH in *E.coli* cells have been performed (Piccinelli, Cella, Maga, unpublished data. Experimental Bach. Sci. thesis of Giovanni Piccinelli). Similarly to hMutYH (Gu and Lu 2001) (Goto et al. 2010), expression of AtMutYH in *E. Coli* showed problems of toxicity and solubility. Therefore, we decided to express AtMutYH in other two peculiar *E.coli* strains, C43 and DE3pLys, which are optimized for expression of toxic proteins. However, also in this case, screening of different protein expression conditions revealed no protein expression also in these strains. We also attempted to clone *AtMutYH* gene in pET30a(+) empty vector, already present in our laboratory. Unfortunately, for unknown reasons, cloning failed. Since we have not been able, so far, to express and purify recombinant AtMutHY, a future perspective could consist in changing the expression system and so the host organism. A possible option could be to clone the AtMutYH synthetic gene in a chloroplast transformation vector in order to transform tobacco plant cells. An advantage of chloroplast transformation is the higher level of expression of the gene of interest and so the higher level of protein production (Verma and Daniell 2007). Moreover, the expression of a plant gene in tobacco cells should result in less toxicity.

To better characterize the SP-BER pathway in plants we decided to investigate plant cells behaviour under stressful conditions. We aimed at silencing AtPOLL in a cellular background deficient for *AtOgg1* or for *AtMutYH* performing *A. tumefaciens*-mediated transformation. To this purpose, *A. thaliana* cell suspension cultures wt (Col-8) or knockout for *AtOgg1* or for *AtMutYH* genes have been obtained as described in the Materials and methods sections. Once reached an appropriate volume and density, cultures were co-cultivated with *A. tumefaciens* previously engineered with pGWB5kdPOLL plasmid, carrying the cassette that expresses an amiRNA to silence AtPOLL. Co-cultivations grew quite slowly, as expected for a cellular background lacking essential proteins involved in fundamental repair pathways. Co-cultivations were propagated weekly, for more than three months. Even though the amount of starting material was low, we decided to extract proteins, at least to check whether we managed to effectively silence AtPOLL. Unfortunately immunoblotting analysis revealed no signal of extracted proteins. Since we thought that the main problems could be related to the quantity and the density of co-

cultivations, we repeated the procedure starting from higher quantities of cultures, propagating them for more than five months. However, also in this case, we were not able to extract enough proteins for further analysis.
Since this route was unsuccessful, our collaborators at the Institute of Plant Sciences Paris Saclay, performed stable transformation of T1 AtMutYH^{KO} mutants, utilizing our pGWB5kdPOLL plasmid, by floral dipping (Clough and Bent 2008). With this procedure, *Arabidopsis* transformants should be obtained at a high rate (0.5–3% of all progeny seed) (Clough and Bent 2008). T2 seeds were harvested. In order to verify whether the transformation, and so the silencing of AtPolλ occurred, we grew T2 mutant plants, extracted DNA and proteins from leaves and performed PCR reactions and Western blot analysis for selection, being able to identify AtMutYH^{KO} and AtPOLL^{Kd} plants. Since UV-B irradiation increases AtPOLL expression we UV-B irradiated pieces of leaves of plants that are deficient for both MutYH glycosylase and Polλ. We expect to observe differences in calli de-differentiation. Unfortunately, we were not able to observe any calli formation. This problem was probably related to media composition and new experiments in different conditions are now scheduled.

6. Conclusions and perspectives

In conclusion, our data support the notion that DNA repair can be a source of rNMPs accumulation, potentially leading to genomic instability. However, future work will be required to determine the precise impact of these events on cells. For example, increased amount of oxidative DNA lesions and accumulation of rNMPs in the brain have been connected to neurodegeneration (Iyama and Wilson 2013). The consequences of TLS with the use of rNMPs in determined by at least three factors: 1) the intrinsic sugar selectivity of Pols (e.g. Pol λ, β or η); 2) the relative Pol levels and/or their selective access to the lesion and 3) the intervention of auxiliary proteins (e.g. PolDIp2). Insertion of rNMPs opposite damaged bases may impact DNA repair in two ways. First, they can affect the work of specialized DNA glycosylases, as shown for 8-oxo-G lesion. In this case, our results indicate that Pols λ, β and η have been shaped by evolution to lower the probability of inserting rAMP opposite the lesion, which would represent the most dangerous situation, due to the poor ability of the DNA glycosylase MUTYH to process the resulting mispair. Second, our data also indicate that rNMPs incorporation toward different lesions can reduce the efficiency of their removal by RNase H2, depending on the type of lesion, thus effectively delaying RER and consequently causing replication stress. However, this event may also give more time for the excision repair systems to remove the damaged bases in front of the inserted rNMPs, which then could be efficiently addressed by RER. Moreover, our findings also suggest a potential role of Pol η in synthesizing long stretches of RNA, which may increase the toxicological consequences of rNMP incorporation in cells lacking RNase H2, for example in AGS patients.

Previous findings (Amoroso et al. 2011) confirmed that Pol λ likely plays a fundamental role in the bypass of 8-oxo-G lesion also in plants. Our attempts regarding a better characterization of proteins involved in SP-BER pathway in plants, in particular of AtOgg1 and AtMutYH glycosylases, have not been exhaustive. Further efforts will be required both for the *in vitro* reconstruction of *A. thaliana* BER pathway and for a comprehensive phenotypic analysis of *A. thaliana* mutants.

References

Albertella, M. R., **C. M. Green**, **A. R. Lehmann**, **M. J. O'Connor**. A Role for Polymerase η in the Cellular Tolerance to Cisplatin-Induced Damage. *Cancer Research.* 2005; 65:9799-9806.

Alt, A., K. Lammens, C. Chiocchini, A. Lammens, J. C. Pieck, D. Kuch, K.-P. Hopfner, and T. Carell. Bypass of DNA Lesions Generated During Anticancer Treatment with Cisplatin by DNA Polymerase η. *Science*. 2007, 318:967-970.

Amoroso, A., L. Concia, C. Maggio, C. Raynaud, C. Bergounioux, E. Crespan, R. Cella, and G. Maga. Oxidative DNA Damage Bypass in Arabidopsis thaliana Requires DNA Polymerase λ and Proliferating Cell Nuclear Antigen 2. *The Plant Cell*. 2011, 23:806.

Amoroso, A., E. Crespan, U. Wimmer, U. Hubscher, and G. Maga. DNA Polymerases and Oxidative Damage: Friends or Foes? *Current Molecular Pharmacology.* 2008, 1:162-170.

Aschner, J. L., and M. Aschner. Nutritional aspects of manganese homeostasis. *Molecular Aspects of Medicine.* 2008, 26:353-362.

Bailey-Serres, J., and R. Mittler. The Roles of Reactive Oxygen Species in Plant Cells. *Plant Physiology.* 2006, 141:311.

Batra, V. K., D. D. Shock, W. A. Beard, C. E. McKenna, and S. H. Wilson. Binary complex crystal structure of DNA polymerase β reveals multiple conformations of the templating 8-oxoguanine lesion. *Proceedings of the National Academy of Sciences of the United States of America*. 2012, 109:113-118.

Beard, W. A., and S. H. Wilson. Structural design of a eukaryotic DNA repair polymerase: DNA polymerase β. *Mutation Research/DNA Repair.* 2000, 460:231-244.

Beard, W. A., and S. H. Wilson. Structure and Mechanism of DNA Polymerase β. *Chemical Reviews*. 2006, 106:361-382.

Bebenek, K., L. C. Pedersen, and T. A. Kunkel. Structure–Function Studies of DNA Polymerase λ. *Biochemistry*. 2014, 53:2781-2792.

Bergoglio, V., E. Ferrari, U. Hübscher, C. Cazaux, and J.-S. Hoffmann. DNA Polymerase β can Incorporate Ribonucleotides during DNA Synthesis of Undamaged and CPD-damaged DNA. *Journal of Molecular Biology*. 2003, 331:1017-1023.

Bertocci, B., A. De Smet, J.-C. Weill, and C.-A. Reynaud. Nonoverlapping Functions of DNA Polymerases Mu, Lambda, and Terminal Deoxynucleotidyltransferase during Immunoglobulin V(D)J Recombination In Vivo. *Immunity.* 2006, 25:31-41.

Bienko, M., C. M. Green, S. Sabbioneda, N. Crosetto, I. Matic, R. G. Hibbert, T. Begovic, A. Niimi, M. Mann, A. R. Lehmann, and I. Dikic. Regulation of Translesion Synthesis DNA Polymerase η by Monoubiquitination. *Molecular Cell*. 2010, 37:396-407.

Bridge, G., S. Rashid, and S. Martin. DNA Mismatch Repair and Oxidative DNA Damage: Implications for Cancer Biology and Treatment. *Cancers.* 2014, 6:1597.

Brown, D. I., B. Lassègue, M. Lee, R. Zafari, J. S. Long, H. I. Saavedra, and K. K. Griendling. Poldip2 Knockout Results in Perinatal Lethality, Reduced Cellular Growth and Increased Autophagy of Mouse Embryonic Fibroblasts. *PLoS ONE.* 2014, 9:e96657.

Brown, J. A., and Z. Suo. Unlocking the Sugar 'Steric Gate' of DNA Polymerases. *Biochemistry*. 2011, 50:1135-1142.

Bubeck, D., M. A. M. Reijns, S. C. Graham, K. R. Astell, E. Y. Jones, and A. P. Jackson. PCNA directs type 2 RNase H activity on DNA replication and repair substrates. *Nucleic Acids Research.* 2011. 39:3652-3666.

Caldecott, K. W. Ribose - An Internal Threat to DNA. *Science.* 2014, 343 :260-261.

Cavanaugh, N. A., W. A. Beard, V. K. Batra, L. Perera, L. G. Pedersen, and S. H. Wilson. Molecular Insights into DNA Polymerase Deterrents for Ribonucleotide Insertion. *Journal of Biological Chemistry.* 2011, 286:31650-31660.

Cavanaugh, N. A., W. A. Beard, and S. H. Wilson. DNA Polymerase β Ribonucleotide Discrimination: INSERTION, MISINSERTION, EXTENSION, AND CODING. *Journal of Biological Chemistry.* 2010, 285:24457-24465.

Cerritelli, S. M., and R. J. Crouch. Ribonuclease H: the enzymes in eukaryotes. *The FEBS Journal.* 2009, 276:1494-1505.

Chen, Y.-w., J. E. Cleaver, F. Hanaoka, C.-f. Chang, and K.-m. Chou. A Novel Role of DNA Polymerase η in Modulating Cellular Sensitivity to Chemotherapeutic Agents. *Molecular Cancer Research.* 2006, 4:257-265.

Chon, H., A. Vassilev, M. L. DePamphilis, Y. Zhao, J. Zhang, P. M. Burgers, R. J. Crouch, and S. M. Cerritelli. Contributions of the two accessory subunits, RNASEH2B and RNASEH2C, to the activity and properties of the human RNase H2 complex. *Nucleic Acids Research*. 2009, 37:96-110.

Chou, K. DNA Polymerase Eta and Chemotherapeutic Agents. *Antioxidants & Redox Signaling.* 2011, 14:2521-2529.

Cilli, P., A. Minoprio, C. Bossa, M. Bignami, and F. Mazzei. Formation and Repair of Mismatches Containing Ribonucleotides and Oxidized Bases at Repeated DNA Sequences. *Journal of Biological Chemistry*. 2015, 290:26259-26269.

Clausen, A. R., M. S. Murray, A. R. Passer, L. C. Pedersen, and T. A. Kunkel. Structure–function analysis of ribonucleotide bypass by B family DNA replicases. *Proceedings of the National Academy of Sciences.* 2013, 110:16802-16807.

Clough, S. J., and A. F. Bent. Floral dip: a simplified method for Agrobacterium -mediated transformation of Arabidopsis thaliana. *The Plant Journal.* 2008, 16:735-743.

Cook, M. S., M. D. Evans, M. Dizdaroglu, and J. Lunec. Oxidative DNA damage: mechanisms, mutation, and disease. *The FASEB Journal.* 2003, 17:1195-1214.

Crespan, E., U. Hübscher, and G. Maga. Expansion of CAG triplet repeats by human DNA polymerases λ and β in vitro, is regulated by flap endonuclease 1 and DNA ligase 1. *DNA Repair*. 2015, 29:101-111.

Crespan, E.; Czabany, T.; Maga, G.; Hübscher, U. Microhomology-mediated DNA strand annealing andelongation by human DNA polymerases λ and β on normal and repetitive DNA sequences. *Nucl. Acids Res.* 2012, 40: 5577–5590.

David, S. S., V. L. O'Shea, and S. Kundu. Base-excision repair of oxidative DNA damage. *Nature.* 2007, 447:941.

Davis, A. J., Chen, D. J. DNA double strand break repair via non-homologous end-joining. *Translational cancer research*. 2013,3:130-143.

Dianov, G. L., and U. Hübscher. Mammalian Base Excision Repair: the Forgotten Archangel. *Nucleic Acids Research*. 2013, 41:3483-3490.

Donigan, K. A., M. P. McLenigan, W. Yang, M. F. Goodman, and R. Woodgate. The Steric Gate of DNA Polymerase ι Regulates Ribonucleotide Incorporation and Deoxyribonucleotide Fidelity. *Journal of Biological Chemistry.* 2014, 289:9136-9145.

Doyle, J. J. Isolation of Plant DNA from Fresh Tissue. *Focus*. 1990, 12:13-15.

Eder, P. S., R. Y. Walder, and J. A. Walder. Substrate specificity of human RNase H1 and its role in excision repair of ribose residues misincorporated in DNA. *Biochimie*. 1993, 75:123-126.

Ferraro, P., E. Franzolin, G. Pontarin, P. Reichard, and V. Bianchi. Quantitation of cellular deoxynucleoside triphosphates. *Nucleic Acids Research*. 2010, 38:e85-e85.

Fortini, P., and E. Dogliotti. Base damage and single-strand break repair: Mechanisms and functional significance of short- and long-patch repair subpathways. *DNA Repair*. 2007, 6:398-409.

Foyer, C. H., and G. Noctor. Redox sensing and signalling associated with reactive oxygen in chloroplasts, peroxisomes and mitochondria. *Physiologia Plantarum.* 2003, 119:355-364.

Frank, E. G., J. P. McDonald, K. Karata, D. Huston, and R. Woodgate. A strategy for the expression of recombinant proteins traditionally hard to purify. *Analytical biochemistry*. 2012, 429:132-139.

Frank, E. G., and R. Woodgate. Increased Catalytic Activity and Altered Fidelity of Human DNA Polymerase ι in the Presence of Manganese. *Journal of Biological Chemistry.* 2007, 282:24689-24696.

Frit, P., Barboule, N., Yuan, Y., Gomez, D., and Calsou, P. Alternative end-joining pathway(s): Bricolage at DNA breaks. *DNA repair.*2014, 17:81-97.

Furrer, A., and B. van Loon. Handling the 3-methylcytosine lesion by six human DNA polymerases members of the B-, X- and Y-families. *Nucleic Acids Research.* 2014, 42:553-566.

Gamborg, O. L., R. A. Miller, and K. Ojima. Nutrient requirements of suspension cultures of soybean root cells. *Experimental Cell Research.* 1968, 50:151-158.

Gasparutto, D., C. Dhérin, S. Boiteux, and J. Cadet. Excision of 8-methylguanine site-specifically incorporated into oligonucleotide substrates by the AlkA protein of Escherichia coli. *DNA Repair*. 2002, 1:437-447.

Ghodgaonkar, Medini M., F. Lazzaro, M. Olivera-Pimentel, M. Artola-Borán, P. Cejka, Martin A. Reijns, Andrew P. Jackson, P.

Plevani, M. Muzi-Falconi, and J. Jiricny. Ribonucleotides Misincorporated into DNA Act as Strand-Discrimination Signals in Eukaryotic Mismatch Repair. *Molecular Cell.* 2013, 50:323-332.

Gill, S. S., and N. Tuteja. Reactive oxygen species and antioxidant machinery in abiotic stress tolerance in crop plants. *Plant Physiology and Biochemistry.* 2010, 48:909-930.

Gosavi, R. A., A. F. Moon, T. A. Kunkel, L. C. Pedersen, and K. Bebenek. The catalytic cycle for ribonucleotide incorporation by human DNA Pol λ. *Nucleic Acids Research.* 2012, 40:7518-7527.

Goto, M., K. Shinmura, Y. Nakabeppu, H. Tao, H. Yamada, T. Tsuneyoshi, and H. Sugimura. Adenine DNA glycosylase activity of 14 Human MutY homolog (MUTYH) variant proteins found in patients with colorectal polyposis and cancer. *Human Mutation*. 2010, 31:E1861-E1874.

Gregory, M. T., G. Y. Park, T. C. Johnstone, Y.-S. Lee, W. Yang, and S. J. Lippard. Structural and mechanistic studies of polymerase η bypass of phenanthriplatin DNA damage. *Proceedings of the National Academy of Sciences of the United States of America.* 2014, 111:9133-9138.

Gu, Y., and A. L. Lu. Differential DNA recognition and glycosylase activity of the native human MutY homolog (hMYH) and recombinant hMYH expressed in bacteria. *Nucleic Acids Research.* 2001, 29: 2666-2674.

Guillam, T. A., Bailey, L. J., Brissett, N. C., Doherty, A. J. PolDIP2 interacts with human PrimPol and enhances its DNA polymerase activities. *Nucleic Acids Research.* 2016, 44: 3317-3329.

Haracska, L., R. E. Johnson, I. Unk, B. Phillips, J. Hurwitz, L. Prakash, and S. Prakash. Physical and Functional Interactions of Human DNA Polymerase η with PCNA. *Molecular and Cellular Biology*. 2001. 21:7199.

Hasanuzzaman, M., K. Nahar, T. I. Anee, and M. Fujita. Glutathione in plants: biosynthesis and physiological role in environmental stress tolerance. *Physiology and Molecular Biology of Plants*. 2017. 23 :249-268.

Hovatter, K. R., and H. G. Martinson. Ribonucleotide-induced helical alteration in DNA prevents nucleosome formation. *Proceedings of the National Academy of Sciences of the United States of America*. 1987, 84:1162-1166.

Hübscher, U., and G. Maga. DNA replication and repair bypass machines. *Current opinion in chemical biology*. 2011, 15:627-635.

Hübscher, U., G. Maga, and S. Spadari. Eukaryotic DNA Polymerases. *Annual Review of Biochemistry.* 2002, 71:133-163.

Iwanga, A., Ouchida, M., Miyazaki, K., Hori, K., Mukai, T. Functional mutation of DNA polymerase β found in human gastric cancer – inability of the base excision repair in vitro. *Mutation Research/DNA Repair.* 1999, 2:121-128.

Iyama, T., and D. M. Wilson. DNA repair mechanisms in dividing and non-dividing cells. *DNA Repair.* 2013, 12:620-636.

Jeong, H.-S., P. S. Backlund, H.-C. Chen, A. A. Karavanov, and R. J. Crouch. RNase H2 of Saccharomyces cerevisiae is a complex of three proteins. *Nucleic Acids Research.* 2004, 32:407-414.

Jeppesen, D. K., Bohr, V. A. Stevnsner, T. DNA repair deficiency in neurodegeneration. *Progress in neurobiology*. 2011, 2:166-200.

Joyce, C. M. Choosing the right sugar: How polymerases select a nucleotide substrate. *Proceedings of the National Academy of Sciences of the United States of America*. 1997, 94:1619-1622.

Kannouche, P., B. C. Broughton, M. Volker, F. Hanaoka, L. H. F. Mullenders, and A. R. Lehmann. Domain structure, localization, and function of DNA polymerase η, defective in xeroderma

pigmentosum variant cells. *Genes & Development*. 2001, 15:158-172.

Kannouche, P. L., J. Wing, and A. R. Lehmann. Interaction of Human DNA Polymerase η with Monoubiquitinated PCNA. *Molecular Cell*. 2004,14:491-500.

Kohda, K., H. Tsunomoto, Y. Minoura, K. Tanabe, and S. Shibutani. Synthesis, Miscoding Specificity, and Thermodynamic Stability of Oligodeoxynucleotide Containing 8-Methyl-2‘-deoxyguanosine. *Chemical Research in Toxicology*. 1996, 9:1278-1284.

Krokan, H. E., Bjørås, M. Base excision repair. *Cold Spring Harbor perspectives in biology*. 2013, 4: a012583-a012583.

Lang, T.; Maitra, M.; Starcevic, D.; Li, S.X.; Sweasy, J.B. A DNA polymerase β mutant from colon cancer cells induces mutations. *Proc. Natl. Acad. Sci.* 2004, 101:6074–6079.

Lazzaro, F., D. Novarina, F. Amara, Danielle L. Watt, Jana E. Stone, V. Costanzo, Peter M. Burgers, Thomas A. Kunkel, P. Plevani, and M. Muzi-Falconi. RNase H and Postreplication Repair Protect Cells from Ribonucleotides Incorporated in DNA. *Molecular Cell*. 2012, 45:99-110.

Lieber, M.R. The mechanism of double-strand DNA break repair by the nonhomologous DNA end joining pathway. *Annu. Rev. Biochem.* 2010, 79:181–211.

Lindsey, B. E., L. Rivero, C. S. Calhoun, E. Grotewold, and J. Brkljacic. Standardized Method for High-throughput Sterilization of Arabidopsis Seeds. *Journal of Visualized Experiments : JoVE.* 2017, 128:56587.

Lujan, S. A., J. S. Williams, A. R. Clausen, A. B. Clark, and T. A. Kunkel. Evidence that ribonucleotides are signals for mismatch repair of leading strand replication errors. *Molecular Cell*. 2013, 50 :437-443.

Maga, G., E. Crespan, E. Markkanen, R. Imhof, A. Furrer, G. Villani, U. Hübscher, and B. van Loon. DNA polymerase δ-interacting protein 2 is a processivity factor for DNA polymerase λ during 8-oxo-7,8-dihydroguanine bypass. *Proceedings of the National Academy of Sciences of the United States of America.* 2013, 110 :18850-18855.

Maga, G., E. Crespan, U. Wimmer, B. van Loon, A. Amoroso, C. Mondello, C. Belgiovine, E. Ferrari, G. Locatelli, G. Villani, and U. Hübscher. Replication protein A and proliferating cell nuclear antigen coordinate DNA polymerase selection in 8-oxo-guanine repair. *Proceedings of the National Academy of Sciences.* 2008, 105 :20689-20694.

Maga, G., G. Villani, E. Crespan, U. Wimmer, E. Ferrari, B. Bertocci, and U. Hübscher. 8-oxo-guanine bypass by human DNA polymerases in the presence of auxiliary proteins. *Nature.* 2007, 447:606.

Makarova, A. V., S. A. N. McElhinny, B. E. Watts, T. A. Kunkel, and P. M. Burgers. Ribonucleotide incorporation by yeast DNA polymerase ζ. *DNA Repair*. 2014, 18:63-67.

Makridakis, N. M., Reichardt, J. K. V. Translesion DNA polymerases and cancer. *Frontiers in genetics*. 2012, 3:174-174.

Markkanen, E. Not breathing is not an option: How to deal with oxidative DNA damage. *DNA Repair*. 2017, 59:82-105.

Markkanen, E., J. Dorn, and U. Hübscher. MUTYH DNA glycosylase: the rationale for removing undamaged bases from the DNA. *Frontiers in Genetics.* 2013, 4.

Marteijn, J. A., H. Lans, W. Vermeulen, and J. H. J. Hoeijmakers. Understanding nucleotide excision repair and its roles in cancer and ageing. *Nature Reviews Molecular Cell Biology*. 2014, 15:465.

Martin, M. J., M. V. Garcia-Ortiz, V. Esteban, and L. Blanco. Ribonucleotides and manganese ions improve non-homologous end

joining by human Polμ. *Nucleic Acids Research.* 2013, 41:2428-2436.

May, M. J., and C. J. Leaver. Oxidative Stimulation of Glutathione Synthesis in Arabidopsis thaliana Suspension Cultures. *Plant Physiology*. 1993, 103:621-627.

Meroni, A., E. Mentegari, E. Crespan, M. Muzi-Falconi, F. Lazzaro, and A. Podestà. The Incorporation of Ribonucleotides Induces Structural and Conformational Changes in DNA. *Biophysical Journal*. 2017, 113:1373-1382.

Moldovan, G.-L., B. Pfander, and S. Jentsch. PCNA, the Maestro of the Replication Fork. *Cell*. 2007, 129:665-679.

Moon, A. F., M. Garcia-Diaz, V. K. Batra, W. A. Beard, K. Bebenek, T. A. Kunkel, S. H. Wilson, and L. C. Pedersen. The X Family Portrait: Structural Insights into Biological Functions of X Family Polymerases. *DNA Repair*. 2007, 6:1709-1725.

Murashige, T., and F. Skoog. A Revised Medium for Rapid Growth and Bio Assays with Tobacco Tissue Cultures. *Physiologia Plantarum*. 1962, 15:473-497.

Nick McElhinny, S. A., D. Kumar, A. B. Clark, D. L. Watt, B. E. Watts, E.-B. Lundström, E. Johansson, A. Chabes, and T. A. Kunkel. Genome instability due to ribonucleotide incorporation into DNA. *Nature chemical biology*. 2010a, 6:774-781.

Nick McElhinny, S. A., and D. A. Ramsden. Polymerase Mu Is a DNA-Directed DNA/RNA Polymerase. *Molecular and Cellular Biology* . 2003, 23:2309-2315.

Nick McElhinny, S. A., B. E. Watts, D. Kumar, D. L. Watt, E.-B. Lundström, P. M. J. Burgers, E. Johansson, A. Chabes, and T. A. Kunkel. Abundant ribonucleotide incorporation into DNA by yeast replicative polymerases. *Proceedings of the National Academy of Sciences of the United States of America*. 2010b, 107:4949-4954.

Nilforoushan, A., A. Furrer, L. A. Wyss, B. van Loon, and S. J. Sturla. Nucleotides with Altered Hydrogen Bonding Capacities Impede Human DNA Polymerase η by Reducing Synthesis in the Presence of the Major Cisplatin DNA Adduct. *Journal of the American Chemical Society.* 2015, 137:4728-4734.

Paredes, F., K. Sheldon, B. Lassègue, H. C. Williams, E. A. Faidley, G. A. Benavides, G. Torres, F. Sanhueza-Olivares, S. M. Yeligar, K. K. Griendling, V. Darley-Usmar, and A. San Martin. Poldip2 is an oxygen-sensitive protein that controls PDH and αKGDH lipoylation and activation to support metabolic adaptation in hypoxia and cancer. *Proceedings of the National Academy of Sciences*. 2018, 115:1789-1794.

Potenski, C. J., Klein, H. L. How the misincorporation of ribonucleotides into genomic DNA can be both harmful and helpful to cells. *Nucleic acids research.* 2014, 42: 10226-10234.

Pryor, J. M., M. P. Conlin, J. Carvajal-Garcia, M. E. Luedeman, A. J. Luthman, G. W. Small, and D. A. Ramsden. Ribonucleotide incorporation enables repair of chromosome breaks by nonhomologous end joining. *Science*. 2018, 36:1126.

Ramsden, D. A. Polymerases in Nonhomologous End Joining: Building a Bridge over Broken Chromosomes. *Antioxidants & Redox Signaling*. 2011, 14:2509-2519.

Reijns, Martin A. M., B. Rabe, Rachel E. Rigby, P. Mill, Katy R. Astell, Laura A. Lettice, S. Boyle, A. Leitch, M. Keighren, F. Kilanowski, Paul S. Devenney, D. Sexton, G. Grimes, Ian J. Holt, Robert E. Hill et al. Enzymatic Removal of Ribonucleotides from DNA Is Essential for Mammalian Genome Integrity and Development. *Cell*. 2012, 149:1008-1022.

Rice, G. I., J. Bond, A. Asipu, R. L. Brunette, I. W. Manfield, I. M. Carr, J. C. Fuller, R. M. Jackson, T. Lamb, T. A. Briggs, M. Ali, H. Gornall, L. R. Couthard, A. Aeby, S. P. Attard-Montalto, E. Bertini, C et al. Mutations involved in Aicardi-Goutières syndrome

implicate SAMHD1 as regulator of the innate immune response. *Nature Genetics.* 2009, 41:829-832.

Roldán-Arjona, T., and R. R. Ariza. Repair and tolerance of oxidative DNA damage in plants. *Mutation Research/Reviews in Mutation Research*. 2009, 681:169-179.

Romani, A. Regulation of magnesium homeostasis and transport in mammalian cells. *Archives of Biochemistry and Biophysics.* 2007, 458:90-102.

Roth, J. A. Homeostatic and toxic mechanisms regulating manganese uptake, retention, and elimination. *Biological Research*. 2006, 39:45-57.

Ruiz, J. F., R. Juárez, M. García-Díaz, G. Terrados, A. J. Picher, S. González-Barrera, A. R. Fernández de Henestrosa, and L. Blanco. Lack of sugar discrimination by human Pol μ requires a single glycine residue. *Nucleic Acids Research.* 2003, 31:4441-4449.

Rychlik, M. P., H. Chon, S. M. Cerritelli, P. Klimek, R. J. Crouch, and M. Nowotny. Crystal Structures of RNase H2 in Complex with Nucleic Acid Reveal the Mechanism of RNA-DNA Junction Recognition and Cleavage. *Molecular Cell*. 2010, 40:658-670.

Sello, S., R. Moscatiello, N. La Rocca, B. Baldan, and L. Navazio. A Rapid and Efficient Method to Obtain Photosynthetic Cell Suspension Cultures of Arabidopsis thaliana. *Frontiers in Plant Science* 2017, 8:1444.

Sharma, P., A. B. Jha, R. S. Dubey, and M. Pessarakli. Reactive Oxygen Species, Oxidative Damage, and Antioxidative Defense Mechanism in Plants under Stressful Conditions. *Journal of Botany*, 2012, 2012:26.

Simonelli, V., S. Camerini, F. Mazzei, B. Van Loon, A. Allione, M. D'Errico, F. Barone, A. Minoprio, F. Ricceri, S. Guarrera, A. Russo, B. Dalhus, M. Crescenzi, U. Hübscher, M. Bjørås et al. Genotype–phenotype analysis of S326C OGG1 polymorphism: a

risk factor for oxidative pathologies. *Free Radical Biology and Medicine.* 2013, 63:401-409.

Smith, N., J. B. Kilpatrick, and G. C. Whitelam. Superfluous Transgene Integration in Plants. *Critical Reviews in Plant Sciences.* 2001, 20 :215-249.

Sobol, R. W., J. K. Horton, R. Kühn, H. Gu, R. K. Singhal, R. Prasad, K. Rajewsky, and S. H. Wilson. Requirement of mammalian DNA polymerase-β in base-excision repair. *Nature.* 1996, 379:183.

Sparks, J. L., H. Chon, S. M. Cerritelli, T. A. Kunkel, E. Johansson, R. J. Crouch, and P. M. Burgers. RNase H2-Initiated Ribonucleotide Excision Repair. *Molecular Cell.* 2012, 47:980-986.

Srivastava, A. K., C. Han, R. Zhao, T. Cui, Y. Dai, C. Mao, W. Zhao, X. Zhang, J. Yu, and Q.-E. Wang. Enhanced expression of DNA polymerase eta contributes to cisplatin resistance of ovarian cancer stem cells. *Proceedings of the National Academy of Sciences.* 2015, 112:4411-4416.

Starcevic, D., Dalal, S., Sweasy, J. Is There a Link Between DNA Polymerase Beta and Cancer? *Cell Cycle*. 2004, 8:996-999.

Steitz, T. A. DNA Polymerases: Structural Diversity and Common Mechanisms. *Journal of Biological Chemistry.* 1999, 274:17395-17398.

Strzalka, W., and C. Aggarwal. Arabidopsis thaliana: Proliferating cell nuclear antigen 1 and 2 possibly form homo- and hetero-trimeric complexes in the plant cell. *Plant Signaling & Behavior.* 2013, 8 :e24837.

Su, Y., M. Egli, and F. P. Guengerich. Mechanism of Ribonucleotide Incorporation by Human DNA Polymerase η. *Journal of Biological Chemistry*. 2016, 291:3747-3756.

Tissier, A., R. Janel-Bintz, S. Coulon, E. Klaile, P. Kannouche, R. P. Fuchs, and A. M. Cordonnier. Crosstalk between replicative and

translesional DNA polymerases: PDIP38 interacts directly with Polη. *DNA Repair*. 2010, 9:922-928.

Traut, T. W. Physiological concentrations of purines and pyrimidines. *Molecular and Cellular Biochemistry*. 1994, 140:1-22.

Tsugama, D., S. Liu, and T. Takano. A rapid chemical method for lysing Arabidopsis cells for protein analysis. *Plant Methods*. 2011, 7:22-22.

Vaisman, A., C. Masutani, F. Hanaoka, and S. G. Chaney. Efficient Translesion Replication Past Oxaliplatin and Cisplatin GpG Adducts by Human DNA Polymerase η. *Biochemistry*. 2000, 39:4575-4580.

Vaisman, A., and R. Woodgate. Redundancy in Ribonucleotide Excision Repair: Competition, Compensation, and Cooperation. *DNA Repair*. 2015, 29:74-82.

van Loon, B., and U. Hübscher. An 8-oxo-guanine repair pathway coordinated by MUTYH glycosylase and DNA polymerase λ. *Proceedings of the National Academy of Sciences of the United States of America*. 2009, 106:18201-18206.

van Loon, B., E. Markkanen, and U. Hübscher. Oxygen as a friend and enemy: How to combat the mutational potential of 8-oxo-guanine. *DNA Repair*. 2010, 9:604-616.

Vengrova, S., and J. Z. Dalgaard. The wild-type Schizosaccharomyces pombe mat1 imprint consists of two ribonucleotides. *EMBO Reports*. 2006, 7:59-65.

Verma, D., and H. Daniell. Chloroplast Vector Systems for Biotechnology Applications. *Plant Physiology*. 2007, 145:1129-1143.

Washington, M. T., L. Prakash, and S. Prakash. Yeast DNA Polymerase η Utilizes an Induced-Fit Mechanism of Nucleotide Incorporation. *Cell*. 2001, 107:917-927.

Waters, L. S., B. K. Minesinger, M. E. Wiltrout, S. D'Souza, R. V. Woodruff, and G. C. Walker. Eukaryotic Translesion Polymerases

and Their Roles and Regulation in DNA Damage Tolerance. *Microbiology and Molecular Biology Reviews : MMBR*. 2009, 73:134-154.

Williams, J. S., A. R. Clausen, S. A. Nick McElhinny, B. E. Watts, E. Johansson, and T. A. Kunkel. Proofreading of ribonucleotides inserted into DNA by yeast DNA polymerase ε. *DNA Repair.* 2012, 11:649-656.

Williams, J. S., D. J. Smith, L. Marjavaara, S. A. Lujan, A. Chabes, and T. A. Kunkel. Topoisomerase 1-mediated Removal of Ribonucleotides from Nascent Leading Strand DNA. *Molecular Cell*. 2013, 49:1010-1015.

Yang, W. An Overview of Y-Family DNA Polymerases and a Case Study of Human DNA Polymerase η. *Biochemistry.* 2014, 53:2793-2803.

Yao, N. Y., J. W. Schroeder, O. Yurieva, L. A. Simmons, and M. E. O'Donnell. Cost of rNTP/dNTP pool imbalance at the replication fork. *Proceedings of the National Academy of Sciences of the United States of America.* 2013, 110:12942-12947.

Zhao, Y., C. Biertümpfel, M. T. Gregory, Y.-J. Hua, F. Hanaoka, and W. Yang. Structural basis of human DNA polymerase η-mediated chemoresistance to cisplatin. *Proceedings of the National Academy of Sciences*. 2012, 109:7269-7274.

List of original manuscripts

9816–9828 *Nucleic Acids Research, 2018, Vol. 46, No. 18* *Published online 8 August 2018*
doi: 10.1093/nar/gky723

p15^{PAF} binding to PCNA modulates the DNA sliding surface

Matteo De March[1,†], Susana Barrera-Vilarmau[2,†], Emmanuele Crespan[3,†], Elisa Mentegari[3], Nekane Merino[4], Amaia Gonzalez-Magaña[4], Miguel Romano-Moreno[4], Giovanni Maga[3], Ramon Crehuet[2], Silvia Onesti[1], Francisco J. Blanco[4,5] and Alfredo De Biasio[1,6,*]

[1]Structural Biology Laboratory, Elettra-Sincrotrone Trieste S.C.p.A., Trieste 34149, Italy, [2]Institute of Advanced Chemistry of Catalonia (IQAC), CSIC, Jordi Girona 18–26, 08034, Barcelona, Spain, [3]Institute of Molecular Genetics, IGM-CNR, via Abbiategrasso 207, 27100 Pavia, Italy, [4]CIC bioGUNE, Parque Tecnológico de Bizkaia Edificio 800, 48160 Derio, Spain, [5]IKERBASQUE, Basque Foundation for Science, Bilbao, Spain and [6]Leicester Institute of Structural & Chemical Biology and Department of Molecular & Cell Biology, University of Leicester, Lancaster Rd, Leicester LE1 7HB, UK

Received October 31, 2017; Revised July 26, 2018; Editorial Decision July 27, 2018; Accepted July 31, 2018

ABSTRACT

p15^{PAF} is an oncogenic intrinsically disordered protein that regulates DNA replication and lesion bypass by interacting with the human sliding clamp PCNA. In the absence of DNA, p15^{PAF} traverses the PCNA ring via an extended PIP-box that contacts the sliding surface. Here, we probed the atomic-scale structure of p15^{PAF}–PCNA–DNA ternary complexes. Crystallography and MD simulations show that, when p15^{PAF} occupies two subunits of the PCNA homotrimer, DNA within the ring channel binds the unoccupied subunit. The structure of PCNA-bound p15^{PAF} in the absence and presence of DNA is invariant, and solution NMR confirms that DNA does not displace p15^{PAF} from the ring wall. Thus, p15^{PAF} reduces the available sliding surfaces of PCNA, and may function as a belt that fastens the DNA to the clamp during synthesis by the replicative polymerase (pol δ). This constraint, however, may need to be released for efficient DNA lesion bypass by the translesion synthesis polymerase (pol η). Accordingly, our biochemical data show that p15^{PAF} impairs primer synthesis by pol η–PCNA holoenzyme against both damaged and normal DNA templates. In light of our findings, we discuss the possible mechanistic roles of p15^{PAF} in DNA replication and suppression of DNA lesion bypass.

INTRODUCTION

Sliding clamps are ring-shaped proteins that tether polymerases and other factors of the replisome to the genomic template, enabling DNA replication and repair. The molecular architecture of sliding clamps is conserved in all domains of life. Proliferating Cell Nuclear Antigen (PCNA)—the eukaryotic sliding clamp—is an 86-kDa homotrimeric ring with a six-fold pseudosymmetric rotation axis running through the centre of the clamp and a central channel lined with lysine and arginine-rich α-helices through which DNA is threaded (1–6). Experimental and computational analyses of the human PCNA–DNA complex showed that the DNA in the channel is tilted and its phosphates transiently interact with a set of basic residues forming a right-hand spiral that matches the DNA pitch (5,7). This dynamic interaction may allow the clamp to slide by rotationally tracking the DNA helix, or by a linear motion uncoupled from the helical pitch, or by a combination of the two modes (8). A recent report based on coarse-grained MD simulations (9) supports that the coupling between rotation and translation in PCNA sliding is weak, and that the translational motion is much faster than the rotational one, suggesting that PCNA slides on the double helix like a washer on a screw, rather than a nut on a screw. Importantly, growing evidence confirms the earlier observation that the PCNA–DNA interaction is critical for the function of the polymerase bound to the clamp (10). A recent report showed that acetylation of conserved lysine residues at the sliding surface of yeast PCNA is induced by DNA lesions and stimulates repair by homologous recombination (11). Acetylation of K20 negatively affects the processivity of the replicative polymerase δ (pol δ), but not that of the translesion synthesis (TLS) polymerase η (pol η), spe-

*To whom correspondence should be addressed. Tel: +44 116 252 5391; Email: adb43@leicester.ac.uk
†The authors wish it to be known that, in their opinion, the first three authors should be regarded as Joint First Authors.

cialized in traversing DNA lesions such as thymine dimers or cisplatin adducts, suggesting that the modulation of the PCNA–DNA interaction can regulate the function of polymerases.

The front face of the PCNA ring contains the site of interaction of polymerases and other proteins, named the PIP-box binding site (3,12). The back face contains the sites of ubiquitylation and sumoylation (13,14). PIP-box interacting partners bind PCNA through a short consensus sequence with the pattern *QXXhXXaa*, where *h* is an aliphatic-hydrophobic residue, *a* aromatic-hydrophobic and *X* any residue (3,12).

The PCNA–associated factor p15^{PAF} (hereafter named p15) is an oncogenic, 11 kDa intrinsically disordered protein that regulates DNA replication and lesion bypass via a PIP-box interaction with PCNA (4,15–18). p15 co-localizes with PCNA in the nucleus of proliferating cells mainly in the S phase of the cell cycle (18–20). Depletion of p15 significantly decreases DNA synthesis (17–20), suggesting that p15 modulates the function of PCNA as a processivity factor. Co-immunoprecipitation from pancreatic cancer cell lines suggests that p15 is part of a DNA-replication complex with PCNA, pol δ and the endonuclease Fen-1 in replication foci (18). During unperturbed DNA replication, PCNA-bound p15 is mono-ubiquitylated at two N-terminal lysines (18) (K14 and K25). UV-induced replication stalling triggers the recruitment of pol η to the damaged site and the degradation of ubiquitylated p15 (18), and Povlsen and coworkers proposed that p15 may compete with pol η for binding to PCNA. However, the molecular mechanisms underlying the function of p15 in DNA replication and DNA lesion bypass remain unclear.

We have previously shown that, in absence of DNA, up to three p15 molecules bind the human trimeric PCNA ring at a site that extends from the PIP-box binding pocket to the clamp inner channel (4), and that the disordered p15 N-termini exit the clamp from the back face and directly interact with DNA (4,21). Negative stain electron microscopy of a p15–PCNA–DNA ternary complex showed particles with DNA in the clamp channel (4), but the molecular details of this assembly remained undefined.

In this work, we characterized the structure of ternary complexes composed of PCNA, DNA and the PCNA-interacting region of p15, by combining experimental and computational approaches. The co-crystal structure of PCNA in complex with two p15 molecules and a 10 bp primed DNA substrate, solved at 3.2 Å resolution, shows the duplex portion of DNA in the PCNA channel leaning towards the subunit not occupied by p15. The p15 residues N-terminal to the PIP-box contact four helices on the ring inner wall, partly shielding the DNA binding site of two subunits. This molecular arrangement is recapitulated by MD simulations of PCNA in complex with two p15 fragments with longer N-termini and a 40 bp DNA duplex. Solution NMR experiments show that DNA does not displace p15 from the inner rim of a PCNA ring in which the three subunits are occupied by p15. Accordingly, when PCNA is co-crystallized with three p15 peptides and DNA, the electron density map does not show features of DNA in the clamp channel. Thus, p15 outcompetes DNA for a common binding site in the clamp channel, and the stoichiometry of binding dictates the available sliding surfaces. Given the inhibitory activity of p15 in TLS (18), we hypothesized that the constraint imposed by p15 to DNA may need to be released for efficient DNA lesion bypass by the TLS polymerase pol η. This agrees with our data showing that p15 downregulates the activity of pol η–PCNA holoenzyme in bypassing a cisplatin-induced DNA lesion and in extending the corresponding undamaged template. Based on our findings, we discuss the possible mechanistic roles of p15 in DNA replication and lesion bypass.

MATERIALS AND METHODS

Protein expression and DNA duplexes

Human PCNA (UniProt: P12004) was produced in *Escherichia coli* BL21(DE3) cells grown in appropriate culture media to obtain protein with natural isotopic abundance or uniform enrichment using a clone with N-terminal His6-tag and PreScission protease cleavage site in a pET-derived plasmid. For NMR samples the protein was purified from the soluble fraction by Co^{2+}-affinity chromatography, cleaved by PreScission protease and polished by gel filtration chromatography (22). All columns and chromatography systems used where from GE Healthcare. Protein elution was monitored by absorbance at 280 nm and confirmed by SDS-PAGE. The purified protein contained the extra sequence GPH- at the N-terminus. The PCNA sample for crystallization was obtained by introducing two additional purification steps (4). The sample cleaved with PreScission protease was dialyzed against 50 mM sodium acetate pH 5.5, 100 mM NaCl. After separation of some precipitated material, the solution was loaded on a HiTrap Heparin HP column equilibrated with the same buffer. After column washing, the protein was eluted with a 0–100% gradient of 50 mM sodium acetate pH 5.5, 2 M NaCl in 20 column volumes (CV). The protein containing fractions of the major peak were dialyzed against 20 mM Tris–HCl buffer pH 7.6, 150 mM NaCl and injected into a HiTrap Chelating HP column loaded with Co^{2+} cations to remove uncleaved PCNA. The flowthrough was loaded on a HiTrap Q Sepharose column and eluted with a 0–60% gradient of 20 mM Tris–HCl pH 7.6, 1 M NaCl in 5 CV. The protein containing fractions were concentrated and polished using a Superdex 200 26/60 column equilibrated with PBS, pH 7.0, and then exchanged into the crystallization buffer (20 mM Tris–HCl, pH 7.5, 10% glycerol, 2 mM DTT) using a PD10 column. Stock solutions in PBS or crystallization buffer were flash-frozen in liquid nitrogen and stored at −80°C. The protein concentrations were measured by absorbance at 280 nm using the extinction coefficient calculated from the amino acid composition (15 930 M^{-1} cm^{-1}). All indicated concentrations of PCNA samples refer to protomer concentrations. dsDNA and pDNA duplexes were obtained by mixing equimolar amounts of the appropriate oligonucleotides, at 93°C for 2 min with subsequent annealing by slow cooling at room temperature.

PCNA complexes crystallization and structure determination

p15$^{50–77}$–PCNA–pDNA complex. Stocks of PCNA, p15$^{50–77}$ and pDNA solutions were mixed to final con-

centrations of 0.4, 0.5 and 1.1 mM, respectively (1:1.2:2.7 protein monomer:peptide:pDNA molar ratio), and incubated at room temperature for 30 min before screening crystallization conditions using the hanging drop vapour diffusion method. Best diffracting co-crystals grew within 2 days at 4°C in droplets obtained by mixing 1 μl of the complex solution and 1 μl of a solution containing 10% polyethylene glycol 3350 in 0.1 M sodium acetate buffer, pH 4.5. The best crystals from the $p15^{50–77}$–PCNA–DNA complex diffracted at 3.2 Å resolution on the ESRF-ID29 beamline, and belonged to $P2_1$ space group. XDS (23) and the CCP4i suite (24) were used for data processing. Molecular replacement was used to place one hPCNA trimer (PDB ID: 4D2G) in the asymmetric unit after removing $p15^{50–77}$ molecule and solvent. Several cycles of refinement using REFMAC5 (25) and model building using COOT (26) were carried out before placing the two $p15^{50–77}$ chains into the $F_o - F_c$ electron density map. NCS and TLS restraints were used. Inspection of the resulting unbiased difference Fourier's map inside the PCNA ring showed some electron density for one DNA strand of the double helix. Due to the disorder and/or partial occupancy the second DNA strand was only partially visible. However, modeling and refining the DNA in the same position as in the PCNA–DNA binary complex (5) gave rise to reasonable crystallographic parameters (i.e. model statistics, *B*-factor values and quality of the $2F_o - F_c$ map) and was consistent with the result from the MD simulations (see text for further details). Data collection and refinement statistics are listed in Supplementary Table ST2. Stereo view of $2F_o - F_c$ electron density map around the $p15^{50–77}$ peptide with higher occupancy is displayed in Supplementary Figure S1. All figures with molecular models were prepared using PyMOL (www.pymol.org). Atomic coordinates and structure factors of $p15^{50–77}$–PCNA–DNA complex have been deposited with PDB ID: 6EHT.

$p15^{41–72}$–PCNA complex. Crystals of $p15^{41–72}$–PCNA complex were obtained by hanging-drop vapor diffusion method at 4°C. Cubic crystals were grown on precipitant solution containing 28% polyethylene glycol 400, 0.2 M $CaCl_2$ in 0.1 M Hepes pH 7.0 buffer. Stocks of PCNA, $p15^{41–72}$ and DNA solutions were mixed to final concentrations of 0.5, 0.5 and 0.5 mM, respectively (1:1:1 protein monomer: peptide: DNA duplex molar ratio), and incubated at room temperature for 30 min before crystallization. Best diffracting co-crystals grew within 1 day and were flash-frozen directly, and diffracted to 2.9 Å resolution on the Elettra XRD1 beamline, and belonged to $P2_1$ space group (Supplementary Table ST2). XDS (23) and the CCP4i suite (24) were used for data processing. Molecular replacement was used to place one hPCNA trimer (PDB ID: 1VYM) in the asymmetric unit. Several cycles of refinement using REFMAC5 (25) and model building using COOT (26) were carried out before placing the three $p15^{41–72}$ chains into the $F_o - F_c$ electron density map. Jelly-Body restraints were used. Inspection of the resulting unbiased difference Fourier's showed no electron density attributable to DNA inside the PCNA ring.

MD simulations

Two 300 ns MD simulation replicas were performed for the same system. The system is a ternary complex composed of PCNA, two p15 peptides spanning residues 47–70 and a 40 bp DNA. The initial MD model was built by combining two different crystal structures: the $p15^{50–77}$–PCNA complex (4) and the PCNA–dsDNA complex (5). The p15 peptide was designed based on the $p15^{50–77}$–PCNA complex structure (4). The seven C-terminal residues are flexible and do not interact with PCNA and were thus excluded, while five extra residues at the flexible N-terminus were added as they are located in the clamp channel, and may transiently interact with DNA, resulting in a final segment $p15^{47–70}$. The DNA segment, with 10 bp in the crystallographic structure, was also extended by 15 bp in each direction of the helical axis. Extension of all fragments was performed using COOT (26). The system was completed by adding TIP3P water molecules in a truncated dodecahedron box at least 1.5 nm away from the DNA or protein atoms. Cl- and Na+ ions were added for charge neutralization and to mimic experimental conditions of 100 mM salt concentration. The system was minimized and equilibrated for 0.1 ns in the NVT ensemble and then for 0.1 ns in the NPT ensemble. All calculations were performed using Gromacs 5.1 (27) and parmBSC1 force field (28), the trajectories were analyzed using MDTraj package (29) and plots were generated using Matplotlib Python Library (30). The stability of the simulations was checked by visual inspection of the trajectories and the RMSD with respect to the starting structure as plotted in Supplementary Figure S2. To track the evolution of the DNA position inside the PCNA ring (Figure 2B), we have followed this procedure: First, the PCNA chains are superimposed for all frames, to eliminate global rotation and translation. Second the centre of each PCNA chain is calculated for all trajectory frames. Third, DNA base-pairs 17–21 for chain F and 20–24 for chain G are selected as those being inside the PCNA ring. Its centre is also calculated for each frame. Fourth, to project into a 2D space, a Principal Component Analysis is performed for the PCNA chain centres, and DNA centres are projected into the first two components of this subspace.

NMR spectroscopy

$^{1}H–^{15}N$ TROSY spectra were recorded at 35°C on a Bruker Avance III 800 MHz (18.8 T) spectrometer equipped with a cryogenically cooled triple resonance z-gradient probe. A 400 ul sample of 100 μM U-[^{2}H,^{13}C, ^{15}N,] PCNA in 20 mM sodium phosphate buffer, 50 mM NaCl, pH 7.0, 20 μM 2,2-dimethyl-2-silapentane-5-sulfonate, 0.01% NaN3, 1 mM DTT and 5% $^{2}H_2O$ was placed in a 5 mm Shigemi NMR tube (without plunger) and increasing volumes of $p15^{50–77}$ or dsDNA stock solutions were added and mixed (by capping and inverting the tube). The peptide and the DNA stocks solutions were prepared in the same buffer as the PCNA samples (except that no NaN_3, DSS or $^{2}H_2O$ was added). For that purpose, and to remove unwanted salts from the synthetic peptide and oligonucleotides, they were dissolved in 20 mM sodium phosphate buffer, 50 mM NaCl, pH 7.0 and desalted on a PD-10 Minitrap G25 column. For

duplex formation, equimolar amounts were mixed and annealed (2 min at 95°C in a thermoblock followed by slow cooling down to room temperature). The duplex and the peptide were concentrated by ultrafiltration up to 20.84 mM (dsDNA) or 9.52 mM ($p15^{50–77}$) and concentrated DTT was added up to 1 mM. Small volumes of the stock peptide solution were added stepwise to the PCNA samples, causing a 7% PCNA dilution. TROSY spectra were measured with 144 or 256 indirect points (alternating between 8 and 14 h total duration). The PCNA–$p15^{50–77}$ sample remained clear during the 6-day long titration. When the peptide was present at an excess molar ratio of 6.4, the observed changes in the PCNA spectrum were judged to be within the experimental error with respect to the previous addition, and PCNA was considered to be saturated with the peptide. Then a volume of dsDNA stock was added to a 1:3 molar ratio (PCNA trimer:DNA duplex). Further additions of DNA did not cause further changes in the PCNA signals. The structural integrity of the DNA duplex was assessed from the imino signals observed in one-dimensional proton spectra, whose intensities increased upon duplex addition. The pH of the PCNA samples was measured at the beginning and at the end of the titrations inside the NMR tubes and found to deviate by less than 0.1 units. Therefore, the small measured shifts are not caused by differences in pH. The titration with the peptide allowed for an extensive transfer of NMR signal assignments from the free PCNA to the $p15^{50–77}$-bound PCNA spectra (with a coverage of 72% of non proline residues). For the $p15^{50–77}$-DNA-bound PCNA the assignment transfer covered 69% of the PCNA signals. The CSP caused by the peptide or the dsDNA were computed as the weighted average distance between the backbone amide ^{1}H and ^{15}N chemical shifts in the free and bound states (31,32).

DNA synthesis assays

Chemicals. Deoxynucleotides were purchased from GeneSpin (Milan, Italy).

Oligonucleotides. The 24-mer template oligonucleotide containing the cis-PtGG adduct was a kind gift from S.J. Sturla (ETH, Zürich) and was prepared and purified as described previously (Nilforoushan, 2015). All other DNA oligonucleotides, all HPLC purified, were synthesized by Biomers.net (Germany). The 18mer primer oligonucleotide was 5′-labeled with carboxyfluorescin (FAM) group. The labeled primer was mixed to the complementary template oligonucleotide at 1:1 (M/M) ratio in the presence of 150 mM Hepes–KOH pH 7.4, 500 mM KCl, 10 mM $MgCl_2$, 250 mM NH_4Ac, heated at 95°C for 5 min and then slowly cooled at room temperature.

Human recombinant pol η. pJM879 (33), expressing N-terminal His-tagged human pol η, was a kind gift from R. Woodgate (NIH, USA). Human recombinant pol η was expressed and purified with a modified protocol: BL21 DE3 competent *E. coli* cells were transformed with pJM879. Plates containing 30 mg/ml kanamycin were used to identify kanamycin-resistant colonies that were picked and grown overnight at 37°C. DNA purified from bacterial cultures using NucleoSpin® Plasmid (NoLid) kit (MACHEREY-NAGEL, Düren, Germany) was digested to confirm the presence of the gene expressing pol η. Transformed *E. coli* cells were used to inoculate a 50 ml starter culture. After overnight growth at 37°C, 12 ml of the starter culture were put into 1 l of LB medium (containing 30 mg/ml kanamycin). After 6 h growth at 37°C, cells were harvested by centrifugation and pellet frozen at –80°C. The pellet was resuspended in 40ml of lysis buffer (50mM Tris–HCl pH 7.5, 0.3 M NaCl, 20 mM imidazole, 10% glycerol, 10 mM b-mercaptoethanol [BME], 1× lysozime (Eurobio, Courtaboeuf, France), 1× ethylenediaminetetraacetic acid [EDTA]-free protease inhibitor (SIGMAFAST™ Protease Inhibitor Cocktail Tablets, Sigma-Aldrich), 1 mM phenylmethane sulfonyl fluoride [PMSF] and lysed through sonication. After ultracentrifugation at 98 000g at 4°C for 1.5 h, the supernatant was loaded onto a 1-ml Ni-NTA column (HisTrap™ HP, GE Healthcare). Column washing was performed with 3 ml of W1 buffer (20 ml Tris–HCl pH 7.5, 1 M NaCl, 20 mM imidazole, 10% glycerol, 10 mM BME) followed by 3 ml of W2 buffer (10 mM Na-phosphate pH 7.7, 0.3 M NaCl, 20 mM imidazole, 10% glycerol, 10 mM BME). Elution of target protein was obtained using buffer H (10 mM Na-phosphate pH 7.7, 0.3 M NaCl, 200 mM imidazole, 10% glycerol, 10 mM BME). The pol η positive fractions (0.5 ml each) were pooled and overnight dialyzed with buffer M (20 mM Na-phosphate pH 7.3, 0.1 M NaCl, 10% glycerol, 10 mM BME), in dialysis cassette (Slide-A-Lyzer™ Dialysis Cassettes, 3.5K MWCO, Thermo Scientific). Pool was then loaded onto a 1-ml cation exchanger column (HiTrap SP, Pharmacia Biotech). Buffer N (20 mM Na-phosphate pH 7.3, 0.5 M NaCl, 10% glycerol, 10 mM BME) was used to elute pol η with a linear gradient. The pol ηpositive fractions (0.5 ml each) were aliquoted and stored at –80°C in 20% final glycerol.

Recombinant ScRF-C was obtained as a kind gift from the laboratory of Alessandro Costa (Francis Crick Institute), and was prepared following the procedure described in (34).

Enzymatic assays. All reactions were performed in a 10 μl final volume using the following conditions: 40 mM Tris pH 8, 1 mM dithiotreitol (DTT), 0.25 mg/ml bovine serum albumin (BSA), 10 mM Mg^{2+} (unless otherwise stated in the figures or figure legends). Enzymes and DNA substrates concentrations are indicated in figure legends. Reactions were incubated at 37°C for 15 min, unless otherwise stated. Reaction mixtures were stopped by addition of standard denaturing gel loading buffer (95% formamide, 10 m methylenediaminetetraacetic acid, xylene cyanol and bromophenol blue), heated at 95°C for 5 min and loaded on a 7-M urea 12% polyacrylamide (PA) gel.

Electronic image manipulation. Linear transformations have been applied in some instance to the whole images using the exposure/brightness filters of Adobe Photoshop CS6 with the sole purpose of reducing excessive background. No masking/enhancement was applied to any specific feature of the images.

RESULTS

Crystallographic evidence for p15–PCNA–DNA interactions

We co-crystallized human PCNA with a 10-bp primed DNA duplex (pDNA, as seen in published crystallographic analysis with both bacterial clamp (35) and *Saccharomyces cerevisiae* PCNA (2) and either the p15 fragment that was previously co-crystallized with PCNA alone ($p15^{50–77}$, comprising the extended PIP-box) (4), or a longer fragment that includes nine additional N-terminal residues ($p15^{41–72}$). In both crystals, incorporation of DNA is confirmed by their blue color, due to the presence of a Cy5 probe attached to the DNA (Figure 1A).

Crystals including the $p15^{50–77}$ peptide diffracted to 3.2 Å resolution, and the Fourier difference map calculated after placing and refining the PCNA ring alone in the asymmetric unit showed two PIP-box sites occupied by the $p15^{50–77}$ peptide and electron density features in the channel that may be attributed to one strand of the DNA duplex. However, electron density from the second strand is weak and the 4-base single stranded overhang invisible (Figure 1B). This suggests partial disorder and/or low occupancy of DNA. We then aligned the previously determined structure of PCNA bound to a 10 bp dsDNA (5) onto the current model and found that the DNA duplex fits reasonably well the residual electron density in the ring channel (Figure 1B). This DNA position, which leans towards the PCNA subunit not occupied by $p15^{50–77}$, also results in the best model statistics, lowest *B*-factors of DNA and best quality of the $2F_o - F_c$ electron density map (Figure 1C, and Supplementary Table ST2) and, importantly, agrees with the results from MD simulations (see below). The electron density for the DNA is still weak, indicating low occupancy and/or the presence of multiple conformations, but allows to propose a model, which shows the duplex portion of the DNA substrate in a similar position to that seen in the PCNA–dsDNA binary model, in the presence of two p15 peptides (Figure 1C). As in the $p15^{50–77}$–PCNA binary structure (4), the stoichiometry of $p15^{50–77}$ binding to PCNA is defined by the crystal packing, where a symmetry-related PCNA molecule occludes the peptide binding site on one subunit. The two $p15^{50–77}$ peptides show different occupancies. The peptide with higher occupancy has its PIP-box (Q62-F69) sitting on at the PCNA front face forming a 3_{10} helical turn, with a type-I β-turn at its N-terminus (P59-Q62) that positions residues P52-T58 to contact PCNA helices αA2 and αB2 on the clamp inner wall (Figure 1C and Supplementary Figure S1). Features of the peptide with lower occupancy are comparable yet weaker, and the peptide N-terminus could be modelled up to V53. Because of the partial disorder of DNA and the presence of a symmetry related loop that plugs the top of the PCNA channel (and may potentially affect both DNA positioning and occupancy, Figure 1B), we resorted to MD simulations to corroborate the crystallographic results and gain further structural insights on the ternary assembly.

Co-crystals of PCNA with $p15^{41–72}$ and pDNA were also obtained and diffracted to 2.9 Å resolution (Supplementary Table ST2). In the electron density map, however, no significant density was observed that may arise from DNA (Figure 1D), suggesting that, although incorporated in the crystal, the DNA is not sufficiently ordered to generate a structured signal. The electron density map showed three p15 fragments spanning residues 50–72 in the corresponding PIP-box sites, with a conformation analogous to that observed in the co-structure with the $p15^{50–77}$ peptide (Figure 1E and Supplementary Figure S1). Notably, due to steric hindrance, the location of the $p15^{41–72}$ peptides would interfere with DNA binding to PCNA in the orientation observed in the PCNA–dsDNA binary structure (Figure 1E), suggesting that p15 may outcompete DNA for binding to the PCNA inner rim.

MD simulation of PCNA in complex with two p15 PIP-boxes and a 40 bp DNA

Two replicas of a 300 ns MD simulation of a ternary complex composed of PCNA, two p15 peptides spanning residues 47–70 and a 40 bp DNA (Supplementary Table ST1) were performed. The initial MD model was built by combining features of two different crystal structures: the $p15^{50–77}$–PCNA complex (4) and the PCNA–dsDNA complex (5) by extending the DNA segment by 15 bp in each direction of the helical axis. The p15 peptide for this model was designed based on the $p15^{50–77}$–PCNA complex structure, by deleting the seven p15 C-terminal residues that are flexible and do not interact with PCNA and adding three extra residues at the flexible N-terminus, as they are located inside the clamp channel, and may transiently interact with DNA. Before starting the simulation, the DNA was moved away from its binding site on the inner wall of the clamp channel to a central position with minimal contacts with PCNA. Along the trajectory, the p15 peptides stay anchored to their binding sites on two PCNA subunits, while DNA rotates and tilts towards the wall of the subunit that is not occupied by p15 (Figure 2A and B, Supplementary Movie S1 and Supplementary Figure S2). At the end of the simulation, the DNA segment within the channel has a position similar to that observed in a previous 250 ns simulation of PCNA bound to a 30 bp DNA in absence of p15, where DNA simultaneously interacts with two adjacent sets of DNA-helix matching residues located on two PCNA subunits, as well as with residues on the clamp back face (5) (Figure 2A). Importantly, the topology of polar interactions between DNA and the PCNA subunit not occupied by p15 coincides with that observed in the crystal structure of the PCNA–dsDNA complex (Figure 2C). These results are consistent with the crystal structure of the $p15^{50–77}$–PCNA–DNA complex presented in this work and the proposed position for the partially disordered and/or incompletely occupied DNA. Altogether, these data suggest that, in the presence of two p15 molecules, a DNA duplex longer than 10 bp may still bind one of the three PCNA sliding surfaces.

Distance analysis of the intermolecular contacts along the MD trajectory shows that p15 residues N-terminal to the PIP-box (residues 52–61) are stably anchored to the inner wall of the PCNA ring, while the extreme N-termini (residues 47–51) remain flexible and thread the channel (Supplementary Figure S3 and Supplementary Movie S1). Overall, the p15 peptides establish limited contacts with

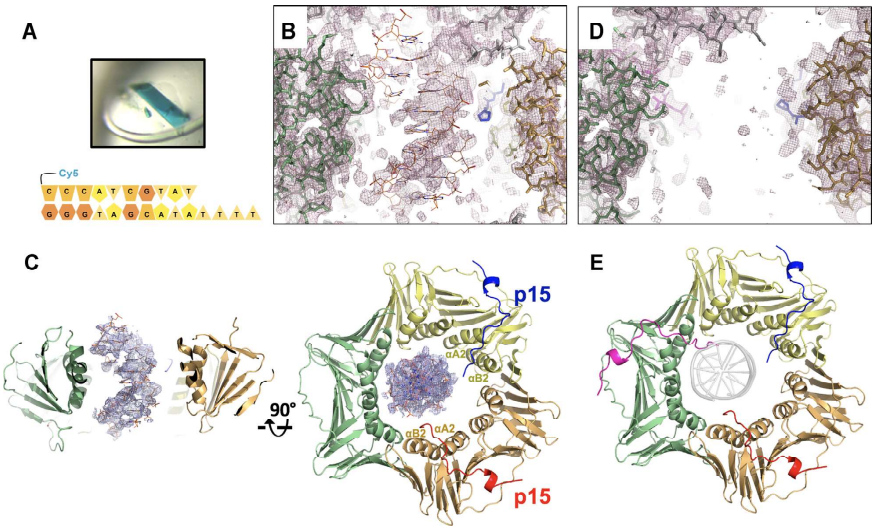

Figure 1. Crystal structures of human PCNA bound to p15 fragments and DNA. (**A**) Blue crystals of $p15^{50–77}$–PCNA–DNA complex. Co-crystals of PCNA mixed with $p15^{41–72}$ and DNA were also blue, confirming incorporation of DNA in the crystal lattice. The cartoon below shows the sequence of the DNA substrate. (**B**) Side view of the $2F_o - F_c$ omit map of the $p15^{50–77}$–PCNA–DNA complex refined without DNA in the model, contoured at 0.7 σ, showing the PCNA central channel. PCNA subunits (green and wheat) and $p15^{50–77}$ peptide in the background (blue) are in stick representation. The loop of a symmetry related PCNA molecule is shown in grey. The DNA, modeled as in the PCNA–dsDNA binary structure (5), is shown in orange. (**C**) Side- and top views of the refined $p15^{50–77}$–PCNA–DNA complex structure. PCNA and $p15^{50–77}$ are shown in ribbon representation, and the protein and peptide chains colored differently. The DNA, shown in orange, is modeled as in the PCNA–dsDNA binary structure. The $2F_o - F_c$ map around DNA is shown contoured at 0.7σ. (**D**) Side view of the $2F_o - F_c$ map of the $p15^{41–72}$–PCNA complex contoured at 0.7σ, showing the PCNA central channel as in (B). (**E**) Top view of $p15^{41–72}$–PCNA complex structure, color-coded as in (C). The DNA shown as a grey transparent ribbon in the same position as in (C) would cause a steric clash with the N-terminus of the p15 peptide on the third PCNA subunit.

DNA. In particular, polar contacts between peptide Y47 and G49 and DNA phosphates are detected. Conversely, DNA shows extensive interactions with the clamp (Figure 2A), and the side chains of many basic residues at the interface can randomly switch between adjacent DNA phosphates on a sub-nanosecond time scale (Supplementary Figure S4), as was observed in the MD simulation of the binary complex (5).

NMR analysis of PCNA binding to the p15 PIP-box and a 10 bp DNA

We characterized the interaction of PCNA with $p15^{50–77}$ and a 10 bp dsDNA (Supplementary Table ST1) by solution NMR. ^{2}H–^{15}N-labeled PCNA was firstly titrated with unlabeled $p15^{50–77}$ and chemical shift perturbations of PCNA backbone amide signals analyzed. Two groups of interacting residues were identified: residues whose signals gradually shift along the titration (Figure 3A and Supplementary Figure S5), implying a fast exchange regime on the NMR time scale, and residues whose signals broaden and disappear (due to signal attenuation below the noise level or untraceable shifting) at substoichiometric concentrations of peptide (Figure 3A and B), indicating an intermediate exchange regime. For the residues of the first group, a dissociation constant of ∼35 μM at 35°C was derived (Supplementary Figure S6), at the same order of magnitude as the 12.5 μM constant previously measured at the same temperature by isothermal calorimetry (4). For some residues of the latter group, new signals appearing at saturation could be tentatively assigned to the bound form (Figure 3A). When projected onto the PCNA surface (Figure 3C), the residues whose signals disappear at substoichiometric peptide concentration strongly overlap with those at the interface in the $p15^{50–77}$–PCNA–DNA crystal structure (Figure 1C), indicating that they interact tightly with PCNA, while the residues whose persisting signals significantly shift are located next to the main binding site (Supplementary Figure S5). Signals of K77, K80 and H153 disappear, while signal of K217 persists but is significantly perturbed (Figure 3B, C and Supplementary Figure S5). These are four of the five residues at the PCNA–DNA interface in the $p15^{50–77}$–PCNA–DNA crystal structure (Figure 1B). This is consistent with the partial overlap between the p15 and DNA binding sites seen in the crystal structure, and suggests that, in solution, p15 may compete with DNA binding.

In order to map the interaction site of DNA onto p15-bound PCNA, a labeled PCNA sample saturated with unlabeled $p15^{50–77}$ was used for a second titration with dsDNA. Signal shift saturation with dsDNA was achieved at 1:3 molar ratio (PCNA trimer:DNA duplex) (Figure 3A). The fact that, in an analogous titration of PCNA with dsDNA in the absence of $p15^{50–77}$, only ∼10% of complex was formed at this molar ratio (5) indicates that the presence of $p15^{50–77}$ increases the apparent DNA affinity for PCNA.

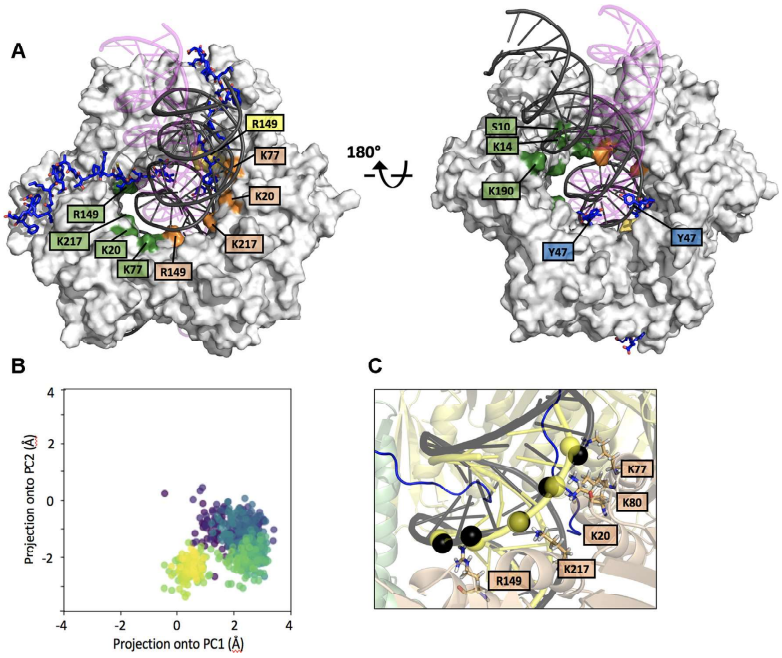

Figure 2. MD simulation of PCNA bound to two $p15^{47–70}$ peptides and a 40 bp DNA (**A**) Superposition of the initial and equilibrium states of the MD trajectory. PCNA is shown as a gray surface and DNA as a ribbon. The DNA in magenta (with transparency), and black correspond to the initial and equilibrium states of the simulation, respectively. PCNA residues whose side chains are engaged in polar contacts with DNA phosphates are labeled. Residues of different PCNA subunits are colored in green, yellow and wheat. (**B**) Principal Component Analysis of the evolution of the DNA position inside the PCNA ring (see Methods section for details). The centre of DNA in each trajectory frame was projected onto the first 2 components of the subspace composed of the centres of the 3 PCNA subunits. Each frame is coloured using the viridis colormap, which goes from dark purple for the first frames to yellow for the last ones. In the initial frame, DNA is close to (0,0), the centre of the three PCNA chains, and it quickly translates to a non-centered position. The final position is retained due to the stabilizing interactions reported in Supplementary Figure S4. (**C**) Close-up of the equilibrium state of the MD trajectory showing the PCNA–DNA interface. Interacting PCNA side chains and DNA phosphates (interatomic side chain nitrogen – DNA phosphorus distance < 4 Å) are shown as sticks and black spheres, respectively. DNA in yellow corresponds to the position in the crystallographic PCNA–dsDNA binary structure (5), with interfacial phosphates shown as spheres.

This result is consistent with the fact that no DNA binding affinity can be biochemically measured for PCNA alone, whereas a weak but detectable affinity for DNA has been previously measured (4) by fluorescence polarization in the presence of $p15^{50–77}$. Like in PCNA alone titrated with ds-DNA or pDNA, backbone amide signal shifts are small (CSP < 0.06 ppm), suggesting that the interaction involves amino acids with long side chains (Figure 3B). The DNA-induced perturbations map to residues within the channel as well as residues that line the $p15^{50–77}$ binding site on the front face of the PCNA ring (Figure 3C). The peptide, however, remains anchored to its binding site since the signals of PCNA residues that disappear in the presence of sub-stoichiometric $p15^{50–77}$ are not recovered by DNA addition (Figure 3A and B). Overall, these data suggest that DNA may thread through the PCNA channel when $p15^{50–77}$ saturates the three PIP-box sites, but that $p15^{50–77}$ remains anchored to the inner wall of the ring. The perturbations near the front face of the ring may arise from transient contacts that the threaded DNA makes with $p15^{50–77}$, slightly altering the position of the side chains. Based on this data, however, we cannot discard the possibility that DNA only partially penetrates the PCNA channel saturated with $p15^{50–77}$, either from the front or back face.

p15-induced inhibition of pol η–PCNA holoenzyme activity

Given the importance of p15 in regulating the activity of pol η during TLS shown in cell-based experiments (18), we performed biochemical studies using purified proteins to gain further mechanistic insight in light of our new structural data. Thus, we first probed the effects of p15 on the activity of pol η–PCNA holoenzyme in extending a DNA primer across a site-specific cisplatin lesion. A time course of pol η bypass in the presence or absence of PCNA and p15 was performed with a DNA template bearing a cisPt(GG) adduct at positions +1 and +2 (Figure 4A). Data shows that pol η alone (40 nM) was able to complete the bypass, resulting in the incorporation of two dCMPs opposite both Gs in the adduct (lanes 6–7, Figure 4A). At increasing times, the +1 product was reduced, being converted into +2 product. Further elongation past the lesion was minimal, as expected from the highly distributive nature of pol η, especially in

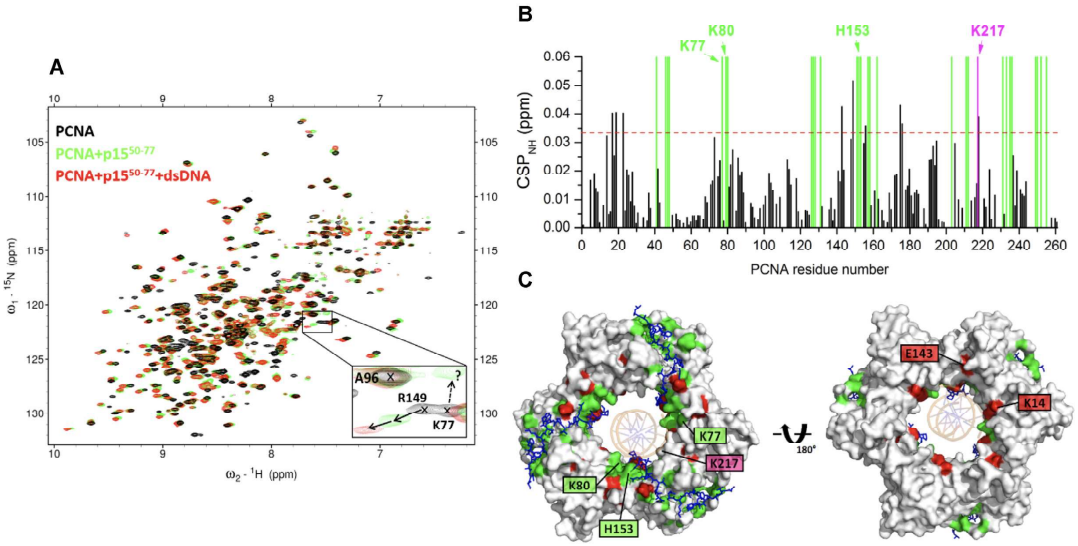

Figure 3. NMR analysis of PCNA binding to $p15^{50–77}$ and a 10 bp dsDNA. (**A**) Superposition of ^{1}H-^{15}N TROSY spectra of 95 μM PCNA in the absence (black) and presence (green) of 606 μM of $p15^{50–77}$ and (red) of 92 μM dsDNA (left) generated with oligonucleotides 3–4 in Supplementary Table S1. Spectra were acquired at 35°C on samples in 20 mM sodium phosphate, 50 mM NaCl, pH 7.0. The expansion shows signals of three representative residues. A96 signal is not perturbed by the addition of either $p15^{50–77}$ or DNA. R149 signal persists upon $p15^{50–77}$ addition, and shifts significantly by the sequential addition of DNA. Conversely, K77 signal disappears at substoichiometric concentrations of $p15^{50–77}$, and is not recovered by DNA addition. The dotted arrow points to a signal that is tentatively assigned to K77 in the $p15^{50–77}$-bound form. (**B**) Chemical shift perturbations (CSP) of backbone amide ^{1}H and ^{15}N NMR resonances induced by DNA. The dotted line indicates the average plus two standard deviations. The green bars indicate the position of residues that disappear upon addition of substoichiometric $p15^{50–77}$, and are not drawn to scale. The residues perturbed by $p15^{50–77}$ and that also appear at the interface of the $p15^{50–77}$–PCNA–DNA crystal structure are labeled. (**C**) Front- and back-face views of PCNA surface. PCNA residues whose amide signals disappear in the presence of substoichiometric $p15^{50–77}$, or are significantly perturbed by DNA are colored green or red, respectively. $p15^{50–77}$ at the three PCNA PIP-box sites is shown in sticks, and DNA in the crystallographic position is shown as and orange ribbon.

replicating damaged templates (36). Addition of a 10-fold excess of PCNA (lanes 4–5) did not significantly affect pol η activity. Such effect is not surprising: while PCNA has been shown to stimulate pol η activity on DNA substrates with blocked ends (36,37) or circular templates (38), this stimulation may not be captured on a DNA substrate with free ends as the one in our assay, because of the rapid turnover of PCNA across the substrate. In addition, if PCNA stimulation of pol η results from an increased affinity for the incorporated nucleotide (38), the saturating nucleotide concentrations used in our experiment would mask the stimulation. On the other hand, addition of equimolar amounts of PCNA and p15 (lanes 2–3) reduced nucleotide incorporation at +2 and +3 positions reproducibly also in independent experiments (Supplementary Figure S7). To rule out the possibility that the inhibitory effect of p15 on pol η activity is due to a defective loading of PCNA onto the primer-template (P/T) junction of the DNA substrate, the TLS experiment was repeated in the presence of *Saccharomyces Cerevisiae* Replication Factor C (ScRF-C), which is able to load human PCNA on DNA (39). Our results (Supplementary Figure S8) show that p15 delays TLS by pol η–PCNA across a cis-Pt lesion even in the presence of RF-C.

The replication experiment was repeated with the same DNA substrate without the lesion (Figure 4B). Again, while pol η alone (lanes 10–13) or in the presence of PCNA (lanes 6–9) showed equal processivity, the addition of PCNA and p15 reduced nucleotide incorporation at position +2 at the initial time point (lane 2), and slowed down the synthesis of the full-length product (lanes 3–5). To confirm that the inhibitory effect of p15 is mediated by the interaction with PCNA and not by a direct interaction with pol η, the activity of pol η in replicating the substrate was tested in the absence or presence of p15 alone, showing that p15 alone does not affect the activity of the polymerase (Supplementary Figure S9). To assess whether a p15 fragment spanning the region interacting with PCNA is sufficient to induce the inhibitory effect on pol η observed with full length p15, pol η activity was tested on the undamaged DNA substrate (Figure 4C) in the presence of PCNA and in the absence (lanes 2 and 3) or in the presence of $p15^{41–72}$ peptide (lanes 4,5) or full length p15 (lanes 6,7). Addition of $p15^{41–72}$ or p15 in combination with PCNA caused a reduction of DNA synthesis with respect to pol η and PCNA alone, which stopped at positions +1 and +2, corresponding to incorporation opposite the first two Gs of the template. These results indicate that p15 or $p15^{41–72}$ in conjunction with PCNA are able to reduce pol η synthesis at comparable levels.

Considering the concentrations of pol η, PCNA and p15 in the assays in Figure 4A and B, and the dissociation con-

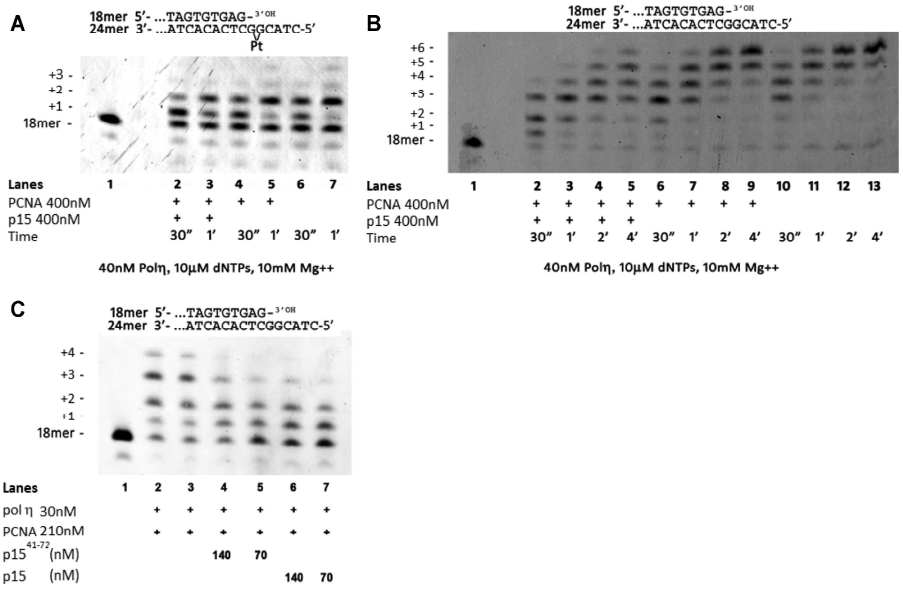

Figure 4. Inhibition of pol η holoenzyme by p15 (**A**) Time course of the reaction of pol η in the presence of PCNA/p15 at equimolar concentrations (Lanes 2 and 3), in the presence of PCNA (Lanes 4 and 5), or with pol η alone (lanes 6 and 7) on a cisPt(GG) template (10 nM), with all four dNTPs at the indicated concentration. (**B**) Time course of the reaction of pol η on the template without the lesion (10 nM), in the presence of PCNA/p15 at equimolar concentrations (lanes 2–5), in the presence of PCNA (lanes 6–9), or pol η alone (lanes 10–13), with all four dNTPs at the indicated concentration. (**C**) Reaction of pol η replicating the undamaged template in the presence of PCNA and in the absence or presence of $p15^{41–72}$ peptide or full length p15. Reactants at the indicated concentrations were incubated at 37°C for 30 s and the reaction was stopped by addition of standard denaturing gel loading buffer. In all these experiments, PCNA was not ubiquitylated. These experiments show that p15 downregulates the activity of pol η–PCNA holoenzyme in bypassing a cisplatin lesion as well as in replicating a normal DNA substrate.

stants for the pol η–PCNA ($K_d = 0.4$ μM, measured by surface plasmon resonance at 25°C) (40) and p15–PCNA ($K_d = 1.1$ μM, measured by ITC at 25°C) (4) binding equilibria, we estimated the relative populations of binary complexes assuming that binding of pol η and p15 to PCNA is mutually exclusive. Under this assumption, 42% of pol η and 23% of p15 are saturated with PCNA. Thus, each dNTP insertion step is carried out by a combination of pol η alone and pol η holoenzyme. However, if p15 did inhibit binding of pol η to PCNA, a drop of pol η activity in the presence of p15 should not be observed, because the latter would favor the formation of free pol η, which shows full activity. Furthermore, the relatively high (30 nM) (36) and low (5 μM) (4) affinity of pol η and p15 for DNA, respectively, rules out that p15 may prevent the access of pol η to the DNA P/T junction. This suggests that inhibition of pol η processivity in the presence of PCNA and p15 is due to the formation of an impaired ternary p15–PCNA–pol η holoenzyme, deficient in primer synthesis against both damaged and normal templates.

DISCUSSION

Topology and stoichiometry of p15 binding to PCNA loaded on DNA

The data reported in this study reveals that DNA can thread through the PCNA ring along with two p15 chains, and that the structure of the p15 segment interacting with PCNA is invariant in the absence or presence of DNA. In our MD simulations, the disordered N-termini of the p15 fragments exit the PCNA back face, a topology analogous to that of full length p15 bound to PCNA in the absence of DNA (4,21). The limited number of contacts between $p15^{50–77}$ and DNA observed in our computational analysis suggests that p15 mostly operates as a passive steric obstacle constraining the DNA in the clamp channel. Critically, p15 shields key residues at the PCNA sliding surfaces, confining DNA in discrete positions, which depend on the p15 stoichiometry of binding (Figure 5A–D). This mode of binding, with DNA partially competing with p15 for a single binding site on the clamp inner ring, is also supported by (i) our NMR study showing that DNA does not disengage p15 from the inner wall of PCNA saturated with p15 and (ii) our structure of PCNA co-crystallized with three p15 peptides and DNA, showing that DNA does not occupy the central channel.

Because p15 is stably associated with PCNA on chromatin during the S phase of the cell cycle (18), it is likely that during replication polymerases and other DNA-editing enzymes bind one or two PCNA sites only, so that the free sites(s) would be available for p15 binding. Indeed, the catalytic subunit of pol δ (p125) and Fen-1 were co-precipitated with p15 and PCNA from pancreatic cell lysates (19). While Fen-1 is a monomeric enzyme that binds PCNA through a

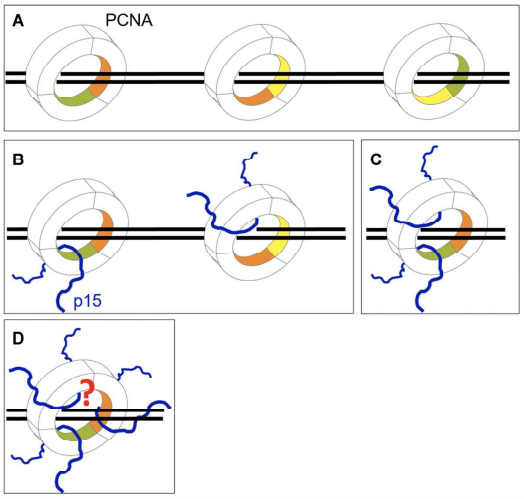

Figure 5. Possible effects of p15 on PCNA sliding (**A**) PCNA can diffuse on DNA contacting three equivalent sliding surfaces, each composed of two homologous sets of basic residues spanning across the interface of two subunits (the 3 PCNA subunits are colored green, yellow and wheat). (**B–D**) The stoichiometry of p15 binding to the PCNA homotrimer defines the available surfaces for clamp sliding. Whether a configuration where PCNA simultaneously binds three p15 chains and DNA, can be achieved, and whether it completely or partially hinders sliding, remains to be determined.

single PIP-box (41), human pol δ consists of four subunits (p125, p66, p50 and p12) and all of them are required for optimal holoenzyme activity (42). Although all four subunits contain potential PIP-box sites, examination of reconstituted holoenzymes in which the PCNA binding motifs have been mutated or inactivated have only been tested for p12 and p66 (43–45), and there may exist multiple subassemblies of pol δ *in vivo* (46,47). Thus, considering its small size and high flexibility, p15 may coexist with pol δ on the same PCNA homotrimer in a replicating cell. Likewise, a comparison of the Fen-1–PCNA (41) (PDB ID: 1UL1) and $p15^{50–77}$–PCNA (4) (PDB ID: 4D20) crystal structures suggests that Fen-1 and p15 may both be accommodated on a single PCNA ring.

The 78-kDa pol η is less bulky than pol δ and binds PCNA mainly through a single PIP-box located at its flexible C-terminus (40). Considering the comparable PIP-box affinities for PCNA (4,40), pol η and p15 may co-exist on one PCNA homotrimer. The recently determined negative stain EM structure of ubiquitylated PCNA bound to pol η and DNA (48), where two PIP-box sites would be free for p15 binding, supports this hypothesis (Figure 6A).

Possible roles of p15 in the holoenzymes with the replicative and TLS polymerases

We propose that p15 is part of the human holoenzyme that replicates the DNA lagging strand, and may function to fasten the DNA within the clamp channel by reducing the accessible sliding surfaces. We and others have shown that the PCNA–DNA interaction is weak and transient (2,4,5,7,9), and recent evidence showed that human pol δ maintains a loose association with PCNA while replicating (49). Because the polymerase needs to maintain a fixed position relative to the phosphodiester backbone at the P/T junction, a constrained orientation of PCNA with respect to the helical pitch may improve the overall stability of the holoenzyme. Such stabilizing role of p15 would explain the negative effects of p15 knockdown on DNA synthesis (19,20).

While a high-resolution structure of a PCNA–polymerase–DNA complex is still awaiting, both the medium resolution EM structure (50) and MD simulations of *Pyrococcus furiosus* (Pfu) PCNA bound to PolB and DNA (51) show that DNA within the clamp is tilted. Particularly, the MD model of the complex in polymerizing mode shows features at the clamp–DNA interface analogous to those observed in the $p15^{50–77}$–PCNA–DNA model presented here, where five conserved positively charged residues, matching the dsDNA B-helix architecture, interact with five consecutive phosphates of one DNA strand, suggesting that this key determinant of the interaction is conserved and may be present in the pol δ holoenzyme. Indeed, mutation of residues at the PCNA–DNA interface impairs both initiation of DNA synthesis (10) and processivity of pol δ (11), suggesting that the PCNA–DNA interactions control both clamping and sliding activities of PCNA in processive DNA replication. In their computational work, Ivanov and co-workers (51) also showed that the repositioning of the PolB core during the conformational switch from polymerizing to editing modes forces the DNA to tilt from one side of the PfuPCNA channel to the other. A 30° change in DNA tilt within the clamp in the catalytic core of the bacterial replisome from polymerizing to editing modes was also observed in the recent cryo-EM work by Lamers and colleagues (52,53). Perhaps, in the human pol δ holoenzyme, p15 plays a role in guiding DNA through the PCNA inner rim in between DNA synthesis and editing steps of the polymerase.

Single molecule experiments suggested that PCNA may slide by rotationally tracking the DNA helix or by a less frequent translational mode uncoupled from the helical pitch (8), while a recent computational work predicts that the coupling between rotation and translation is weak (9), suggesting that the translational mode is prevalent. Thus, p15 binding to PCNA may increase the rotation-translation coupling by reducing the available sliding surfaces (Figure 5). This, together with the DNA binding activity of the p15 disordered N-terminus, may result in a slower diffusion of PCNA on DNA. Therefore, p15 might regulate the sliding velocity of PCNA, and this function may be required for the DNA damage response to prevent a rapid drift of PCNA from stalled forks in between polymerase swapping events.

Upon encounter of a DNA lesion, pol δ dissociates from PCNA, which becomes ubiquitylated, and is replaced by pol η that replicates DNA past the lesion (54,55). While the ubiquitin moieties of ubiquitylated-PCNA may interact with the C-terminal ubiquitin binding motif (UBZ) of pol η, a large body of data argues that ubiquitylation of PCNA is not strictly necessary for pol η recruitment and activity in TLS (38,56,57). Notably, a recent report unambiguously demonstrates that the binding of pol η to PCNA, and DNA

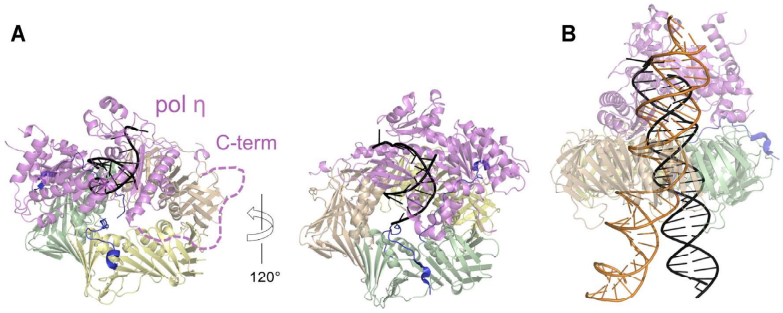

Figure 6. Structural models of pol η-PCNA holoenzymes with p15 and DNA. (**A**) The PCNA trimer of the p15$^{50–77}$–PCNA crystal structure (PDB ID: 4D2G) was superposed to PCNA of the low-resolution structure of human pol η–PCNA–DNA generated from EM data (PDB ID: 3JA9 and 3JAA) (33). DNA is shown in black. The vacant PIP-box site on PCNA (subunit wheat) was occupied by the C-terminal PIP-box of pol η using the crystal structure of human PCNA bound to pol η residues 700–710 (chain W of PDB ID 2ZVK) (40). The dashed line indicates the flexible pol η C-terminus (residues 433–699). (**B**) The PCNA trimer of the structure of p15$^{50–77}$–PCNA–DNA complex (PDB: 6EHT) was superposed to PCNA of the pol η–PCNA–DNA (48) complex (PDB: 3JA9 and and 3JAA). The DNA of the first complex (elongated to 40 bp) is shown as an orange ribbon, that of the latter (elongated to 25 bp) as a black ribbon. According to these models, it is possible that p15 may co-exist with pol η on the same PCNA ring. However, the constraint on DNA within the clamp channel imposed by p15 may hinder the translocation of pol η holoenzyme on DNA.

synthesis by a pol η holoenzyme are both independent of PCNA monoubiquitylation (36).

During unperturbed replication, p15 is mono-ubiquitylated at K15 and K24 and is degraded by the proteasome after UV irradiation or cisplatin treatment (18). Degradation of ubiquitylated p15 upon DNA damage is required for the recruitment of pol η to the replication foci and efficient lesion bypass, and the authors suggested that p15 may prevent the binding of pol η to PCNA. In this work, we showed that p15 has an inhibitory activity on the pol η–PCNA holoenzyme in synthesizing past the 5′dG of a 1,2-d(GpG) cisplatin DNA adduct and in extending the undamaged template. Importantly, a p15 fragment spanning only the region of interaction with PCNA is sufficient to inhibit pol η activity. Rather than preventing pol η from binding to PCNA, our data suggests that p15 inhibits pol η activity by associating to the holoenzyme, a possibility supported by structural considerations (Figure 6A). Although the DNA in the EM map of pol η bound to ubiquitylated PCNA and DNA is not fully defined (48), the DNA duplex within PCNA lies close to one of the clamp subunits, in a position different from that observed in our p15–PCNA–DNA complex structure (Figure 6B). We propose that the constraint imposed to DNA by p15 in the central channel of PCNA may hinder the advancement of DNA in the pol η active site required for the incorporation of the nucleotide opposite to the 5′dG of the DNA template. Thus, after the insertion of the first dCMP, the polymerase may become 'idle' and dissociate from PCNA. Further high-resolution structural studies on pol η holoenzyme will shed light on this possibility.

DATA AVAILABILITY

Atomic coordinates of p15$^{50–77}$–PCNA–DNA and p15$^{41–72}$–PCNA complexes have been deposited in the Protein Databank under the accession codes 6EHT and 6GWS, respectively. Assignments of backbone amide NMR resonances of human PCNA bound to p15$^{50–77}$ and DNA are deposited in the Biological Magnetic Resonance database BMRB under accession code 27558.

SUPPLEMENTARY DATA

Supplementary Data are available at NAR Online.

ACKNOWLEDGEMENTS

We thank Adriana L. Rojas (CIC bioGUNE) for help with crystal structure determination, and Pietro Roversi (University of Leicester) for his useful comments. We acknowledge CERIC-ERIC for the use of the XRD1 beamline at Elettra Sincrotrone Trieste. The authors thankfully acknowledge the computer resources, technical expertise and assistance provided by the Red Española de Supercomputación, the Barcelona Supercomputing Centre, and the Catalan CSUC. *Author Contributions*: G.M., R.C., S.O., F.J.B. and A.D.B. guided the research experiments. M.D.M., A.G.-M. and M.R.-M. crystallised the complexes, solved and refined the crystal structures. S.B.-V. performed and analyzed the MD data. E.M. and E.C. purified pol η and performed the functional assays. N.M. purified PCNA and p15^{PAF} proteins. F.J.B. performed and A.D.B. analyzed the NMR experiments. A.D.B. wrote the manuscript with contributions from all other authors.

FUNDING

Italian Association for Cancer Research [iCARE fellowship from AIRC and the European Commission to A.D.B. and AIRC Grant IG14718 to S.O., IG20762 to G.M and MFAG18811 to E.C.]; Spanish Ministry of Economy and Competitiveness [CTQ2017-83810-R grant to F.J.B.]; CIC bioGUNE acknowledges MINECO for the Severo Ochoa Excellence Accreditation [SEV-2016-0644]; S.B-V. and A.G.-M. acknowledge fellowships from MINECO [BES-2013-063991 and BES-2015-075847]; M.R.-M. is supported by a pre-doctoral fellowship from the Basque

Government [PRE_2016_2_0249]. Funding for open access charge: University of Leicester.
Conflict of interest statement. None declared.

REFERENCES

1. Krishna,T.S., Kong,X.P., Gary,S., Burgers,P.M. and Kuriyan,J. (1994) Crystal structure of the eukaryotic DNA polymerase processivity factor PCNA. *Cell*, **79**, 1233–1243.
2. McNally,R., Bowman,G.D., Goedken,E.R., O'Donnell,M. and Kuriyan,J. (2010) Analysis of the role of PCNA-DNA contacts during clamp loading. *BMC Struct. Biol.*, **10**, 3.
3. Mailand,N., Gibbs-Seymour,I. and Bekker-Jensen,S. (2013) Regulation of PCNA-protein interactions for genome stability. *Nat. Rev. Mol. Cell Biol.*, **14**, 269–282.
4. De Biasio,A., de Opakua,A.I., Mortuza,G.B., Molina,R., Cordeiro,T.N., Castillo,F., Villate,M., Merino,N., Delgado,S., Gil-Carton,D. *et al.* (2015) Structure of p15(PAF)-PCNA complex and implications for clamp sliding during DNA replication and repair. *Nat. Commun.*, **6**, 6439.
5. De March,M., Merino,N., Barrera-Vilarmau,S., Crehuet,R., Onesti,S., Blanco,F.J. and De Biasio,A. (2017) Structural basis of human PCNA sliding on DNA. *Nat. Commun.*, **8**, 13935.
6. De March,M. and De Biasio,A. (2017) The dark side of the ring: role of the DNA sliding surface of PCNA. *Crit. Rev. Biochem. Mol. Biol.*, **52**, 663–673.
7. Ivanov,I., Chapados,B.R., McCammon,J.A. and Tainer,J.A. (2006) Proliferating cell nuclear antigen loaded onto double-stranded DNA: dynamics, minor groove interactions and functional implications. *Nucleic Acids Res.*, **34**, 6023–6033.
8. Kochaniak,A.B., Habuchi,S., Loparo,J.J., Chang,D.J., Cimprich,K.A., Walter,J.C. and van Oijen,A.M. (2009) Proliferating cell nuclear antigen uses two distinct modes to move along DNA. *J. Biol. Chem.*, **284**, 17700–17710.
9. Daitchman,D., Greenblatt,H.M. and Levy,Y. (2018) Diffusion of ring-shaped proteins along DNA: case study of sliding clamps. *Nucleic Acids Res.*, **46**, 5935–5949.
10. Fukuda,K., Morioka,H., Imajou,S., Ikeda,S., Ohtsuka,E. and Tsurimoto,T. (1995) Structure-function relationship of the eukaryotic DNA replication factor, proliferating cell nuclear antigen. *J. Biol. Chem.*, **270**, 22527–22534.
11. Billon,P., Li,J., Lambert,J.P., Chen,Y., Tremblay,V., Brunzelle,J.S., Gingras,A.C., Verreault,A., Sugiyama,T., Couture,J.F. *et al.* (2017) Acetylation of PCNA sliding surface by Eco1 promotes genome stability through homologous recombination. *Mol. Cell*, **65**, 78–90.
12. De Biasio,A. and Blanco,F.J. (2013) Proliferating cell nuclear antigen structure and interactions: too many partners for one dancer? *Adv. Protein Chem. Struct. Biol.*, **91**, 1–36.
13. Freudenthal,B.D., Gakhar,L., Ramaswamy,S. and Washington,M.T. (2010) Structure of monoubiquitinated PCNA and implications for translesion synthesis and DNA polymerase exchange. *Nat. Struct. Mol. Biol.*, **17**, 479–484.
14. Freudenthal,B.D., Brogie,J.E., Gakhar,L., Kondratick,C.M. and Washington,M.T. (2011) Crystal structure of SUMO-modified proliferating cell nuclear antigen. *J. Mol. Biol.*, **406**, 9–17.
15. De Biasio,A., Ibanez de Opakua,A., Cordeiro,T.N., Villate,M., Merino,N., Sibille,N., Lelli,M., Diercks,T., Bernado,P. and Blanco,F.J. (2014) p15PAF is an intrinsically disordered protein with nonrandom structural preferences at sites of interaction with other proteins. *Biophys. J.*, **106**, 865–874.
16. Yu,P., Huang,B., Shen,M., Lau,C., Chan,E., Michel,J., Xiong,Y., Payan,D.G. and Luo,Y. (2001) p15(PAF), a novel PCNA associated factor with increased expression in tumor tissues. *Oncogene*, **20**, 484–489.
17. Emanuele,M.J., Ciccia,A., Elia,A.E. and Elledge,S.J. (2011) Proliferating cell nuclear antigen (PCNA)-associated KIAA0101/PAF15 protein is a cell cycle-regulated anaphase-promoting complex/cyclosome substrate. *Proc. Natl. Acad. Sci. U.S.A.*, **108**, 9845–9850.
18. Povlsen,L.K., Beli,P., Wagner,S.A., Poulsen,S.L., Sylvestersen,K.B., Poulsen,J.W., Nielsen,M.L., Bekker-Jensen,S., Mailand,N. and Choudhary,C. (2012) Systems-wide analysis of ubiquitylation dynamics reveals a key role for PAF15 ubiquitylation in DNA-damage bypass. *Nat. Cell Biol.*, **14**, 1089–1098.
19. Hosokawa,M., Takehara,A., Matsuda,K., Eguchi,H., Ohigashi,H., Ishikawa,O., Shinomura,Y., Imai,K., Nakamura,Y. and Nakagawa,H. (2007) Oncogenic role of KIAA0101 interacting with proliferating cell nuclear antigen in pancreatic cancer. *Cancer Res.*, **67**, 2568–2576.
20. Chang,C.N., Feng,M.J., Chen,Y.L., Yuan,R.H. and Jeng,Y.M. (2013) p15(PAF) is an Rb/E2F-regulated S-phase protein essential for DNA synthesis and cell cycle progression. *PLoS One*, **8**, e61196.
21. Cordeiro,T.N., Chen,P.C., De Biasio,A., Sibille,N., Blanco,F.J., Hub,J.S., Crehuet,R. and Bernado,P. (2017) Disentangling polydispersity in the PCNA-p15PAF complex, a disordered, transient and multivalent macromolecular assembly. *Nucleic Acids Res.*, **45**, 1501–1515.
22. De Biasio,A., Sanchez,R., Prieto,J., Villate,M., Campos-Olivas,R. and Blanco,F.J. (2011) Reduced stability and increased dynamics in the human proliferating cell nuclear antigen (PCNA) relative to the yeast homolog. *PLoS One*, **6**, e16600.
23. Kabsch,W. (2010) Integration, scaling, space-group assignment and post-refinement. *Acta Crystallogr. D. Biol. Crystallogr.*, **66**, 133–144.
24. Winn,M.D., Ballard,C.C., Cowtan,K.D., Dodson,E.J., Emsley,P., Evans,P.R., Keegan,R.M., Krissinel,E.B., Leslie,A.G., McCoy,A. *et al.* (2011) Overview of the CCP4 suite and current developments. *Acta Crystallogr. D. Biol. Crystallogr.*, **67**, 235–242.
25. Murshudov,G.N., Skubak,P., Lebedev,A.A., Pannu,N.S., Steiner,R.A., Nicholls,R.A., Winn,M.D., Long,F. and Vagin,A.A. (2011) REFMAC5 for the refinement of macromolecular crystal structures. *Acta Crystallogr. D. Biol. Crystallogr.*, **67**, 355–367.
26. Emsley,P., Lohkamp,B., Scott,W.G. and Cowtan,K. (2010) Features and development of Coot. *Acta Crystallogr. D. Biol. Crystallogr.*, **66**, 486–501.
27. Abraham,M.J., Murtola,T., Schulz,R., Pail,S., Smith,J.C., Hess,B. and Lindhal,E. (2015) GROMACS: High performance molecular simulations through multi- level parallelism from laptops to supercomputers. *SoftwareX*, **1–2**, 19–25
28. Ivani,I., Dans,P.D., Noy,A., Perez,A., Faustino,I., Hospital,A., Walther,J., Andrio,P., Goni,R., Balaceanu,A. *et al.* (2016) Parmbsc1: a refined force field for DNA simulations. *Nat. Methods*, **13**, 55–58.
29. McGibbon,R.T., Beauchamp,K.A., Harrigan,M.P., Klein,C., Swails,J.M., Hernandez,C.X., Schwantes,C.R., Wang,L.P., Lane,T.J. and Pande,V.S. (2015) MDTraj: A modern open library for the analysis of molecular dynamics trajectories. *Biophys. J.*, **109**, 1528–1532.
30. Hunter,J.D. (2007) Matplotlib: A 2D graphics environment. *Comput. Sci. Eng.*, **9**, 90–95.
31. Sanchez,R., Torres,D., Prieto,J., Blanco,F.J. and Campos-Olivas,R. (2007) Backbone assignment of human proliferating cell nuclear antigen. *Biomol. NMR Assign.*, **1**, 245–247.
32. De Biasio,A., Campos-Olivas,R., Sanchez,R., Lopez-Alonso,J.P., Pantoja-Uceda,D., Merino,N., Villate,M., Martin-Garcia,J.M., Castillo,F., Luque,I. *et al.* (2012) Proliferating Cell Nuclear Antigen (PCNA) interactions in solution studied by NMR. *PLoS One*, **7**, e48390.
33. Frank,E.G., McDonald,J.P., Karata,K., Huston,D. and Woodgate,R. (2012) A strategy for the expression of recombinant proteins traditionally hard to purify. *Anal. Biochem.*, **429**, 132–139.
34. Yeeles,J.T.P., Janska,A., Early,A. and Diffley,J.F.X. (2017) How the eukaryotic replisome achieves rapid and efficient DNA replication. *Mol. Cell*, **65**, 105–116.
35. Georgescu,R.E., Kim,S.S., Yurieva,O., Kuriyan,J., Kong,X.P. and O'Donnell,M. (2008) Structure of a sliding clamp on DNA. *Cell*, **132**, 43–54.
36. Hedglin,M., Pandey,B. and Benkovic,S.J. (2016) Characterization of human translesion DNA synthesis across a UV-induced DNA lesion. *Elife*, **5**, e19788.
37. Haracska,L., Unk,I., Prakash,L. and Prakash,S. (2006) Ubiquitylation of yeast proliferating cell nuclear antigen and its implications for translesion DNA synthesis. *Proc. Natl. Acad. Sci.*, **103**, 6477–6482.
38. Haracska,L., Johnson,R.E., Unk,I., Phillips,B., Hurwitz,J., Prakash,L. and Prakash,S. (2001) Physical and functional interactions of human DNA polymerase eta with PCNA. *Mol. Cell. Biol.*, **21**, 7199–7206.

39. Dzantiev,L., Constantin,N., Genschel,J., Iyer,R.R., Burgers,P.M. and Modrich,P. (2004) Defined human system that supports bidirectional mismatch-provoked excision. *Mol. Cell*, **15**, 31–41.
40. Hishiki,A., Hashimoto,H., Hanafusa,T., Kamei,K., Ohashi,E., Shimizu,T., Ohmori,H. and Sato,M. (2009) Structural basis for novel interactions between human translesion synthesis polymerases and proliferating cell nuclear antigen. *J. Biol. Chem.*, **284**, 10552–10560.
41. Sakurai,S., Kitano,K., Yamaguchi,H., Hamada,K., Okada,K., Fukuda,K., Uchida,M., Ohtsuka,E., Morioka,H. and Hakoshima,T. (2005) Structural basis for recruitment of human flap endonuclease 1 to PCNA. *EMBO J.*, **24**, 683–693.
42. Xie,B., Mazloum,N., Liu,L., Rahmeh,A., Li,H. and Lee,M.Y.W.T. (2002) Reconstitution and characterization of the human DNA polymerase delta four-subunit holoenzyme. *Biochemistry*, **41**, 13133–13142.
43. Li,H., Xie,B., Zhou,Y.J., Rahmeh,A., Trusa,S., Zhang,S.F., Gao,Y., Lee,E.Y.C. and Lee,M.Y.W.T. (2006) Functional roles of p12, the fourth subunit of human DNA polymerase delta. *J. Biol. Chem.*, **281**, 14748–14755.
44. Rahmeh,A.A., Zhou,Y.J., Xie,B., Li,H., Lee,E.Y.C. and Lee,M.Y.W.T. (2012) Phosphorylation of the p68 subunit of Pol delta acts as a molecular switch to regulate its interaction with PCNA. *Biochemistry*, **51**, 416–424.
45. Zhang,S.F., Zhou,Y.J., Trusa,S., Meng,X., Lee,E.Y.C. and Lee,M.Y.W.T. (2007) A novel DNA damage response - rapid degradation of the p12 subunit of DNA polymerase delta. *J. Biol. Chem.*, **282**, 15330–15340.
46. Meng,X., Zhou,Y., Zhang,S., Lee,E.Y., Frick,D.N. and Lee,M.Y. (2009) DNA damage alters DNA polymerase delta to a form that exhibits increased discrimination against modified template bases and mismatched primers. *Nucleic Acids Res.*, **37**, 647–657.
47. Meng,X., Zhou,Y.J., Lee,E.Y.C., Lee,M.Y.W.T. and Frick,D.N. (2010) The p12 subunit of human polymerase delta modulates the rate and fidelity of DNA synthesis. *Biochemistry*, **49**, 3545–3554.
48. Lau,W.C., Li,Y., Zhang,Q. and Huen,M.S. (2015) Molecular architecture of the Ub-PCNA/Pol eta complex bound to DNA. *Sci. Rep.*, **5**, 15759.
49. Hedglin,M., Pandey,B. and Benkovic,S.J. (2016) Stability of the human polymerase delta holoenzyme and its implications in lagging strand DNA synthesis. *Proc. Natl. Acad. Sci.*, **113**, E1777–E1786.
50. Mayanagi,K., Kiyonari,S., Saito,M., Shirai,T., Ishino,Y. and Morikawa,K. (2009) Mechanism of replication machinery assembly as revealed by the DNA ligase-PCNA-DNA complex architecture. *Proc. Natl. Acad. Sci.*, **106**, 4647–4652.
51. Xu,X., Yan,C., Kossmann,B.R. and Ivanov,I. (2016) Secondary interaction interfaces with PCNA control conformational switching of DNA polymerase PolB from polymerization to editing. *J. Phys. Chem. B*, **120**, 8379–8388.
52. Fernandez-Leiro,R., Conrad,J., Yang,J.C., Freund,S.M., Scheres,S.H. and Lamers,M.H. (2017) Self-correcting mismatches during high-fidelity DNA replication. *Nat. Struct. Mol. Biol.*, **24**, 140–143.
53. Fernandez-Leiro,R., Conrad,J., Scheres,S.H. and Lamers,M.H. (2015) cryo-EM structures of the E. coli replicative DNA polymerase reveal its dynamic interactions with the DNA sliding clamp, exonuclease and tau. *Elife*, **4**, e11134.
54. Biertumpfel,C., Zhao,Y., Kondo,Y., Ramon-Maiques,S., Gregory,M., Lee,J.Y., Masutani,C., Lehmann,A.R., Hanaoka,F. and Yang,W. (2010) Structure and mechanism of human DNA polymerase eta. *Nature*, **465**, 1044–1048.
55. Waters,L.S., Minesinger,B.K., Wiltrout,M.E., D'Souza,S., Woodruff,R.V. and Walker,G.C. (2009) Eukaryotic translesion polymerases and their roles and regulation in DNA damage tolerance. *Microbiol. Mol. Biol. Rev.*, **73**, 134–154.
56. Hoege,C., Pfander,B., Moldovan,G.L., Pyrowolakis,G. and Jentsch,S. (2002) RAD6-dependent DNA repair is linked to modification of PCNA by ubiquitin and SUMO. *Nature*, **419**, 135–141.
57. O'Donnell,M., Langston,L. and Stillman,B. (2013) Principles and concepts of DNA replication in bacteria, archaea, and eukarya. *Cold Spring Harb. Perspect. Biol.*, **5**, a010108.

Biophysical *Journal*
Article

Biophysical Society

The Incorporation of Ribonucleotides Induces Structural and Conformational Changes in DNA

Alice Meroni,[1] Elisa Mentegari,[2] Emmanuele Crespan,[2] Marco Muzi-Falconi,[1,*] Federico Lazzaro,[1] and Alessandro Podestà[3,*]
[1]Dipartimento di Bioscienze, Università degli Studi di Milano, Milano, Italy; [2]DNA Enzymology and Molecular Virology, Institute of Molecular Genetics IGM-CNR, Pavia, Italy; and [3]Dipartimento di Fisica and C.I.Ma.I.Na, Università degli Studi di Milano, Milano, Italy

ABSTRACT Ribonucleotide incorporation is the most common error occurring during DNA replication. Cells have hence developed mechanisms to remove ribonucleotides from the genome and restore its integrity. Indeed, the persistence of ribonucleotides into DNA leads to severe consequences, such as genome instability and replication stress. Thus, it becomes important to understand the effects of ribonucleotides incorporation, starting from their impact on DNA structure and conformation. Here we present a systematic study of the effects of ribonucleotide incorporation into DNA molecules. We have developed, to our knowledge, a new method to efficiently synthesize long DNA molecules (hundreds of basepairs) containing ribonucleotides, which is based on a modified protocol for the polymerase chain reaction. By means of atomic force microscopy, we could therefore investigate the changes, upon ribonucleotide incorporation, of the structural and conformational properties of numerous DNA populations at the single-molecule level. Specifically, we characterized the scaling of the contour length with the number of basepairs and the scaling of the end-to-end distance with the curvilinear distance, the bending angle distribution, and the persistence length. Our results revealed that ribonucleotides affect DNA structure and conformation on scales that go well beyond the typical dimension of the single ribonucleotide. In particular, the presence of ribonucleotides induces a systematic shortening of the molecules, together with a decrease of the persistence length. Such structural changes are also likely to occur in vivo, where they could directly affect the downstream DNA transactions, as well as interfere with protein binding and recognition.

INTRODUCTION

Current opinion on the evolution of genetic information suggests that DNA was selected as the storage molecule because it is more stable with respect to its ancient precursor, RNA (1). The only difference between DNA and RNA is the presence of a hydroxyl group on the ribose of RNA monomers (rNMPs). Such group makes RNA unstable and less suitable to safely store genetic information (2).

Recent works reported that large amounts of ribonucleotides are misincorporated into chromosomes during DNA replication, even though DNA polymerases are extremely accurate enzymes (3–5). The frequency of incorporation in budding yeast is estimated to be ~1 every 700 nucleotides, making ribonucleotides the most frequent noncanonical nucleotides incorporated into the genome (6).

The elevated levels of ribonucleotides incorporated may suggest that this is not a mere error of DNA polymerases, but that it may have some beneficial roles. Indeed, it was recently demonstrated that ribonucleotides help a specific DNA repair pathway in discriminating the newly synthesized strand from the template filament (7,8). However, ribonucleotides are not permanent in DNA, because cells possess specific mechanisms to remove them from the genome (6,9). The persistence of rNMPs is an endogenous source of genome instability and replication stress (5,10–12).

RNase H enzymes are able to recognize and cleave embedded rNMPs (13), and are responsible for the major pathway that processes genomic rNMPs. Interestingly, defects in RNase H2 function represent the major cause of a rare genetic disorder, Aicardi-Goutieres syndrome (14).

How rNMPs embedded in chromosomal DNA may interfere with DNA-protein interactions has not been investigated yet, although it has been reported that nucleosomes assembly on DNA is reduced when even a single ribonucleotide is present (15). Understanding the structural changes imposed upon DNA molecules by the presence of

Submitted March 6, 2017, and accepted for publication July 25, 2017.

*Correspondence: marco.muzifalconi@unimi.it or alessandro.podesta@mi.infn.it

Federico Lazzaro and Alessandro Podestà contributed equally to this article.

Editor: Karin Musier-Forsyth.

http://dx.doi.org/10.1016/j.bpj.2017.07.013

ribonucleotides is essential to determine the biological impact of their persistence in the genome. It is thus crucial to explore and investigate those effects at the single-molecule level.

During the 1990s, the first ribonucleotides containing DNA (RC-DNA) molecules were crystallized. These were very short self-complementary oligonucleotides with embedded ribonucleotides. X-ray diffraction analyses suggested that the presence of ribonucleotides induce a complete change toward the A-conformation, both when they are in the middle or at the ends of the molecules (16–18). In solution studies, such as nuclear magnetic resonance, the transition observed was partial (19,20). Molecular dynamics simulations suggested that even with 50% of ribonucleotide substitutions, B-DNA is not fully converted to A-DNA, although the ribose caused local perturbations (21). In addition, atomic force microscopy (AFM) measurements showed that ribonucleotides also perturb the backbone elasticity (22–24) with respect to DNA in the B-form, although these studies report different trends of the persistence length in relation to the presence of ribonucleotides. In conclusion, only a few single-molecule studies on the structural properties of RC-DNAs are available in the literature, and furthermore, in some cases apparently contradictory results are reported. And in most cases, short RC-DNA molecules are studied, although in biologically relevant cases (such as in vivo), the molecules are much longer.

Here we present the results of a systematic study of the structural effects of ribonucleotide incorporation into DNA carried out taking advantage of, to our knowledge, a novel protocol to synthesize several-hundred-of-basepairs-long RC-DNA molecules. RC-DNA molecules were produced via enzymatic synthesis by a mutant *Taq* polymerase (I614K), able to introduce ribonucleotides (rNTPs) in addition to deoxynucleotides (dNTPs). We were therefore able to produce numerous populations of RC-DNA molecules, as well as their controls without ribonucleotides, that have been studied at the single-molecule level by means of AFM. The main advantage of AFM is the possibility of studying large ensembles of molecules, by quantitatively analyzing each molecule individually, therefore obtaining robust average values of relevant structural and conformational observables (25–28). In particular, we have characterized the scaling of the contour length with the number of basepairs, the scaling of the end-to-end distance with the curvilinear distance, the bending angle distribution, and the persistence length of DNA molecules, showing that the presence of ribonucleotides affects the DNA structure and conformation well beyond the scale of the single ribonucleotide, up to full molecular length. The observed changes are also likely to take place in physiological conditions such as the cell environment, and consequently influence DNA transactions occurring in vivo.

MATERIALS AND METHODS

Taq polymerase production

The pTaq plasmid was site-directed mutagenized using primers TAQI614K for 5′-TGG CCC TGG ACT ATA GCC AGA AAG AGC TCA GGG TGC TGG CCC A-3′ and TAQI614Krev 5′-TGG GCC AGC ACC CTG AGC TCT TTC TGG CTA TAG TCC AGG GCC A-3′. BL21(DE3) *Escherichia coli* cells harboring pTaq or pTaqI614K were grown in selective medium and protein expression was induced by IPTG addition. Protein extraction and purification was done by GeneSpin (Milan, Italy).

RC-DNAs synthesis

Polymerase chain reaction (PCR) was performed with either wild-type (WT) or I614K *Taq* polymerase in the presence of dATP, dGTP, and dTTP 0.2 mM, dCTP 0.1 mM for normal DNAs, and plus rCTP 0.8 mM only for RC-DNAs. Nucleotides were purchased from GeneSpin. The 464- and 727-basepair (bp) fragments were amplified from pGEM3Zf plasmid using primer pairs 5′-TCG GGA AAC CTG TCG TGC C-3′/5′-CAG CGT GAG CTA TGA GAA AG-3′ and 5′-TCG GGA AAC CTG TCG TGC C-3′/5′-TCA GCA GAG CGC AGA TAC CA-3′, respectively. The 646-bp fragment was amplified from pNB187 plasmid using primers 5′-TAG TTG AAG CAT TAG GTC CC-3′/5′-CTT CTC AAA TAT GCT TCC CA-3′; the 960- and the 1079-bp fragments were amplified from pFL39.3 with primers 5′-AAA GAG TTA CTC AAG AAT AA-3′/5′-CAA AAC GGC ATT TAA GAA GC-3′ and 5′-GGA CGA GGC AAG CTA AAC AG-3′/5′-CAA AAC GGC ATT TAA GAA GC-3′, respectively. The complete sequences are reported in Fig. S8. PCR reactions were carried out in multiple independent samples and then pooled to increase the product yield. The samples were loaded onto 1% agarose gel and the band corresponding to the amplification product was excised and purified using silica columns (The Wizard SV Gel and PCR Clean-Up System; Promega, Fitchburg, WI) according to the manufacturer's instructions. This last step was necessary to further clean the samples from template plasmid and primers. All the samples were finally resuspended in ultrapure Milli-Q water (Millipore, Billerica, MA).

PCR with radiolabeled nucleotides

PCR reactions were performed adding α^{32}P-dCTP or α^{32}P-rCTP (PerkinElmer, Waltham, MA) in addition to the nonradioactive dCTP or rCTP, respecting the final concentrations described above for RC-DNAs. Samples were drop-dialyzed on 0.025-μm membranes (Millipore) and further cleaned by ethanol precipitation. Samples were then run in a 2% agarose gel that was dried and exposed on a phosphor storage screen; images were acquired using a Phosphoimager (Typhoon FLA 7000; GE Healthcare, Buckinghamshire, UK).

Alkaline gel and Southern blot

Alkaline gel electrophoresis was performed as described in (29). Briefly, samples were incubated for 2 h at 55°C in 0.3 M NaOH and then run in alkaline gel (1% agarose in Milli-Q water with 1 mM EDTA and 250 mM NaOH) previously equilibrated in its alkaline running buffer (1 mM EDTA, 250 mM NaOH). DNA was transferred to a charged nylon membrane (GeneScreen Plus Hybridization Transfer Membrane; PerkinElmer) by Southern blotting and hybridized with the radiolabeled 464-bp fragment as a probe (prepared by a DECAprime II DNA Labeling Kit; Ambion, Austin, TX). Images were acquired using a Phosphoimager (Typhoon FLA 7000; GE Healthcare).

AFM imaging

The procedure is described in detail in (30). Samples were deposited on freshly cleaved mica of the highest quality (V1, ruby muscovite; Ted Pella,

Redding, CA) in a Mg^{2+}-containing buffer (5 mM $MgCl_2$, 10 mM NaCl, 10 mM HEPES-Na, pH 7.5 in Milli-Q H_2O). Incubation time ranged from 2 to 10 min at room temperature, then the samples were gently washed dropwise with 1–2 mL of Milli-Q water, and dried under a clean nitrogen stream. Images were captured in air, using a Multimode Nanoscope IV AFM (Bruker, Billerica, MA) working in tapping mode, equipped with rigid cantilevers (~300 kHz resonance frequency) and single-crystal silicon tips with nominal radius of curvature below 10 nm. The scan rate was typically 1.5–2 Hz, the scan area 2 × 1 μm, with a sampling resolution of 1 and 2 nm/pixel in the fast and slow scan directions, respectively.

Analysis of AFM data

Raw images were first flattened by subtracting polynomials up to the third order, using only the flat mica surface as reference for the fit. DNA and RC-DNA molecules were semiautomatically traced using FiberApp software (31), to obtain the spatial coordinates of the backbones. Calibration of the scanner was checked by scanning a calibration grating and the determined correction factors (always <2–3%) were applied to the coordinates, when needed. The traces were analyzed using custom MATLAB (The MathWorks, Natick, MA) routines. We evaluated the following statistical quantities describing structural/mechanical and conformational properties of semirigid polymers, as described in our previous works (26,30): the mean contour length $\langle l \rangle$, the mean squared end-to-end distance $\langle R^2(L) \rangle$ of segments of the molecules with a curvilinear length (curvilinear distance) L, the distribution of bending angles $\theta(L)$ (as well as $\langle \cos(\theta(L)) \rangle$ and $\langle \theta^2(L) \rangle$), and the persistence length P. If DNA molecules are in a well-defined form (either B or A), the $\langle l \rangle$ versus n of the bp curve is a straight line with a slope equal to r_A or r_B, the rise per residues of the A and B forms, respectively, with units nm/bp. A reduction of the contour length independent on bp simply shifts the curve vertically by a constant offset c, but does not alter the slope of the curve. According to the wormlike chain (WLC) model, in two dimensions the mean squared end-to-end distance $\langle R^2 \rangle_{2D}$ increases as the curvilinear distance L increases, and depends on the persistence length P of DNA as (25,26):

$$\langle R^2(L) \rangle_{2D} = 4PL\left[1 - \frac{2P}{L}\left(1 - e^{-\frac{L}{2P}}\right)\right]. \quad (1)$$

Estimation of the fraction of incorporated rCTP. To estimate the percentage $\%rCTP$ of rCTP incorporated into RC-DNA molecules, we use Eq. 2, i.e., we multiply the fraction of sites along the DNA backbone available for rCTP incorporation (the GC content $\%GC$) by the estimated frequency of incorporation, $f_{\text{incorporation}}$ (defined and calculated with Eq. 3 in the Results and Discussion):

$$\%rCTP_{\text{incorporated}} = \%GC \cdot f_{\text{incorporation}} \cdot 100. \quad (2)$$

Apparent B to A transition fraction. An apparent fraction of basepairs in the DNA molecules that have switched from B to A conformation can be calculated by assuming that whenever an rCTP is incorporated, the hosting basepair switches from the B to the A form. The B-to-A transition fraction represents the fraction of basepairs that undergo such transition. Following (32,33), the total number of available basepairs before rCTP incorporation is $N = (l_0 - c)/r_B$, where l_0 is the measured contour length; c is a possible systematic shortening of the molecules, as discussed before (the negative intercept of the $\langle l \rangle$ versus n of basepairs curve shown in Fig. 4); and $r_B = 0.34$ nm/bp is the B-form helical rise. After rCTP incorporation, N_A basepairs switch to the A conformation whereas N_B basepairs remain in the B conformation, such that $N = N_B + N_A$. In terms of contour length, $N_B\, r_B + N_A\, r_A = (l_0 - c) - |\Delta l|$, where $r_A = 0.26$ nm/bp is the A-form helical rise and Δl is the measured difference in contour length upon ribonucleotide introduction. It follows that the bases in A form are $N_A = |\Delta l|/(r_B - r_A)$, and the B to A transition fraction N_A/N can be calculated as $N_A/N = [|\Delta l|/(l_0 - c)] \times [r_B/(r_B - r_A)]$.

Statistical analysis. Length data are reported in the figures and tables as mean value ± effective error. The mean values and the SDs have been obtained by a Gaussian fit of the distributions of experimental values (see Fig. S4 for some representative distributions of contour length values). The effective errors have been calculated by summing in quadrature the SDs of the mean and a systematic error of ± 1% due to the z-piezo calibration. The error associated to the persistence length, extracted by fitting Eq. 1 to the average end-to-end distance curves of the samples, has been estimated by applying the fit to a few set of data obtained by adding a Gaussian noise to the average curves, whose width was set equal to the SD of the mean associated to each experimental value (the resulting error bar is comparable to the marker size, and it is not shown in the graphs). The significance of the observed differences in the value of relevant parameters was evaluated applying a two-tailed t-test.

RESULTS AND DISCUSSION

Synthesis of RC-DNA molecules

DNA molecules with incorporated ribonucleotides are generally synthesized chemically by a stepwise addition of nucleotides, whose limit is the chain extension step; as a result, with this methodology, only relatively short molecules are produced. Such short RC-DNAs molecules (10–30 bp) have been studied by several techniques (16,21,22), reproducing environments quite far from the physiological one.

We propose, to our knowledge, a new approach to synthesize RC-DNA molecules that exploits many consecutives cycles of an enzymatic reaction known as PCR. PCR is performed with the *Thermus aquaticus* DNA Polymerase (*Taq* pol), a very versatile enzyme, able to sustain multiple reaction cycles to amplify a defined DNA sequence exponentially (34). *Taq* pol is endowed with a high capability of discrimination between dNTPs and rNTPs; we took advantage of a known mutant version that is able to incorporate ribonucleotides more efficiently (35). We mutated the *Taq* pol with a single amino acid substitution at Isoleucine 614 to Lysine, making the enzyme more prone to binding and introducing rNTPs (35). The incorporation rates range from 150- to 1500-fold with respect to the WT *Taq* pol, depending on the rNTP species (rCTP, rATP, rGTP, or rTTP) (35). We expressed and purified both the WT and I614K *Taq* pols from *E. coli* cells, as described in Materials and Methods.

PCR allows the synthesis of a significant number of linear molecules, thanks to repetitive cycles of reaction. We set PCR conditions for the I614K *Taq* pol, in the presence of all four dNTPs and of rCTP, the most common ribonucleotide found in the DNA of living cells (36,37). To verify the effective rCTP incorporation, PCRs were performed using radiolabeled α^{32}P-rCTP, and the amplification products (464 bp) were then purified and visualized by autoradiography after agarose gel electrophoresis. The radioactive signal corresponding to a band of 464 bp indicates that the I614K *Taq* pol is indeed introducing α^{32}P-rCTP, although with low efficiency compared to α^{32}P-dCTP (Fig. 1).

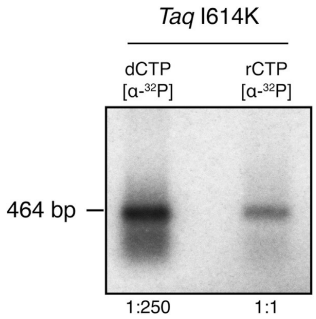

FIGURE 1 *Taq* polymerase I614K introduces rCTP in PCR products. DNA is amplified by I614K *Taq* pol mutant in the presence of radiolabeled α^{32}P-dCTP or α^{32}P-rCTP, and then it is separated onto an agarose gel, after purification through drop-dialysis and ethanol precipitation. The radioactive signal visible in the rCTP lane confirms that PCR products contain rNMPs.

From the published kinetic parameters of I614K *Taq* pol (35) it is possible to theoretically estimate such frequency of incorporation, using

$$f_{\text{incorporation}} = \frac{v_{d\text{CTP}}}{v_{r\text{CTP}}} = \frac{\frac{K_{\text{cat}}^{d\text{CTP}}}{K_m^{d\text{CTP}}}[d\text{CTP}]}{\frac{K_{\text{cat}}^{r\text{CTP}}}{K_m^{r\text{CTP}}}[r\text{CTP}]}. \quad (3)$$

In our PCR conditions, the mutant *Taq* pol introduces one rCTP every 19 dCTP, in front of each guanosine residue (*G*), respecting the Watson-Crick basepairing. In fact, its misincorporation rates are small, regardless of the fact that I614K mutation confers less fidelity to the polymerase (38), as we verified by sequencing (data not shown).

To assess to what extent ribonucleotides are present in RC-DNA molecules, we exploited alkaline gel electrophoresis. PCR reactions were performed with I614K *Taq* pol in the presence or absence of rCTP and the products (see Fig. S1) were separated by gel electrophoresis in alkaline conditions; here the DNA is denatured and its backbone hydrolyzed at ribonucleotide positions, generating smaller fragments (4). Fig. 2 shows the degree of alkaline degradation of the 464-bp fragments, synthesized either in the absence or presence of rCTP. The molecules produced without rCTP migrate as a sharp band, whereas the ones containing rCTP generate a smear of smaller fragments, confirming the presence of ribonucleotides in most of them.

The presence of rNMPs in the template strand could interfere with the *Taq* pol activity in the following reaction cycles, as reported for other polymerases (39,40). To exclude this, we tested the ability of the mutant *Taq* pol to bypass ribonucleotides in the template by using a primer extension assay. The I614K *Taq* polymerase efficiently bypasses embedded rCMP in DNA (Fig. S2); a slight

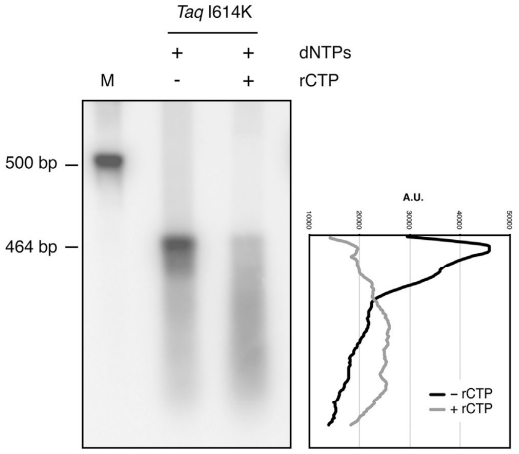

FIGURE 2 RC-DNA molecules are sensitive to alkaline hydrolysis. DNA is amplified in the presence or absence of rCTP and run in alkaline conditions. The DNA backbone is hydrolyzed in correspondence to ribonucleotides, resulting in a population of smaller molecules. Only molecules produced in the presence of rCTP are hydrolyzed and their corresponding band is converted to a smear signal. DNA is detected by Southern blotting hybridization, using the radiolabeled 464-bp fragment as a probe. The chart on the right displays the lane profiles in the presence or absence of rCTP.

pausing before the rNMP can be detected at enzyme concentrations much lower than those used in PCR reactions. Our synthesis strategy allows us, therefore, to obtain full-length amplified sequences.

AFM imaging and characterization of RC-DNAs

Once the RC-DNA production has been validated, we generated several DNA molecules with different lengths and features. We produced and purified DNA and RC-DNA molecules with five different lengths in basepairs (464, 646, 727, 960, and 1079), and subjected them to AFM imaging. As described in detail in the Materials and Methods, DNA molecules were deposited onto a negatively charged mica surface, where they adsorb thanks to the mediation of magnesium divalent ions, which bridge the negative charges of the DNA backbone and the mica surface. Fig. 3 shows three representative AFM images of DNA and RC-DNA molecules produced with either WT or I614K *Taq* polymerases. Typically, the DNA molecules are well contrasted, thanks to the Mg^{2+} buffer, which provides a clean way to bind the molecules to the mica surface, preserving the atomic smoothness and cleanliness of the freshly cleaved substrates. Because the efficiency of PCR decreases when the mutated *Taq* is used, and when ribonucleotides are added to the reaction, AFM maps typically feature a decreasing number of molecules per unit area. Some molecules from both WT and I614K *Taq* pol (~20%) exhibited severe

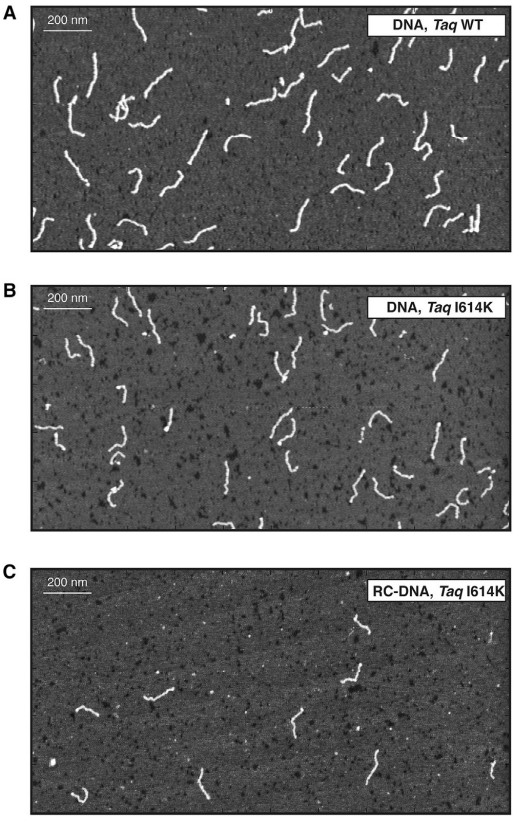

FIGURE 3 Representative AFM topographies of 464-bp molecules. Molecules are deposited on mica and imaged in air by AFM. (*A*) Shown here are DNA molecules synthesized with WT and (*B*) I614K *Taq* pol in the presence of dNTPs, and (*C*) RC-DNA molecules synthesized with the addition of rCTP by the I614K *Taq* polymerase. The size of the image is $2 \times 1\ \mu m^2$.

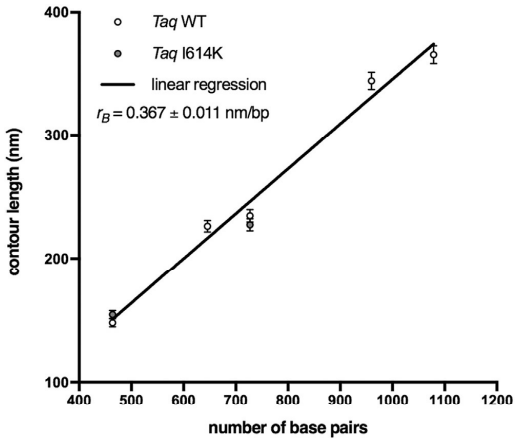

FIGURE 4 DNA molecules from WT and I614K *Taq* pol retain canonical B conformation. Measured contour length values are plotted versus the number of basepairs of each DNA population analyzed (464, 646, 727, 960, and 1079), produced either by WT or I614K *Taq* polymerases. The linear fit ($R^2 = 0.9851$) exhibits a slope ($r_B = 0.367 \pm 0.011$ nm/bp) close to the one typical of B DNA conformation. The length of the molecules produced by the mutated I614K *Taq* pol agrees with the length of the corresponding molecules produced by the WT *Taq* pol, within the error. The number of analyzed 464-, 646-, 727-, 960-, and 1079-bp WT *Taq* pol molecules is 146, 92, 74, 67, and 46, respectively; the number of analyzed 464- and 727-bp I614K *Taq* pol molecules is 176 and 47, respectively.

irregularities in their shape and dimensions, such as overlapping and condensed regions, protruding asperities, etc., and were not considered for the analysis. These molecules were excluded on the basis of a visual analysis as well as of the analysis of representative profiles, as shown in Fig. S3. As detailed in Materials and Methods, molecules from several AFM topographic profiles were semiautomatically traced to calculate the relevant structural and conformational quantities (contour length, rise per residue, bending angle distribution, and end-to-end distance curve).

To validate our experimental imaging conditions, we have first characterized the conformational properties of DNA molecules produced by the WT *Taq* pol with dNTPs only. The scaling of the average contour length of linear DNA molecules with respect to the number of basepairs (464, 646, 727, 960, and 1079) is shown in Fig. 4.

The slope of the contour length versus number-of-base-pairs curve represents the rise per residue r of the molecules. We found $r_B = 0.367 \pm 0.011$ nm/bp, which is close to the value for the B form of DNA ($r_B = 0.34$ nm/bp), and significantly larger than the rise per residue of the A form ($r_A = 0.26$ nm/bp). Notably, the intercept c of the fitting line in Fig. 4 is negative ($c = -21.3 \pm 7.2$ nm), witness to a reduction of the contour length of the molecules, irrespective of the number of basepairs, of ~60 bp in the B form. The reduction of the length of DNA molecules imaged in air is commonly observed (32,33,41), and the reason is still debated, although the prevalent hypothesis is that of a partial transition from B to A conformation. Such transition is often assessed based on the comparison of the measured contour length to the one expected for the B form, by considering only one molecular length (i.e., a given number of base-pairs). This procedure, however, cannot capture accurately the scaling of the contour length with the number of base-pairs, especially in those cases when a systematic alteration of the contour length is not attributable to a distributed, yet partial, transition. In the case of this study, we have evidence that the scaling of the DNA lengths, despite a systematic shortening, is the one typical of the B form (Fig. 4); we argue therefore that the constant shortening must be well localized within the molecule, which is at odds with the idea of a uniformly distributed shortening as expected by

a uniform (yet only partial) B to A transition. Recently, Japaridze et al. (32) reported a similar evidence of molecular shortening, and by means of tip-enhanced Raman spectroscopy they were able to localize the shortened DNA tracts at the molecules' free ends. We have carefully checked the calibration of our instrument, and we exclude this as the reason for the observed shortening (data not shown).

Reference DNA molecules synthesized by the I614K *Taq* pol have also been characterized (for a few selected lengths), and the measured lengths agree within error with those of the WT *Taq* pol, indicating that there is no alteration of DNA synthesized by the mutant *Taq* polymerase (Fig. 4). Our data suggest therefore that reference DNA molecules (WT and I614K *Taq* pol) are in the B-form, although there are shortened domains within the molecules. These samples represent the controls for the investigation of the effects of ribonucleotide incorporation. The latter have been assessed first by looking at changes of the contour length of the molecules upon ribonucleotide incorporation.

Interestingly, when comparing RC-DNA samples (464, 646, 727, and 960 bp) to their reference molecules without ribonucleotides, we observed a systematic shortening, except in the case of the 960-bp population (see Figs. 5 and S4 for the distribution of measured length values). We

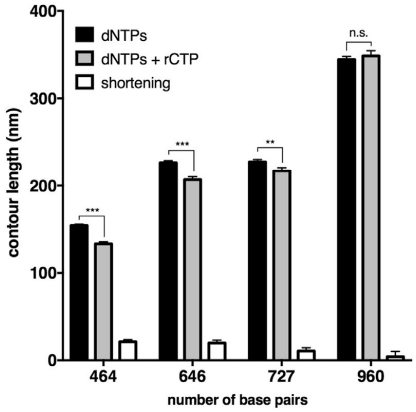

FIGURE 5 The incorporation of rCTPs induces shortening of DNA molecules. Solid bars represent the mean contour length of four different sets of molecules, produced with dNTPs or with the addition of rCTP. Open bars represent the difference in contour length (shortening) observed upon ribonucleotide incorporation. In the case of 464-, 646-, and 727-bp populations, the shortening of the contour length is significant according to the two-tailed *t*-test (with $p \leq 0.001$, 0.001, and 0.010, respectively), and this can be attributed to ribonucleotide incorporation. The 960-bp sample did not show a significant decrease in length ($p = 0.50$). Error bars represent the combination of the standard deviation of the mean and the calibration error, as explained in Materials and Methods. The number of analyzed 464-, 646-, 727-, and 960-bp dNTPs/dNTPs+rCTP molecules is 176/157, 92/92, 47/57, and 61/26, respectively. All plotted values are reported in Table S1.

attribute the shortening of the contour length to the presence of rCTP. In fact, apart from the rCTP incorporation, nothing else is different from the control DNA molecules; moreover, the molecules generated by the I614K *Taq* pol have been shown to be equivalent in terms of length to the ones from the WT *Taq* (Fig. 4). We also exclude that the shortening effect is due to increased truncation of PCR products when ribonucleotides are present in the template DNA strand: the primer extension assay described above demonstrated that the I614K *Taq* polymerase efficiently bypasses embedded rCMP, without prematurely ending the synthesis reaction (see Fig. S2 and Supporting Materials and Methods). The measured length differences between DNA and RC-DNA molecules are all significant according to the two-tailed *t*-test, with the exception of the 960-bp DNA sample that is not significant. Indeed, this is the sample with the lowest expected percentage of basepairs containing an rCMP (1.8%, and reported in Table 1) that was determined by Eq. 2, which considers the GC content and the ribonucleotide incorporation frequency. As for the others, we expect a 3.1% of basepairs containing a ribonucleotide in the 464-bp, 2.3% in the 646-bp, and 3.0% in the 727-bp molecules (Table 1). These data suggest that the number of embedded ribonucleotides could be crucial to induce detectable alterations of the contour length; however, there seems to be no clear correlation of the contour length shortening with the original GC content (reported in Table 1), especially when comparing the 646- and 727-bp samples (the shortening is more pronounced in 646-bp RC-DNAs, despite the smaller GC content). In addition to the absolute amount of GC pairs, it is important to consider their spatial distribution along the molecules (see Fig. S5 for a graphical representation of the distribution of GCs). We notice that in the case of the 646-bp sequence, the majority of available positions for rCTP incorporation consist of single bases, and that G or C clusters contain a maximum of three adjacent bases (as detailed in Table 1). Although the I614K *Taq* polymerase could be able to insert consecutive ribonucleotides, this would be a very inefficient and unfavorable reaction (35). As a consequence, despite the higher expected quantity of rCTP in the 727 bp, this sample probably presents a lesser degree of incorporation. In its sequence, there are actually fewer single positions available, and more, and longer, GC clusters, made of two to six consecutive C or G (Table 1).

Because double-stranded RNA molecules are known to be in the A form (42,43), and RNA-containing oligonucleotides have been shown to undergo a partial B to A transition (19,21), one can tentatively estimate an apparent fraction of basepairs that underwent a B to A transition upon rCTP incorporation, assuming that whenever an rCTP is incorporated, the hosting basepair switches from the B to the A form. The extent of such transition is calculated using the equations given in Materials and Methods. Fractions of the B-to A apparent transitions are 0.67, 0.41, 0.22, and

TABLE 1 Features of RC-DNA Molecules

bp	%GC (%)	Total Number of G+C	Number of Clusters with 6–4 G or C	Number of Clusters with 2–3 G or C	Number of Single G or C	Total Number of rCTP Incorporated	%rCTP (%)
464	58	269	4	50	143	14	3.1
646	43	279	0	51	159	15	2.3
727	57	413	5	77	224	22	3.0
960	34	325	3	45	215	17	1.8

GC content percentage, the GC clustering degree, and the estimated rCTP incorporation (absolute and percentage content) in the investigated DNA sequences. Clusters consist of consecutive nucleotides of the same species; here we have reported the sum of G and C clusters in one DNA strand, which is identical in the other complementary strand. Clusters are divided into two main groups: one made from 6 to 4 units, the other from 2 to 3. The number of isolated G or C present in the sequence is also reported. The total number of rCTP incorporated represents the estimated amount of rCTP incorporated into the molecule (with the percentage value) calculated using Eq. 2, as described in Materials and Methods.

0.05 for 464-, 646-, 727-, and 960-bp fragments, respectively. These estimated fractions are surprisingly high, because the ribonucleotide incorporation ratio (one rCTP every 19 bp) would lead to a B to A transition fraction up to one order-of-magnitude smaller. A reasonable explanation could be that the incorporation of one rCTP triggers the transition from the B to A form not only in correspondence to that single basepair, but also along the surrounding nucleotides (a B/A junction), extending across several tens of basepairs (corresponding to a few cooperative lengths, ~10 basepairs each (44,45)). At present, however, we do not have clear evidence that a (partial) B to A transition is the leading mechanism behind the observed shortening of DNA molecules upon ribonucleotide incorporation.

To further investigate the nature of the rCTP action on the DNA structure, we have investigated the mesoscopic conformation and elasticity of RC-DNAs. To this purpose, we have characterized the distribution of bending angles along the molecules' backbones as a function of the curvilinear separation L, as well as the scaling of the mean squared end-to-end distance $\langle R^2 \rangle_{2D}$ (Eq. 1), as described in the Materials and Methods. Equation 1 is valid for molecules equilibrated on two dimensions, where P refers to the persistence length of the molecules in the three dimensions, i.e., in the bulk solution. Noticeably, the ratio $(R/L)^2$ depends only on the ratio P/L, which also represents the asymptotic scaling of the normalized curves at large distances. The measured ratio of higher moments of the angle distribution $\langle \theta^4 \rangle / \langle \theta^2 \rangle^2$ is close to three (see Supporting Materials and Methods and Fig. S6), which is the theoretical WLC value for full equilibration of the molecules in two dimensions (25). The values of P for DNA and RC-DNA samples are obtained by fitting Eq. 1 to the R^2 versus L curves (the representative curve for the 464-bp sample is shown in Fig. S7). Typically, the WLC model fitted with good accuracy the experimental data across the 0–120-nm distance range. Fig. 6, *A–C*, shows the scaling of the normalized mean squared end-to-end distance $(R/L)^2$. The mean squared end-to-end distance R^2 has been normalized by L^2 to better appreciate the change in the slope (i.e., in the persistence lengths P) upon incorporation of rCTP, and the extrapolated persistence length values are plotted in Fig. 6 *D* and reported in Table S1. First, we noticed that for the 464- and 727-bp samples (from I614K *Taq* pol) the measured values of the persistence length are higher than the value of ~50 nm, typically for DNA molecules with a ~50% GC content (25,26). However, this is consistent with the fact that high GC content is known to induce stiffening, with an increase of the persistence length (46). Remarkably, the incorporation of ribonucleotides into the molecules with higher GC content (464 and 727 bp) induced a significant shortening of the persistence length, according to the two-tailed *t*-test (Fig. 6 *D*; Table S1).

The 960-bp sample is the only one not showing any appreciable reduction of the persistence length, in addition to the absence of the shortening of the contour length, as shown previously. However, as for the shortening of contour length, we could not define a clear trend of the persistence length shortening with the GC content, probably because the rCTP incorporation is not simply proportional to the available sites; the latter in turn are not uniformly distributed along the molecules, but present with different degrees of clustering and spatial distribution (Fig. S5; Table 1).

The molecules containing rCTP seem to be equilibrated to a good extent on the mica surface, and their R^2 versus L curves can be fitted by the WLC model across a wide range of distances; these evidences suggest that the incorporation of rCTP exerts an influence on the DNA structure that goes well beyond the scale of the single ribonucleotide. In this study, we observe that, upon rCTP incorporation, the structure and conformation of DNA molecules change significantly and on the mesoscopic scale. In particular, the observed reduction of the persistence length P suggests that ribonucleotides induce a softening of DNA molecules (Fig. 6 *D*) in addition to causing a significant shortening (Fig. 5). The extension of the effects of the rCTP incorporation in dsDNA is remarkable, because one would expect an effective rCTP content of a few percent (Table 1). The action of a single ribonucleotide, namely its effect on the DNA structure, extends far beyond its linear dimension. Attributing the observed changes of conformational and elastic properties to a B to A transition—based on the fact that RNA is in the A form—is not at all straightforward, and this conclusion would not at present be fully supported by the data. On one side, DNA in the A form in

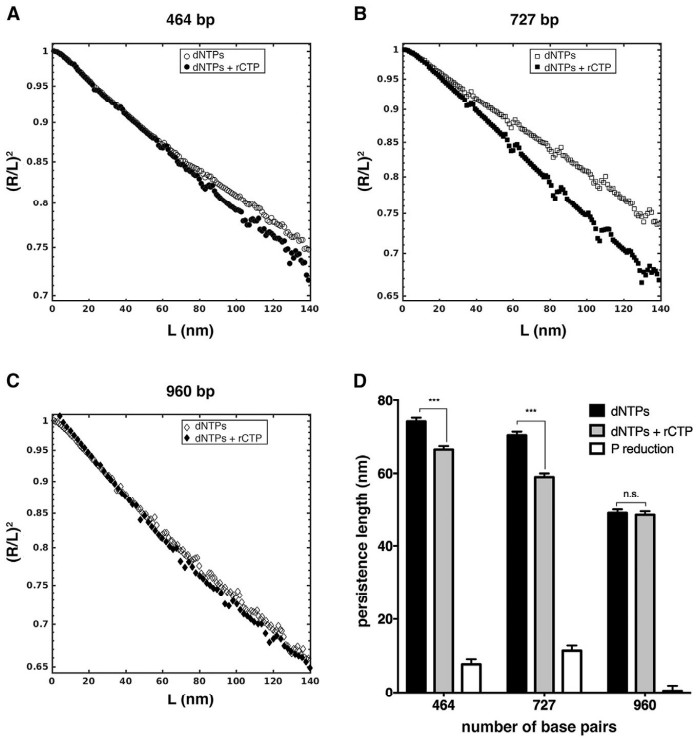

FIGURE 6 rCTP incorporation affects end-to-end distance and persistence length of DNA molecules. (*A–C*) Shown here is the scaling of the normalized mean squared end-to-end distance $(R/L)^2$ as a function of the curvilinear distance L for 464-, 727-, and 960-bp samples. Differences in the slope of the curves are appreciable for 464- and 727 bp, but not for 960 bp. In (*D*) are represented persistence length values of the same samples (*solid bars*): 464- and 727 bp showed extremely significant decrease in P upon rCTP incorporation (with $p \leq 0.001$, according to the two-tailed t-test), whereas the 960-bp samples did not show any difference ($p = 0.10$). Open bars represent the persistence length shortening between the two compared samples. See Materials and Methods for details on error bars. The number of analyzed 464-, 727-, and 960-bp dNTPs/dNTPs+rCTP molecules is 176/157, 47/57, and 61/26, respectively. All plotted values are reported in Table S1.

solution is reported to be stiffer than in the B form (47), at odd with our observations; on the other side, DNA in the A form deposited on mica at different ethanol concentrations showed decreasing values of the persistence length at increasing B to A transition fractions, a trend similar to that observed by us, at least in the general terms. Concerning the published single-molecule studies on the bending rigidity (persistence length) of ribonucleotide-containing DNA molecules, including double-stranded RNA, either stiffer (23) or softer and slightly stiffer molecules (22) have been reported, depending on the sequence context and the positions of ribonucleotides. It emerged that besides the absolute content, which determines the extent of the incorporation, the distribution of ribonucleotide along the molecular backbone also is important in determining structural changes (22). Chiu et al. (22) concluded that the incorporation of ribonucleotides locally induces a significant (torsional) distortion of the sugar-phosphate backbone, affecting the elastic, and structural properties of the molecule as a whole. Relating such a torsional alteration to the observed mesoscopic changes of the DNA molecules conformation, namely the shortening of the molecules, and the reduction of the persistent length, is not trivial. Intuitively, a torsional alteration, especially if distributed along the molecular backbone, even if not uniformly, can lead to a shortening of the molecule. It was recently proposed that the rotational stiffening caused by the ribonucleotide-induced torsion of the sugar-phosphate backbone can hamper the rotational fluctuations, resulting in bending stiffening, rather than the opposite, at least as long as the electrostatic component of the persistence length is concerned (48). Under the hypothesis that the incorporation of ribonucleotides induces the formation of B/A junctions, which are known to be significantly bent (49), one could also consider the role of these bent domains in decreasing the apparent persistence length of DNA molecules (50). Further investigations are therefore required, by means of both experimental techniques and structural simulations, to unravel the fine mechanisms underlying the observed structural and conformational changes in DNA molecules upon ribonucleotide incorporation. In particular, the influence of the base sequence should be directly investigated and assessed, at similar GC content.

CONCLUSIONS

In this work, we present, to our knowledge, a novel approach to study the effects of ribonucleotides

incorporation into DNA. Our synthesis strategy exploited the use of a mutant version of the *Taq* polymerase (I614K) in PCR reactions allowing us to generate populations of long (several hundreds of basepairs) RC-DNAs, which are more biologically relevant than short oligonucleotides. In particular, we have studied the ribonucleotides-induced changes in the structural and conformational properties of DNA at the single-molecule level by means of atomic force microscopy. Our systematic and statistical study highlighted the impact of ribonucleotides intrusions on the DNA double helix. We found that their presence alters DNA structural properties. All the investigated DNA molecules, with the exception of the longest molecules with the lowest GC content (960 bp), showed a significant reduction in the contour length upon rCTP introduction compared to their cognate molecules without rCTP. As observed in RNA molecules, it is the presence of the extra hydroxyl group on ribonucleotides that leads to a compaction of the DNA backbone. From the biochemical parameters of the I614K *Taq* polymerase (38) we estimated an incorporation frequency of 1/19 (rCTP/dCTP), representing 2–3% of the total number of basepairs. By contrast, the calculated apparent B to A transition fraction ranges between 20 and 60%. Although we do not have concluding evidence that this structural transition is the mechanism triggered by the ribonucleotide insertion, these figures suggest that the ribonucleotide effect on DNA structure extends remarkably on a scale that goes well beyond the typical dimension of a single ribonucleotide, affecting the full length of the molecule. Together with the shortening, RC-DNA molecules become more flexible, as demonstrated by the reduction of the persistence length. This is another indication that the effect of even a tiny fraction of incorporated ribonucleotides affects the DNA molecules on a global scale. A deeper understanding of the observed phenomena would require a precise quantification of the extent of rCTP incorporation, as well as of their spatial distribution along the RC-DNA molecules. Nevertheless, rCTP incorporation is nearly controlled by the number of positions available, given by the GC content.

In our system, control DNA molecules retain their native B conformation, supporting the idea that changes upon ribonucleotide introduction are likely to occur also in vivo. Along the genome of living cells there are hotspots of ribonucleotide incorporation, and the most frequently incorporated ribonucleotide is rCTP (36,37). We speculate that the induced structural and conformational alterations can contribute to the negative outcome of ribonucleotide persistence in DNA. These alterations could be easily transferred to DNA transactions that rely on structure recognition, such as protein binding. For instance, it is reported that ribonucleotides prevent nucleosome assembly on DNA (15), probably reshaping their positioning. Therefore, our strategy to study the effect of ribonucleotide incorporation of long supported DNA fragments could contribute to a better understanding of their harmful consequences upon genome stability.

SUPPORTING MATERIAL

Supporting Materials and Methods, eight figures, and one table are available at http://www.biophysj.org/biophysj/supplemental/S0006-3495(17)30811-1.

AUTHOR CONTRIBUTIONS

M.M.-F., F.L., and A.P. conceived the study and designed the experiments. A.M. and A.P. performed the main experiments and analyzed the data. E.M. and E.C. performed the control experiment reported in Fig. S2. A.M. and A.P. wrote the manuscript. M.M.-F. and F.L. revised the manuscript. All authors participated in scientific discussions.

ACKNOWLEDGMENTS

A.M. thanks Francesca Borghi for support in AFM imaging, and Barbara Sciandrone for support in radioactive DNA dialysis. We thank Prof. A. Aliverti and Prof. P. Plevani for critical discussions, and G. Maga for support in the control experiments.

A.P. thanks the Department of Physics of the University of Milano for financial support under the project "Piano di Sviluppo dell'Ateneo per la Ricerca 2014. Linea B: Supporto per i Giovani Ricercatori". The M.M.-F. lab is funded by AIRC (no. 15631), MIUR, and Telethon (GGP15227). F.L. is funded by AIRC and Fondazione Cariplo (TRIDEO 2014 Id. 15724) and Fondazione CARIPLO (RIF. 2013-0798). E.M. and E.C. are supported by AIRC individual grant MFAG2016 18811.

REFERENCES

1. Gilbert, W. 1986. Origin of life: the RNA world. *Nature.* 319:618.
2. Li, Y., and R. R. Breaker. 1999. Kinetics of RNA degradation by specific base catalysis of transesterification involving the 2′-hydroxyl group. *J. Am. Chem. Soc.* 121:5364–5372.
3. Hiller, B., M. Achleitner, …, A. Roers. 2012. Mammalian RNase H2 removes ribonucleotides from DNA to maintain genome integrity. *J. Exp. Med.* 209:1419–1426.
4. Nick McElhinny, S. A., B. E. Watts, …, T. A. Kunkel. 2010. Abundant ribonucleotide incorporation into DNA by yeast replicative polymerases. *Proc. Natl. Acad. Sci. USA.* 107:4949–4954.
5. Nick McElhinny, S. A., D. Kumar, …, T. A. Kunkel. 2010. Genome instability due to ribonucleotide incorporation into DNA. *Nat. Chem. Biol.* 6:774–781.
6. Sparks, J. L., H. Chon, …, P. M. Burgers. 2012. RNase H2-initiated ribonucleotide excision repair. *Mol Cell.* 47:980–986.
7. Ghodgaonkar, M. M. M., F. Lazzaro, …, J. Jiricny. 2013. Ribonucleotides misincorporated into DNA act as strand-discrimination signals in eukaryotic mismatch repair. *Mol. Cell.* 50:323–332.
8. Lujan, S. A., J. S. Williams, …, T. A. Kunkel. 2013. Ribonucleotides are signals for mismatch repair of leading-strand replication errors. *Mol. Cell.* 50:437–443.
9. Kim, N., S. N. Huang, …, S. Jinks-Robertson. 2011. Mutagenic processing of ribonucleotides in DNA by yeast topoisomerase I. *Science.* 332:1561–1564.
10. Conover, H. N., S. A. Lujan, …, J. L. Argueso. 2015. Stimulation of chromosomal rearrangements by ribonucleotides. *Genetics.* 201:951–961.

11. Lazzaro, F., D. Novarina, …, M. Muzi-Falconi. 2012. RNase H and postreplication repair protect cells from ribonucleotides incorporated in DNA. *Mol. Cell.* 45:99–110.
12. Reijns, M. A. M., B. Rabe, …, A. P. Jackson. 2012. Enzymatic removal of ribonucleotides from DNA is essential for mammalian genome integrity and development. *Cell.* 149:1008–1022.
13. Cerritelli, S. M., and R. J. Crouch. 2009. Ribonuclease H: the enzymes in eukaryotes. *FEBS J.* 276:1494–1505.
14. Crow, Y. J., A. Leitch, …, A. P. Jackson. 2006. Mutations in genes encoding ribonuclease H2 subunits cause Aicardi-Goutières syndrome and mimic congenital viral brain infection. *Nat. Genet.* 38:910–916.
15. Hovatter, K. R., and H. G. Martinson. 1987. Ribonucleotide-induced helical alteration in DNA prevents nucleosome formation. *Proc. Natl. Acad. Sci. USA.* 84:1162–1166.
16. Egli, M., N. Usman, and A. Rich. 1993. Conformational influence of the ribose 2′-hydroxyl group: crystal structures of DNA-RNA chimeric duplexes. *Biochemistry.* 32:3221–3237.
17. Ban, C., B. Ramakrishnan, and M. Sundaralingam. 1994. A single 2′-hydroxyl group converts B-DNA to A-DNA. Crystal structure of the DNA-RNA chimeric decamer duplex d(CCGGC)r(G)d(CCGG) with a novel intermolecular G-C base-paired quadruplet. *J. Mol. Biol.* 236:275–285.
18. Wahl, M. C., and M. Sundaralingam. 2000. B-form to A-form conversion by a 3′-terminal ribose: crystal structure of the chimera d(CCAC TAGTG)r(G). *Nucleic Acids Res.* 28:4356–4363.
19. Jaishree, T. N., G. A. van der Marel, …, A. H. Wang. 1993. Structural influence of RNA incorporation in DNA: quantitative nuclear magnetic resonance refinement of d(CG)r(CG)d(CG) and d(CG)r(C)d(TAGCG). *Biochemistry.* 32:4903–4911.
20. Chou, S. H., P. Flynn, …, B. Reid. 1991. High-resolution NMR studies of chimeric DNA-RNA-DNA duplexes, heteronomous basepairing, and continuous base stacking at junctions. *Biochemistry.* 30:5248–5257.
21. DeRose, E. F., L. Perera, …, R. E. London. 2012. Solution structure of the Dickerson DNA dodecamer containing a single ribonucleotide. *Biochemistry.* 51:2407–2416.
22. Chiu, H.-C., K. D. Koh, …, F. Storici. 2014. RNA intrusions change DNA elastic properties and structure. *Nanoscale.* 6:10009–10017.
23. Abels, J. A., F. Moreno-Herrero, …, N. H. Dekker. 2005. Single-molecule measurements of the persistence length of double-stranded RNA. *Biophys. J.* 88:2737–2744.
24. Herrero-Galán, E., M. E. Fuentes-Perez, …, J. R. Arias-Gonzalez. 2013. Mechanical identities of RNA and DNA double helices unveiled at the single-molecule level. *J. Am. Chem. Soc.* 135:122–131.
25. Rivetti, C., M. Guthold, and C. Bustamante. 1996. Scanning force microscopy of DNA deposited onto mica: equilibration versus kinetic trapping studied by statistical polymer chain analysis. *J. Mol. Biol.* 264:919–932.
26. Podestà, A., M. Indrieri, …, D. Dunlap. 2005. Positively charged surfaces increase the flexibility of DNA. *Biophys. J.* 89:2558–2563.
27. Lia, G., M. Indrieri, …, D. Dunlap. 2008. ATP-dependent looping of DNA by ISWI. *J. Biophotonics.* 1:280–286.
28. Podestà, A., L. Imperadori, …, D. Dunlap. 2004. Atomic force microscopy study of DNA deposited on poly L-ornithine-coated mica. *J. Microsc.* 215:236–240.
29. Sambrook, J., and D. W. Russell. 2006. Alkaline agarose gel electrophoresis. *CSH Protoc.*:2006 Jun 1;2006(1). pii: pdb.prot4027. http://dx.doi.org/10.1101/pdb.prot4027.
30. Meroni, A., F. Lazzaro, …, A. Podestà. 2017. Characterization of structural and configurational properties of DNA by atomic force microscopy. *In* Methods in Molecular Biology. J. M. Walker, editor. Humana Press, New York, NY.
31. Usov, I., and R. Mezzenga. 2015. FiberApp: an open-source software for tracking and analyzing polymers, filaments, biomacromolecules, and fibrous objects. *Macromolecules.* 48:1269–1280.
32. Japaridze, A., D. Vobornik, …, G. Dietler. 2016. Toward an effective control of DNA's submolecular conformation on a surface. *Macromolecules.* 49:643–652.
33. Rivetti, C., and S. Codeluppi. 2001. Accurate length determination of DNA molecules visualized by atomic force microscopy: evidence for a partial B- to A-form transition on mica. *Ultramicroscopy.* 87:55–66.
34. Chien, A., D. B. Edgar, and J. M. Trela. 1976. Deoxyribonucleic acid polymerase from the extreme thermophile *Thermus aquaticus*. *J. Bacteriol.* 127:1550–1557.
35. Patel, P. H., and L. A. Loeb. 2000. Multiple amino acid substitutions allow DNA polymerases to synthesize RNA. *J. Biol. Chem.* 275:40266–40272.
36. Koh, K. D., S. Balachander, …, F. Storici. 2015. Ribose-seq: global mapping of ribonucleotides embedded in genomic DNA. *Nat. Methods.* 12:251–257, 3, 257.
37. Clausen, A. R., S. A. Lujan, …, T. A. Kunkel. 2015. Tracking replication enzymology in vivo by genome-wide mapping of ribonucleotide incorporation. *Nat. Struct. Mol. Biol.* 22:185–191.
38. Patel, P. H., H. Kawate, …, L. A. Loeb. 2001. A single highly mutable catalytic site amino acid is critical for DNA polymerase fidelity. *J. Biol. Chem.* 276:5044–5051.
39. Clausen, A. R., S. Zhang, …, T. A. Kunkel. 2013. Ribonucleotide incorporation, proofreading and bypass by human DNA polymerase δ. *DNA Repair (Amst.).* 12:121–127.
40. Clausen, A. R., M. S. Murray, …, T. A. Kunkel. 2013. Structure-function analysis of ribonucleotide bypass by B family DNA replicases. *Proc. Natl. Acad. Sci. USA.* 110:16802–16807.
41. Sanchez-Sevilla, A., J. Thimonier, …, J. Barbet. 2002. Accuracy of AFM measurements of the contour length of DNA fragments adsorbed on mica in air and in aqueous buffer. *Ultramicroscopy.* 92:151–158.
42. Langridge, R., and P. J. Gomatos. 1963. The structure of RNA. *Science.* 141:1024.
43. Arnott, S., D. W. L. Hukins, and S. D. Dover. 1972. Optimised parameters for RNA double-helices. *Biochem. Biophys. Res. Commun.* 48:1392–1399.
44. Ivanov, V. I., L. E. Minchenkova, …, C. Zimmer. 1996. The detection of B-form/A-form junction in a deoxyribonucleotide duplex. *Biophys. J.* 71:3344–3349.
45. Ivanov, V. I., D. Y. Krylov, …, L. E. Minchenkova. 1983. B-A transition in DNA. *J. Biomol. Struct. Dyn.* 1:453–460.
46. Hormeño, S., B. Ibarra, …, J. R. Arias-Gonzalez. 2011. Mechanical properties of high-G.C content DNA with A-type base-stacking. *Biophys. J.* 100:1996–2005.
47. Charney, E., H.-H. Chen, and D. C. Rau. 1991. The flexibility of A-form DNA. *J. Biomol. Struct. Dyn.* 9:353–362.
48. Dobrynin, A. V. 2005. Electrostatic persistence length of semiflexible and flexible polyelectrolytes. *Macromolecules.* 38:9304–9314.
49. Selsing, E., R. D. Wells, …, S. Arnott. 1979. Bent DNA: visualization of a base-paired and stacked A-B conformational junction. *J. Biol. Chem.* 254:5417–5422.
50. Rouzina, I., and V. A. Bloomfield. 1998. DNA bending by small, mobile multivalent cations. *Biophys. J.* 74:3152–3164.

2600–2614 *Nucleic Acids Research, 2017, Vol. 45, No. 5* *Published online 19 December 2016*
doi: 10.1093/nar/gkw1275

Ribonucleotide incorporation by human DNA polymerase η impacts translesion synthesis and RNase H2 activity

Elisa Mentegari[1], Emmanuele Crespan[1], Laura Bavagnoli[1], Miroslava Kissova[1], Federica Bertoletti[1], Simone Sabbioneda[1], Ralph Imhof[2], Shana J. Sturla[3], Arman Nilforoushan[3], Ulrich Hübscher[2], Barbara van Loon[2] and Giovanni Maga[1,*]

[1]DNA Enzymology & Molecular Virology and Cell Nucleus & DNA replication Units, Institute of Molecular Genetics IGM-CNR, via Abbiategrasso 207, I-27100 Pavia, Italy, [2]Department of Molecular Mechanisms of Disease, University of Zürich, Winterthurerstrasse 190, CH-8057 Zürich, Switzerland and [3]Department of Health Sciences and Technology, ETH Zurich, Schmelzbergstrasse 9, CH-8092 Zürich, Switzerland

Received September 15, 2016; Revised December 05, 2016; Editorial Decision December 06, 2016; Accepted December 07, 2016

ABSTRACT

Ribonucleotides (rNs) incorporated in the genome by DNA polymerases (Pols) are removed by RNase H2. Cytidine and guanosine preferentially accumulate over the other rNs. Here we show that human Pol η can incorporate cytidine monophosphate (rCMP) opposite guanine, 8-oxo-7,8-dihydroguanine, 8-methyl-2'-deoxyguanosine and a cisplatin intrastrand guanine crosslink (cis-PtGG), while it cannot bypass a 3-methylcytidine or an abasic site with rNs as substrates. Pol η is also capable of synthesizing polyribonucleotide chains, and its activity is enhanced by its auxiliary factor DNA Pol δ interacting protein 2 (PolDIP2). Human RNase H2 removes cytidine and guanosine less efficiently than the other rNs and incorporation of rCMP opposite DNA lesions further reduces the efficiency of RNase H2. Experiments with XP-V cell extracts indicate Pol η as the major basis of rCMP incorporation opposite cis-PtGG. These results suggest that translesion synthesis by Pol η can contribute to the accumulation of rCMP in the genome, particularly opposite modified guanines.

INTRODUCTION

Several thousands to millions of ribonucleotides (rNMPs) are interspersed among the DNA bases of eukaryotic genomes (1). The presence of the 2′-OH group makes the sugar phosphate backbone of RNA 100 000-fold more prone to spontaneous hydrolysis than DNA. In addition, rNMPs induce B- to A-form transition in the double helix, potentially affecting protein-DNA interactions and the catalytic activity of DNA polymerases (Pols), topoisomerases and ligases and leading to further DNA damage (2). Thus, rNMPs in the genome constitute the most abundant DNA lesions in eukaryotic cells (3,4).

Deep sequencing studies in *Saccharomyces cerevisiae* found that cytosine and guanosine were the most abundant rNMPs in the genome (5–7). Their relative genomic abundance did not reflect their intracellular concentrations, with regard to their ratios with respect to those of adenosine and uracil, nor with respect to the relative G+C and A+T genomic content, suggesting that factors beside nucleotide pool concentrations and template sequence influence the accumulation of specific rNMPs in the genome.

Incorporation of rNMPs into the genome of proliferating cells, is predominantly mediated by the replicative Pols δ and ϵ (1). However, biochemical studies revealed that also several specialized repair Pols have poor sugar discrimination abilities (8–17), making rNMP incorporation during DNA repair or translesion synthesis (TLS) a likely event *in vivo*, given that the intracellular ribonucleoside triphosphates (rNTPs) concentrations are 100- to 1000-fold higher than those of deoxyribonucleoside triphosphates (dNTPs). In the context of TLS, rNMPs incorporation opposite a DNA lesion may delay subsequent removal of either the rNMPs or the damaged base, as recently was shown in the case of TLS over a 8-oxo-7,8-dihydroguanine (8-oxo-G) lesion by human Pols β and λ (16,18).

The process of TLS is mainly carried out by Y-family Pols η, ι and κ (19,20). One study (14) reported that human Pol ι has sugar discrimination values between 1000 and 6000 and can bypass abasic (AP) sites or 8-oxo-G lesions using rNTPs as substrates. On the contrary, yeast Pol η showed

*To whom correspondence should be addressed. Tel: +39 0382 546 354; Fax: +39 0382 422 286; Email: maga@igm.cnr.it
Present address: Barbara van Loon, Department of Cancer Research and Molecular Medicine, Norwegian University of Science and Technology, Erling Skjalgssons gt 1, N-7491 Trondheim, Norway.

limited rNMP incorporation for undamaged DNA templates or opposite a cyclobutane pyrimidine dimer (CPD) (21). A recent study that appeared during the preparation of the present work showed more robust rNMPs incorporation and elongation by human Pol η on both undamaged DNA and during TLS of a CPD or a 8-oxo-G lesion (17). The same study also provided the crystal structure of Pol η in complex with an incoming rCTP paired to a template 8-oxo-G, showing that the enzyme can accommodate both the C-8 OH group of the oxidized base and the 2′-OH group of the ribose sugar of the incoming nucleotide, due to its wide active site. However, whether TLS using rNMPs is a general feature of human Pol η, or it is limited to specific lesions, is currently not known.

Human Pol η is essential for TLS over CPDs, and its absence in humans causes a variant form of the genetic disease *Xeroderma pigmentosum* (XP-V) (20,22). Pol η is also involved in the bypass of other DNA lesions, such as 8-oxo-G and AP sites, and it plays an important role in bypassing the intrastrand crosslinks between two adjacent guanines caused by the anticancer drug cisplatin (cis-PtGG) (23). Thus, its ability to use rNTPs instead of dNTPs during TLS may have physiologically relevant consequences.

Once incorporated, rNMPs can be removed by the ribonucleotide excision repair (RER) pathway, which is initiated by the RNase H2 enzyme (4,24–26). This ribonuclease can specifically introduce a nick on the 5′-side of the DNA/RNA junction when 1 to 4 rNMPs are embedded in DNA. This cleavage subsequently triggers nick translation by the Pol δ holoenzyme, with the generation of a flap that is cut by the Flap endonuclease 1, resulting in the elimination of the RNA/DNA hybrid tract and re-synthesis of an intact DNA strand. Both the yeast *Schizosaccharomyces pombe* (27) and the *Escherichia coli* RNase H2 (18) were shown to incise cytidine monophosphate (rCMP) opposite 8-oxo-G. However, the impact of rNMP incorporation opposite damaged bases on the catalytic efficiency of human RNase H2 have not been carefully investigated yet.

In this work, we characterize the capacity of human Pol η to incorporate rNMPs opposite undamaged guanine or five different lesions: 8-oxo-G, 8-methyl-2′-deoxyguanosine (8-met-G), cis-PtGG, 3-methyldeoxycytidine (3-met-C) and an AP site. We also characterize the cleavage specificity of the human trimeric RNase H2 with respect to all four rNMP:dNMP base pairs, as well as its ability to cleave rCMP incorporated opposite 8-oxo-G, 8-met-G and cis-PtGG lesions. In addition we evaluated the effects in these reactions of the auxiliary protein proliferating cell nuclear antigen (PCNA) and also of DNA Pol δ interacting protein 2 (PolDIP2), which was shown to stimulate Pol η catalytic activity (28). Our results support the notion that Pol η can contribute to the genomic accumulation of rCMP, particularly opposite modified guanines.

MATERIALS AND METHODS

Chemicals

Deoxynucleotides were purchased from GeneSpin (Milan, Italy). Ribonucleotides were purchased by GE Healthcare (Uppsala, Sweden). Labeled [γ-^{32}P]ATP was purchased from Hartmann Analytic GmbH (Braunschweig, Germany). All other reagents were of analytical grade and purchased from Fluka or Merck.

Oligonucleotides

The 24mer oligonucleotide containing the cis-PtGG adduct was prepared and purified as described previously (29). All other DNA oligonucleotides were synthesized by Purimex (Grebenstein, Germany) and purified from polyacrylamide denaturing gels. When indicated, oligonucleotides were 5'-labeled with T4 polynucleotide kinase (New England Biolabs) and [γ-^{32}P]ATP, according to the manufacturer's protocol or directly synthesized as 5′-labeled with carboxyfluorescin (FAM) group. Each labeled primer was mixed to the complementary template oligonucleotide at 1:1 (M/M) ratio in the presence of 25mM Tris-HCl pH 8 and 50mM KCl, heated at 75 C for 10 min and then slowly cooled at room temperature.

A complete listing of sequences of the oligonucleotides used is given in the Supplementary Methods.

Enzymes and proteins

Recombinant human PCNA and PolDIP2 were expressed and purified as described (28). The bacterial clone for the expression of human Pol η was a kind gift from R. Woodgate (NIH, USA). Human recombinant Pol η was expressed and purified as described (30). The MIC1066 *E. coli* strain and the expression plasmid for the simultaneous expression of the three subunits of human RNase H2 were a kind gift of R. J. Crouch (National Institute of Child Health and Human development, Bethesda, MD, USA). The heterotrimeric human recombinant RNase H2 was expressed and purified as described (31), with the following modifications: cells were lysed for 30 min on ice in 20 mM KPO4 buffer pH 7.4, 300 mM NaCl, 30 mM Imidazole, 10 mg ml^{-1} lysozyme, 0.05% phenylmethylsulfonyl fluoride and protease inhibitors. The lysate was sonicated and cleared by ultracentrifugation at 38 000 rpm in a Ti70 Beckman rotor. The cleared lysate was loaded onto a FPLC-NiNTA column (G&E Healthcare) equilibrated in 20 mM KPO4 buffer pH 7.4, 300 mM NaCl, 30 mM imidazole, 5% glycerol. The protein was eluted with a 30–500 mM linear gradient of imidazole in the equilibration buffer. The fractions containing the enzyme in 20% glycerol were stored separately in liquid nitrogen.

Cell lines and culturing conditions

XP-V patient-derived XP30R0 fibroblast cells transformed with simian virus 40 were a gift from Alan Lehman (University of Sussex, Brighton, UK). XP-V cells were grown in a humidified 5% CO_2 atmosphere in Dulbecco's modified Eagle's medium containing GlutaMAX-I supplemented with 10% fetal bovine serum and 100 U/ml penicillin–streptomycin (all obtained from Gibco, Invitrogen). To complement XP-V cells, human Pol η mammalian expression vector pJRM56 (kindly provided by Roger Woodgate, NIH, USA) was used. pJRM56 or empty pcDNA 3.1 (Invitrogen) constructs were transiently transfected into XP-V cells using lipofectamine (Invitrogen) according to man-

ufacturers protocol. Alternatively XP30RO cells stably expressing eGFP-Polη were used (32,33). Cells were harvested 48 h respectively after transfection or seeding and whole-cell extract (WCE) were prepared. Cells were harvested 48 h after the transfection and WCE prepared.

Cell extracts and western blot

Cell extracts were prepared as described (34). Proteins were separated on 10% Bis-Tris poly-acrylamide gels and transferred to Immobilon-FL membrane (Millipore) for immunoblotting analysis. Primary antibodies against Pol η (Abcam), Pol β (custom made antibody) and Tubulin (Sigma) were detected using infrared dye-conjugated secondary antibodies (LI-COR Biosciences). For signal visualization the Odyssey Scanner (LI-COR Biosciences) was used.

Enzymatic assays

All reactions were in a 10 μl final volume. Pol η reaction buffer: 40 mM Tris pH 8, 1 mM dithiotreitol, 0.25 mg/ml bovine serum albumin (BSA). Mg^{2+} was included at 5 mM, unless otherwise stated in the figures or figure legends. RNase H2 reaction buffer: 50 mM Tris-HCl pH 8.5, 25 mM NaCl, 50 μg ml^{-1} BSA, 1 mM 2-mercaptoethanol, 1% glycerol, 5 mM Mg^{2+}. Enzymes and DNA substrates concentrations are indicated in the figures or figure legends. Reactions were incubated at 37°C for 5 min, unless otherwise stated in the figures or figure legends. For denaturing gel analysis of the DNA products, the reaction mixtures were stopped by addition of standard denaturing gel loading buffer (95% formamide, 10 mM ethylenediaminetetraacetic acid, xylene cyanol and bromophenol blue), heated at 95°C for 5 min and loaded on a 7 M urea 12% polyacrylamide (PA) gel. The reaction products were analyzed by using Molecular Dynamics Phosphoimager (Typhoon Trio, GE Healthcare) and quantified by the program Image Quant.

Kinetic analysis

Due to the highly distributive nature of the reaction and the relatively low efficiency of rNTP incorporation, the Pols and the DNA substrate were used at similar concentrations. This implies that, at equilibrium, the concentration of the binary enzyme-DNA complex does not approximate the total enzyme concentration, but there is always a fraction of enzyme not bound to the DNA substrate, which does not participate in catalysis. Thus, in order to account for the fraction of enzyme not bound to the DNA substrate at equilibrium, the variation of the nucleotide incorporation rates (v) as a function of the nucleotide substrate concentration was fitted to the modified Briggs-Haldane equation:

$$v = \frac{k\mathrm{cat}\,E_0 S}{(S \cdot a) + (K_\mathrm{d} \cdot b)} \quad (1)$$

where k_{cat} is the apparent catalytic rate, E_0 is the input enzyme concentration, S is the variable nucleotide substrate concentration, K_d is the apparent equilibrium dissociation constant of the nucleotide substrate from the catalytically active ternary complex, a and b are two constants, whose values were kept fixed during the computer fitting and were calculated from the expressions:

$$a = \frac{1}{1 + \frac{Kd}{K'}} \quad (2)$$

$$b = \frac{1}{\left(1 + \frac{K'}{S'}\right)} \quad (3)$$

where K_d is the same as in Equation (1), K' is the apparent dissociation constant for binding to the DNA substrate and S' is the concentration of DNA use in each experiment. The value of K' used for the fitting process for Pol η was 11 nM (35).

In the case of RNase H2, the apparent initial velocities were plotted as a function of the DNA substrate concentrations and fitted to the Michaelis-Menten equation:

$$v = \frac{k\mathrm{cat}\,E_0 S}{K_\mathrm{M} + S} \quad (4)$$

here k_{cat} is the apparent catalytic rate, E_0 is the input enzyme concentration, S is the variable DNA substrate concentration, K_M is the apparent Michaelis constant.

Fitting was obtained with the GraphPad Prism 3.0 computer program.

Electronic image manipulation

Linear transformations have been applied in some instance to the whole images using the exposure/brightness filters of Adobe Photoshop CS6 with the sole purpose of reducing excessive background. No masking/enhancement was applied to any specific feature of the images. Solid lines identify different portions of the same gel brought next for clarity of presentation.

RESULTS

Incorporation of ribonucleotides by human Pol η

Human Pol η was incubated in the presence of a mixture of the four rNTPs or dNTPs, each present at its average intracellular concentration. Incorporation was measured as a function of increasing concentrations of Mg^{2+} or Mn^{2+} cofactors. As shown in Figure 1A, Pol η incorporated multiple rNMPs in the presence of physiological concentration (5 mM) of Mg^{2+} (Figure 1A, lane 9), but also at Mn^{2+} concentrations as low as 0.1 mM, even displaying more robust activity than with Mg^{2+}, at relatively high Mn^{2+} concentrations (0.5–1 mM) (Figure 1A, lanes 4 and 5). The 5 mM Mg^{2+} concentration was then used for all subsequent experiments. Pol η showed remarkable fidelity, being able to significantly incorporate rCMP only opposite an undamaged guanine (Figure 1B). When dCTP or rCTP were titrated into the reaction, robust incorporation of both nucleotides was observed opposite the template G, along with some misincorporation events leading to a +2 product (Figure 1C, lanes 4–7 and 12–15). The kinetic parameters for rCMP versus dCMP incorporation opposite a normal G are summarized in Table 1. On this template, the discrimination factor for deoxy- versus ribonucleotide incorporation by Pol η

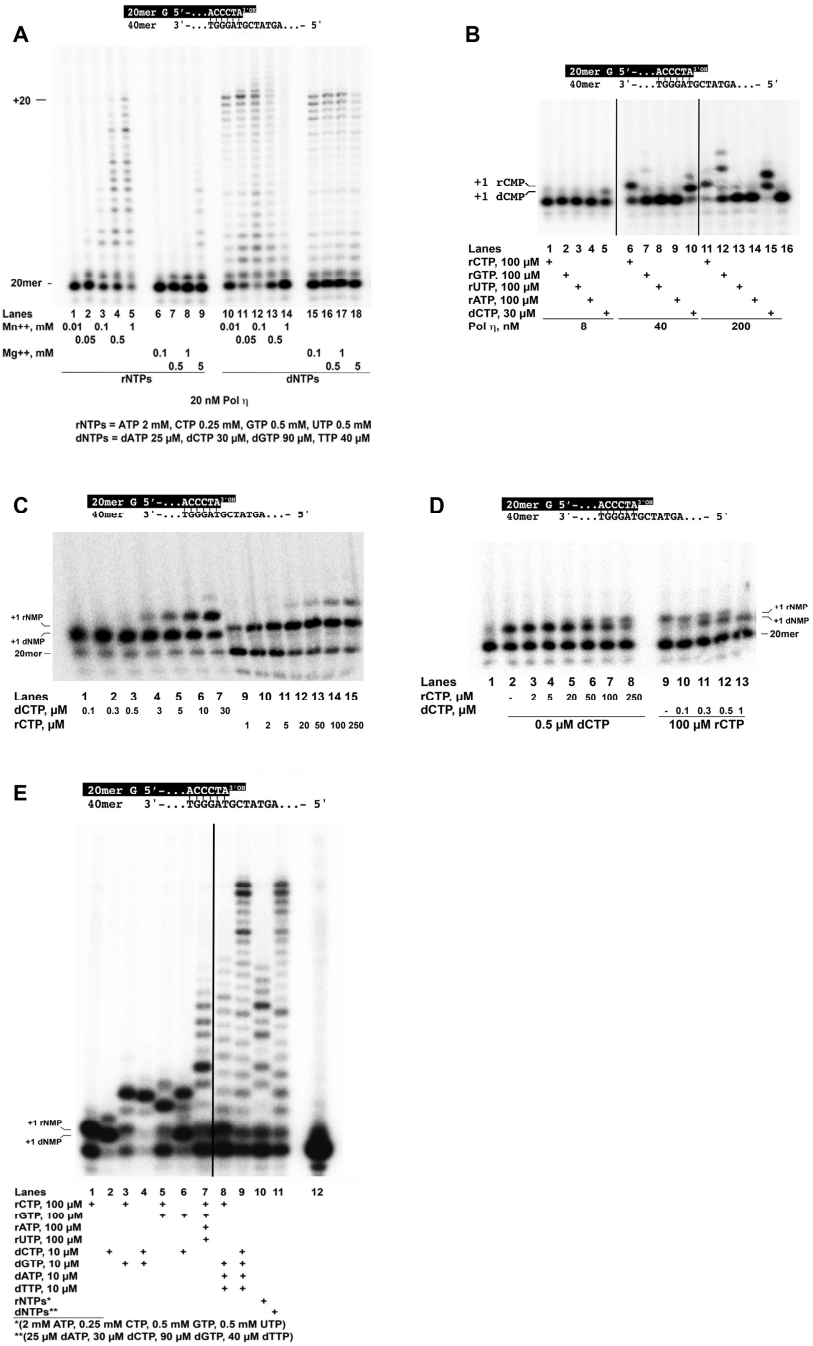

Figure 1. Incorporation and elongation of ribonucleotides by human Pol η. The sequence of the 5′ ^{32}P-labeled 20/40mer substrate (50 nM) used in all the experiments is indicated on top of each panel. (**A**) Pol η (20 nM) was incubated in the presence of non-equimolar mixtures of rNTPs (lanes 1–9) or dNTPs

was 400. Since the products arising from rCMP incorporation had a different electrophoretic mobility with respect to those due to dCMP incorporation, it was possible to simultaneously visualize both incorporation events in the same reaction. Indeed, titrating rCTP in the reaction, in the presence of fixed amounts of dCTP, led to the accumulation of the +1 rCMP product with concomitant reduction of the +1 dCMP product (Figure 1D, lanes 3–8). The same pattern was observed in the reciprocal experiment, i.e. titrating dCTP while keeping rCTP fixed (Figure 1D, lanes 9–13). These results confirmed that dCTP and rCTP can compete for incorporation opposite G. Comparable amounts of either products were observed at a rCTP/dCTP (M/M) ratio between 500 (Figure 1D, lane 8) and 300 (Figure 1D, lane 11), in agreement with the selectivity value derived from the kinetic analysis.

Pol η can synthesize hybrid DNA/RNA chains

Next, different combinations of the four deoxy- or ribonucleotides were tested, according to the template sequence. As shown in Figure 1E, after rCMP incorporation at position +1, Pol η was able to efficiently elongate by incorporating either deoxy- (Figure 1E, lane 3) or ribo-GMP (lane 5) opposite C at position +2. Similarly, efficient elongation was observed starting from a dCMP-terminated primer, with either deoxy- or ribo-GMP (Figure 1E, lanes 4 and 6). Long products were synthesized by Pol η when provided with all four rNTPs at equimolar (Figure 1E, lane 7) or physiological (lane 10) concentration ratios. Comparable products were observed when rCTP was provided in combination with the three remaining dNTPs (Figure 1E, lane 8). These products, however, were shorter than those synthesized in the presence of dNTPs only (Figure 1 E, lanes 9 and 11). Overall, these results indicated that Pol η can efficiently elongate rNMP-terminated primers, synthesizing both RNA and RNA/DNA polynucleotide chains.

Translesion synthesis of 8-oxo-G by Pol η with ribonucleotides

Pol η can perform faithful bypass of 8-oxo-G, inserting dCMP. When rCTP was provided in the reaction, robust incorporation opposite 8-oxo-G was observed for both a 1-nt gapped (Figure 2A, lanes 1–6) or an open primer/template (Figure 2B, lanes 1–5). The kinetic parameters for rCMP and dCMP incorporation opposite 8-oxo-G are summarized in Table 1. The selectivity of Pol η for dCMP versus rCMP incorporation opposite the lesion was increased 3.5-fold, with respect to a normal G, showing a value of 1428. Pol η could also incorporate both dAMP and rAMP, opposite the lesion (Figure 2C). The selectivity for dAMP versus rAMP was in the order of 3800, while the preference for dCMP versus rAMP incorporation was 12 700 (Table 1). Interestingly, the fidelity of lesion bypass was increased with rNTPs relative to dNTPs, with a 3.3-fold preference for dCMP versus dAMP incorporation and an 8.9-fold preference for rCMP versus rAMP incorporation, respectively (Table 1). These values were also in agreement with those reported in a recent study (17). When all four dNTPs or rNTPs were provided, Pol η could perform efficient TLS (Figure 2D, compare lane 1 with lane 5). The products synthesized in the presence of rNTPs were sensitive to RNase treatment (Figure 2D, lane 3), confirming that they were authentic RNA chains. These results indicated that Pol η can synthesize RNA chains as a result of TLS past an 8-oxo-G lesion.

Pol η bypasses 8-met-G, but not 3-met-C with ribonucleotides

We extended our investigation of Pol η bypass to the 3-met-C and 8-met-G alkylation lesions. As shown in Figure 3A, Pol η incorporated all four dNMPs opposite 3-met-C or 8-met-G (Figure 3A, lanes 2–5; 11–14). On the contrary, while none of the rNMPs was incorporated opposite 3-met-C (Figure 3A, lanes 1–9), robust rCMP incorporation was observed opposite 8-met-G (lane 16). Titration of dCTP or rCTP in the reaction revealed the accumulation of the expected +2 product (Figure 3B), indicating efficient TLS by Pol η with both deoxy- and ribonucleotides. The kinetic parameters for 8-met-G bypass are summarized in Table 1. The selectivity for dCMP versus rCMP incorporation by Pol η opposite 8-met-G was 693, which is only slightly higher than the selectivity measured opposite a normal G. To the best of our knowledge, this is the first report of bypass of the 8-met-G lesion by a human pol with rNTPs.

Next, the effect of the auxiliary proteins PCNA and PolDIP2 was tested. PCNA did not stimulate rCMP incorporation opposite 8-met-G by Pol η (Figure 3C, compare lanes 1–4 with lanes 7–10). On the other hand, a significant stimulation was observed in the presence of PolDIP2 (Figure 3C, lanes 11–14). Kinetic analysis showed that PolDIP2 increased the apparent catalytic efficiency (k_{cat}/K_M) for rCMP incorporation by 6-fold, lowering the selectivity value of Pol η for dCMP versus rCMP incorporation to 111 (Table 1). PolDIP2 stimulated TLS by Pol η past 8-met-G also when all four dNTPs or rNTPs were provided to the reaction at their average physiological concentrations (Figure 3 D). However, the length of the RNA chains synthesized were limited to about 5 nt (Figure 3D, lanes 5–8), while full length products were detected with dNTPs (Figure 3D, lanes 1–4). When PCNA was added in the reaction in a molar excess with respect to PolDIP2, TLS by Pol η with rNTPs was partially inhibited (Supplementary Figure S1A, lane 4). However, this effect was abolished when the PolDIP2 concentration was increased (lane 8), suggesting a

←

(lanes 10–18) and different amounts of Mn2+ (lanes 1–5; 10–14) or Mg 2+ (lanes 6–9; 15–18). The final concentrations of the individual rNTPs and dNTPs are indicated on the bottom of the panel. (**B**) Increasing amounts of Pol η were titrated in the presence of fixed concentrations of each individual rNTP (lanes 1–4; 6–9; 11–14) or dCTP (lanes 5, 10, 15). Lane 16, control reaction in the absence of nucleotides. (**C**) Pol η (40 nM) was tested in the presence increasing concentrations of dCTP (lanes 1–7) or rCTP (lanes 9–15). **D**. Pol η (20 nM) was tested in the presence of a fixed dose of dCTP and increasing concentrations of rCTP (lanes 2–8) or a fixed dose of rCTP and increasing concentrations of dCTP (lanes 9–13). Lane 1, control reaction in the absence of nucleotides. (**E**) Pol η (40 nM) was tested in the presence of various combinations of dNTPs or rNTPs. Lane 12, control reaction in the absence of nucleotides.

Table 1. Kinetic parameters for nucleotide incorporation opposite G, 8oxoG or 8metG by Pol η

Nucleotide	K_M, μM[a]	k_{cat}, min^{-1}	k_{cat}/K_M M^{-1} s^{-1}	f_{rel}[b] (dCTP/rCTP)	f_{rel} (dCTP/dATP)	f_{rel} (dCTP/rATP)	f_{rel} (rCTP/dATP)	f_{rel} (rCTP/rATP)
39/100mer G								
dCTP	0.20 ± 0.05	1.9 ± 0.05	1.60×10^5	400	n.a.	n.a.	n.a.	n.a.
rCTP	15 ± 0.3	0.40 ± 0.1	0.40×10^3					
39/100mer 8oxoG								
dCTP	0.50 ± 0.02	1.8 ± 0.01	0.60×10^5	1428	3.30	12 765		
rCTP	117 ± 4	0.30 ± 0.01	42				2.30×10^{-3}	8.90
dATP	0.30 ± 0.01	0.32 ± 0.01	0.18×10^5					
rATP	247 ± 5	0.07 ± 0.02	4.70					
39/72mer 8metG								
dCTP	2.70 ± 0.1	1.10 ± 0.02	6.80×10^3	693	n.a.	n.a.	n.a.	n.a.
rCTP	187 ± 3	0.11 ± 0.03	9.80					
rCTP + PolDIP2	100 ± 2	0.37 ± 0.04	61	111				
18/24mer GG								
dCTP	0.30 ± 0. 3	2.50 ± 0.2	1.40×10^5	546	n.a.	n.a.	n.a.	n.a.
rCTP	26 ± 0.5	0.40 ± 0.2	256					
18/24mer cis-Pt								
dCTP	1.50 ± 1	1.20 ± 0.1	1.30×10^4	1212	n.a.	n.a.	n.a.	n.a.
rCTP	113 ± 5	0.07 ± 0.01	11					

[a]Kinetic parameters have been calculated as indicated in the 'Materials and Methods' section. Values are the means of three independent experiments ±S.D.
[b]Relative incorporation frequency, f_{rel} was calculated as the ratio between the k_{cat}/K_M values for the indicated nucleotide pairs.

possible competition between PCNA and Pol η for binding to PolDIP2.

Pol η bypasses cis-PtGG but not an abasic site with ribonucleotides

Pol η is the main enzyme involved in the bypass of the intrastrand guanine crosslinks caused by the anticancer drug cisplatin (cis-PtGG) (36). When tested in the presence of each of the four rNTPs, Pol η was capable of incorporating rCMP opposite the lesion (Figure 4A, lane 10). The products observed with rGTP and rUTP as substrates resulted from the incorporation of dNTPs contaminating the commercial preparation used, as judged by their electrophoretic mobility, which was similar to those of products obtained with dCTP as substrate (Figure 4A, compare lanes 8, 9 with lane 7; Supplementary Figure S1B and C). Interestingly, the incorporation of rCMP was largely limited to the +1 product (Figure 4A, lane 10), corresponding to incorporation opposite the first guanine (termed 3′-G, according to the template strand orientation) of the adduct, similar to what has been observed for the insertion of non-canonical dNTPs opposite Pt-GG by Pol η (29), while dCMP was correctly incorporated opposite both guanines, yielding the expected +2 product (Figure 4A, lane 2). Titration of dCTP (Figure 4B) or rCTP (Figure 4C) into the reaction confirmed that rCMP incorporation was limited to opposite the 3′-G of cisPt-GG (Figure 4C, lanes 9–4). PolDIP2 stimulated rCMP (Figure 4D) and dCMP (Figure 4E) incorporation by Pol η opposite cis-PtGG, but even in the presence of PolDIP2, rCMP incorporation was limited to the first position (Figure 4 D, lanes 5–13). When a primer/template bearing a rCMP opposite the 3′-G of the lesion was tested, only dCMP, but not rCMP, was incorporated opposite the 5′-G (Figure 4F). Interestingly, when a primer/template with a dCMP opposite the 3′-G was used, no incorporation of rCMP was observed either (Figure 4G). Overall, these results indicated that bypass of a cis-PtGG adduct by Pol η can lead to incorporation of rCMP opposite the first guanine (3′-G) only. The bypass, however, can be subsequently completed by incorporating dCMP opposite the 5′-G. The selectivity for dCMP versus rCMP incorporation opposite the two guanines on the undamaged template was 546, similar to the one observed on the template with a single guanine (Table 1). This selectivity was increased to about 1200, opposite the 3′-G of cisPt-GG, a value similar to the one observed for 8-oxo-G (Table 1). In a competition experiment, dCTP was titrated in the presence of the cisPt-GG template and fixed amounts of rCTP, resulting in the accumulation of the +1 dCMP product with concomitant reduction of the +1 rCMP product (Figure 4 H, lanes 2–6). The same pattern was observed in the reciprocal experiment, i.e. titrating rCTP while keeping dCTP fixed (Figure 4H, lanes 7–10). These results confirmed that dCTP and rCTP can compete for incorporation opposite the 3'-G of a cisPt-GG adduct. Comparable amounts of either products were observed at a rCTP/dCTP (M/M) ratio of 1/1000 (Figure 4H, lanes 4 and 10), in agreement with the selectivity value derived from the kinetic analysis (Table 1). Simultaneous incorporation of rCMP and dCMP opposite the lesion was also observed in a similar competition experiment carried out with XP-V/η extracts (Figure 4I, lane 6), suggesting that rCMP incorporation opposite the cisPt-GG lesion by Pol η can also occur in a cellular context.

Finally, when tested in the presence of an AP site, Pol η was unable to significantly incorporate rNMPs opposite the lesion (Supplementary Figure S1D, lanes 1–4), even in the presence of PolDIP2 (lanes 7–10), with the exception of a very weak incorporation of rCMP (Supplementary Figure S1F, lane 10), while it efficiently bypassed the lesion with either dATP or all four dNTPs (Supplementary Figure S1D, lanes 5, 6, 11 and 12).

Ribonucleotide-mediated lesion bypass in XP-V cell extracts

The rCMP incorporation opposite 8-oxo-G was measured in extracts from XP-V cells lacking Pol η, in comparison with the same XP-V cell line complemented with ectopic expression of human Pol η (XP-V/h). As shown in Supplementary Figure S1E, TLS of 8-oxo-G with rCMP was detected in both XP-V and XP-V/η extracts (lanes 1–3). When this activity was normalized to the total Pol activity (measured as incorporation of dCMP opposite a normal G, Supplementary Figure S1F), rCMP incorporation was reduced

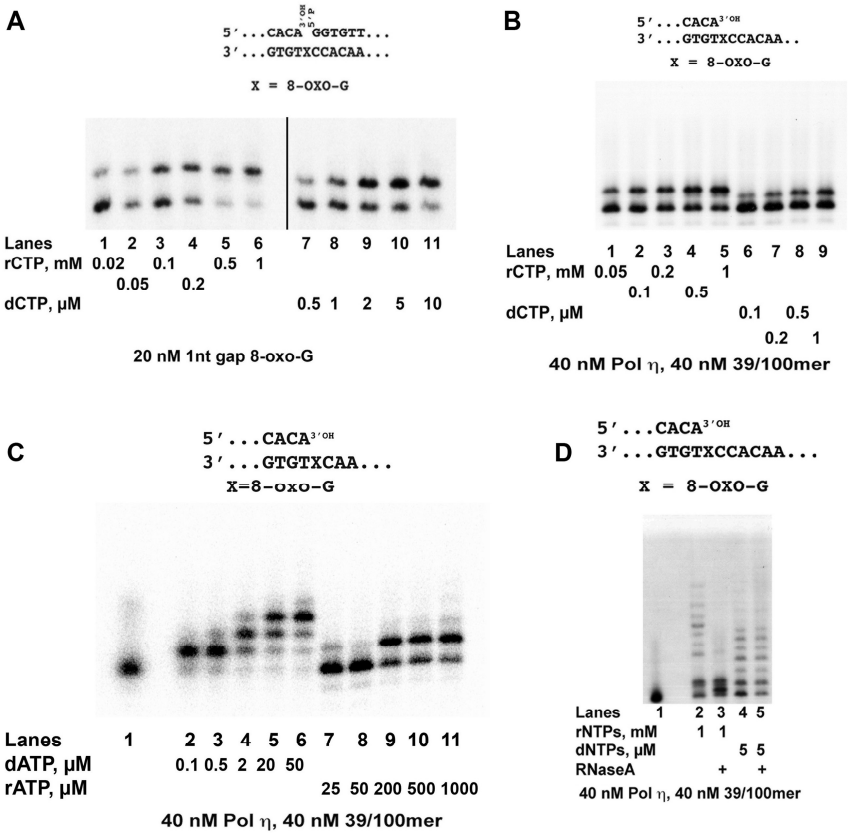

Figure 2. Translesion synthesis of 8-oxo-G by Pol η with ribonucleotides. The sequences of the 5′ ^{32}P-labeled DNA substrates used are indicated on top of each panel. (**A**) Pol η (40 nM) was incubated with the 1-nt gapped 8-oxo-G template, in the presence of increasing concentrations of rCTP (lanes 1–6) or dCTP (lanes 7–11). (**B**) Pol η was incubated with the 39/100-mer 8-oxo-G template, in the presence of increasing concentrations of rCTP (lanes 1–5) or dCTP (lanes 6–9). (**C**) Pol η was incubated with the 39/100-mer 8-oxo-G template, in the presence of increasing concentrations of dATP (lanes 2–6) or rATP (lanes 7–11). Lane 1, control reaction in the absence of nucleotides. (**D**) Pol η was incubated with the 39/100-mer 8-oxo-G template, in the presence of all four rNTPs (lanes 2, 3) (1 mM each, final concentration) or dNTPs (lanes 4, 5) (5 μM each, final concentration). 2 Units of RNaseA (lanes 3, 5) or buffer (lanes 2, 4) were added after 10 min and the incubation continued for additional 5 min. Lane 1, control reaction in the absence of nucleotides.

by about 25% in the absence of Pol η (Supplementary Figure S1G). The majority of rCMP incorporation opposite 8-oxo-G has been shown to be carried out by Pol β (16). Western blot analysis of the extracts confirmed that both Pol β and Pol η were present in the extracts (Supplementary Figure S1H). Thus, the apparently modest contribution of Pol η to rCMP incorporation opposite 8-oxo-G, could be explained by the competition of Pol β. On the other hand, when the extracts were tested with the cis-PtGG template, bypass was observed only in XP-V/η cells, with either dCMP or rCMP (Supplementary Figure S1I), in agreement with the notion that Pol η contributes most to TLS past this lesion. Collectively, these data suggest that the frequency of rNMP incorporation opposite a certain lesion is a function of (i) the type of TLS pols potentially acting on that lesion, (ii) their sugar selectivity and (iii) their relative affinity for the lesion.

Cleavage of rCMP opposite normal or damaged guanines by human RNase H2

In a 1993 report of the first purification from mammalian cells of the enzyme later identified as RNase H2, Eder *et al.* showed that the efficiency of the enzyme depended on the identity of the base pair being cleaved (37). To verify this property, we expressed and purified the recombinant human trimeric RNase H2 (Supplementary Figure S3A) and tested it with all four ribo-to-deoxynucleoside base pairs. Time course experiments were performed with increasing amounts of the 40/40mer ds DNA oligonucleotide substrates, bearing either a rC:dG, rG:dC, rA:dT or rU:dA pair at a specific position. The strand containing the single rNMPs was 5′-labeled so that after cleavage by RNase H2, products of a defined length were generated and resolved by sequencing gel electrophoresis. Representative experi-

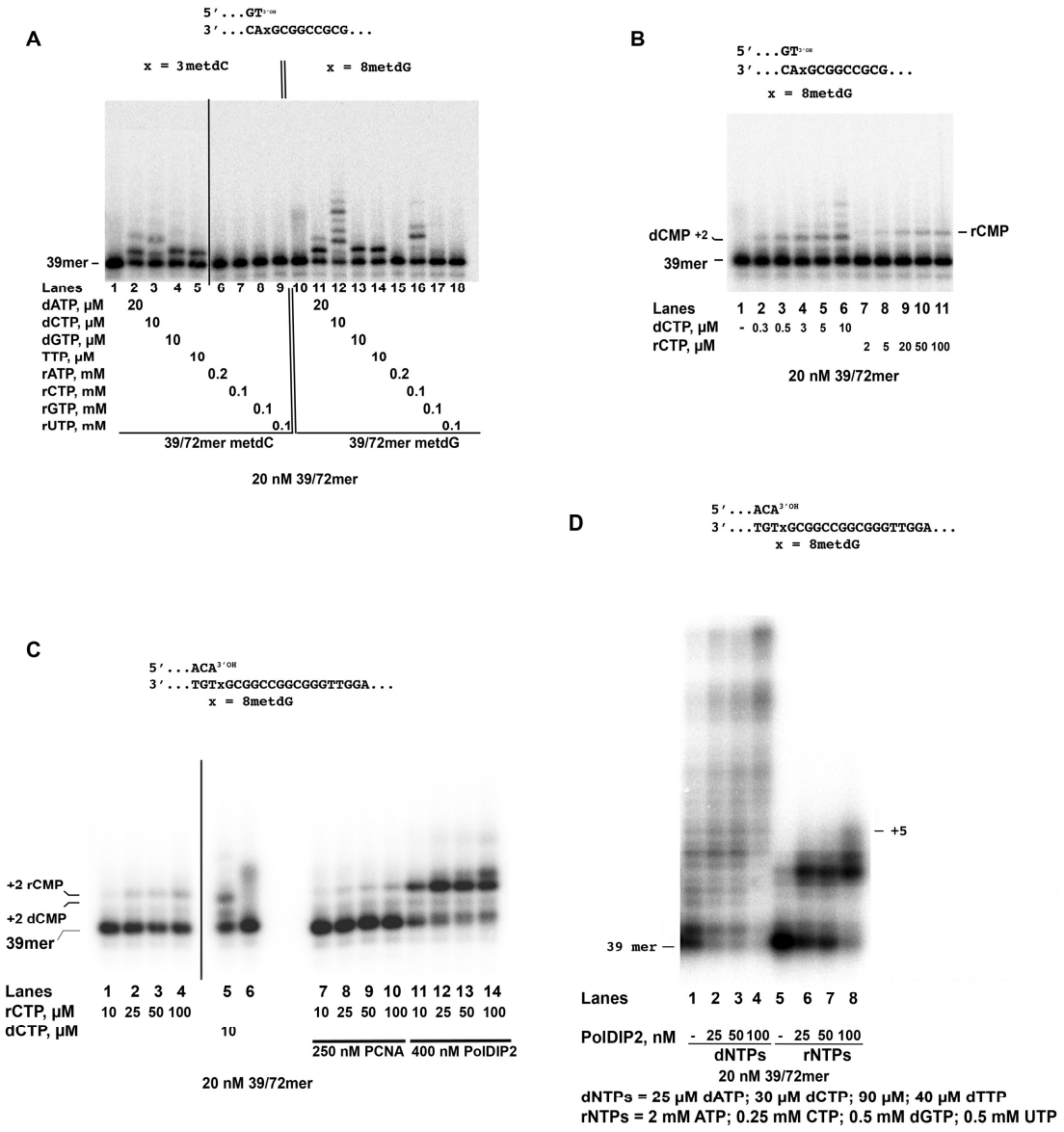

Figure 3. Pol η bypass of 8-met-G and 3-met-C with ribonucleotides. The sequences of the 5′ ^{32}P-labeled DNA substrates used are indicated on top of each panel. (**A**) A total of 20 nM Pol η was incubated in the presence of the 3-met-C (lanes 1–9) or 8-met-G (lanes 10–18) 39/72mer substrates and a fixed concentration of each dNTP (lanes 2–5; 11–14) or rNTP (lanes 6–9; 15–18). Lanes 1 and 10, control reactions without nucleotides. (**B**) 20 nM Pol η was incubated with the 8-met-G substrate, in the presence of increasing concentrations of dCTP (lanes 2–6) or rCTP (lanes 7–11). Lane 1, control reaction in the absence of nucleotides. (**C**) 20 nM Pol η was incubated with the 8-met-G substrate, in the presence of rCTP (lanes 1–4; 7–14) or dCTP (lane 5) and in the absence (lanes 1–5) or in the presence of PCNA (lanes 7–10) or PolDIP2 (lanes 11–14). Lane 6, control reaction in the absence of nucleotides. (**D**) A total of 20 nM Pol η was incubated with the 8-met-G substrate, in the presence of non-equimolar mixtures of dNTPs (lanes 1–4) or rNTPs (lanes 5–8) and in the absence (lanes 1, 5) or in the presence of increasing concentrations of PolDIP2 (lanes 2–4; 6–8). The final concentrations of the individual rNTPs and dNTPs are indicated on the bottom of the panel.

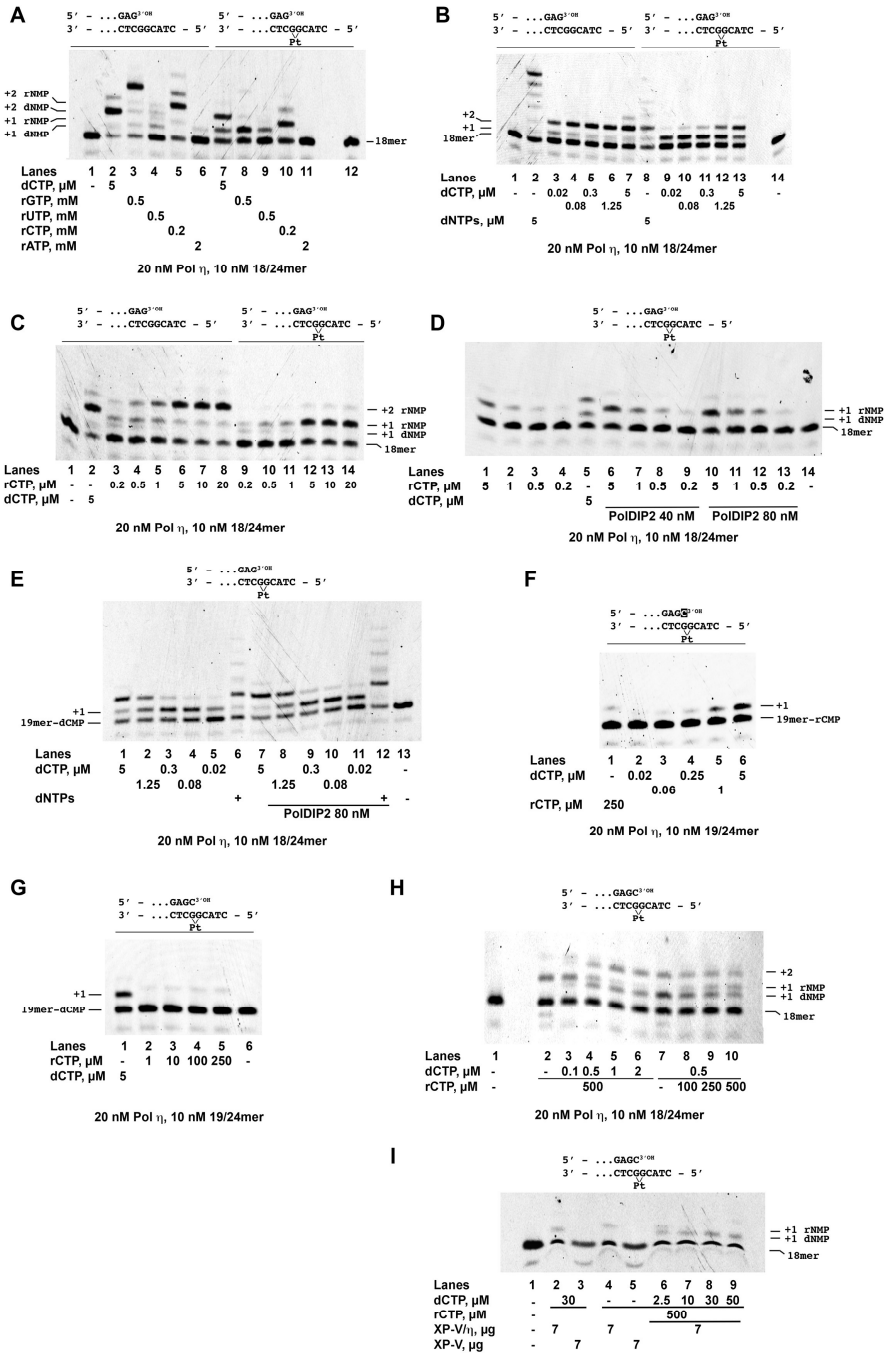

Figure 4. Pol η bypass of cis-PtGG and abasic site with ribonucleotides. The 5′ FAM-labeled DNA substrates used are indicated on top of each panel. (**A**) Pol η was incubated with the undamaged (lanes 1–6) or the cis-PtGG (lanes 7–12) templates, with dCTP (lanes 5, 7) or each rNTP (lanes 3–6; 8–11).

Table 2. Kinetic parameters for RNase H2 cleavage of different ribo-/deoxynucleoside basepairs

Basepair	K_M (nM)[a]	k_{cat} (min^{-1})	k_{cat}/K_M (M^{-1}, s^{-1})	efficiency (-fold)
rA:dT	10 ± 3	6.7 ± 0.2	11×10^6	6.1
rU:dA	12 ± 2	3.1 ± 0.5	4.3×10^6	2.4
rC:dG	8 ± 2	0.9 ± 03	1.8×10^6	1
rG:dC	27 ± 5	1.2 ± 0.3	0.7×10^6	0.4

[a]Kinetic parameters have been calculated as indicated in the 'Materials and Methods' section. Values are the means of four independent experiments ±S.D.

ments are shown in Supplementary Figure S2A–D, while the kinetic parameters are summarized in Table 2. Human RNase H2 had a strong preference for rA:dT cleavage, followed by rU:dA. Interestingly, rC:dG and rG:dC pairs were cleaved with a 6-fold and 15-fold reduced efficiency with respect to rA:dT. RNase H2 subunit H2B contains a PCNA-binding domain and PCNA has been shown to interact with RNase H2 and direct it to the DNA substrate. We therefore tested whether PCNA could rescue the reduced catalytic activity of human RNase H2 with rC- or rG-containing substrates. As shown in Supplementary Figure S2B and C, however, PCNA did not stimulate rC:dG or rG:dC cleavage by RNase H2.

Next, we evaluated whether rCMP paired to a damaged guanine may affect RNase H2 cleavage. RNase H2 showed a 3.4-fold reduced efficiency in removing rCMP when it was opposite 8-oxo-G versus G (Figure 5A and B). On the other hand, no differences were seen in cleavage efficiency between rC:dG and rC:8metG pairs (Figure 5C and D). RNase H2 exhibited reduced cleavage efficiency of rCMP opposite both the 3′-G and 5′-G of cis-PtGG relative to the controls (Supplementary Figure S2D). Since rCMP incorporation by Pol η can occur only opposite the 3′-G (see Figure 4), we better characterized RNase H2 cleavage at this position (Figure 5E). Quantification of the results indicated a 3.8-fold reduced cleavage efficiency by RNase H2 when rCMP was opposite the 3′-G of a cis-PtGG lesion, relative to it being opposite an undamaged guanine at the same position (Figure 5F). Overall, these results indicated that rCMP opposite an undamaged guanine is already less efficiently cleaved by RNase H2, and incorporation of rCMP as a result of TLS can further reduce the efficiency of its removal by RNase H2.

DISCUSSION

In the present study, we addressed the possible consequences of rNMPs incorporation by human Pol η in the context of TLS of five different lesions (8-oxo-G, 8-met-G, 3met-C, cis-PtGG and AP site), by studying not only the incorporation by Pol η *per se*, but also the subsequent cleavage of the incorporated rNMPs by human RNase H2 and the impact of auxiliary proteins in the TLS process. In fact, the incorporation of rNMPs in the context of TLS would result in an aberrant base pair, in which the rNMP is placed opposite the original DNA lesion. As a result, the cell will need to act upon *two paired lesions*: the rNMP on the newly synthesized strand and the original lesion on the template strand.

We found that human Pol η, at physiological concentrations of Mg^{2+} and rNMPs, has robust DNA-dependent RNA Pol activity, being able to synthesize several nucleotides-long RNA chains, either on undamaged DNA or during TLS. Thus, Pol η behaves differently from Pols β and λ, whose activity is limited to the incorporation of one or two rNMPs (16), but similar to the X-family Pol μ (9,13) or the Y-family Pol ι (14).

These results suggest that Pol η may amplify the number of rNMPs incorporated into the genome, for example if TLS occurs on a gapped DNA intermediate behind the replication fork, as has been suggested. Such long RNA chains may represent an additional challenge to the cell. It has been observed that in *S. cerevisiae*, deletion of the Rad30 gene (encoding yeast Pol η) reduces the toxic effects due to inactivation of RNaseH1 and RNase H2, both required to remove RNA chains longer than 4 nt (38). The same studies indicated Pol ζ as the TLS enzyme essential to relieve the cells from the stress due to excessive rNMPs accumulation in the genome. Replicative pols δ and ϵ can bypass only a limited number (< 4) of rNMPs in the template strand (39,40), while Pol ζ can easily copy a template containing multiple rNMPs (38). These findings, together with studies on yeast strains expressing a mutant Pol η with increased ability to incorporate rNMPs (21), support the hypothesis that Pol η leads to the accumulation of long stretches of RNA in the genome in cells lacking RNase H2

←

Lanes 1, 12, control reactions without nucleotides. (**B**) Pol η was incubated with the undamaged (lanes 1–7) or the cis-PtGG (lanes 8–14) templates, in the presence of dNTPs (lanes 2, 8) or dCTP (lanes 3–7; 9–13). Lanes 1, 14, control reactions without nucleotides. (**C**) Pol η was incubated with the undamaged (lanes 1–8) or the cis-PtGG (lanes 9–14) templates, in the presence of rCTP (lanes 3–14). Lane 1, control reaction without nucleotides. Lane 2, control reaction with dCTP. (**D**) Pol η was incubated with the cis-PtGG template in the presence of rCTP (lanes 1–4; 6–13) and in the absence (lanes 1–4) or in the presence of PolDIP2 (lanes 6–13). Lane 5, control reaction with dCTP. Lane 14, control reaction without nucleotides. (**E**) Pol η was incubated with the cis-PtGG template in the presence of dNTPs (lanes 6, 12) or dCTP (lanes 1–5; 7–11) and in the absence (lanes 1–6) or in the presence of PolDIP2 (lanes 7–12). Lane 13, control reaction without nucleotides. (**F**) Pol η was incubated with the cis-PtGG template bearing a rCMP opposite the 3′-G of the lesion, in the presence of rCTP (lane 1) or dCTP (lanes 2–6). (**G**) Pol η was incubated with the cis-PtGG template bearing a dCMP opposite the 3′-G of the lesion, in the presence of dCTP (lane 1) or rCTP (lanes 2–5). Lane 6, control reaction without nucleotides. (**H**) Pol η (20 nM) was tested in the presence of a fixed dose of rCTP and increasing concentrations of dCTP (lanes 2–6) or a fixed dose of dCTP and increasing concentrations of rCTP (lanes 7–10). Lane 1, control reaction in the absence of nucleotides. (**I**) XP-V (lanes 3, 5) or XP-V/η (lanes 2, 4, 6–9) extracts, were incubated with the cis-PtGG template in the presence of dCTP alone (lanes 2, 3), rCTP alone (lanes 4, 5) or both nucleotides at different M/M ratios (lanes 6–9). Lane 1, control reaction in the absence of extracts.

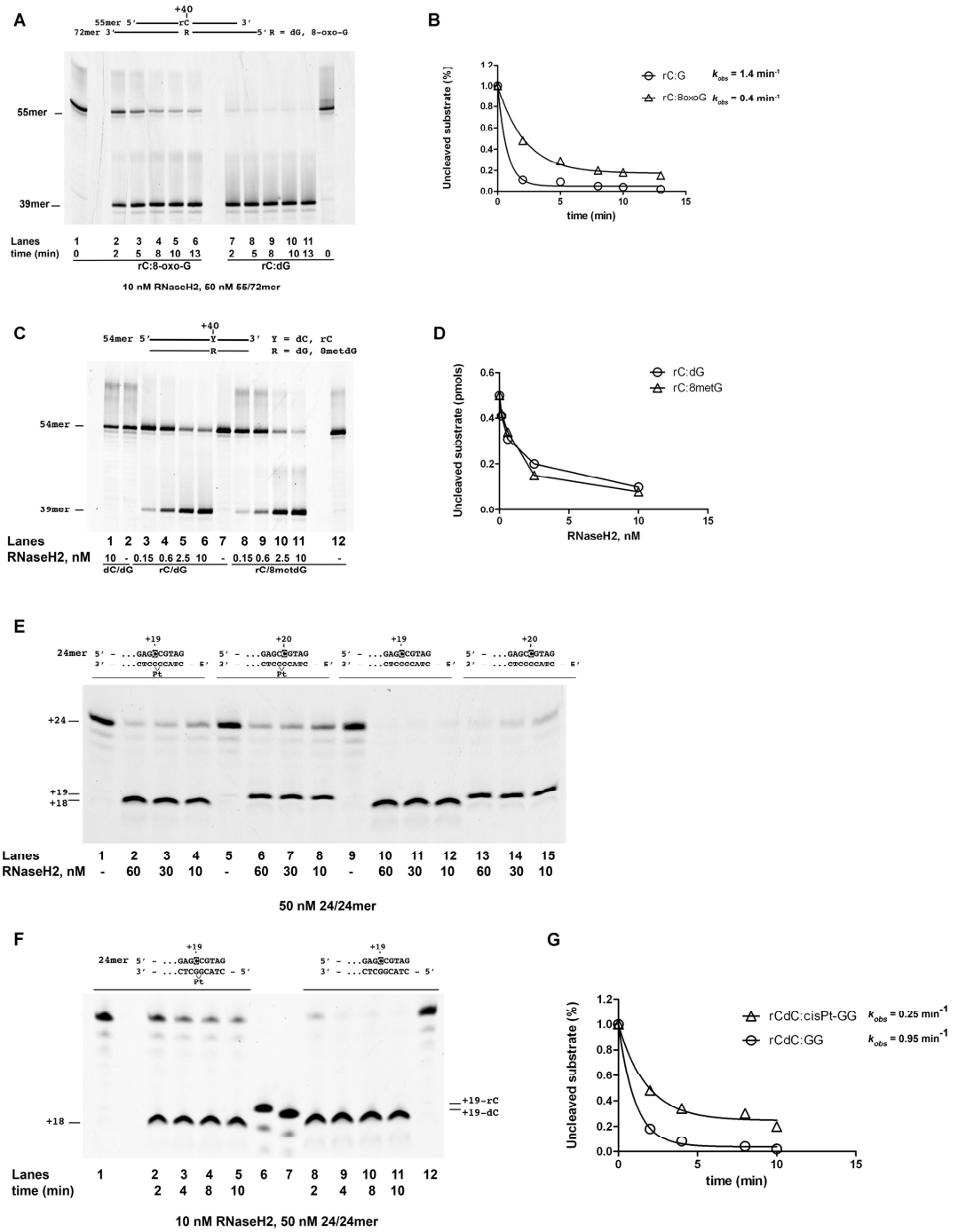

Figure 5. Cleavage of rCMP opposite normal or damaged guanines by human RNase H2. The 5′ FAM-labeled templates used are indicated on top of each panel. Asterisks indicate the labeled strands. (**A**) Time course of RNase H2 digestion of the DNA substrate containing a single rCMP opposite 8-oxo-G

and H1. In the next replication round, these RNA tracts will require Pol ζ for TLS.

Our results show that Pol η can bypass only certain lesions using rNMPs. It can easily perform TLS incorporating rCMP past a 8-oxo-G or 8-met-G, but not past 3-met-C or an AP site. Also, the nature of the lesion can influence its sugar selectivity. While the dCMP versus rCMP preference for incorporation opposite 8-met-G was similar to the one opposite a normal guanine (693 versus 400, respectively, Table 1), selectivity of dCMP opposite 8-oxo-G increased to a value of about 1400 (Table 1). Also, the fidelity of 8-oxo-G bypass was increased: the preference for rCMP versus rAMP incorporation was 8.9, while the one for dCMP versus dAMP was 3.3 (Table 1). A recent study, appearing during the preparation of this manuscript, found a similar increase in fidelity for the bypass of 8-oxo-G by human Pol η (17).

The 8-Met-G is an major alkylation product of deoxyguanosine and has miscoding properties (41). No human glycosylase has been identified so far, that can remove this lesion (42). Thus, its tolerance may rely principally on the TLS pathway. However, the capacity of human Pols to perform TLS over 8-met-G remains largely unknown. Interestingly, this modification occurs at the same position of the purine ring as in the 8-oxo-G, giving us the opportunity to compare the effects of two different substituents at the C-8 of the guanine. We found that Pol η can easily misincorporate different dNMPs opposite 8-met-G, while the complementary rCMP was the only rNMP inserted opposite this lesion. Efficient elongation past 8-met-G was observed with both dNMP and rNMP insertion. To the best of our knowledge, this is the first report of bypass of 8-met-G by a human TLS Pol.

Another important role for Pol η is in resistance toward the anticancer drug cis-Pt, which causes inter- or intrastrand crosslinks of two adjacent purines, in most cases guanines. These crosslinks block replication fork progression, requiring bypass by a specialized TLS Pol. The most frequent intrastrand crosslink is the cis-PtGG lesion. Among human Pols, Pol η has been shown to be the most proficient in bypassing cis-PtGG lesions (36). Accordingly, cells lacking Pol η, are hypersensitive to cis-Pt treatment (43,44). In cancer cells, Pol η overexpression is induced by cis-Pt treatment and its levels correlate with chemoresistance and poor clinical outcomes of several tumors, such as non-small-lung or ovarian cancers (44,45).

We found that human Pol η bypasses a cis-PtGG intrastrand crosslink by incorporating rCMP opposite the 3′-G of the lesion, then completing the bypass by incorporating dCMP opposite the 5′-G of the lesion. No rCMP incorporation could be observed opposite the 5′-G, either starting from a rCMP- or a dCMP-terminated primer. Crystal structures of Pol η in complex with a cis-PtGG and an incoming dCTP (46–48) clearly shows that incorporation opposite the 5′-G requires structural rearrangements to adsorb the 30° roll imposed by the crosslink between the two guanines. As a result, the 5′-G of the adduct can adopt either an inactive 'open' conformation or a catalytically active 'stacked' conformation. Even in the stacked conformation, the distance between the 3′-OH and the α-phosphate of the incoming dCTP poised for insertion opposite the 5′-G, is increased with respect to the complex formed with the 3′-G as the templating base, further decreasing the catalytic rate. Thus, it is possible that the presence of a 2′-OH group in the sugar of the incoming nucleotide cannot be accommodated opposite the 5′-G in the stacked conformation.

The rNMPs incorporated into the genome can be removed by RNase H2. However, very little is known about the ability of human RNase H2 in processing rNMPs incorporated opposite DNA lesions. Human RNase H2 is a heterotrimer composed of the H2A subunit that contains the catalytic site and the H2B and H2C subunits, which contribute essential structural roles (49,50). H2B also interacts with PCNA (31), which is important for the recruitment of the RNase H2 heterotrimer to DNA repair sites (51). RNase H2 knockout mice show embryonic lethality (52,53), while mutations in the RNase H2 subunits are linked to human diseases such as the Aicardi-Goutieres Syndrome (AGS) (54) and Systemic Lupus Erythematosus (SLE) (55). Thus, alterations in the catalytic efficiency of RNase H2, leading to rNMP accumulation, can have important physiological consequences (56).

We observed that human RNase H2 processes rNMPs paired to their complementary dNMPs with preference in the order rA>rU>rC>rG. The reasons for such a preference are not clear. The available crystal structures of mammalian RNase H2 enzymes (57,58) were not solved in complex with a nucleic acid substrate. However, the structure of the enzyme-substrate complex of *Thermotoga maritima* RNase H2 (59) shows that for the DNA/RNA junction, cleavage requires structural rearrangement of the sugar-phosphate backbone with rotation of the phosphodiester bond. It is tempting to speculate that such local backbone distortion my be energetically less favoured when the rNMP to be cleaved is part of a more stable rC:dG or rG:dC pair relative to rA:dT or rU:dA. Overall, these results suggest that besides the preferential incorporation of rCMP and dGMP by replicative Pols, also the lower efficiency of their removal by RNase H2 may contribute to the observed preferential accumulation of these two rNMPs in the genome.

We also observed a different preference of RNase H2 in the removal of rCMP opposite DNA lesions. A rCMP op-

←

(lanes 1–6) or undamaged guanine (lanes 7–12). (**B**) Quantification of the experiment shown in panel A. Data points were fitted to the simple exponential ([substrate]/[substrate+ product]) = $e^{-k_{obs}t}$. (**C**) RNase H2 was titrated in the presence of the DNA substrate containing a single rCMP opposite an undamaged guanine (lanes 3–6) or opposite a 8-met-G lesion (lanes 8–11). Lanes 7, 12, control reactions in the absence of enzyme. Lanes 1, 2, control reactions with the DNA substrate bearing a dCMP opposite guanine with or without enzyme, respectively. (**D**) Quantification of the experiment shown in panel C. No curve fitting was applied. (**E**) RNase H2 was titrated in the presence of the DNA substrate containing a single rCMP opposite either the 3' G (lanes 1 - 4) or the 5' G (lanes 5 - 8) of a cis-PtGG lesion (lanes 1 – 8) or the same guanines in an undamaged template (lanes 9–15). (**F**) Time course of RNase H2 digestion of the DNA substrate containing a single rCMP opposite the 3′-G of a cis-PtGG lesion (lanes 1 – 10) or the same guanine in an undamaged template (lanes 8–12) Lanes 6, 7, rCMP- and dCMP-terminated 19mer oligonucleotides, respectively, as markers. (**G**) Quantification of the experiment shown in panel E. Data points were fitted to the simple exponential ([substrate]/[substrate + product]) = $e^{-k_{obs}t}$.

Table 3. Theoretical rCMP versus dCMP incorporation frequencies opposite normal and modified G by Pol η in different cell types

Tissue	rCTP/dCTP ratio	Template G f(rCTP/dCTP)[c] × 10^{-3}	Template 8-oxo-G f(rCTP/dCTP)[c] × 10^{-3}	Template cisPt-GG f(rCTP/dCTP)[c] × 10^{-3}	Template 8metG f(rCTP/dCTP)[c] × 10^{-3}
Skin fibroblasts[a]	18	45	12	15	26
Lymphocytes[b]	200	500	140	165	288
Liver[b]	36	86	24	27	49

[a]The rCTP and dCTP concentrations have been taken from (64).
[b]The rCTP and dCTP concentrations have been taken from (63).
[c]Frequencies of incorporation for each ribo-/deoxy-nucleoside substrate pair were calculated according to the Cornish-Bowden relationship: $f(\mathrm{rCTP/dCTP}) = (k\mathrm{cat}/K_M)_{\mathrm{rCTP}}/(k\mathrm{cat}/K_M)_{\mathrm{dCTP}} \bullet [\mathrm{rCTP}]/[\mathrm{dCTP}]$ using the values from Table 1 and (63,64).

posite 8-met-G was processed with the same efficiency as opposite a normal guanine, while a substantial drop in efficiency was observed when rCMP was opposite an 8–oxo-G or the 3′-G of a cis-PtGG lesion. Intriguingly, this order of preference is paralleled by Pol η, with incorporation of rCMP opposite 8-met-G being more favoured with respect to opposite 8-oxo-G or cisPt-GG. Thus, the increased probability of rCMP incorporation opposite 8-met-G may be compensated by a higher efficiency of its removal by RNase H2. On the contrary, incorporation of rCMP opposite 8-oxo-G or cis-PtGG may lead to a substantial delay in their processing by RNase H2.

Auxiliary proteins can also influence rNMPs incorporation during TLS. In this context, PCNA has been shown to interact with both Pol η and RNase H2 and to recruit both proteins at DNA repair foci (31,51,60). We did not find any stimulation of rNMP incorporation by Pol η or of rNMP cleavage by RNase H2 with PCNA. PolDIP2 is another recently identified auxiliary protein, which has been shown to stimulate the activity of Pols λ and η (28) and PrimPol (61). When tested in our system, PolDIp2 was able to significantly stimulate rNMP incorporation by Pol η on both undamaged DNA and during TLS of 8-oxo-G, 8-met-G and cis-PtGG.

In summary, the data presented here add novel details to the complex emerging picture of the consequences of rNMP incorporation during DNA repair. When considered in the context of recent data obtained for Pols λ and β (16), these results show that at least three key elements must cooperate in determining the consequences of TLS with rNMPs: (i) the intrinsic sugar selectivity of Pols (e.g. Pol λ, β or η); (ii) the relative Pol levels and/or their selective access to the lesion and (iii) the action of auxiliary proteins (e.g. PolDIp2). For example, while Pol η has lower sugar selectivity for dCMP versus rCMP incorporation opposite 8-oxo-G than Pols λ and β, experiments with cell extracts clearly indicate that the majority of rCMP insertion opposite the lesion is carried out by the more abundantly expressed Pol β (16), which can effectively compete with Pols λ and η for access to this lesion. On the other hand, the specificity of Pol η for TLS over the cis-PtGG adduct, makes rNMPs incorporation opposite this lesion almost exclusively dependent on the selectivity of this Pol. The auxiliary factor PolDIP2 can also further modulate the frequency of rNMP incorporation during TLS by Pol η. PCNA can functionally interact with both Pol η and PolDIP2 (28,62). Our *in vitro* data suggest the possibility that Pol η and PCNA may compete for their binding to PolDIP2 in a mutually exclusive way, an observation that deserves further investigations.

In turn, the complex lesions generated as a result of rNMP incorporation opposite damaged bases may impact DNA repair in two ways. First, they can affect the action of specialized DNA glycosylases, as shown in the case of the 8-oxo-G lesion, (16). In this context, the present data indicate that Pol η, similarly to Pols λ and β, has been shaped by evolution to minimize the risk of inserting rAMP opposite the lesion, which would represent the most dangerous situation, due to the poor ability of the DNA glycosylase MUTYH to process the resulting mispair (16).

Second, the novel information presented here, also clearly indicates that insertion of rNMPs opposite different lesions can reduce the efficiency of their removal by RNase H2, thus effectively delaying RER. However, RNase H2 is still able to correctly process a rNMP paired to a damaged base, albeit at a reduced rate, depending on the lesion. This indicates that the cell is still able to resolve the complex damage resulting from incorporating rNMPs during TLS. Thus, while this event may potentially cause replication stress, delaying the action of RNase H2 may also give more time for the excision repair systems to remove lesions opposite the rNMPs, which then could be efficiently addressed by RER once the complementary DNA strand is freed from the damaged bases. Finally, the findings reported here also suggest a potential role of Pol η in synthesizing long stretches of RNA. As shown in Table 3 for the case of rCMP incorporation, the theoretical frequencies of rNMPs versus dNMPs incorporation by Pol η are higher for undamaged G, than for all the three lesions considered here (8-oxo-G, cisPt-GG and 8-met-G), ranging from 4 to 50%, depending on the particular cell type (63,64). Intracellular dCTP concentrations measured in normal tissues are generally comprised between 0.3 and 30 μM, while rCTP concentrations range between 15 and 400 μM (63). However, other nucleotides show much higher differences, most notably rGTP and rATP, with respect to their corresponding dNTPs (64). Thus, depending on the cellular context, synthesis of long RNA stretches by Pol η may increase the toxicological consequences of rNMP incorporation in cells lacking RNase H2, for example in AGS patients.

SUPPLEMENTARY DATA

Supplementary Data are available at NAR Online.

FUNDING

Italian Association of Cancer Research AIRC Grant [IG15868 to G.M]; AIRC StartUP [12710 to S.S.]; University of Zurich and Swiss National Science Foundation Grant [152621 to B.v.L.]; Swiss National Science Foundation [156280]; ETH Research Commission [ETH-43 14-1 to S.J.S.]. Funding for open access charge: Italian Association of Cancer Research AIRC Grant [IG15868].
Conflict of interest statement. None declared.

REFERENCES

1. Nick McElhinny,S.A., Watts,B.E., Kumar,D., Watt,D.L., Lundstrom,E.B., Burgers,P.M., Johansson,E., Chabes,A. and Kunkel,T.A. (2010) Abundant ribonucleotide incorporation into DNA by yeast replicative polymerases. *Proc. Natl. Acad. Sci. U.S.A.*, **107**, 4949–4954.
2. Caldecott,K.W. (2014) Molecular biology. Ribose–an internal threat to DNA. *Science*, **343**, 260–261.
3. Cerritelli,S.M. and Crouch,R.J. (2016) The balancing act of ribonucleotides in DNA. *Trends Biochem. Sci.*, **41**, 434–445.
4. Williams,J.S., Lujan,S.A. and Kunkel,T.A. (2016) Processing ribonucleotides incorporated during eukaryotic DNA replication. *Nat. Rev. Mol. Cell Biol.*, **17**, 350–363.
5. Clausen,A.R., Lujan,S.A., Burkholder,A.B., Orebaugh,C.D., Williams,J.S., Clausen,M.F., Malc,E.P., Mieczkowski,P.A., Fargo,D.C., Smith,D.J. *et al.* (2015) Tracking replication enzymology in vivo by genome-wide mapping of ribonucleotide incorporation. *Nat. Struct. Mol. Biol.*, **22**, 185–191.
6. Ding,J., Taylor,M.S., Jackson,A.P. and Reijns,M.A. (2015) Genome-wide mapping of embedded ribonucleotides and other noncanonical nucleotides using emRiboSeq and EndoSeq. *Nat. Protoc.*, **10**, 1433–1444.
7. Keszthelyi,A., Daigaku,Y., Ptasinska,K., Miyabe,I. and Carr,A.M. (2015) Mapping ribonucleotides in genomic DNA and exploring replication dynamics by polymerase usage sequencing (Pu-seq). *Nat. Protoc.*, **10**, 1786–1801.
8. Bergoglio,V., Ferrari,E., Hubscher,U., Cazaux,C. and Hoffmann,J.S. (2003) DNA polymerase beta can incorporate ribonucleotides during DNA synthesis of undamaged and CPD-damaged DNA. *J. Mol. Biol.*, **331**, 1017–1023.
9. Nick McElhinny,S.A. and Ramsden,D.A. (2003) Polymerase mu is a DNA-directed DNA/RNA polymerase. *Mol. Cell. Biol.*, **23**, 2309–2315.
10. Ruiz,J.F., Juarez,R., Garcia-Diaz,M., Terrados,G., Picher,A.J., Gonzalez-Barrera,S., Fernandez de Henestrosa,A.R. and Blanco,L. (2003) Lack of sugar discrimination by human Pol mu requires a single glycine residue. *Nucleic Acids Res.*, **31**, 4441–4449.
11. Cavanaugh,N.A., Beard,W.A. and Wilson,S.H. (2010) DNA polymerase beta ribonucleotide discrimination: insertion, misinsertion, extension, and coding. *J. Biol. Chem.*, **285**, 24457–24465.
12. Gosavi,R.A., Moon,A.F., Kunkel,T.A., Pedersen,L.C. and Bebenek,K. (2012) The catalytic cycle for ribonucleotide incorporation by human DNA Pol lambda. *Nucleic Acids Res.*, **40**, 7518–7527.
13. Martin,M.J., Garcia-Ortiz,M.V., Esteban,V. and Blanco,L. (2013) Ribonucleotides and manganese ions improve non-homologous end joining by human Polmu. *Nucleic Acids Res.*, **41**, 2428–2436.
14. Donigan,K.A., McLenigan,M.P., Yang,W., Goodman,M.F. and Woodgate,R. (2014) The steric gate of DNA polymerase iota regulates ribonucleotide incorporation and deoxyribonucleotide fidelity. *J. Biol. Chem.*, **289**, 9136–9145.
15. Makarova,A.V., Nick McElhinny,S.A., Watts,B.E., Kunkel,T.A. and Burgers,P.M. (2014) Ribonucleotide incorporation by yeast DNA polymerase zeta. *DNA Rep.*, **18**, 63–67.
16. Crespan,E., Furrer,A., Rosinger,M., Bertoletti,F., Mentegari,E., Chiapparini,G., Imhof,R., Ziegler,N., Sturla,S.J., Hubscher,U. *et al.* (2016) Impact of ribonucleotide incorporation by DNA polymerases beta and lambda on oxidative base excision repair. *Nat. Commun.*, **7**, 10805.
17. Su,Y., Egli,M. and Guengerich,F.P. (2016) Mechanism of ribonucleotide incorporation by human DNA polymerase eta. *J. Biol. Chem.*, **291**, 3747–3756.
18. Cilli,P., Minoprio,A., Bossa,C., Bignami,M. and Mazzei,F. (2015) Formation and Repair of Mismatches Containing Ribonucleotides and Oxidized Bases at Repeated DNA Sequences. *J. Biol. Chem.*, **290**, 26259–26269.
19. Hubscher,U., Maga,G. and Spadari,S. (2002) Eukaryotic DNA polymerases. *Annu. Rev. Biochem.*, **71**, 133–163.
20. Hubscher,U. and Maga,G. (2011) DNA replication and repair bypass machines. *Curr. Opin. Chem. Biol.*, **15**, 627–635.
21. Donigan,K.A., Cerritelli,S.M., McDonald,J.P., Vaisman,A., Crouch,R.J. and Woodgate,R. (2015) Unlocking the steric gate of DNA polymerase eta leads to increased genomic instability in Saccharomyces cerevisiae. *DNA Rep.*, **35**, 1–12.
22. Prakash,S., Johnson,R.E. and Prakash,L. (2005) Eukaryotic translesion synthesis DNA polymerases: specificity of structure and function. *Annu. Rev. Biochem.*, **74**, 317–353.
23. Yang,W. (2014) An overview of Y-Family DNA polymerases and a case study of human DNA polymerase eta. *Biochemistry*, **53**, 2793–2803.
24. Rydberg,B. and Game,J. (2002) Excision of misincorporated ribonucleotides in DNA by RNase H (type 2) and FEN-1 in cell-free extracts. *Proc. Natl. Acad. Sci. U.S.A.*, **99**, 16654–16659.
25. Sparks,J.L., Chon,H., Cerritelli,S.M., Kunkel,T.A., Johansson,E., Crouch,R.J. and Burgers,P.M. (2012) RNase H2-initiated ribonucleotide excision repair. *Mol. Cell*, **47**, 980–986.
26. Vaisman,A. and Woodgate,R. (2015) Redundancy in ribonucleotide excision repair: Competition, compensation, and cooperation. *DNA Rep.*, **29**, 74–82.
27. Sastre-Moreno,G., Sanchez,A., Esteban,V. and Blanco,L. (2014) ATP insertion opposite 8-oxo-deoxyguanosine by Pol4 mediates error-free tolerance in Schizosaccharomyces pombe. *Nucleic Acids Res.*, **42**, 9821–9837.
28. Maga,G., Crespan,E., Markkanen,E., Imhof,R., Furrer,A., Villani,G., Hubscher,U. and van Loon,B. (2013) DNA polymerase delta-interacting protein 2 is a processivity factor for DNA polymerase lambda during 8-oxo-7,8-dihydroguanine bypass. *Proc. Natl. Acad. Sci. U.S.A.*, **110**, 18850–18855.
29. Nilforoushan,A., Furrer,A., Wyss,L.A., van Loon,B. and Sturla,S.J. (2015) Nucleotides with altered hydrogen bonding capacities impede human DNA polymerase eta by reducing synthesis in the presence of the major cisplatin DNA adduct. *J. Am. Chem. Soc.*, **137**, 4728–4734.
30. Frank,E.G., McDonald,J.P., Karata,K., Huston,D. and Woodgate,R. (2012) A strategy for the expression of recombinant proteins traditionally hard to purify. *Anal. Biochem.*, **429**, 132–139.
31. Chon,H., Vassilev,A., DePamphilis,M.L., Zhao,Y., Zhang,J., Burgers,P.M., Crouch,R.J. and Cerritelli,S.M. (2009) Contributions of the two accessory subunits, RNASEH2B and RNASEH2C, to the activity and properties of the human RNase H2 complex. *Nucleic Acids Res.*, **37**, 96–110.
32. Kannouche,P., Broughton,B.C., Volker,M., Hanaoka,F., Mullenders,L.H. and Lehmann,A.R. (2001) Domain structure, localization, and function of DNA polymerase eta, defective in xeroderma pigmentosum variant cells. *Genes Dev.*, **15**, 158–172.
33. Bienko,M., Green,C.M., Sabbioneda,S., Crosetto,N., Matic,I., Hibbert,R.G., Begovic,T., Niimi,A., Mann,M., Lehmann,A.R. *et al.* (2010) Regulation of translesion synthesis DNA polymerase eta by monoubiquitination. *Mol Cell*, **37**, 396–407.
34. Furrer,A. and van Loon,B. (2014) Handling the 3-methylcytosine lesion by six human DNA polymerases members of the B-, X- and Y-families. *Nucleic Acids Res.*, **42**, 553–566.
35. Washington,M.T., Prakash,L. and Prakash,S. (2001) Yeast DNA polymerase eta utilizes an induced-fit mechanism of nucleotide incorporation. *Cell*, **107**, 917–927.
36. Vaisman,A., Masutani,C., Hanaoka,F. and Chaney,S.G. (2000) Efficient translesion replication past oxaliplatin and cisplatin GpG adducts by human DNA polymerase eta. *Biochemistry*, **39**, 4575–4580.
37. Eder,P.S., Walder,R.Y. and Walder,J.A. (1993) Substrate specificity of human RNase H1 and its role in excision repair of ribose residues misincorporated in DNA. *Biochimie*, **75**, 123–126.
38. Lazzaro,F., Novarina,D., Amara,F., Watt,D.L., Stone,J.E., Costanzo,V., Burgers,P.M., Kunkel,T.A., Plevani,P. and

Muzi-Falconi,M. (2012) RNase H and postreplication repair protect cells from ribonucleotides incorporated in DNA. *Mol. Cell*, **45**, 99–110.
39. Clausen,A.R., Zhang,S., Burgers,P.M., Lee,M.Y. and Kunkel,T.A. (2013) Ribonucleotide incorporation, proofreading and bypass by human DNA polymerase delta. *DNA Rep.*, **12**, 121–127.
40. Clausen,A.R., Murray,M.S., Passer,A.R., Pedersen,L.C. and Kunkel,T.A. (2013) Structure-function analysis of ribonucleotide bypass by B family DNA replicases. *Proc. Natl. Acad. Sci. U.S.A.*, **110**, 16802–16807.
41. Kohda,K., Tsunomoto,H., Minoura,Y., Tanabe,K. and Shibutani,S. (1996) Synthesis, miscoding specificity, and thermodynamic stability of oligodeoxynucleotide containing 8-methyl-2'-deoxyguanosine. *Chem. Res. Toxicol.*, **9**, 1278–1284.
42. Gasparutto,D., Dherin,C., Boiteux,S. and Cadet,J. (2002) Excision of 8-methylguanine site-specifically incorporated into oligonucleotide substrates by the AlkA protein of Escherichia coli. *DNA Rep.*, **1**, 437–447.
43. Albertella,M.R., Green,C.M., Lehmann,A.R. and O'Connor,M.J. (2005) A role for polymerase eta in the cellular tolerance to cisplatin-induced damage. *Cancer Res.*, **65**, 9799–9806.
44. Chen,Y.W., Cleaver,J.E., Hanaoka,F., Chang,C.F. and Chou,K.M. (2006) A novel role of DNA polymerase eta in modulating cellular sensitivity to chemotherapeutic agents. *Mol. Cancer Res.*, **4**, 257–265.
45. Srivastava,A.K., Han,C., Zhao,R., Cui,T., Dai,Y., Mao,C., Zhao,W., Zhang,X., Yu,J. and Wang,Q.E. (2015) Enhanced expression of DNA polymerase eta contributes to cisplatin resistance of ovarian cancer stem cells. *Proc. Natl. Acad. Sci. U.S.A.*, **112**, 4411–4416.
46. Alt,A., Lammens,K., Chiocchini,C., Lammens,A., Pieck,J.C., Kuch,D., Hopfner,K.P. and Carell,T. (2007) Bypass of DNA lesions generated during anticancer treatment with cisplatin by DNA polymerase eta. *Science*, **318**, 967–970.
47. Ummat,A., Rechkoblit,O., Jain,R., Roy Choudhury,J., Johnson,R.E., Silverstein,T.D., Buku,A., Lone,S., Prakash,L., Prakash,S. *et al.* (2012) Structural basis for cisplatin DNA damage tolerance by human polymerase eta during cancer chemotherapy. *Nat. Struct. Mol. Biol.*, **19**, 628–632.
48. Zhao,Y., Biertumpfel,C., Gregory,M.T., Hua,Y.J., Hanaoka,F. and Yang,W. (2012) Structural basis of human DNA polymerase eta-mediated chemoresistance to cisplatin. *Proc. Natl. Acad. Sci. U.S.A.*, **109**, 7269–7274.
49. Cerritelli,S.M. and Crouch,R.J. (2009) Ribonuclease H: the enzymes in eukaryotes. *FEBS J.*, **276**, 1494–1505.
50. Reijns,M.A., Bubeck,D., Gibson,L.C., Graham,S.C., Baillie,G.S., Jones,E.Y. and Jackson,A.P. (2011) The structure of the human RNase H2 complex defines key interaction interfaces relevant to enzyme function and human disease. *J. Biol. Chem.*, **286**, 10530–10539.
51. Bubeck,D., Reijns,M.A., Graham,S.C., Astell,K.R., Jones,E.Y. and Jackson,A.P. (2011) PCNA directs type 2 RNase H activity on DNA replication and repair substrates. *Nucleic Acids Res.*, **39**, 3652–3666.
52. Hiller,B., Achleitner,M., Glage,S., Naumann,R., Behrendt,R. and Roers,A. (2012) Mammalian RNase H2 removes ribonucleotides from DNA to maintain genome integrity. *J. Exp. Med.*, **209**, 1419–1426.
53. Reijns,M.A., Rabe,B., Rigby,R.E., Mill,P., Astell,K.R., Lettice,L.A., Boyle,S., Leitch,A., Keighren,M., Kilanowski,F. *et al.* (2012) Enzymatic removal of ribonucleotides from DNA is essential for mammalian genome integrity and development. *Cell*, **149**, 1008–1022.
54. Crow,Y.J., Leitch,A., Hayward,B.E., Garner,A., Parmar,R., Griffith,E., Ali,M., Semple,C., Aicardi,J., Babul-Hirji,R. *et al.* (2006) Mutations in genes encoding ribonuclease H2 subunits cause Aicardi-Goutieres syndrome and mimic congenital viral brain infection. *Nat. Genet.*, **38**, 910–916.
55. Gunther,C., Kind,B., Reijns,M.A., Berndt,N., Martinez-Bueno,M., Wolf,C., Tungler,V., Chara,O., Lee,Y.A., Hubner,N. *et al.* (2015) Defective removal of ribonucleotides from DNA promotes systemic autoimmunity. *J. Clin. Invest.*, **125**, 413–424.
56. Pizzi,S., Sertic,S., Orcesi,S., Cereda,C., Bianchi,M., Jackson,A.P., Lazzaro,F., Plevani,P. and Muzi-Falconi,M. (2015) Reduction of hRNase H2 activity in Aicardi-Goutieres syndrome cells leads to replication stress and genome instability. *Hum. Mol. Gen.*, **24**, 649–658.
57. Shaban,N.M., Harvey,S., Perrino,F.W. and Hollis,T. (2010) The structure of the mammalian RNase H2 complex provides insight into RNA.NA hybrid processing to prevent immune dysfunction. *J. Biol. Chem.*, **285**, 3617–3624.
58. Figiel,M., Chon,H., Cerritelli,S.M., Cybulska,M., Crouch,R.J. and Nowotny,M. (2011) The structural and biochemical characterization of human RNase H2 complex reveals the molecular basis for substrate recognition and Aicardi-Goutieres syndrome defects. *J. Biol. Chem.*, **286**, 10540–10550.
59. Rychlik,M.P., Chon,H., Cerritelli,S.M., Klimek,P., Crouch,R.J. and Nowotny,M. (2010) Crystal structures of RNase H2 in complex with nucleic acid reveal the mechanism of RNA-DNA junction recognition and cleavage. *Mol. Cell*, **40**, 658–670.
60. Kannouche,P.L., Wing,J. and Lehmann,A.R. (2004) Interaction of human DNA polymerase eta with monoubiquitinated PCNA: a possible mechanism for the polymerase switch in response to DNA damage. *Mol. Cell*, **14**, 491–500.
61. Guilliam,T.A., Bailey,L.J., Brissett,N.C. and Doherty,A.J. (2016) PolDIP2 interacts with human PrimPol and enhances its DNA polymerase activities. *Nucleic Acids Res.*, **44**, 3317–3329.
62. Tissier,A., Janel-Bintz,R., Coulon,S., Klaile,E., Kannouche,P., Fuchs,R. P. and Cordonnier,A. M. (2010) Crosstalk between replicative and translesional DNA polymerases: PDIP38 interacts directly with Pol eta *DNA Repair (Amst)* **9**, 922–928.
63. Traut,T.W. (1994) Physiological concentrations of purines and pyrimidines. *Mol. Cell. Biochem.*, **140**, 1–22.
64. Ferraro,P., Franzolin,E., Pontarin,G., Reichard,P. and Bianchi,V. (2010) Quantitation of cellular deoxynucleoside triphosphates. *Nucleic Acids Res*, **38**, e85.

genes

MDPI

Review

DNA Polymerases λ and β: The Double-Edged Swords of DNA Repair

Elisa Mentegari, Miroslava Kissova, Laura Bavagnoli, Giovanni Maga * and Emmanuele Crespan *

Institute of Molecular Genetics, IGM-CNR, via Abbiategrasso 207, 27100 Pavia, Italy; elisa.mentegari01@universitadipavia.it (E.M.); miroslava.kissova01@universitadipavia.it (M.K.); bavagnoli@igm.cnr.it (L.B.)

* Correspondence: maga@igm.cnr.it (G.M.); emmanuelecrespan@gmail.com (E.C.); Tel.: +39-0382-546354 (G.M.); +39-0382-546346 (E.C.)

Academic Editor: Richard T. Pomerantz
Received: 1 June 2016; Accepted: 24 August 2016; Published: 31 August 2016

Abstract: DNA is constantly exposed to both endogenous and exogenous damages. More than 10,000 DNA modifications are induced every day in each cell's genome. Maintenance of the integrity of the genome is accomplished by several DNA repair systems. The core enzymes for these pathways are the DNA polymerases. Out of 17 DNA polymerases present in a mammalian cell, at least 13 are specifically devoted to DNA repair and are often acting in different pathways. DNA polymerases β and λ are involved in base excision repair of modified DNA bases and translesion synthesis past DNA lesions. Polymerase λ also participates in non-homologous end joining of DNA double-strand breaks. However, recent data have revealed that, depending on their relative levels, the cell cycle phase, the ratio between deoxy- and ribo-nucleotide pools and the interaction with particular auxiliary proteins, the repair reactions carried out by these enzymes can be an important source of genetic instability, owing to repair mistakes. This review summarizes the most recent results on the ambivalent properties of these enzymes in limiting or promoting genetic instability in mammalian cells, as well as their potential use as targets for anticancer chemotherapy.

Keywords: DNA polymerases; DNA repair; translesion synthesis; cancer chemotherapy; mutagenesis

1. Introduction

DNA polymerases (Pols) β and λ belong to the Pol family X. In mammalian cells, the X family comprises four members: Pol β, λ, μ and terminal deoxynucleotidyl transferase (TdT). All of the members possess a highly homologous C-terminal catalytic or β-like domain. In addition, Pol λ, μ and TdT contain an extended N-terminus, with additional domains. While the functions of Pol μ and TdT seem to be restricted to specialized forms of DNA double-strand break repair, such as non-homologous end joining (NHEJ) and V(D)J recombination, Pol β and λ play more diversified roles, participating in different DNA repair pathways. Because of their partially overlapping roles, Pol β and λ are regulated along the cell cycle, through mainly post-translational modifications [1–4]. In addition, their function is also under the control of cell cycle checkpoints [5,6]. Since these Pols are involved in the tolerance of various kinds of DNA damages, including those caused by anticancer chemo- or radio-therapy, and their overexpression may lead to genetic instability, they are being regarded as attractive targets for cancer chemotherapy. Below, we will provide a summary of the roles of Pol β and λ in the various repair pathways, their regulation and the state of the art in the development of specific inhibitors for these enzymes.

2. Pol β and λ in the Base Excision Repair Pathway

Pol β and λ use their polymerase and 5′-deoxyribose 5′-phosphate (dRP)-lyase activities during single-nucleotide base excision repair (BER) [7].

The BER pathway contributes to the maintenance of genome integrity, since it repairs DNA lesions caused by alkylation, oxidation, depurination/depyrimidination and deamination [8] that, if not removed, could cause mutations by mispairing or lead to strand breaks during replication. Enzymes acting during BER excise the damaged nucleotide and replace it with the correct one [9].

In eukaryotes, the pathway is divided into short-patch (SP) BER, devoted to the replacement of single damaged nucleotides, and long-patch (LP) BER to repair two or more damaged nucleotides. Pol β is the solely Pol involved in SP BER, while in LP BER, it is involved in the incorporation of the first nucleotide, whereas the elongation step is carried out by replicative Pols [10]. Both pathways start with the damaged base being recognized; then, a DNA glycosylase hydrolizes the N-glycosidic bond removing the base from the sugar-phosphate backbone. At this point, the AP (abasic or apurinic/apyrimidinic) site generated in this way is further processed by apurinic/apyrimidinic endonuclease 1 (APE1), the main 5′ AP endonuclease in human cells, which cleaves the phosphodiester bond 5′ to the AP site, generating a 5′dRP and a 3′-OH. The 5′dRP is removed by Pol β, as it possesses intrinsic dRP-lyase activity, leaving a phosphate at the 5′-end. Subsequently, Pol β can fill the gap, and finally, ligase III in complex with its accessory protein XRCC1 ligates the nicked DNA in the SP BER [10,11]. Experiments performed on mouse cells demonstrated that ligase III, which possesses nuclear and mitochondrial forms, is fundamental for the maintenance of the mitochondrial DNA (mtDNA) integrity, while it is not required in nuclear BER [12,13]. In LP BER, the final ligation step is instead performed by ligase I [11]. Like Pol β, also Pol λ is involved in BER: while Pol β is the main enzyme for BER, Pol λ involvement in BER is supported by the observation that it can substitute Pol β in BER reactions in vitro [8]. Indeed, it has been shown that Pol λ is the preferred Pol involved in the specialized BER, which removes 7,8-dihydro-8-oxoguanine (8-oxo-G):A mispairs, initiated by the glycosylase MUTYH [14] (see also below).

3. Pol β and λ in the Translesion Synthesis Pathway

DNA integrity is fundamental for the inheritance of complete and correct genetic information. Cells are exposed not only to exogenous attacks, such as ionizing radiation, ultraviolet light and chemical agents, but they also have to cope with endogenous mechanisms generating reactive metabolites that are threatening for DNA. Despite multiple repair pathways evolved in order to correct damages occurring in DNA, other mechanisms are necessary to tolerate DNA lesions without actually repairing them. DNA damage tolerance processes are important in promoting cell survival and, in some cases, contribute to the generation of mutations [15]. During the S phase, when the replication machinery encounters a lesion along DNA, replicative Pols are unable to bypass it and to incorporate the right nucleotide opposite the damaged site, leading to fork stalling. In such a situation, the translesion synthesis (TLS) mechanism is activated.

TLS is one of the major damage tolerance systems in which specialized polymerases, known as TLS Pols, substitute for replicative Pols in copying across DNA lesions during replication [8]. TLS Pols are able to use damaged DNA bases as a template and to insert nucleotides opposite them.

Two non-mutually exclusive models for lesion bypass by TLS Pols have been proposed: the polymerase-switching model and the gap-filling model. At the replication fork, where replicative Pols are acting, a switch occurs in the presence of DNA damage through protein-protein interactions, so that replicative Pols are substituted by TLS Pols. After lesion bypass with relative accuracy, an additional switch takes place, and the replicative Pol is restored in order to continue accurate DNA synthesis [15]. It has also been proposed that TLS takes place outside replication forks, in a gap-filling model. In this scenario the replication machinery leaves a single-strand DNA (ssDNA) gap opposite a DNA lesion because of suppressing events that occur downstream of the damage, leaving to TLS Pols the role of filling the gap [15].

TLS Pols are present in all three domains of life, and they mainly belong to the Y family of DNA Pols; however, also Pol β and λ play a role in specialized forms of TLS, even if it is not their primary task [16].

3.1. Bypass of the 7,8-Dihydro-8-Oxoguanine (8-oxo-G) Lesion

Oxidative lesions are one of the most frequently-observed base modifications; they derive from the action of reactive oxygen species (ROS) [17]. Hydroxyl radicals, in particular, can generate adducts at diverse positions of purines, since they add to the double bonds of DNA bases. The C_8-OH adducts of guanine, such as 7-hydro-8-hydroxyguanine and 7,8-dihydro-8-oxoguanine (8-oxo-G), and the C_2-OH adduct of adenine are the most studied oxidative lesions [17]. 8-oxo-G is a particularly relevant lesion because it is widely present in DNA (10^3 to 10^4 per cell per day) [18] and because of its well-established mutagenic potential in bacterial and mammalian cells. It is a miscoding lesion that can generate G:C to T:A transversions; it accumulates with age, mainly in the mitochondrial genome, and it is involved in different types of tumors and neurodegenerative diseases (e.g., Parkinson and Alzheimer diseases) [17].

8-oxo-G can be bypassed by replicative Pol α, δ and ξ in an error-prone manner since, in many cases, instead of inserting the correct cytosine (C) opposite to the damage, they incorporate an adenine (A) [16]. In order to face this threatening damage, prokaryotic and eukaryotic cells evolved two different BER systems: an 8-oxo-G DNA glycosylase 1 (OGG1)-dependent pathway and a MUTHY-dependent pathway [18]. In all tissues, the OGG1 initiates the short patch BER recognizing the damaged G when paired with a C, catalyzing the removal of 8-oxo-G. The AP site generated in this way is a substrate of APE1, then DNA Pol β fills the gap, and DNA ligase III/XRCC1 complex performs the ligation step [16,17]. In replicating tissues, when the replication machinery encounters the 8-oxo-G, it often incorporates an A instead of a C; the glycosylase MUTYH has the ability to recognize the mispair, but excides the A. At this point, APE1 incises the DNA, then DNA Pol λ with the help of Proliferating cell nuclear antigen (PCNA) and replication protein A (RP-A) incorporates the correct C opposite the 8-oxo-G left on the template strand within the gap [14]. The newly-formed C:8-oxo-G pair can subsequently become the substrate of the OGG1-dependent short patch BER [16].

Since both Pol λ and β have a role in BER, there should be a mechanism allowing the selection of one or the other to repair the 8-oxo-G lesion. Experiments suggested that PCNA and RP-A have a role in this discriminatory mechanism, recruiting Pol λ instead of Pol β towards the 8-oxo-G lesion facing a window gap. Pol λ is the most efficient in the MUTYH-initiated pathway, ensuring error-free TLS with correct Deoxycytidine triphosphate (dCTP) incorporation opposite 8-oxo-G; its fidelity is increased by the association with PCNA and RP-A, ensuring a 750-fold preference for dCTP incorporation opposite to 8-oxoG on 1-nt gap with respect to Deoxyadenosine triphosphate (dATP) incorporation. The other main polymerase involved in BER, Pol β can substitute for Pol λ, but at the expense of a reduced fidelity, leading to frequent misincorporation of dATP opposite 8-oxo-G (in 20% to 30% of cases). In fact, Pol β is 145-fold less efficient than Pol λ in bypassing 8-oxo-G damage on 1-nt gaps inserting the correct dCTP [18].

3.2. Bypass of Abasic Sites and the 2-Deoxyribonolactone Lesion

Reactive oxygen species (ROS) have also the ability to cause the accumulation of oxidized AP sites [19]. Among the oxidized AP sites produced by oxidative stress, the C1′-oxidized abasic site 2-deoxyribonolactone (L) is a frequently-encountered lesion, representing about 10% of total 2-deoxyribose oxidation [20]. L can be caused also by long wave UV irradiation, organometallic oxidants and by antitumor drugs, such as neocarzinostatin and the enediyne antibiotic C-1027 [21]. The presence of L in the DNA strand, on the other hand, can be particularly dangerous during the S phase, since it can lead to the arrest of the replication fork.

AP sites are usually handled by the BER pathway, where an AP endonuclease, mainly APE1 in mammalian cells, incises AP sites, thus generating ssDNA breaks with 3′-OH and 5′-deoxyribose-

5′-phosphate (5′-dRp) termini. Pol β, through its 5′-dRp-lyase activity residing in its 8-kDa domain, can remove the 5′-dRp residue [22,23]. Pol λ possesses a homologous 8-kDa domain, which also allows elimination of 5′-dRp [24]. Both Pol λ and β can bypass non-oxidized AP sites, but with diverse mechanisms. In most cases, Pol λ skips the lesion and gives rise to a -1 frameshift deletion, while Pol β generally incorporates a dATP opposite the AP site [21,25]. Moreover, Pol λ is more efficient than Pol β in performing TLS when an AP site is present, especially when the concentration of nucleotides is low [25].

On the contrary, when L lesion or chemically-reduced AP sites are present, Pol β cannot excise the modified sugar. Therefore, LP BER is activated in order to process such lesions. However, during unsuccessful attempts to repair L through SP BER, when Pol β attacks the 5′-dRp residue through the active site of its N-terminal lysine 72 (K72), it becomes covalently trapped on DNA via the formation of an amide bond with K72, resulting in the formation of DNA-protein cross-links (DPC) [22–24,26,27].

In in vitro experiments, performed using either Mn^{2+} or Mg^{2+} as the cofactor, Pol β exhibited the ability of bypassing L, and, its capacity of performing TLS over such a lesion, was enhanced in the presence of the auxiliary protein PCNA. Pol β mainly incorporates dATP opposite L and, to a minor extent, dCTP. Thus, L bypass, similarly to the case of the normal AP site, is most of the times mutagenic. On the other hand, similar experiments revealed that Pol λ is unable to bypass L damage, even when nucleotide concentrations were high [21].

3.3. Pol δ-Interacting Protein 2 as an Auxiliary Factor for Pol λ during TLS

In the presence of a DNA lesion, a switch between replicative Pols and TLS Pols allows lesion bypass can occur. DNA Pol δ-interacting protein 2 (PolDIP2), also known as Pol δ interacting protein 38 (PDIP38), is a protein of 368 aa that makes contact with the p50 subunit of Pol δ and with PCNA [28], the processivity clamp whose ubiquitination seems to favor the access of TLS Pols to the lesioned DNA site [29]. In effect, in the presence of PolDIP2, Pol δ increases its affinity for PCNA by about two-fold [30].

PolDIP2 also physically interacts with TLS Pol η, ζ and Rev1, even if the physiological meaning of this event is still required to be fully elucidated. Indeed, PolDIP2 can associate to the ubiquitin-binding zinc finger domain of Pol η, the domain that mediates the interaction of Pol η with ubiquitinated PCNA. An intriguing possibility is that PolDIP2 might have a role in the TLS pathway, contributing to the switch between Pol η and TLS Pols [30].

While PolDIP2 does not seem to stimulate either Pol β or Pol ι, it has been found to physically interact with Pol λ, the main actor in bypassing faithfully the 8-oxo-G lesion by inserting in most cases the right cytidine. Pol λ forms a complex with PolDIP2 through its catalytic domain. Experiments demonstrated that PolDIP2 association with Pol λ, as well as to Pol η, positively regulates their ability to perform correct 8-oxo-G bypass. PolDIP2 enhances both the processivity and catalytic activity of Pol λ and η, thus favoring a speeding up of the bypass process, not only of 8-oxo-G damage, but of other DNA lesions, as well, such as abasic sites and cyclobutane thymine dimers. In particular, PolDIP2 favors the switch from Pol δ to Pol λ in TLS of the 8-oxo-G lesion [30].

Moreover, silencing of PolDIP2 in mouse embryonic fibroblasts (MEFs) results in increased sensitivity of cells to oxidative agents, an effect very similar to the one displayed by Pol λ-null cells. When PolDIP2 was silenced in Pol $\lambda^{-/-}$ fibroblasts, the sensitivity further increases, thus suggesting that cells need both Pol λ and PolDIP2 for effective DNA damage response. [30]. Interestingly, PolDIP2 has been also shown to activate the intracellular oxidase NADPH oxidase 4 (Nox4), thus increasing endogenous ROS levels. Since this protein shuttles from the cytoplasm to the nucleus in response to proliferative stimuli, it is intriguing to speculate that during replication, when the risk of incurring mutations due to oxidized bases is higher, PolDIP2 stops stimulating Nox4 and aids TLS Pols in bypassing oxidative DNA damages caused by endogenous ROS.

4. Pol β and λ and the Incorporation of Ribonucleotides in the Genome

The selectivity of the incorporation of dNTPs is from 10-fold to 10^6-fold greater with respect to ribonucleotide monophosphates (rNMPs) incorporation, depending on the identity of the polymerase, on the base examined and on rNMP:Deoxynucleoside Monophosphate (dNMP) ratio [31]. However, in spite of their specificity, replicative Pols discriminate dNMPs imperfectly, and so, they can frequently incorporate rNMPs during DNA replication since in mammalian cells, as well as in yeast cells, rNMPs' concentration is 10- to 100-fold higher than dNMPs' concentration. [32,33].

Lacking the reactive hydroxyl group in position 2′ of the ribose ring, DNA is more stable and resistant to cleavage than RNA [31]. Therefore, for the cell, it is important to remove rNMPs in order to preserve the integrity of the genome. Indeed, most DNA Pols evolved to avoid incorporation of rNMPs during DNA synthesis, as they could lead to spontaneous strand breaks and stalling of Pols at the replication fork [32]. Most misincorporated rNTPs are removed through the RNaseH2-initiated ribonucleotide excision repair (RER) pathway [34].

Besides replication, rNMPs can be inserted in the genome by Pols also during reparative pathways. Until now, 17 Pols, including cytidyl-transferase Rev1 and telomerase, are known to be present in human cells, many of which participate in DNA repair pathways [16].

Reparative Pols are low-fidelity Pols that do not possess 3′ to 5′ exonuclease activity, so they cannot proofread rNMPs erroneously inserted as replicative Pols do. For high-fidelity Pols, the range of sugar selectivity is from 500 to 4,400,000, while for reparative low-fidelity Pols, the values range is between 1.3 and 50,000. This difference is probably ascribed to the overall flexibility and arrangement of their active sites [35].

Several studies have shown that family X Pols can incorporate rNMPs during the synthesis of undamaged DNA, but with varying sugar selectivity. Pol μ displays the lowest discrimination capability, in the range of 1- to 10-fold preference for dNMPs over rNMPs incorporation, thus possessing both DNA and RNA polymerase activities [36]. Pol μ can incorporate rNMPs and dNMPs with similar efficiency, because it possesses a glycine residue at the predicted "steric gate" position [37] where, instead, Pol β and λ have Tyr or Phe residues, thus achieving a higher sugar selection [35]. It has been shown that Pol λ has a sugar selectivity of 5100 to 7500 and Pol β of 1690 to 3200 for incorporation of rCMP opposite a guanine, depending on the structure of the template [38], in agreement with similar results [35,39]. These findings suggest that Pol β and λ can incorporate rNMPs opposite undamaged DNA bases [38]. Moreover, examining the impact of rNMPs' incorporation opposite the 8-oxo-G lesion, Pol λ displayed the ability to bypass such a lesion on a 1-nt gap template incorporating the correct dCMP in the majority of cases. Pol β, on the other hand, having a lower selectivity for rNMPs, can bypass the lesion also inserting rCMP (wrong sugar/right base), but at least excluding in most cases rAMP (wrong sugar/wrong base) [38]. Incorporation of rNMPs opposite an 8-oxo-G lesion has also been shown to negatively impact the subsequent action of the glycosylases OGG1 and MUTYH, thus substantially delaying BER [38,40].

Thus, Pol β can be a source of rNMPs' incorporation into genomic DNA, both during BER (that is opposite normal DNA bases) and during the bypass of 8-oxo-G. Pol β is the major Pol expressed in post-mitotic neurons, which are cells with dNTP levels markedly lower than rNTP levels, with a poor expression of RNaseH2 and that undergo severe oxidative stress. Therefore, post-mitotic neurons ability to use rNMPs may have physiological relevance in enhancing the deleterious effects of DNA oxidation in the brain [38].

5. Pol β and λ in Specialized Forms of DNA Double Stand Break Repair

Double-strand breaks (DSBs) represent the most dangerous damages occurring in DNA since they can lead to cell death if left unrepaired or cause chromosomal rearrangements if misrepaired. DSBs can result from endogenous sources, such as ROS, which can alter in different ways DNA bases, or they can arise from programmed processes, including V(D)J recombination and class switch recombination (CSR). Moreover, also, exogenous sources, like IR and ultraviolet (UV) light, can induce DNA DSBs [41].

Cells have evolved two main general mechanisms to face these genotoxic lesions, homologous recombination (HR) and non-homologous and joining (NHEJ) [41]. HR acts exclusively during the S phase, while NHEJ, the main DSB repair pathway in higher organisms, acts throughout the cell cycle [8]. The "classical" NHEJ starts with binding of the Ku70/80 heterodimer to the ends of the broken double-stranded DNA molecule, a step that allows successive binding of NHEJ factors. Pol μ and λ participate in the NHEJ pathway. They can bind to Ku:DNA complexes through their N-terminal breast cancer carboxy-terminal (BRCT) domains [42], providing their gap-filling activity before the final ligation step, which is performed by the XRCC4-ligase IV complex. Pol λ tends to fill gaps with ends that have partially complementary overhangs, while Pol μ can synthesize DNA without the presence of complementarity between the primer and template strand [43].

Besides classical NHEJ, an alternative Ku-independent and ligase IV-independent NHEJ pathway exists. It has been proposed that this alternative end-joining (A-EJ) pathway proceeds through microhomology-mediated end joining (MMEJ) [41–43]. It seems that in MMEJ, terminal microhomology (MH) can substitute for the presence of Ku protein [42]. This mechanism relies on MH regions (five to 25 nucleotides) that anneal to form a synaptic complex causing the formation of gaps on both DNA strands. These gaps are subsequently filled by Pols and finally ligated by DNA ligase 3 (Lig3) or DNA ligase 1 (Lig1) [41–43].

Evidence supports the involvement of Pol λ in MMEJ. When DSBs occur, nucleases create 3′ssDNA overhangs with terminal MH. The idea is that Pol λ promotes the creation of stable synapsis at MH regions, with the formation of long DNA gaps on both strands. The elongation step follows, during which the 9-1-1 complex increases the processivity of Pol λ, which makes contact with the 5′-phosphate of the terminal downstream nucleotide when the gap size reaches 1 nt, thus ensuring precise gap-filling. Finally, Lig1 seals the nick [43]. This reaction is also stimulated by the flap endonuclease 1 (FEN1) [43].

In vitro experiments demonstrated that Pol β is not able to promote annealing and elongation of long ssDNA 3′ overhangs possessing a single short MH region. On the other hand, it was capable of promoting the annealing and elongation of short (five nucleotides) 3′ ssDNA overhangs, even more efficiently than pol λ, in sequences containing CAG triplet repeats. Moreover, on such substrates, Pol β leads to the expansion of CAG triplets [43]. This observation, along with the fact that Pol β is the most highly expressed Pol in post-mitotic neurons, may suggest a role of MMEJ in the CAG repeats' expansion linked to neurodegenerative diseases, such as the Huntington disease.

6. Pol β and λ Roles in Genetic Instability

Pols have an extremely important role in repairing DNA damage, protecting the cells. In fact, the damage, if not repaired, can lead to mutagenesis. However, unscheduled activation of repair Pols or alteration of their levels, can be detrimental for the cell, leading to genetic instability. For this reason, repair Pols must be tightly regulated. In recent years, further details about the regulation of Pol β and λ and their relationships with cell cycle checkpoints have emerged.

6.1. Pol λ

As summarized above, Pol λ plays a fundamental role during non-homologous end joining (NHEJ) and the bypass of DNA lesions. Some of these lesions, such as AP sites or oxidized bases, can slow down or even block replication fork progression [17,44]. As a consequence, the S phase checkpoint, relying on the ATR protein kinase pathway, is activated [6], which is responsible for cell survival in the presence of a stalled replication fork [45]. ATR activation leads to the phosphorylation and activation of the checkpoint kinase 1 (Chk1), which initiates a cascade of phosphorylation events that ultimately delays S phase progression [46] and activates the recruitment of DNA repair factors. Zucca et al. demonstrated that the downregulation of Pol λ resulted in the activation of the ATR/Chk1 pathway [5]. Cells permanently silenced for Pol λ accumulated replication stress, as evidenced by increased γH2AX histone foci, and showed phosphorylation of ATR and Chk1. Inhibition of Pol λ and Chk1 function resulted in cell lethality. One possible explanation is that, in the presence of Pol λ,

oxidized bases can be efficiently bypassed [16]. However, in its absence, the accumulation of oxidized bases causes the block of the replication fork, slowing the repair of DNA damage and accumulating SS breaks. This causes the activation of the ATR-Chk1 pathway repair leading to the delay of the S phase of the cell cycle. These results highlighted the role of Pol λ in replication fork stability [5]. DNA Pol λ stability is also regulated during cell cycle by phosphorylation. Frouin et al. demonstrated that Pol λ interacts in the late S and G2 phases with Cdk2 in vivo, and it is phosphorylated by the Cdk2/cyclin A complex in vitro at Ser167, Ser17, Ser230 and Thr553 [3]. Markkanen et al. demonstrated that phosphorylation of Pol λ promotes its placement to 8-oxo-G lesions on chromatin, while Pol λ that is not phosphorylated and, as a consequence, is not involved in DNA repair is ubiquitinated by E3 ubiquitin ligase Mule and subsequently degraded via the ubiquitin-proteasome pathway [4]. The regulation by phosphorylation/ubiquitination probably allows Pol λ to properly repair the DNA damage during the S phase of the cell cycle.

In a large study [47], Pol λ has been found overexpressed in the 24% of various human solid tumors. Moreover, a cancer-related variant of Pol λ, the R438W mutant, was described, having low fidelity, impaired NHEJ capability and inducing genomic instability. These results highlight a role of Pol λ deregulation/mutation in promoting tumorigenesis [48,49].

6.2. Pol β

Pol β is the major polymerase involved in BER, its levels are regulated mainly through ubiquitination by the E3 ubiquitin ligases Mule and CHIP. Ubiquitination leads to Pol β degradation. The Mule inhibitor protein ARF and the human ubiquitin-specific protease 47 (USP47) deubiquitinating enzyme counteract this effect during DNA damage response, ensuring the maintenance of balanced levels of Pol β [1,2]. However, Fang et al. demonstrated that the XRCC1/Pol β complex formation prevents the ubiquitination and degradation of Pol β, which is otherwise ubiquitinated on Lys206 and Lys244 and targeted for proteasome-mediated degradation. The authors proposed that Pol β stability depends on the binding to XRCC1. Such a mechanism is used for DNA repair pathway choice, depending on the requirement of Pol β for the repair of specific damage (as in BER), while XRCC1, which is stable also as a monomer, is involved also in Pol β-independent repair pathways, such as NHEJ and NER [50].

Literature data demonstrated that 30% of tumors in human express several Pol β variants [51,52], and about 48% are characterized by aminoacidic substitutions [53,54]. The most common tumor-associated variants of Pol β are listed in Table 1.

Table 1. Polymerase β variants identified and involved in cancer.

Polymerase β Variant	Human Tumor Type
K289M [55] E288K [54] S229L [56] R152C [57]	Colorectal cancer
E295K G231D L22P Y265C D160N [51] T889C [58]	Gastric cancer
I260M [59]	Prostate cancer
P242R [60]	Evidence of chromosomal aberrations in human mammary cells
K167I [61]	Esophageal cancer

As described above, the DNA substrate for Pol β is a single-nucleotide gap generated by the excision of a damaged base [11]. Ray. et al. reviewed that the variants reported can lead to genomic instability in several ways: the Pol β variant could misincorporate nucleotides in the gap, as is the case of Pol β variant K289M [55], leading to a mutagenesis process; the Pol β variant with slow or no polymerase activity (as is the case of the G231D and E295K variants, respectively [51]) does not insert any nucleotides in the gap, leading to the accumulation of double-strand breaks; the failure to remove the group from a dRP by the Pol β variant with slow lyase activity (L22P variant) [51] could also result in genomic instability [62].

Overexpression of Pol β is present in 30% of tumors, mostly solid tumors (gastric, uterine, prostate, thyroid and ovarian cancer) [47] and in chronic myeloid leukemia [63]. Bergoglio et al. demonstrated that overexpression of Pol β by only two-fold in cells is enough to promote genome instability, suggesting that Pol β regulation has a key role in vivo [64]. It has been demonstrated that overexpression of Pol β improved the mutator phenotype because of the genotoxic effects of oxidized damages [65]. Moreover, the alteration of Pol β expression in irradiated cells strengthened the genetic changes associated with a malignant phenotype [66].

Overexpression of Pol β could also cause genome instability, probably interfering with normal cellular processes. Starcevic et al. demonstrated that Pol β interacts with TRF2 protein [53], a telomeric DNA binding protein that has an important role in the maintenance of telomeres [67]. The authors supposed that overexpression of Pol β could sequestrate TRF2, causing the telomeres' ends' fusion, leading to chromosomal instability [53]. Polymerase β plays an important role in repairing DNA damage also during meiosis (Prophase I), maintaining genomic stability [56].

Trinucleotides repeat (TNR) instability is a feature of several neurological diseases, including Huntington disease (HD) and myotonic dystrophy 1 (MD1). Many studies linked the TNR expansion in somatic cells to erroneous DNA repair involving BER, nucleotide excision repair (NER) and mismatch repair (MMR). For a comprehensive review, see Goula and Merienne, 2013 [68]. Mounting evidence supports a crucial role of Pol β modulation by different BER factors in mediating somatic TNR expansion [69]. Moreover, recent findings showed that the MMR protein MutSβ physically interacts at the (CAG)n or (CTG)n hairpin with Pol β, which catalyze TNR expansion after hairpin incision [70].

7. Pols β and λ as Targets for Anticancer Chemotherapy

The concept of the DNA-repair interference as a potential adjuvant approach to overcome intrinsic or acquired tumor resistance is gaining substantial attention. Regarding the inhibition of DNA repair pathways, it is desirable to avoid harming normal cells. Therefore, preferably pathways that are alternatively activated just in cancer cells should be selectively targeted. Additionally, many proteins involved in repair pathways coordinate other pathways and functions, and their inhibition would lead to a catastrophe in cellular context. Thus, different inhibitors of key proteins in DNA repair have been developed [71,72].

Many studies have proposed a mutagenic role of deregulated specialized Pols in cancer. Research conducted by Albertella et al. [47] has offered the evidence that nearly 50% of different human tumors showed overexpression of one or more specialized Pols. The fact that Pols can help cancer cells tolerate DNA damage makes them interesting candidates for targeted therapy.

As summarized above, Pol β and λ play essential roles in DNA repair and DNA damage tolerance repair pathways. Abolishing the functions of these Pols appears then to be a powerful strategy in sensitizing tumor cells towards the conventional DNA damaging chemotherapy.

Mounting evidence confirmed that overexpression of Pol β is a frequent event occurring in tumorigenesis. Pol β plays an important role in BER, an important drug-resistant determinant, due to the ability to rapidly and efficiently repair the DNA lesions induced by several chemotherapeutic agents [73]. Importantly, different human tumors are characterized by enhanced expression of Pol β, whose downregulation correlates with increased responsiveness to chemotherapy [74]. The ability of Pol β to bypass damaged DNA is largely exploited by cancer cells in order to boost their survival [75].

This is of particular clinical interest, as Pol β expression is increased in more than 30% of different human tumors [47], mostly ovarian, breast, uterus and prostate cancer. The same group confirmed the overexpression of Pol λ in 24% of various human tumors, which is comparable to the Pol β overexpression occurrence. Like Pol β, Pol λ has been proven to play a role in BER, as well [76,77]. Moreover, Pol λ physically and functionally interacts with the key components of NHEJ, the Ku antigen and the XRCC4/DNA ligase IV complex; indeed, Pol λ is central to the double-strand break repair pathway. The involvement of Pol λ in processes to safeguard the DNA integrity and ability to bypass some DNA lesions [14] contributing to the survival of cancer cells addresses the possibility to target this polymerase in the tumoral setting. Thus, different inhibitors for Pol β and λ are under study as potential anticancer agents.

7.1. Pol β Natural Inhibitors

The first attempts to discover the inhibitors of Pol β conducted by Mizushina et al. revealed that long chain fatty acids suppressed Pol activity [78]. Since the 1990s, several inhibitors of both polymerase [79–89] and lyase activity [90–96] of Pol β have been described. Of these, several natural compounds, like glycoglycerolipids [97], triterpenoids [81] and sulfolipids [98], are endowed with potent Pol β inhibitory activity; however, they unspecifically act on Pol α, as well. Other natural products, such as oleanolic acid, edgeworin, harbinatic acid and myristinin A, display a low micromolar inhibitory activity in biochemical assays and little toxicity [82,99,100]. Prunasin, a natural glucoside extracted from *Perilla frutescens* and *Artemisia vulgaris*, was demonstrated to be a specific Pol β inhibitor [101], since it did not act on mammalian Polα and TdT, plant Pols, HIV-1 Reverse Transcriptase nor on any prokaryotic Pol.

7.2. Pol β Synthetic Small Molecule Inhibitors

The deoxynucleotide analogue NSC-124854 identified by the group of Jaiswal et al. is an effective Pol β inhibitor, active against colorectal cancer cells with an EC_{50} value of 5.3 μM [102]. The small molecule methoxamine (MX) binds to and modifies AP sites, inhibiting lesion processing by the dRP-lyase activity of DNA polymerase β [103]. MX works in synergy with therapeutic alkylating agents (e.g., temozolomide (TMZ)) in order to potentiate their anti-tumoral potency in solid tumors [104,105], and has entered the phase I clinical trial process. The majority of the TMZ-induced DNA base adducts are removed by N-methylpurine DNA glycosylase (MPG), which initiates BER, leaving AP sites. Tang et al. [106] reported that potentiation of TMZ with MX, in glioma cells, is greatly enhanced by MPG overexpression. However, Pol β overexpression abrogated TMZ potentiation by MX, suggesting that cells proficient for BER readily repair AP sites in the presence of MX, and Pol β might be used to predict the effectiveness of MX-mediated potentiation of TMZ in cancer treatment. Potent Pol β inhibitors based on the rhodanine scaffold were recently discovered by the group of Strittmatter et al. [107]. Of 30 active compounds, 14 small-molecules have displayed specificity for Pol β. Additionally, several of the discovered compounds sensitized colorectal cancer cells towards DNA-damaging agents.

Noteworthy, Pol β activation and induction, which contribute to neuronal death, have been described in Alzheimer's and Parkinson's disease [108–110]. On that account, inhibitors of Pol β may provide a neuronal-specific activity, representing a successful strategy to combat this neurodegenerative disease. In 2015, the screening of more than 20,000 natural and millions of drug-like agents has been performed, leading to the identification of the 5-methoxyflavone endowed with the ability to inhibit DNA Pol β-mediated neurodegeneration without causing toxicity to normal neurons [111].

7.3. Pol λ Natural Inhibitors

Petasiphenol, a natural compound extracted from the Japanese plant *Petasites japonicus*, was proven to selectively inhibit Pol λ activity, but resulted in being ineffective towards the structurally-related Pol β, as well as towards replicative Pols [112]. The antioxidant and anti-inflammatory compound

curcumin has been shown to inhibit Pol λ selectively and to suppress the growth of a human gastric cancer cell line [113]. Another potent natural compound that inhibits Pol λ activity belongs to the category of catechin derivatives and has been obtained from green tea *Camellia sinensis* [114]. However, this compound inhibited also Pol α and HIV-1 RT. The natural compounds from the class of tetralols, nodulisporol and nodulisporone, produced by a fungus (*Nodulisporium* sp.), were found to specifically inhibit Pol λ at the micromolar level [115]. In 2014, Mizushina et al. discovered that extracts from germinated soybean (*Glycine max* L.), composed mainly by glucosyls, specifically inhibited the activity of eukaryotic Pol λ and possessed anti-inflammatory properties [116].

7.4. Pol λ Synthetic Small Molecule Inhibitors

Specific methoxy-derivatives of resveratrol, a known antioxidant compound, were found to selectively inhibit Pol λ, but not the related Pol β and TdT [117].

In silico screening of more than 9000 compounds in order to discover molecular probes that selectively inhibit Pol λ yielded there novel classes of Pol λ inhibitors: rhodanines, carbohydrazides and the compounds with the 2,4-pentadione element [118]. Of these, rhodanines resulted in being the most potent Pol λ inhibitors. Further research on the rhodanine derivatives revealed ten compounds that proved to specifically target Pol λ [107] and synergistically potentiated the killing of colorectal cancer cells by DNA-damaging agents.

7.5. Dual Pols λ and β Natural Inhibitors

Some inhibitors identified in the past manifested dual activity on both Pol β and Pol λ. An example of such a natural inhibitor is solanapyrone A, which was discovered in 2002 by the group of Mizushina et al. [119]. Kimura et al. identified two azaphilones, kasanosins A and B, as specific Pol β and Pol λ inhibitors [120]. Other classes of natural compounds that inhibit specifically mammalian X family Pols (λ, β, TdT), with the strongest inhibitory activity towards Pol β, are represented by diallyl sulfides isolated from *Allium sativum* [121]. Interestingly, these compounds did not inhibit the activities of family A, B and Y Pols, as well as other DNA-metabolic enzymes, such as HIV-1 RT, T7 RNA polymerase and T4 polynucleotide kinase.

8. Conclusions and Perspectives

One of the most intriguing observations of the last decade, has been the realization that while only four Pols (α, δ, ε and γ) are necessary and sufficient for the duplication of both nuclear and mitochondrial DNA, more than a dozen additional Pols are required in mammalian cells to ensure the maintenance of the genetic information. Biochemical, structural and genetic studies have revealed that these specialized Pols are endowed with special properties, which make them uniquely fit for a particular DNA repair event, it being either a special pathway or even a special DNA lesion. However, several of these enzymes have potentially overlapping roles, thus requiring careful regulation, in terms of expression levels, intracellular localization and timing of recruitment to a particular subcellular compartment. When such a tight regulation fails, these enzymes can be detrimental, rather than beneficial, to the cell, causing mutations and genetic instability.

This situation is well exemplified by the case of Pol β and λ. These enzymes play essential roles in many different repair pathways. Pol β is the main enzyme involved in BER, and it is essential during development, especially in the brain, as testified by the embryonic lethality of Pol β knockout mice. Pol λ, on the other hand, is not essential, at least for mouse development, since Pol λ knockout mice are viable and fertile. However, alterations of its levels have been clearly linked to various forms of DNA damage accumulation and genetic instability.

Both of these enzymes are thus fundamentally beneficial to the cell. However, in some special contexts, they can exert deleterious effects. For example, under unbalanced dNTP/rNTP pool ratios, both enzymes can incorporate rNMPs into DNA, causing mutations, DNA fragility and delaying BER of oxidized bases. During MMEJ of ends containing repetitive sequences, Pol β can also contribute to

the deleterious expansion of CAG triplets. Finally, overexpression of both Pols has been clearly linked to tumorigenesis.

In this respect, such a dual aspect of Pol β and λ action, might be exploited for the better. In fact, understanding their mechanisms of (de)regulation is a key step towards their exploitation as potential antitumoral targets. For example, inhibition of Pol β has been shown to sensitize tumors towards conventional DNA damaging agents, while suppression of Pol λ has been shown to induce synthetic lethality when combined with Chk1 inhibitors.

Unfortunately, of the dozens of Pol λ and β inhibitors that have been described to date, both natural and small molecule compounds, only a small part is sufficiently selective and active in a non-toxic nanomolar range. In order to achieve improvements of the current treatment options, there is an imminent need to identify novel selective inhibitors targeting Pol λ and Pol β in tumor cells. The approach of the concurrent inhibition of DNA repair mechanisms and the use of systemic antitumoral therapy offers the rationale to potentiate selective tumor killing. However, knowledge of tumor background, comprehension of the altered DNA-repair mechanism, is essential in order to tailor the adequate antitumoral therapy. The research of novel promising agents to be exploited in anticancer therapy must thus be advanced, in order to optimize their selectivity, efficacy and reduce the mutagenic risk for healthy cells.

Acknowledgments: Work in the authors' laboratory has been supported by the Italian Cancer Research Association (AIRC) Grant IG15868. AIRC supports open access publishing.

Conflicts of Interest: The authors declare no conflict of interest.

References

1. Khoronenkova, S.V.; Dianov, G.L. The emerging role of mule and ARF in the regulation of base excision repair. *FEBS Lett.* **2011**, *585*, 2831–2835. [PubMed]
2. Parsons, J.L.; Dianova, I.I.; Khoronenkova, S.V.; Edelmann, M.J.; Kessler, B.M.; Dianov, G.L. Usp47 is a deubiquitylating enzyme that regulates base excision repair by controlling steady-state levels of DNA polymerase β. *Mol. Cell* **2011**, *41*, 609–615. [PubMed]
3. Frouin, I.; Toueille, M.; Ferrari, E.; Shevelev, I.; Hubscher, U. Phosphorylation of human DNA polymerase λ by the cyclin-dependent kinase cdk2/cyclin a complex is modulated by its association with proliferating cell nuclear antigen. *Nucl. Acids Res.* **2005**, *33*, 5354–5361. [PubMed]
4. Markkanen, E.; Hübscher, U.; van Loon, B. Regulation of oxidative DNA damage repair: The adenine: 8-oxo-guanine problem. *Cell Cycle* **2012**, *11*, 1070–1075. [PubMed]
5. Zucca, E.; Bertoletti, F.; Wimmer, U.; Ferrari, E.; Mazzini, G.; Khoronenkova, S.; Grosse, N.; van Loon, B.; Dianov, G.; Hubscher, U.; et al. Silencing of human DNA polymerase λ causes replication stress and is synthetically lethal with an impaired S phase checkpoint. *Nucl. Acids Res.* **2013**, *41*, 229–241. [PubMed]
6. Cimprich, K.A.; Cortez, D. ATR: An essential regulator of genome integrity. *Nat. Rev. Mol. Cell. Biol.* **2008**, *9*, 616–627. [PubMed]
7. Moon, A.F.; Garcia-Diaz, M.; Batra, V.K.; Beard, W.A.; Bebenek, K.; Kunkel, T.A.; Wilson, S.H.; Pedersen, L.C. The X family portrait: Structural insights into biological functions of X family polymerases. *DNA Repair* **2007**, *6*, 1709–1725. [PubMed]
8. Bebenek, K.; Pedersen, L.C.; Kunkel, T.A. Structure-function studies of DNA polymerase λ. *Biochemistry* **2014**, *53*, 2781–2792. [PubMed]
9. Dianov, G.L.; Hübscher, U. Mammalian base excision repair: The forgotten archangel. *Nucl. Acids Res.* **2013**, *41*, 3483–3490. [PubMed]
10. Fortini, P.; Dogliotti, E. Base damage and single-strand break repair: Mechanisms and functional significance of short- and long-patch repair subpathways. *DNA Repair* **2007**, *6*, 398–409. [PubMed]
11. Beard, W.A.; Wilson, S.H. Structure and mechanism of DNA polymerase β. *Chem. Rev.* **2006**, *106*, 361–382. [PubMed]
12. Gao, Y.; Katyal, S.; Lee, Y.; Zhao, J.; Rehg, J.E.; Russell, H.R.; McKinnon, P.J. DNA ligase III is critical for mtDNA integrity but not Xrcc1-mediated nuclear DNA repair. *Nature* **2011**, *471*, 240–244. [PubMed]

13. Simsek, D.; Furda, A.; Gao, Y.; Artus, J.; Brunet, E.; Hadjantonakis, A.-K.; van Houten, B.; Shuman, S.; McKinnon, P.J.; Jasin, M. Crucial roles for DNA ligase III in mitochondria but not in Xrcc1-dependent repair. *Nature* **2011**, *471*, 245–248. [PubMed]
14. Maga, G.; Villani, G.; Crespan, E.; Wimmer, U.; Ferrari, E.; Bertocci, B.; Hubscher, U. 8-oxo-guanine bypass by human DNA polymerases in the presence of auxiliary proteins. *Nature* **2007**, *447*, 606–608. [PubMed]
15. Waters, L.S.; Minesinger, B.K.; Wiltrout, M.E.; D'Souza, S.; Woodruff, R.V.; Walker, G.C. Eukaryotic translesion polymerases and their roles and regulation in DNA damage tolerance. *Microbiol. Mol. Biol. Rev.* **2009**, *73*, 134–154. [PubMed]
16. Hübscher, U.; Maga, G. DNA replication and repair bypass machines. *Curr. Opin. Chem. Biol.* **2011**, *15*, 627–635. [PubMed]
17. Amoroso, A.; Crespan, E.; Wimmer, U.; Hubscher, U.; Maga, G. DNA polymerases and oxidative damage: Friends or foes? *Curr. Mol. Pharmacol.* **2008**, *1*, 162–170. [PubMed]
18. Maga, G.; Crespan, E.; Wimmer, U.; van Loon, B.; Amoroso, A.; Mondello, C.; Belgiovine, C.; Ferrari, E.; Locatelli, G.; Villani, G.; et al. Replication protein a and proliferating cell nuclear antigen coordinate DNA polymerase selection in 8-oxo-guanine repair. *Proc. Natl. Acad. Sci. USA* **2008**, *105*, 20689–20694. [PubMed]
19. Malyarchuk, S.; Castore, R.; Harrison, L. DNA repair of clustered lesions in mammalian cells: Involvement of non-homologous end-joining. *Nucl. Acids Res.* **2008**, *36*, 4872–4882. [PubMed]
20. Cunniffe, S.; O'Neill, P.; Greenberg, M.M.; Lomax, M.E. Reduced repair capacity of a DNA clustered damage site comprised of 8-oxo-7,8-dihydro-2′-deoxyguanosine and 2-deoxyribonolactone results in an increased mutagenic potential of these lesions. *Mutat. Res.* **2014**, *762*, 32–39. [PubMed]
21. Crespan, E.; Pasi, E.; Imoto, S.; Hübscher, U.; Greenberg, M.M.; Maga, G. Human DNA polymerase β, but not λ, can bypass a 2-deoxyribonolactone lesion together with proliferating cell nuclear antigen. *ACS Chem. Biol.* **2013**, *8*, 336–344. [PubMed]
22. Quiñones, J.L.; Thapar, U.; Yu, K.; Fang, Q.; Sobol, R.W.; Demple, B. Enzyme mechanism-based, oxidative DNA–protein cross-links formed with DNA polymerase β in vivo. *Proc. Natl. Acad. Sci. USA* **2015**, *112*, 8602–8607. [PubMed]
23. Quiñones, J.L.; Demple, B. When DNA repair goes wrong: BER-generated DNA-protein crosslinks to oxidative lesions. *DNA Repair* **2016**, *44*, 103–109. [PubMed]
24. Stevens, A.J.; Guan, L.; Bebenek, K.; Kunkel, T.A.; Greenberg, M.M. DNA polymerase λ inactivation by oxidized abasic sites. *Biochemistry* **2013**, *52*, 975–983. [PubMed]
25. Blanca, G.; Villani, G.; Shevelev, I.; Ramadan, K.; Spadari, S.; Hübscher, U.; Maga, G. Human DNA polymerases λ and β show different efficiencies of translesion DNA synthesis past abasic sites and alternative mechanisms for frameshift generation. *Biochemistry* **2004**, *43*, 11605–11615. [PubMed]
26. DeMott, M.S.; Beyret, E.; Wong, D.; Bales, B.C.; Hwang, J.-T.; Greenberg, M.M.; Demple, B. Covalent trapping of human DNA polymerase β by the oxidative DNA lesion 2-deoxyribonolactone. *J. Biol. Chem.* **2002**, *277*, 7637–7640. [PubMed]
27. Arian, D.; Hedayati, M.; Zhou, H.; Bilis, Z.; Chen, K.; DeWeese, T.L.; Greenberg, M.M. Irreversible inhibition of DNA polymerase β by small molecule mimics of a DNA lesion. *J. Am. Chem. Soc.* **2014**, *136*, 3176–3183. [PubMed]
28. Liu, L.; Rodriguez-Belmonte, E.M.; Mazloum, N.; Xie, B.; Lee, M.Y. Identification of a novel protein, pdip38, that interacts with the p50 subunit of DNA polymerase δ and proliferating cell nuclear antigen. *J. Biol. Chem.* **2003**, *278*, 10041–10047. [PubMed]
29. Tissier, A.; Janel-Bintz, R.; Coulon, S.; Klaile, E.; Kannouche, P.; Fuchs, R.P.; Cordonnier, A.M. Crosstalk between replicative and translesional DNA polymerases: Pdip38 interacts directly with Polη. *DNA Repair* **2010**, *9*, 922–928. [PubMed]
30. Maga, G.; Crespan, E.; Markkanen, E.; Imhof, R.; Furrer, A.; Villani, G.; Hübscher, U.; van Loon, B. DNA polymerase δ-interacting protein 2 is a processivity factor for DNA polymerase λ during 8-oxo-7,8-dihydroguanine bypass. *Proc. Natl. Acad. Sci. USA* **2013**, *110*, 18850–18855. [PubMed]
31. McElhinny, S.A.N.; Kumar, D.; Clark, A.B.; Watt, D.L.; Watts, B.E.; Lundström, E.-B.; Johansson, E.; Chabes, A.; Kunkel, T.A. Genome instability due to ribonucleotide incorporation into DNA. *Nat. Chem. Biol.* **2010**, *6*, 774–781.
32. Yao, N.Y.; Schroeder, J.W.; Yurieva, O.; Simmons, L.A.; O'Donnell, M.E. Cost of rNTP/dNTP pool imbalance at the replication fork. *Proc. Natl. Acad. Sci. USA* **2013**, *110*, 12942–12947. [PubMed]

33. Clausen, A.R.; Murray, M.S.; Passer, A.R.; Pedersen, L.C.; Kunkel, T.A. Structure–function analysis of ribonucleotide bypass by b family DNA replicases. *Proc. Natl. Acad. Sci. USA* **2013**, *110*, 16802–16807. [PubMed]
34. Reijns, M.A.; Rabe, B.; Rigby, R.E.; Mill, P.; Astell, K.R.; Lettice, L.A.; Boyle, S.; Leitch, A.; Keighren, M.; Kilanowski, F.; et al. Enzymatic removal of ribonucleotides from DNA is essential for mammalian genome integrity and development. *Cell* **2012**, *149*, 1008–1022. [PubMed]
35. Brown, J.A.; Suo, Z. Unlocking the sugar "steric gate" of DNA polymerases. *Biochemistry* **2011**, *50*, 1135–1142. [PubMed]
36. Nick McElhinny, S.A.; Ramsden, D.A. Polymerase mu is a DNA-directed DNA/RNA polymerase. *Mol. Cell. Biol.* **2003**, *23*, 2309–2315. [PubMed]
37. Martin, M.J.; Garcia-Ortiz, M.V.; Esteban, V.; Blanco, L. Ribonucleotides and manganese ions improve non-homologous end joining by human polμ. *Nucl. Acids Res.* **2013**, *41*, 2428–2436. [CrossRef] [PubMed]
38. Crespan, E.; Furrer, A.; Rösinger, M.; Bertoletti, F.; Mentegari, E.; Chiapparini, G.; Imhof, R.; Ziegler, N.; Sturla, S.J.; Hübscher, U.; et al. Impact of ribonucleotide incorporation by DNA polymerases β and λ on oxidative base excision repair. *Nat. Commun.* **2016**, *7*, 10805. [CrossRef] [PubMed]
39. Gosavi, R.A.; Moon, A.F.; Kunkel, T.A.; Pedersen, L.C.; Bebenek, K. The catalytic cycle for ribonucleotide incorporation by human DNA Pol λ. *Nucl. Acids Res.* **2012**, *40*, 7518–7527. [CrossRef]
40. Cilli, P.; Minoprio, A.; Bossa, C.; Bignami, M.; Mazzei, F. Formation and repair of mismatches containing ribonucleotides and oxidized bases at repeated DNA sequences. *J. Biol. Chem.* **2015**, *290*, 26259–26269. [CrossRef] [PubMed]
41. Frit, P.; Barboule, N.; Yuan, Y.; Gomez, D.; Calsou, P. Alternative end-joining pathway(s): Bricolage at DNA breaks. *DNA Repair* **2014**, *17*, 81–97. [CrossRef] [PubMed]
42. Lieber, M.R. The mechanism of double-strand DNA break repair by the nonhomologous DNA end joining pathway. *Annu. Rev. Biochem.* **2010**, *79*, 181–211. [CrossRef] [PubMed]
43. Crespan, E.; Czabany, T.; Maga, G.; Hübscher, U. Microhomology-mediated DNA strand annealing and elongation by human DNA polymerases λ and β on normal and repetitive DNA sequences. *Nucl. Acids Res.* **2012**, *40*, 5577–5590. [CrossRef] [PubMed]
44. Barone, F.; McCulloch, S.D.; Macpherson, P.; Maga, G.; Yamada, M.; Nohmi, T.; Minoprio, A.; Mazzei, F.; Kunkel, T.A.; Karran, P.; et al. Replication of 2-hydroxyadenine-containing DNA and recognition by human mutsalpha. *DNA Repair* **2007**, *6*, 355–366. [CrossRef] [PubMed]
45. Marechal, A.; Zou, L. DNA damage sensing by the ATM and ATR kinases. *Cold Spring Harb. Perspect. Biol.* **2013**, *5*, a012716. [CrossRef] [PubMed]
46. Kelly, T.J.; Brown, G.W. Regulation of chromosome replication. *Annu. Rev. Biochem.* **2000**, *69*, 829–880. [CrossRef] [PubMed]
47. Albertella, M.R.; Lau, A.; O'Connor, M.J. The overexpression of specialized DNA polymerases in cancer. *DNA Repair* **2005**, *4*, 583–593. [CrossRef] [PubMed]
48. Capp, J.-P.; Boudsocq, F.; Bergoglio, V.; Trouche, D.; Cazaux, C.; Blanco, L.; Hoffmann, J.-S.; Canitrot, Y. The R438W polymorphism of human DNA polymerase λ triggers cellular sensitivity to camptothecin by compromising the homologous recombination repair pathway. *Carcinogenesis* **2010**, *31*, 1742–1747. [CrossRef] [PubMed]
49. Terrados, G.; Capp, J.-P.; Canitrot, Y.; García-Díaz, M.; Bebenek, K.; Kirchhoff, T.; Villanueva, A.; Boudsocq, F.; Bergoglio, V.; Cazaux, C.; et al. Characterization of a natural mutator variant of human DNA polymerase λ which promotes chromosomal instability by compromising NHEJ. *PLoS ONE* **2009**, *4*, e7290. [CrossRef]
50. Fang, Q.; Inanc, B.; Schamus, S.; Wang, X.H.; Wei, L.; Brown, A.R.; Svilar, D.; Sugrue, K.F.; Goellner, E.M.; Zeng, X.; et al. HSP90 regulates DNA repair via the interaction between XRCC1 and DNA polymerase β. *Nat. Commun.* **2014**, *5*, 5513. [CrossRef] [PubMed]
51. Iwanaga, A.; Ouchida, M.; Miyazaki, K.; Hori, K.; Mukai, T. Functional mutation of DNA polymerase β found in human gastric cancer–inability of the base excision repair in vitro. *Mutat. Res.* **1999**, *435*, 121–128. [CrossRef]
52. Dobashi, Y.; Shuin, T.; Tsuruga, H.; Uemura, H.; Torigoe, S.; Kubota, Y. DNA polymerase β gene mutation in human prostate cancer. *Cancer Res.* **1994**, *54*, 2827–2829. [PubMed]
53. Starcevic, D.; Dalal, S.; Sweasy, J.B. Is there a link between DNA polymerase β and cancer? *Cell Cycle* **2004**, *3*, 998–1001. [CrossRef] [PubMed]

54. Donigan, K.A.; Sun, K.W.; Nemec, A.A.; Murphy, D.L.; Cong, X.; Northrup, V.; Zelterman, D.; Sweasy, J.B. Human polb gene is mutated in high percentage of colorectal tumors. *J. Biol. Chem.* **2012**, *287*, 23830–23839. [CrossRef] [PubMed]
55. Lang, T.; Maitra, M.; Starcevic, D.; Li, S.X.; Sweasy, J.B. A DNA polymerase β mutant from colon cancer cells induces mutations. *Proc. Natl. Acad. Sci. USA* **2004**, *101*, 6074–6079. [CrossRef] [PubMed]
56. Nemec, A.A.; Murphy, D.L.; Donigan, K.A.; Sweasy, J.B. The s229l colon tumor-associated variant of DNA polymerase β induces cellular transformation as a result of decreased polymerization efficiency. *J. Biol. Chem.* **2014**, *289*, 13708–13716. [CrossRef] [PubMed]
57. Zhou, T.; Pan, F.; Cao, Y.; Han, Y.; Zhao, J.; Sun, H.; Zhou, X.; Wu, X.; He, L.; Hu, Z.; et al. R152c DNA pol beta mutation impairs base excision repair and induces cellular transformation. *Oncotarget* **2016**, *7*, 6902–6915. [PubMed]
58. Tan, X.; Wang, H.; Luo, G.; Ren, S.; Li, W.; Cui, J.; Gill, H.S.; Fu, S.W.; Lu, Y. Clinical significance of a point mutation in DNA polymerase beta (polb) gene in gastric cancer. *Int. J. Biol. Sci.* **2015**, *11*, 144–155. [CrossRef] [PubMed]
59. Dalal, S.; Hile, S.; Eckert, K.A.; Sun, K.-W.; Starcevic, D.; Sweasy, J.B. Prostate-cancer-associated i260m variant of DNA polymerase β is a sequence-specific mutator. *Biochemistry* **2005**, *44*, 15664–15673. [CrossRef] [PubMed]
60. Yamtich, J.; Nemec, A.A.; Keh, A.; Sweasy, J.B. A germline polymorphism of DNA polymerase beta induces genomic instability and cellular transformation. *PLoS Genet.* **2012**, *8*, e1003052. [CrossRef] [PubMed]
61. Wang, Y.; Zang, W.; Du, Y.; Chen, X.; Zhao, G. The k167i variant of DNA polymerase β that is found in esophageal carcinoma patients impairs polymerase activity and BER. *Sci. Rep.* **2015**, *5*, 15986. [CrossRef] [PubMed]
62. Ray, S.; Menezes, M.R.; Senejani, A.; Sweasy, J.B. Cellular roles of DNA polymerase β. *Yale J. Biol. Med.* **2013**, *86*, 463–469. [PubMed]
63. Louat, T.; Servant, L.; Rols, M.P.; Bieth, A.; Teissie, J.; Hoffmann, J.S.; Cazaux, C. Antitumor activity of 2′,3′-dideoxycytidine nucleotide analog against tumors up-regulating DNA polymerase β. *Mol. Pharmacol.* **2001**, *60*, 553–558. [PubMed]
64. Bergoglio, V.; Frechet, M.; Philippe, M.; Bieth, A.; Mercier, P.; Morello, D.; Lacroix-Tricki, M.; Delsol, G.; Hoffmann, J.S.; Cazaux, C. Evidence of finely tuned expression of DNA polymerase β in vivo using transgenic mice. *FEBS Lett.* **2004**, *566*, 147–150. [CrossRef] [PubMed]
65. Frechet, M.; Canitrot, Y.; Cazaux, C.; Hoffmann, J.S. DNA polymerase β imbalance increases apoptosis and mutagenesis induced by oxidative stress. *FEBS Lett.* **2001**, *505*, 229–232. [CrossRef]
66. Frechet, M.; Canitrot, Y.; Bieth, A.; Dogliotti, E.; Cazaux, C.; Hoffmann, J.S. Deregulated DNA polymerase β strengthens ionizing radiation-induced nucleotidic and chromosomal instabilities. *Oncogene* **2002**, *21*, 2320–2327. [CrossRef] [PubMed]
67. Fotiadou, P.; Henegariu, O.; Sweasy, J.B. DNA polymerase β interacts with TRF2 and induces telomere dysfunction in a murine mammary cell line. *Cancer Res.* **2004**, *64*, 3830–3837. [CrossRef] [PubMed]
68. Goula, A.-V.; Merienne, K. Abnormal base excision repair at trinucleotide repeats associated with diseases: A tissue-selective mechanism. *Genes* **2013**, *4*, 375. [CrossRef] [PubMed]
69. Liu, Y.; Wilson, S.H. DNA base excision repair: A mechanism of trinucleotide repeat expansion. *Trends Biochem. Sci.* **2012**, *37*, 162–172. [CrossRef] [PubMed]
70. Guo, J.; Gu, L.; Leffak, M.; Li, G.-M. MutSβ promotes trinucleotide repeat expansion by recruiting DNA polymerase β to nascent (CAG) n or (CTG) n hairpins for error-prone DNA synthesis. *Cell Res.* **2016**, *26*, 775–786. [CrossRef] [PubMed]
71. Ding, J.; Miao, Z.H.; Meng, L.H.; Geng, M.Y. Emerging cancer therapeutic opportunities target DNA-repair systems. *Trends Pharmacol. Sci.* **2006**, *27*, 338–344. [CrossRef] [PubMed]
72. Madhusudan, S.; Hickson, I.D. DNA repair inhibition: A selective tumour targeting strategy. *Trends Mol. Med.* **2005**, *11*, 503–511. [CrossRef] [PubMed]
73. Liu, L.; Nakatsuru, Y.; Gerson, S.L. Base excision repair as a therapeutic target in colon cancer. *Clin. Cancer Res.* **2002**, *8*, 2985–2991. [PubMed]
74. Canitrot, Y.; Cazaux, C.; Frechet, M.; Bouayadi, K.; Lesca, C.; Salles, B.; Hoffmann, J.S. Overexpression of DNA polymerase β in cell results in a mutator phenotype and a decreased sensitivity to anticancer drugs. *Proc. Natl. Acad. Sci. USA* **1998**, *95*, 12586–12590. [CrossRef] [PubMed]

75. Lange, S.S.; Takata, K.; Wood, R.D. DNA polymerases and cancer. *Nat. Rev. Cancer* **2011**, *11*, 96–110. [CrossRef] [PubMed]
76. Lebedeva, N.A.; Rechkunova, N.I.; Dezhurov, S.V.; Khodyreva, S.N.; Favre, A.; Blanco, L.; Lavrik, O.I. Comparison of functional properties of mammalian DNA polymerase λ and DNA polymerase β in reactions of DNA synthesis related to DNA repair. *Biochim. Biophys. Acta* **2005**, *1751*, 150–158. [CrossRef] [PubMed]
77. Fiala, K.A.; Abdel-Gawad, W.; Suo, Z. Pre-steady-state kinetic studies of the fidelity and mechanism of polymerization catalyzed by truncated human DNA polymerase λ. *Biochemistry* **2004**, *43*, 6751–6762. [CrossRef] [PubMed]
78. Mizushina, Y.; Tanaka, N.; Yagi, H.; Kurosawa, T.; Onoue, M.; Seto, H.; Horie, T.; Aoyagi, N.; Yamaoka, M.; Matsukage, A.; et al. Fatty acids selectively inhibit eukaryotic DNA polymerase activities in vitro. *Biochim. Biophys. Acta* **1996**, *1308*, 256–262. [CrossRef]
79. Ono, K.; Nakane, H.; Fukushima, M.; Chermann, J.C.; Barre-Sinoussi, F. Differential inhibitory effects of various flavonoids on the activities of reverse transcriptase and cellular DNA and RNA polymerases. *Eur. J. Biochem.* **1990**, *190*, 469–476. [CrossRef] [PubMed]
80. Chen, J.; Zhang, Y.H.; Wang, L.K.; Sucheck, S.J.; Snow, A.M.; Hecht, S.M. Inhibitors of DNA polymerase β from schoepfia californica. *Chem. Commun.* **1998**, 2769–2770. [CrossRef]
81. Tanaka, N.; Kitamura, A.; Mizushina, Y.; Sugawara, F.; Sakaguchi, K. Fomitellic acids, triterpenoid inhibitors of eukaryotic DNA polymerases from a basidiomycete, *Fomitella fraxinea*. *J. Nat. Prod.* **1998**, *61*, 193–197. [CrossRef] [PubMed]
82. Deng, J.Z.; Sun Di-An, A.; Starck, S.R.; Hecht, S.M.; Cerny, R.L.; Engen, J.R. Chrysochlamic acid, a new diterpenoid-substituted quinol from chrysochlamys ulei that inhibits DNA polymerase β. *J. Chem. Soc. Perkin Trans. 1* **1999**, *24*, 1147–1149. [CrossRef]
83. Sun, D.A.; Deng, J.Z.; Starck, S.R.; Hecht, S.M. Mispyric acid, a new monocyclic triterpenoid with a novel skeleton from *Mischocarpus pyriformis* that inhibits DNA polymerase β. *J. Am. Chem. Soc.* **1999**, *121*, 6120–6124. [CrossRef]
84. Sun, D.A.; Starck, S.R.; Locke, E.P.; Hecht, S.M. DNA polymerase β inhibitors from *Sandoricum koetjape*. *J. Nat. Prod.* **1999**, *62*, 1110–1113. [CrossRef] [PubMed]
85. Deng, J.Z.; Starck, S.R.; Hecht, S.M. DNA polymerase β inhibitors from *Baeckea gunniana*. *J. Nat. Prod.* **1999**, *62*, 1624–1626. [CrossRef] [PubMed]
86. Deng, J.Z.; Starck, S.R.; Hecht, S.M.; Ijames, C.F.; Hemling, M.E. Harbinatic acid, a novel and potent DNA polymerase β inhibitor from *Hardwickia binata*. *J. Nat. Prod.* **1999**, *62*, 1000–1002. [CrossRef] [PubMed]
87. Ma, J.; Starck, S.R.; Hecht, S.M. DNA polymerase β inhibitors from *Tetracera boiviniana*. *J. Nat. Prod.* **1999**, *62*, 1660–1663. [CrossRef] [PubMed]
88. Deng, J.Z.; Starck, S.R.; Hecht, S.M. Pentacyclic triterpenoids from freziera sp. that inhibit DNA polymerase β. *Bioorg. Med. Chem.* **2000**, *8*, 247–250. [CrossRef]
89. Deng, J.Z.; Starck, S.R.; Sun, D.A.; Sabat, M.; Hecht, S.M. A new 7,8-euphadien-type triterpenoid from *Brackenridgea nitida* and *Bleasdalea bleasdalei* that inhibits DNA polymerase β. *J. Nat. Prod.* **2000**, *63*, 1356–1360. [CrossRef] [PubMed]
90. Hecht, S.M. Inhibitors of the lyase activity of DNA polymerase β. *Pharm. Biol.* **2003**, *41*, 68–77. [CrossRef]
91. Prakash Chaturvedula, V.S.; Gao, Z.; Hecht, S.M.; Jones, S.H.; Kingston, D.G. A new acylated oleanane triterpenoid from *Couepia polyandra* that inhibits the lyase activity of DNA polymerase β. *J. Nat. Prod.* **2003**, *66*, 1463–1465. [CrossRef] [PubMed]
92. Li, S.S.; Gao, Z.; Feng, X.; Jones, S.H.; Hecht, S.M. Plant sterols as selective DNA polymerase β lyase inhibitors and potentiators of *Bleomycin cytotoxicity*. *Bioorg. Med. Chem.* **2004**, *12*, 4253–4258. [CrossRef] [PubMed]
93. Li, S.S.; Gao, Z.; Feng, X.; Hecht, S.M. Biscoumarin derivatives from edgeworthia gardneri that inhibit the lyase activity of DNA polymerase β. *J. Nat. Prod.* **2004**, *67*, 1608–1610. [CrossRef] [PubMed]
94. Prakash Chaturvedula, V.S.; Hecht, S.M.; Gao, Z.; Jones, S.H.; Feng, X.; Kingston, D.G. New neolignans that inhibit DNA polymerase β lyase. *J. Nat. Prod.* **2004**, *67*, 964–967. [CrossRef] [PubMed]
95. Chaturvedula, V.S.; Zhou, B.N.; Gao, Z.; Thomas, S.J.; Hecht, S.M.; Kingston, D.G. New lupane triterpenoids from *Solidago canadensis* that inhibit the lyase activity of DNA polymerase β. *Bioorg. Med. Chem.* **2004**, *12*, 6271–6275. [CrossRef] [PubMed]
96. Feng, X.; Gao, Z.; Li, S.; Jones, S.H.; Hecht, S.M. DNA polymerase β lyase inhibitors from *Maytenus putterlickoides*. *J. Nat. Prod.* **2004**, *67*, 1744–1747. [CrossRef] [PubMed]

97. Ogawa, A.; Murate, T.; Izuta, S.; Takemura, M.; Furuta, K.; Kobayashi, J.; Kamikawa, T.; Nimura, Y.; Yoshida, S. Sulfated glycoglycerolipid from Archaebacterium inhibits eukaryotic DNA polymerase alpha, β and retroviral reverse transcriptase and affects methyl methanesulfonate cytotoxicity. *Int. J. Cancer* **1998**, *76*, 512–518. [CrossRef]
98. Mizushina, Y.; Watanabe, I.; Ohta, K.; Takemura, M.; Sahara, H.; Takahashi, N.; Gasa, S.; Sugawara, F.; Matsukage, A.; Yoshida, S.; et al. Studies on inhibitors of mammalian DNA polymerase α and β: Sulfolipids from a pteridophyte, *Athyrium niponicum*. *Biochem. Pharmacol.* **1998**, *55*, 537–541. [CrossRef]
99. Gao, Z.; Maloney, D.J.; Dedkova, L.M.; Hecht, S.M. Inhibitors of DNA polymerase β: Activity and mechanism. *Bioorg. Med. Chem.* **2008**, *16*, 4331–4340. [CrossRef] [PubMed]
100. Maloney, D.J.; Deng, J.Z.; Starck, S.R.; Gao, Z.; Hecht, S.M. (+)-myristinin A, a naturally occurring DNA polymerase β inhibitor and potent DNA-damaging agent. *J. Am. Chem. Soc.* **2005**, *127*, 4140–4141. [CrossRef] [PubMed]
101. Mizushina, Y.; Takahashi, N.; Ogawa, A.; Tsurugaya, K.; Koshino, H.; Takemura, M.; Yoshida, S.; Matsukage, A.; Sugawara, F.; Sakaguchi, K. The cyanogenic glucoside, prunasin (D-mandelonitrile-β-D-glucoside), is a novel inhibitor of DNA polymerase β. *J. Biochem.* **1999**, *126*, 430–436. [CrossRef] [PubMed]
102. Jaiswal, A.S.; Banerjee, S.; Aneja, R.; Sarkar, F.H.; Ostrov, D.A.; Narayan, S. DNA polymerase β as a novel target for chemotherapeutic intervention of colorectal cancer. *PLoS ONE* **2011**, *6*, e16691. [CrossRef] [PubMed]
103. Horton, J.K.; Prasad, R.; Hou, E.; Wilson, S.H. Protection against methylation-induced cytotoxicity by DNA polymerase β-dependent long patch base excision repair. *J. Biol. Chem.* **2000**, *275*, 2211–2218. [CrossRef] [PubMed]
104. Taverna, P.; Liu, L.; Hwang, H.S.; Hanson, A.J.; Kinsella, T.J.; Gerson, S.L. Methoxyamine potentiates DNA single strand breaks and double strand breaks induced by temozolomide in colon cancer cells. *Mutat. Res.* **2001**, *485*, 269–281. [CrossRef]
105. Fishel, M.L.; He, Y.; Smith, M.L.; Kelley, M.R. Manipulation of base excision repair to sensitize ovarian cancer cells to alkylating agent temozolomide. *Clin. Cancer Res.* **2007**, *13*, 260–267. [CrossRef]
106. Tang, J.B.; Svilar, D.; Trivedi, R.N.; Wang, X.H.; Goellner, E.M.; Moore, B.; Hamilton, R.L.; Banze, L.A.; Brown, A.R.; Sobol, R.W. N-methylpurine DNA glycosylase and DNA polymerase β modulate BER inhibitor potentiation of glioma cells to temozolomide. *Neuro-oncology* **2011**, *13*, 471–486. [CrossRef] [PubMed]
107. Strittmatter, T.; Brockmann, A.; Pott, M.; Hantusch, A.; Brunner, T.; Marx, A. Expanding the scope of human DNA polymerase λ and β inhibitors. *ACS Chem. Biol.* **2014**, *9*, 282–290. [CrossRef] [PubMed]
108. Copani, A.; Sortino, M.A.; Caricasole, A.; Chiechio, S.; Chisari, M.; Battaglia, G.; Giuffrida-Stella, A.M.; Vancheri, C.; Nicoletti, F. Erratic expression of DNA polymerases by β-amyloid causes neuronal death. *FASEB J.* **2002**, *16*, 2006–2008. [CrossRef] [PubMed]
109. Copani, A.; Hoozemans, J.J.; Caraci, F.; Calafiore, M.; Van Haastert, E.S.; Veerhuis, R.; Rozemuller, A.J.; Aronica, E.; Sortino, M.A.; Nicoletti, F. DNA polymerase-β is expressed early in neurons of alzheimer's disease brain and is loaded into DNA replication forks in neurons challenged with β-amyloid. *J. Neurosci.* **2006**, *26*, 10949–10957. [CrossRef] [PubMed]
110. Zhang, Z.; Cao, X.; Xiong, N.; Wang, H.; Huang, J.; Sun, S.; Liang, Z.; Wang, T. DNA polymerase-β is required for 1-methyl-4-phenylpyridinium-induced apoptotic death in neurons. *Apoptosis* **2010**, *15*, 105–115. [CrossRef] [PubMed]
111. Merlo, S.; Basile, L.; Giuffrida, M.L.; Sortino, M.A.; Guccione, S.; Copani, A. Identification of 5-methoxyflavone as a novel DNA polymerase-β inhibitor and neuroprotective agent against β-amyloid toxicity. *J. Nat. Prod.* **2015**, *78*, 2704–2711. [CrossRef] [PubMed]
112. Mizushina, Y.; Kamisuki, S.; Kasai, N.; Ishidoh, T.; Shimazaki, N.; Takemura, M.; Asahara, H.; Linn, S.; Yoshida, S.; Koiwai, O.; et al. Petasiphenol: A DNA polymerase λ inhibitor. *Biochemistry* **2002**, *41*, 14463–14471. [CrossRef] [PubMed]
113. Mizushina, Y.; Hirota, M.; Murakami, C.; Ishidoh, T.; Kamisuki, S.; Shimazaki, N.; Takemura, M.; Perpelescu, M.; Suzuki, M.; Yoshida, H.; et al. Some anti-chronic inflammatory compounds are DNA polymerase λ-specific inhibitors. *Biochem. Pharmacol.* **2003**, *66*, 1935–1944. [CrossRef]
114. Mizushina, Y.; Saito, A.; Tanaka, A.; Nakajima, N.; Kuriyama, I.; Takemura, M.; Takeuchi, T.; Sugawara, F.; Yoshida, H. Structural analysis of catechin derivatives as mammalian DNA polymerase inhibitors. *Biochem. Biophys. Res. Commun.* **2005**, *333*, 101–109. [CrossRef] [PubMed]

115. Kamisuki, S.; Ishimaru, C.; Onoda, K.; Kuriyama, I.; Ida, N.; Sugawara, F.; Yoshida, H.; Mizushina, Y. Nodulisporol and nodulisporone, novel specific inhibitors of human DNA polymerase λ from a fungus, *Nodulisporium* sp. *Bioorg. Med. Chem.* **2007**, *15*, 3109–3114. [CrossRef] [PubMed]
116. Mizushina, Y.; Kuriyama, I.; Yoshida, H. Inhibition of DNA polymerase λ and associated inflammatory activities of extracts from steamed germinated soybeans. *Food Funct.* **2014**, *5*, 696–704. [CrossRef] [PubMed]
117. Locatelli, G.A.; Savio, M.; Forti, L.; Shevelev, I.; Ramadan, K.; Stivala, L.A.; Vannini, V.; Hubscher, U.; Spadari, S.; Maga, G. Inhibition of mammalian DNA polymerases by resveratrol: Mechanism and structural determinants. *Biochem. J.* **2005**, *389*, 259–268. [CrossRef] [PubMed]
118. Strittmatter, T.; Bareth, B.; Immel, T.A.; Huhn, T.; Mayer, T.U.; Marx, A. Small molecule inhibitors of human DNA polymerase λ. *ACS Chem. Biol.* **2011**, *6*, 314–319. [CrossRef] [PubMed]
119. Mizushina, Y.; Kamisuki, S.; Kasai, N.; Shimazaki, N.; Takemura, M.; Asahara, H.; Linn, S.; Yoshida, S.; Matsukage, A.; Koiwai, O.; et al. A plant phytotoxin, solanapyrone A, is an inhibitor of DNA polymerase β and λ. *J. Biol. Chem.* **2002**, *277*, 630–638. [CrossRef] [PubMed]
120. Kimura, T.; Nishida, M.; Kuramochi, K.; Sugawara, F.; Yoshida, H.; Mizushina, Y. Novel azaphilones, kasanosins A and B, which are specific inhibitors of eukaryotic DNA polymerases β and λ from talaromyces sp. *Bioorg. Med. Chem.* **2008**, *16*, 4594–4599. [CrossRef] [PubMed]
121. Nishida, M.; Hada, T.; Kuramochi, K.; Yoshida, H.; Yonezawa, Y.; Kuriyama, I.; Sugawara, F.; Yoshida, H.; Mizushina, Y. Diallyl sulfides: Selective inhibitors of family X DNA polymerases from garlic (*Allium sativum* L.). *Food Chem.* **2008**, *108*, 551–560. [CrossRef] [PubMed]

nature COMMUNICATIONS

ARTICLE

Received 29 Jun 2015 | Accepted 22 Jan 2016 | Published 26 Feb 2016

DOI: 10.1038/ncomms10805 OPEN

Impact of ribonucleotide incorporation by DNA polymerases β and λ on oxidative base excision repair

Emmanuele Crespan[1,*], Antonia Furrer[2,*], Marcel Rösinger[2], Federica Bertoletti[1], Elisa Mentegari[1], Giulia Chiapparini[1], Ralph Imhof[2], Nathalie Ziegler[3], Shana J. Sturla[3], Ulrich Hübscher[2,†], Barbara van Loon[2,**] & Giovanni Maga[1,**]

Oxidative stress is a very frequent source of DNA damage. Many cellular DNA polymerases (Pols) can incorporate ribonucleotides (rNMPs) during DNA synthesis. However, whether oxidative stress-triggered DNA repair synthesis contributes to genomic rNMPs incorporation is so far not fully understood. Human specialized Pols β and λ are the important enzymes involved in the oxidative stress tolerance, acting both in base excision repair and in translesion synthesis past the very frequent oxidative lesion 7,8-dihydro-8-oxoguanine (8-oxo-G). We found that Pol β, to a greater extent than Pol λ can incorporate rNMPs opposite normal bases or 8-oxo-G, and with a different fidelity. Further, the incorporation of rNMPs opposite 8-oxo-G delays repair by DNA glycosylases. Studies in Pol β- and λ-deficient cell extracts suggest that Pol β levels can greatly affect rNMP incorporation opposite oxidative DNA lesions.

[1] DNA Enzymology & Molecular Virology Unit, Institute of Molecular Genetics IGM-CNR, via Abbiategrasso 207, I-27100 Pavia, Italy. [2] Department of Molecular Mechanisms of Disease, University of Zürich, CH-8057 Zürich, Switzerland. [3] Department of Health Sciences and Technology, ETH Zurich, CH-8092 Zürich, Switzerland. * These authors contributed equally to this work. ** These authors jointly supervised this work. † Present address: Department of Chemistry and Biology, Konstanz Research School Chemical Biology, University of Konstanz, Universitätsstrasse 10, 78457 Konstanz, Germany (U.H.). Correspondence and requests for materials should be addressed to B.V.L. (email: bvanloon@vetbio.uzh.ch) or to G.M. (email: maga@igm.cnr.it).

DNA polymerases (Pols) are specialized enzymes that selectively use deoxynucleoside triphosphates (dNTPs) as building blocks for DNA synthesis. However, despite their specificity, replicative Pols can incorporate ribonucleoside monophosphates (rNMPs) during DNA replication (more than 1,000,000 rNMPs per mammalian genome)[1–3]. Such rNMPs incorporation has been suggested to assist recognition of the newly synthesized strand by mismatch repair[4,5]. However, it can also constitute a major threat to genome stability[6,7]. The sugar-phosphate backbone of RNA is much more prone to strand breakage than DNA, potentially resulting in the accumulation of strand breaks. In addition, rNMPs incorporation could decrease the rate of DNA replication[2,8–10]. Due to the intrinsic 3′→5′ proofreading exonuclease activity replicative Pols can excise incorporated rNMPs to a variable extent[9,11]. The majority of rNMPs is however removed by the RNaseH2-dependent ribonucleotide excision repair[12]. Genetic studies in yeast have shown that RNaseH2 mutants suffer replication stress and require translesion synthesis (TLS) to avoid accumulation of rNMPs in the genome[13]. The embryonic lethality of RNaseH2-null mice as well as the severe phenotype of the Aicardi–Goutières syndrome in humans, due to mutations in RNaseH2, indicate that removal of rNMPs from the DNA is essential also in mammals[14].

Besides replication, DNA repair is another potential source of rNMPs incorporation. This may become particularly relevant in post-mitotic cells, such as neurons. To date, 17 Pols, including the cytidyl-transferase Rev1 and telomerase, have been identified in human cells[15], many of which are specialized in various DNA repair pathways. Among them, family X enzymes Pols β, μ and λ participate in base excision repair (BER), non-homologous end joining and in specialized form of TLS of oxidative lesions[16,17]. Several studies have shown that family X Pols can incorporate rNMPs during synthesis of undamaged DNA (reviewed in ref. 18), but with varying sugar selectivity. Pol μ displayed the lowest discrimination, in the range of 1- to 10-fold preference for dNMPs over rNMPs incorporation[19,20]. On the other hand, Pols β and λ showed sugar selectivity in the 3,000–50,000 range, depending on the particular base pair involved[21–23]. While Pol μ lacks a suitable 'steric gate' amino acid side chain (usually Glu, Tyr or Phe), used by the majority of Pols for sugar discrimination[24], Pols β and λ achieve the sugar selection using a protein backbone segment to exclude rNTPs[21,23]. Thus, both the active site architecture and the particular mechanism of sugar selection may account for the very diverse range of selectivity measured for the different Pols.

Genomes of living organisms are constantly exposed to various damaging agents. Among the most frequently generated DNA base modifications, are the oxidative lesions, particularly 7,8-dihydro-8-oxoguanine (8-oxo-G). During DNA replication 8-oxo-G lesions in the template strand lead to high frequency of misincorporation, generating A:8-oxo-G mismatches. The repair of these mismatches requires the sequential action of the MutY homologue (MutYH) and 8-oxo-G DNA glycosylase (OGG1), as well as of a specialized TLS Pol. We have previously shown that Pol λ is the most accurate in MutYH-initiated pathway, ensuring correct dCMP incorporation opposite 8-oxo-G, while Pol β can substitute for Pol λ, but at the expense of a reduced fidelity, leading to frequent misincorporation of dAMP opposite the lesion[25]. So far, it is not known whether DNA repair synthesis by Pols β and λ, either during BER or 8-oxo-G bypass, could contribute to genomic rNMPs accumulation. Since approximately 1,000–10,000 oxidative DNA lesions, of which 8-oxo-G is one of the most abundant, are generated spontaneously every day in each cell[26], understanding to what extent repair Pols incorporate rNMPs and how this event could influence DNA repair, remains an important issue.

In the present study, we compare the ability of the two BER Pols β and λ to incorporate rNMPs versus dNMPs opposite all four undamaged bases as well as 8-oxo-G, within a range of Mg^{2+}, Mn^{2+} and nucleotide concentrations matching those believed to normally occur in the cell. In addition, we examine the impact of rNMPs incorporation opposite 8-oxo-G on the subsequent BER initiated by the human OGG1 (hOGG1) and MutYH glycosylases. Finally, we measure incorporation of rNMPs opposite 8-oxo-G in extracts from cells deficient in either Pol λ or Pol β. Our results suggest that Pol β, to a greater extent than Pol λ, plays a role in rNMP incorporation opposite oxidative DNA damage.

Results

Metal-dependent rNMPs incorporation by Pol β and λ. The identity of the divalent metal cation Mg^{2+} or Mn^{2+}, required by all Pols for catalytic activity[27], can profoundly influence both Pol efficiency and the fidelity. The levels of Mg^{2+} and Mn^{2+} in the cells are tightly regulated and their physiological range of concentrations is quite different. While Mg^{2+} on average is present at concentrations ranging from 1 to 20 mM (refs 28,29), Mn^{2+} is usually found in the 0.01–0.2 mM range[30,31]. Different studies have shown that Pols β (ref. 23) and λ (ref. 22) can incorporate rNMPs *in vitro*. However, these studies often were conducted in the presence of one metal activator (either Mg^{2+} or Mn^{2+}) at a fixed dose. To compare the influence of Mg^{2+} and Mn^{2+} on the ability of Pols β and λ to incorporate rNMPs, DNA polymerization assays were performed on a 20/40mer primer/template (p/t) oligonucleotide, in the presence of different concentrations of the two metal activators, encompassing their respective physiological ranges. Similarly, mixtures of all four rNTPs or dNTPs were non-equimolar, to ensure that each individual nucleotide matched the previously published cellular concentrations[32,33]. As shown in Fig. 1a,b, Pols β and λ were able to incorporate rNMPs at physiological (1–5 mM) Mg^{2+} concentrations, while significant rNMPs incorporation in the presence of Mn^{2+} occurred only at 0.5–1 mM concentrations, higher than those normally measured in the cell. Thus, Mg^{2+} appeared to be the most relevant physiological activator for rNMPs incorporation by Pols β and λ, even though it cannot be excluded that in particular cell types or physiological conditions, Mn^{2+} concentrations may be high. Next, the fidelity of rNMPs incorporation was tested for all the 16 possible base pairs in the presence of Mg^{2+}. It must be noted here that commercial rNTPs stocks often contain small (<1%) amounts of contaminating dNTPs, which, owing to the relatively high rNTPs concentrations used in the assay and the high affinity of Pols λ and β for the nucleotides, could also be incorporated. However, since the products resulting from rNMP incorporation were migrating slower than those arising from dNMP incorporation, they could be easily distinguished on the sequencing gels. As shown in Supplementary Fig. 1A, Pol λ was able to insert each rNMP opposite its complementary templating base (lanes 5, 9, 19 and 25). No significant misincorporation was observed, with the exception of very low rGMP incorporation opposite G (lane 17). Pol β (Supplementary Fig. 1B), on the other hand, was able to incorporate rCMP opposite G and, to a lower extent, rGMP opposite C (lanes 19 and 27), while rUMP and rAMP incorporation opposite their complementary bases was at the limit of detection (lanes 7 and 11).

Overall, these data revealed differences in the ability and fidelity of Pols β and λ to select and incorporate rNMPs opposite undamaged bases.

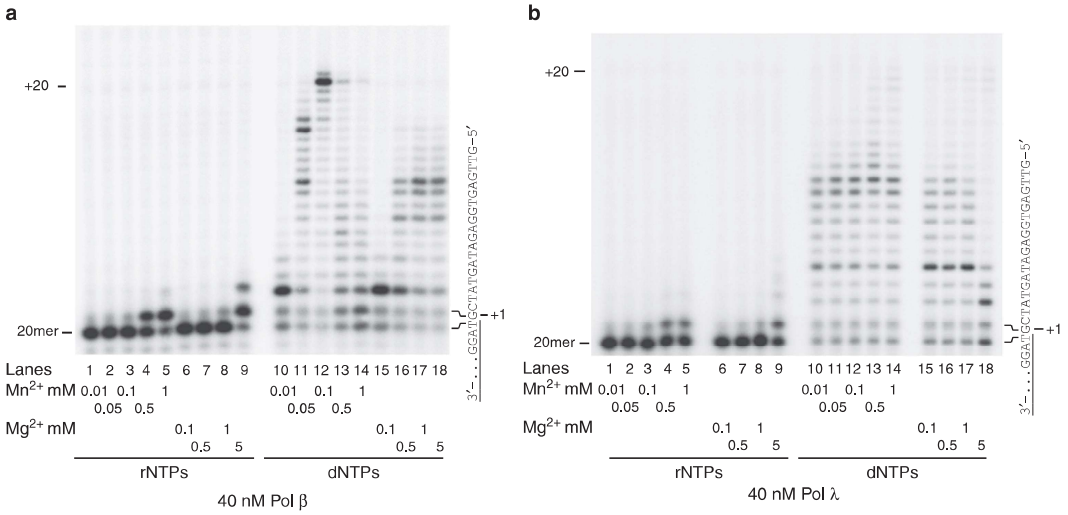

rNTPs = ATP 2 mM, CTP 0.25 mM, GTP 0.5 mM, UTP 0.5 mM
dNTPs = dATP 25 μM, dCTP 30 μM, dGTP 90 μM, dTTP 40 μM

Figure 1 | Nucleotide incorporation by DNA polymerases β and λ under different Mg^{2+} and Mn^{2+} conditions. (**a**,**b**) Pol β (**a**) and λ (**b**) activity was assayed in the presence of increasing Mn^{2+} or Mg^{2+} concentrations and with all four rNTPs or dNTPs at fixed concentrations in their physiological range. The sequence of the template strand of the 5′-labelled 20-G/40mer p/t is shown on the right side of each panel. The rNTPs and dNTPs concentrations used are indicated at the bottom of each panel.

rNMPs incorporation opposite 8-oxo-G by Pol λ. Besides undamaged DNA, repair Pols could potentially incorporate rNMPs opposite damaged DNA bases. 8-oxo-G, a frequent oxidative base damage, is a cognate substrate of Pol λ (refs 34,35). To test the ability of Pol λ to use rNTPs for incorporation opposite 8-oxo-G, Pol λ activity was determined in the presence of each of the four rNTPs on a 39/100mer p/t or a single nucleotide (1 nt)-gap template, both bearing at the +1 position either 8-oxo-G, or G. The 1 nt-gap template was chosen since it resembles a BER intermediate. On both templates, Pol λ significantly incorporated only rCMP opposite a normal G (Supplementary Fig. 2A, lane 4; Supplementary Fig. 2C, lane 10), while it incorporated both rCMP and rAMP opposite and 8-oxo-G (Supplementary Fig. 2B,C, lanes 5 and 6). On both substrates, some incorporation opposite a normal G or 8-oxo-G was also occurring in the presence of rGTP (Supplementary Fig. 2A, lane 2; Supplementary Fig. 2B, lane 3; Supplementary Fig. 2C, lanes 3 and 8). However, as indicated by the faster electrophoretic mobility of the resulting +1 product, such events were due to contaminating dNTPs in the commercial rGTP stock. Only minimal rGMP incorporation was seen opposite 8-oxo-G on the 1 nt-gap template (Supplementary Fig. 2C, lane 3). Incorporation was monitored as a function of dCTP, rCTP, dATP or rATP concentrations (Fig. 2) on both substrates and the corresponding kinetic parameters and sugar selectivity are reported in Table 1. Pol λ showed a 7,500-fold selectivity for dCTP over rCTP as substrates for synthesis opposite a normal G on the BER-mimicking template, which was in line with previously published data[22]. However, this selectivity increased to 14,000 opposite an 8-oxo-G. On this template, Pol λ showed also a strong preference for dAMP incorporation versus rAMP opposite an 8-oxo-G, with a selectivity of 17,200. Interestingly, the relative fidelity of 8-oxo-G bypass by Pol λ on the BER-mimicking template was not changed in the presence of rNTPs, since rCTP was preferred over rATP as a substrate, to a similar extent as dCTP over dATP (5.5-fold and 4.5-fold, respectively). On the 39/100-mer p/t, Pol λ showed a 5,140-fold selectivity for dCMP versus rCMP incorporation opposite a normal G, which increased to 12,800 opposite an 8-oxo-G. Interestingly, both the selectivity and the fidelity of Pol λ for rAMP incorporation opposite 8-oxo-G, were decreased on this substrate, with respect to the 1 nt gap. The selectivity value for dAMP versus rAMP was 3,000-fold, while the preference for rCMP versus rAMP incorporation was 0.9, indicating that both rNMPs could be equally used by Pol λ, to bypass the lesion on this template.

Taken together, these data clearly indicated that the structure of the DNA substrate influenced the fidelity and sugar selectivity of Pol λ during 8-oxo-G bypass in the presence of rNTPs.

Fidelity of rNMPs incorporation opposite 8-oxo-G by Pol β. Pol β has been shown to frequently misincorporate dAMP opposite an 8-oxo-G[34]. As shown in Supplementary Fig. 2D, with the 1 nt gap BER-mimicking template, Pol β readily incorporated both rCMP and rAMP opposite 8-oxo-G (lanes 1 and 2), while only rCMP was inserted opposite a normal G (lane 9). As already noted above, with rUTP and rGTP, only incorporation of contaminating dNTPs was detected. Substrate titrations with increasing concentrations of dCTP, rCTP, dATP or rATP were performed on both the 39/100 mer p/t and the 1 nt-gap templates (Fig. 3). The results of the kinetic analysis (Table 1) showed that on the 1 nt gap BER-mimicking template Pol β displayed a sugar selectivity for dCTP versus rCTP as substrates for the incorporation opposite a normal G of 3,400, which is in agreement with published data[18,23]. Contrary to Pol λ, this value was not increased in the presence of an 8-oxo-G lesion and

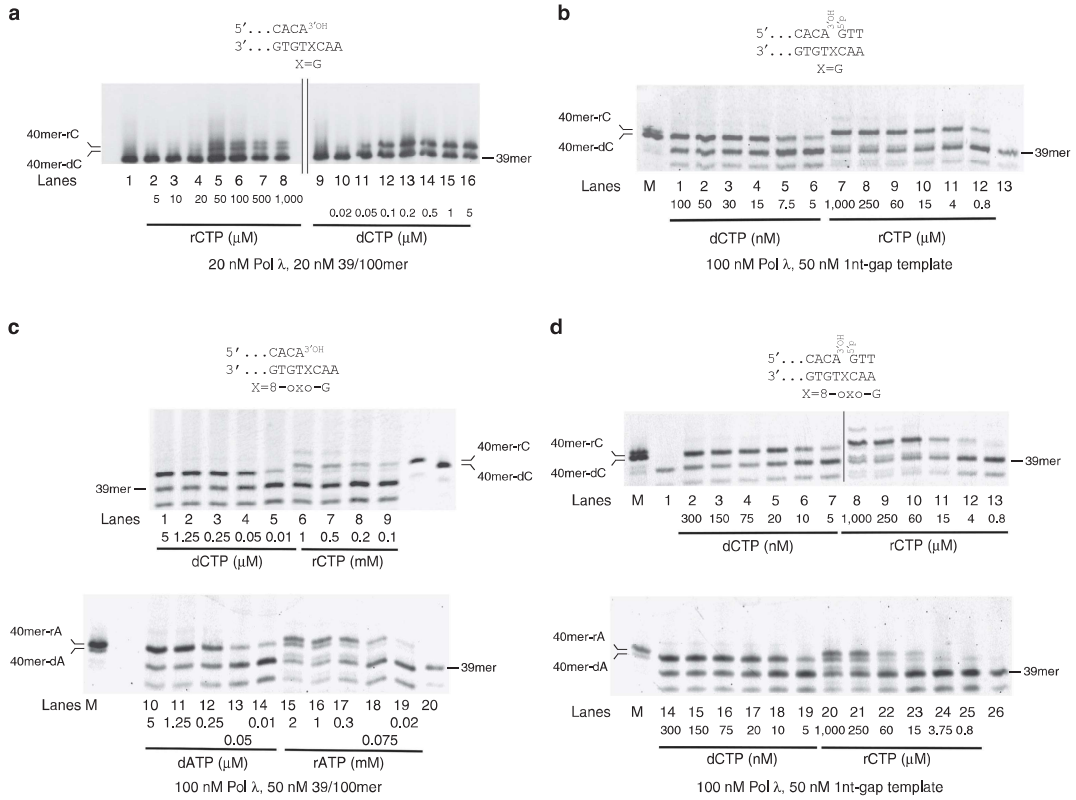

Figure 2 | The fidelity of 8-oxo-G bypass by DNA polymerase λ in the presence of rNTPs is influenced by the structure of the DNA template. (**a**) Pol λ activity was measured on the undamaged 5′-labelled 39/100mer p/t, in the presence of increasing concentrations of rCTP or dCTP. Lane 1, control reaction in the absence of nucleotides. (**b**) As in **a**, but in the presence of the undamaged 5′-labelled 39/60/100mer 1 nt-gap template. M, a mixture of 5′-labelled 40mer oligonucleotides bearing either dCMP or rCMP as the terminal nucleotide, as markers. Lane 13, control reaction in the absence of nucleotides. (**c**) Pol λ activity was measured on the 5′-labelled 39/100mer p/t containing 8-oxo-G, in the presence of different concentrations of dCTP and rCTP (top panel), or dATP and rATP (bottom panel). 5′-Labelled 40mer oligonucleotides bearing either dCMP, rCMP, dAMP or rAMP as the terminal nucleotide, were used as markers. Lane 20, control reaction without nucleotides. (**d**) As in **c**, but in the presence of the 5′-labelled 39/60/100mer 1 nt-gap 8-oxo-G template. Lane M, 5′-labelled 40mer oligonucleotides bearing either dCMP, rCMP, dAMP or rAMP as the terminal nucleotide, were used as markers.

measured 3,200. Interestingly, on the same template containing 8-oxo-G, Pol β showed strong discrimination against rAMP incorporation, with selectivity value of 25,600. The preference for dAMP versus rAMP incorporation opposite 8-oxo-G was 13.4-fold, while the one for dCMP versus dAMP incorporation was only 1.65-fold. On the p/t, the selectivity values were 1,690 and 4,680 for dCMP versus rCMP incorporation opposite a normal G and an 8-oxo-G, respectively. On this template however, the selectivity for dAMP versus rAMP incorporation opposite the lesion was 2,800. The fidelity was similar, with a twofold preference for rCMP versus rAMP utilization and a threefold for dCMP versus dAMP.

These data suggested that Pol β was sensitive to the structure of the DNA template, similarly to Pol λ. In particular, while Pol β showed lower sugar selectivity for rCMP versus dCMP incorporation than Pol λ on the 1 nt gap BER-mimicking template, its bypass fidelity with rNMPs was higher, since it strongly preferred rCMP versus rAMP incorporation opposite the lesion.

To directly visualize simultaneous incorporation of rCMP or dCMP opposite 8-oxo-G, competition experiments were carried out on the 1 nt-gap template (Supplementary Fig. 2E). The products coming from the incorporation of either rCMP or dCMP could be distinguished on the gel, as they differ in electrophoretic mobility. By titrating increasing amounts of one nucleotide (either dCTP or rCTP), in the presence of a fixed amount of the other competing nucleotide, both Pol λ (lanes 1–11) and Pol β (lanes 12–16) showed a dose-dependent increase in the band corresponding to the nucleotide titrated into the reaction, while the band corresponding to the incorporation of the nucleotide at a fixed concentration, decreased. These experiments confirmed that rCTP and dCTP compete as substrates for incorporation opposite 8-oxo-G by both Pols.

rNMPs opposite 8-oxo-G impair repair by hOGG1 and MutYH. Removal of 8-oxo-G paired to dC in double-stranded (ds) DNA, is predominantly accomplished by the BER glycosylase OGG1 (ref. 36). Since the data presented above clearly showed that rCMP could be incorporated opposite 8-oxo-G by the specialized repair Pols β and λ, we next asked whether this fundamental

Table 1 | Kinetic parameters for rNMPs incorporation by DNA polymerases λ and β.

	K_m* (μM)	k_{cat}* (min^{-1})	k_{cat}/K_m* ($M^{-1}s^{-1}$)	f_{inc}† dNTP/rNTP	f_{inc} rNTP/dNTP	f_{inc} C versus A
1nt-gap control						
Pol λ						
rCTP	83 ± 4	0.024 ± 0.003	4.8		1.3×10^{-4}	NA
dCTP	0.018 ± 0.004	0.039 ± 0.002	3.6×10^4	7,500		NA
Pol β						
rCTP	47 ± 3	0.034 ± 0.002	12		2.9×10^{-4}	NA
dCTP	0.03 ± 0.004	0.074 ± 0.002	4.1×10^4	3,400		NA
1nt-gap 8-oxo-G						
Pol λ						
rCTP	50 ± 10	0.06 ± 0.003	20		7.1×10^{-5}	5.5
dCTP	0.007 ± 0.001	0.12 ± 0.01	28×10^4	14,000		4.5
rATP	185 ± 20	0.04 ± 0.01	3.6		5.8×10^{-5}	
dATP	0.015 ± 0.001	0.056 ± 0.01	6.2×10^4	17,200		
Pol β						
rCTP	29 ± 1	0.018 ± 0.002	10.3		3.1×10^{-4}	13.4
dCTP	0.01 ± 0.01	0.02 ± 0.001	3.3×10^4	3,200		1.6
rATP	367 ± 30	0.017 ± 0.003	0.77		3.9×10^{-5}	
dATP	0.017 ± 0.002	0.021 ± 0.002	2×10^4	25,600		
39/100mer control						
Pol λ						
rCTP	38 ± 0.5	0.008 ± 0.0003	3.5		1.9×10^{-4}	NA
dCTP	0.03 ± 0.005	0.032 ± 0.007	18×10^3	5,140		NA
Pol β						
rCTP	64 ± 7	0.015 ± 0.003	3.9		6×10^{-4}	
dCTP	0.05 ± 0.01	0.02 ± 0.002	6.6×10^3	1,690		
39/100mer 8-oxo-G						
Pol λ						
rCTP	155 ± 18	0.02 ± 0.004	2.1		0.7×10^{-4}	0.9
dCTP	0.05 ± 0.004	0.08 ± 0.008	27×10^3	12,800		4
rATP	200 ± 5	0.027 ± 0.009	2.2		3.3×10^{-4}	
dATP	0.15 ± 0.004	0.06 ± 0.01	6.6×10^3	3,000		
Pol β						
rCTP	73 ± 13	0.007 ± 0.002	1.6		2.1×10^{-4}	2
dCTP	0.04 ± 0.01	0.018 ± 0.002	7.5×10^3	4,680		3
rATP	150 ± 15	0.007 ± 0.003	0.8		5.7×10^{-4}	
dATP	0.15 ± 0.02	0.021 ± 0.003	2.3×10^3	2,800		

*The meaning of the kinetic parameters K_m, k_{cat} and k_{cat}/K_m and their calculations are described in the Methods section. Values are the means of two independent estimates ± s.d.
†f_{inc}, relative incorporation frequencies for the different nucleotide pairs, defined as the ratio of the respective k_{cat}/K_m values.

glycosylase reaction was affected by pairing of rC base to an 8-oxo-G. A glycosylase assay was performed, with hOGG1 and a ds DNA oligonucleotide bearing either a dC:8-oxo-G or a rC:8-oxo-G base pair. Interestingly, the 8-oxo-G incorporated opposite rCMP could be removed by hOGG1, even though at a fourfold slower rate (Fig. 4a; Supplementary Fig. 3A). Besides rC:8-oxo-G pair, both Pols β and λ may also generate rA:8-oxo-G mispairs (Figs 2 and 3). MutYH is the BER glycosylase responsible for the recognition and removal of dA erroneously paired with 8-oxo-G[37]. To address if MutYH can also act on rA:8-oxo-G mispair, a glycosylase assay was performed using ds DNA oligonucleotide substrate bearing either a dA:8-oxo-G or a rA:8-oxo-G mismatch. While MutYH very efficiently removed dA opposite 8-oxo-G, its activity on a rA:8-oxo-G mismatch was severely impaired with respect to the normal dA:8-oxo-G substrate (Fig. 4b; Supplementary Fig. 3B). Overall, these results indicate that incorporation of rNMPs opposite 8-oxo-G may impair repair of the damaged base by the BER pathway, potentially posing a threat to genomic stability.

rCMP incorporation opposite 8-oxo-G in cell extracts. The data presented above, indicated that both Pols β and λ used rCTP as a substrate to bypass an 8-oxo-G lesion, generating a rC:8-oxo-G base pair, which was subsequently processed by hOGG1 with lowered efficiency. To better estimate to which extent Pols β and λ contribute to this potentially harmful event, we measured the incorporation opposite 8-oxo-G on a BER mimicking 1 nt-gap template, in extracts from mouse embryonic fibroblasts (MEFs) either proficient or deficient for Pol β or λ. Besides Pols β and λ, many other specialized Pols present in the cell, such as Pols μ, ν, η, ι, θ or κ, can efficiently fill 1 nt gaps. Like Pols β and λ, they are all resistant to the inhibitor aphidicolin, while replicative Pols α, δ and ε are sensitive to this inhibitor. The specialized Pol ζ is also aphidicolin sensitive, but its contribution to rNMPs incorporation in the cell was proposed to be minimal[38]. To determine the extent to which Pol β or λ contribute to potentially harmful rCMP incorporation opposite 8-oxo-G among specialized DNA repair Pols, aphidicolin was added to the reactions, thus blocking the incorporation by family B Pols α, δ, ε and ζ. The specific incorporation frequency (expressed as pmols of rCMP incorporated opposite 8-oxo-G per μg of extract) was calculated in each extract and normalized to the normal DNA synthesis (pmols of dCMP opposite guanine per μg of extract). As shown in Fig. 4c on the 1-nt gap on BER-mimicking template, Pol $\beta^{-/-}$ MEFs displayed severely reduced rCMP incorporation opposite 8-oxo-G, with respect to Pol $\beta^{+/+}$, as well as to Pol $\lambda^{+/+}$ and Pol $\lambda^{-/-}$ MEFs (compare lanes 1–3 with 4–12). In contrast, incorporation of dCMP opposite normal G was almost equal between Pol $\beta^{-/-}$ and Pol $\beta^{+/+}$ MEFs (Supplementary Fig. 3C,

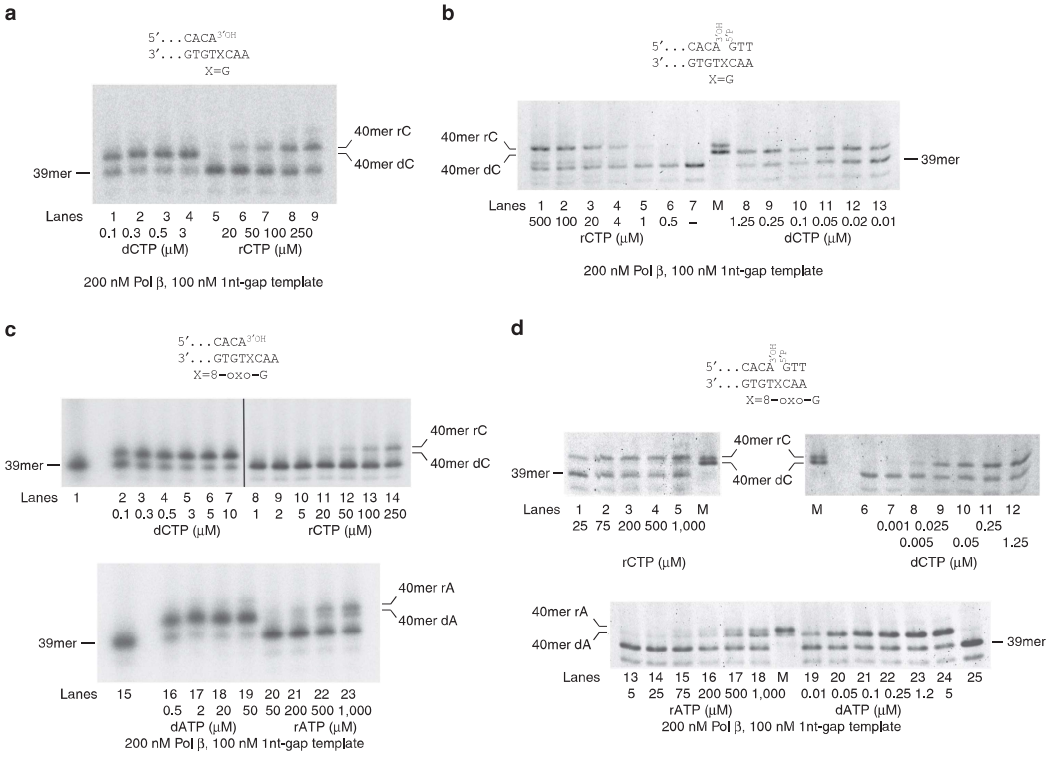

Figure 3 | DNA polymerase β bypasses 8-oxo-G more faithfully in the presences of rNTPs than dNTPs. (**a**) Pol β activity was measured on the undamaged 5′-labelled 39/100mer p/t, in the presence of increasing concentrations of rCTP or dCTP. (**b**) As in **a**, but in the presence of the undamaged 5′-labelled 39/60/100mer 1nt-gap template. M, a mixture of 5′-labelled 40mer oligonucleotides bearing either dCMP or rCMP as the terminal nucleotide, as markers. Lane 7, control reaction in the absence of nucleotides. (**c**) Pol β activity was measured on the 5′-labelled 39/100mer p/t containing 8-oxo-G, in the presence of different concentrations of dCTP and rCTP (top panel), or dATP and rATP (bottom panel). 5′-Labelled 40mer oligonucleotides bearing either dCMP, rCMP, dAMP or rAMP as the terminal nucleotide, were used as markers. Lanes 1 and 15, control reactions without nucleotides. (**d**) As in **c**, but in the presence of the 5′-labelled 39/60/100mer 1nt-gap 8-oxo-G template. Lanes M, 5′-labelled 40mer oligonucleotides bearing either dCMP, rCMP, dAMP or rAMP as the terminal nucleotide, were used as markers. Lane 25, control reaction in the absence of nucleotides.

compare lanes 11 and 12 with lanes 14 and 15) and comparable with Pol λ extracts (Supplementary Fig. 3C,D). These data thus suggest that, among the aphidicolin-resistant Pols, Pol β seems to be responsible for most of the rCMP incorporation opposite 8-oxo-G in the extracts, while no statistically significant differences were found between Pol λ proficient and deficient cells (Fig. 4d).

Discussion

Pols β and λ are the two major Pols involved in BER, one of the major DNA repair pathways operating in both resting and proliferating cells. In addition to providing the necessary gap-filling synthesis, we have previously shown that both Pols also operate in a specialized type of TLS in the context of MutYH-initiated repair of 8-oxo-G:A mismatches[25]. Since the contribution of BER to the incorporation of rNMPs into the genome is at present not fully understood, we decided to investigate the selectivity and fidelity of Pols β and λ with respect to rNMPs incorporation opposite normal and damaged bases under physiological concentrations of metal activators and nucleotides. Among the possible DNA damages, we selected 8-oxo-G, the very frequent oxidative stress DNA lesion, as a physiologically relevant example. Previous studies already revealed different sugar discrimination values among these Pols[18], however, only with Mg^{2+} or with Mn^{2+} as the metal activator, as well as on different substrates. By comparing Pols β and λ under identical conditions (that is, in the presence of Mg^{2+} and on the same substrates), we also found clear differences in their sugar discrimination ability. Pol λ showed sugar selectivity of 5,100–7,500 and Pol β of 1,690–3,200 for incorporation of rCMP opposite a guanine, depending on the structure of the template (Table 1). These values were in agreement with previous studies, reporting rCTP/dCTP selectivity values of 4,000 and 2,000–8,000 for Pols λ and β, respectively[18,21–23]. While these findings suggest that Pols λ and β can incorporate rNMPs in normal DNA, currently little is known about their ability to introduce rNMPs when the template bears oxidative DNA damage. In a recent study, it was indicated that Pol ι and, to a much lesser extent, Pol η, perform TLS of 8-oxo-G damage by incorporating rNMPs[39]. Interestingly, in our study we found that the presence of an 8-oxo-G damage on the template strand significantly affected the Pol λ selectivity for rNTP/dNTP. On its preferred 1 nt-gap template, Pol λ showed a

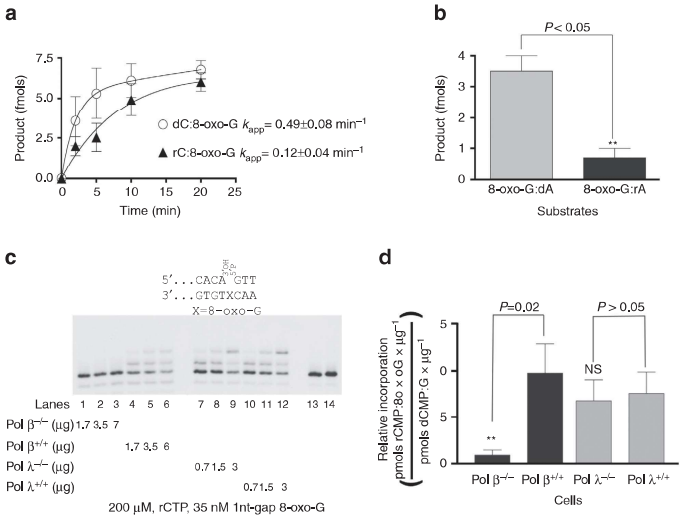

Figure 4 | Incorporation of rNMPs opposite 8-oxo-G inhibits DNA repair and is reduced in the absence of DNA polymerase β. (**a**) Time course of the excision products accumulation generated by hOGG1 in the presence of a 8-oxo-G:dC (empty circles) or 8-oxo-G:rC (filled triangles) base pairs. The k_{app} values refer to the apparent rates for the exponential phase. Values are the mean of three independent replicates, error bars represent ± s.d. A representative experiment is shown in Supplementary Fig. 3A. (**b**) Quantification of the excision products generated by MutYH in the presence of a 8-oxo-G:dA (grey bars) or 8-oxo-G:rA (black bars) mismatch. Values are the mean of three independent replicates as the one presented in Supplementary Fig. 3B, error bars represent ± s.d. The *P* values were calculated by two-tailed Student's *t*-test. (**c**) Increasing amounts of the different cell extracts were titrated in the presence of the 1 nt-gap template bearing an 8-oxo-G and 200 μM rCTP. Lanes 13 and 14, control reactions in the absence of extracts. (**d**) The rCMP incorporation activity (expressed as pmols of rCTP incorporated opposite 8-oxo-G per μg of proteins of each extract) was normalized to the total DNA polymerase activity (expressed as pmols of dCMP incorporated opposite undamaged dG per μg of proteins of each extract). Values are the mean of three independent replicates like the one shown in **c**, error bars represent ± s.d. The *P* values were calculated by two-tailed Student's *t*-test.

twofold increase in its preference for dCMP incorporation relative to rCMP incorporation opposite the lesion. Its fidelity was, on the other hand, unaffected since it preferred rCMP over rAMP to the same extent as dCMP over dAMP. We have shown previously that Pol λ is preferred over Pol β in the specialized MutYH-dependent BER of A:8-oxo-G mismatches[25,34,37], due to its higher efficiency of incorporation opposite the lesion of the correct dCMP over the incorrect dAMP. The present data indicate that Pol λ will also minimize the chances of incorporating rNMPs opposite this lesion.

Pol β showed lower selectivity values than Pol λ for rCMP incorporation opposite an 8-oxo-G (Table 1). However, while Pol β can incorporate dAMP opposite 8-oxo-G almost as efficiently as dCMP[34], when tested on the BER intermediate-mimicking 1 nt-gap template, it displayed a 13-fold preference for rCMP incorporation with respect to rAMP, compared with 1.6-fold preference for dCMP over dAMP on the same template (Table 1). In the crystal structure of the ternary complexes of Pol β with a (*syn*)8-oxo-G:(*anti*)dATP base pair[40], the templating oxidized guanine was accommodated in the enzyme's active site in its *syn* conformation by a hydrogen bond between the 8-O of the guanine and the side chain of Arg283. The sugar-phosphate backbone around the lesion was also displaced of about 3.4 Å. The structure of a ternary complex of Pol β with an incoming rCTP and an undamaged template[41], on the other hand, showed that a repulsive interaction between the backbone carbonyl of Tyr271 and the 2'OH group of the ribose counteracted base pairing of rCTP with the template G in the active site. In addition, rNTP binding disrupts a hydrogen bond between the hydroxyl group of Tyr271 and the primer end base, further disturbing the active site geometry. Thus, the combination of structural rearrangements required to accommodate both a templating 8-oxo-G in its *syn* conformation and an incoming rATP, may exacerbate the unfavourable interactions of Tyr271 with the ribose sugar and the primer end, thereby favouring the thermodynamically more stable rCTP pairing opposite 8-oxo-G. Crystal structures of Pol β in complex with an 8-oxo-G template and an incoming rNTP are needed to further clarify the molecular basis for this difference.

Experiments with extracts from cells defective in either Pol β or λ showed that, after inhibition of Pols α, δ, ε and ζ by aphidicolin, the majority of rCMP incorporation opposite 8-oxo-G was catalysed by Pol β. Interestingly, Pol λ seemed not to contribute significantly to rCMP-mediated bypass of 8-oxo-G. This is also in agreement with our kinetic data, showing that Pol λ discriminates against rCMP incorporation much more than Pol β (Table 1).

While the bulk of rNMPs incorporation in proliferating cells is due to DNA replication, our *in vitro* data suggest that also DNA synthesis during DNA repair on oxidative stress, among which the highly prominent is BER, may be a source of rNMPs incorporation.

On the basis of the selectivity values and on the known intracellular nucleotide concentrations[32,33], we estimated the theoretical frequency of rCMP versus dCMP incorporation opposite a normal G or 8-oxo-G for three representative mammalian tissues. As shown in Table 2, Pol β may incorporate rCMP opposite a normal G with frequencies about twofold higher than Pol λ (0.38–5.8% versus 0.23–2.6%, respectively). These values are in agreement with the previously estimated average frequency of rNMPs incorporation by Pol β of 1.2% (ref. 23). In addition, under physiological rCTP/dCTP

Table 2 | Estimated misincorporation frequencies of rCTP versus dCTPs opposite 8-oxo-G or a normal G, for DNA polymerases β and λ under physiological dNTPs/rNTPs concentrations.

Tissue	rCTP/dCTP ratio	Template G	Template 8-oxo-G
		f(rCTP/dCTP)* $\times 10^{-3}$	f(rCTP/dCTP)* $\times 10^{-3}$
Pol λ			
Skin fibroblasts†	18†	2.3	1.3
Lymphocytes‡	200‡	26	14
Liver‡	13‡	1.7	0.9
Pol β			
Skin fibroblasts	18†	5.2	5.6
Lymphocytes	200‡	58	62
Liver	13‡	3.8	4

*Frequencies of incorporation for each ribo-/deoxy-nucleotide substrate pair were calculated according to the Cornish-Bowden relationship: f(rCTP/dCTP) = (k_{cat}/K_mrCTP)/(k_{cat}/K_mdCTP)•(rCTP)/(dCTP) using the values from Table 1 for the 1-nt gap and from refs 32,33.
†The rCTP and dCTP concentrations have been taken from ref. 33.
‡The rCTP and dCTP concentrations have been taken from ref. 32.

ratios, Pol β may incorporate rCMP opposite 8-oxo-G fourfold more frequently than Pol λ (Table 2). Our data show that Pol λ can bypass an 8-oxo-G with either rCMP or rAMP, depending on the template. However, its high discrimination against rNMPs incorporation and its preference for dCMP over dAMP, ensures that, even with strongly unbalanced rNTPs/dNTPs ratios, the vast majority of incorporation events will lead to dCMP incorporation (Table 2). Pol β, on the other hand, which is endowed with a lower sugar selectivity than Pol λ, during bypass of 8-oxo-G on a 1 nt-gap template, strongly discriminates against rAMP incorporation, thus ensuring that, at least, bypass will result in the incorporation of rCMP (wrong sugar/correct base) opposite the lesion, rather than rAMP (wrong sugar/wrong base). This distinction could become relevant, since we have shown here that the presence of rAMP opposite 8-oxo-G strongly inhibits the repair initiated by the MutYH glycosylase, while incorporation of rCMP would result in a 8-oxo-G:rC base pair, which can be still repaired by the OGG1 glycosylase, but at a reduced rate (Fig. 4a,b). During the final revision of the present manuscript, it has been reported that incorporation of rNMPs opposite 8-oxo-G in the context of CAG triplet repeats sequences, can negatively affect its subsequent repair, lending further support to our results[42]. Recent data also indicated that *Schizosaccharomyces pombe* RNaseH2 can remove rCMP incorporated opposite 8-oxo-G[43], while *Escherichia coli* RNaseH2 in the presence of MutYH showed reduced efficiency in removing rAMP opposite 8-oxo-G[42], suggesting that the ribonucleotide excision repair pathway can limit the deleterious effects of rNMPs accumulation during DNA repair, but possibly with some loss of efficiency. Thus, during evolution, it seems that specialized TLS Pols have been optimized to reduce the possible deleterious consequences of rNMPs incorporation opposite DNA lesions.

In summary, the data presented in this work support the notion that DNA repair can be a source of rNMPs accumulation, potentially leading to genomic instability. However, future work will be required to determine its precise impact to the cell. For example, accumulation of rNMPs in the brain, as well as the increase in the amount of oxidative DNA lesions, have been linked to neurodegeneration[44,45]. Given that Pol β is the most abundantly expressed Pol in adult neurons, where dNTPs pools are much lower than rNTPs and RNaseH2 is poorly expressed, its ability to incorporate rNMPs when copying both undamaged and damaged DNA, as shown in the present work, may contribute to these processes.

Methods

Chemicals. Deoxynucleotides were purchased from GeneSpin (Milan, Italy). Ribonucleotides were purchased by GE Healthcare (Uppsala, Sweden). The rNTPs stocks were double checked in house by HPLC for dNTPs contamination, which was found to be below the limit of detection (> 99.6% purity). Labelled [γ-^{32}P]ATP was purchased from Hartmann Analytic GmbH (Braunschweig, Germany). Adenosine, guanosine, cytidine and uridine standards were obtained from Sigma (St Louis, MO, USA). All the other reagents were of analytical grade and purchased from Fluka or Merck.

Oligonucleotides. DNA oligonucleotides were synthesized by Purimex (Grebenstein, Germany) and purified from polyacrylamide denaturing gels. When indicated, oligonucleotides were 5′-labelled with T4 polynucleotide kinase (New England Biolabs) and [γ-^{32}P]ATP, according to the manufacturer's protocol. Each labelled primer was mixed to the complementary template oligonucleotide at 1:1 (M/M) ratio in the presence of 25 mM Tris-HCl pH 8 and 50 mM KCl, heated at 75 °C for 10 min and then slowly cooled down at room temperature.

Oligonucleotide sequences. 40-mer template:
3′-ATAGGTGGTTATGATGGGATGCTATGATAGAGGTGAGTTG-5′.
The sequence underlined corresponds to the four templating bases at position +1, generated on annealing of the template to the 18merA, 19merT, 20merG and 21merC primers, respectively.
18merA primer:
5′-TATCCACCAATACTACCC-3′,
19merT primer:
5′-TATCCACCAATACTACCCT-3′,
20merG primer:
5′-TATCCACCAATACTACCCTA-3′,
21merC primer:
5′-TATCCACCAATACTACCCTAC-3′.
For the generation of the 1 nt-gap template, the 100mer was annealed to the 39-mer primer and to the 60-mer downstream oligo, which has been 5′-phosphorylated with unlabelled ATP by using T4 polynucleotide kinase (NEB).
100 mer template:
3′-ATGTTGGTTCTCGTATGCTGCCGGTCACG GCTTAAGTGTXCCAC AACACACAACCAACACCACCACAACACACCAACAACCACAACACACAC AACCAC AC-5′,
where X = G or 8-oxo-G. The sequence underlined is the one complementary to the 39-mer primer.
39-mer primer:
5′-TACAACCAAGAGCATACGACGGCCAGTGCCGAATTCACA-3′
60-mer downstream oligonucleotide:
5′-GGTGTTGTGTGTTGGTTGTGGTGGTGTTGTGTGGTTGTTGGTGTTG TGTGTGTTGGTGTG-3′.

Enzymes and proteins. Human recombinant Pols λ and β (ref. 34) and human recombinant glycosylases MutYH and hOGG1 (refs 37,46), were used.

Cell lines and culturing conditions. Immortalized Pol $\lambda^{+/+}$, Pol $\lambda^{-/-}$, Pol $\beta^{+/+}$ and Pol $\beta^{-/-}$ MEFs[47,48] were grown in a humidified 5% CO_2 atmosphere in Dulbecco's modified Eagle's medium containing GlutaMAX-I supplemented with 10% fetal bovine serum and 100 U ml^{-1} penicillin–streptomycin (all obtained from Gibco, Invitrogen).

DNA polymerase assays. All reactions were done in a final volume of 10 µl and incubated for 10 min at 37 °C in the presence of 5′-labelled p/t at the concentrations stated in the figure legends. Pol λ, β reaction buffer: 50 mM Tris pH 7.5, 1 mM DTT, 0.2 mg ml^{-1} BSA. Mg^{++} was included for all Pols at 5 mM, unless

otherwise stated in the figures or figure legends. When crude extracts were used, the reaction mixture was supplemented with 0.1 mg ml^{-1} aphidicolin and 1 μM of a 49mer single-stranded DNA oligonucleotide with a non-complementary sequence to the DNA substrate, to inhibit exonuclease degradation. Crude whole-cell extracts were prepared as described in ref. 49. Proteins, Mg^{2+}, Mn^{2+} and nucleotides were in the concentration specified in the figures and figure legends. For denaturing gel analysis of the DNA products, the reaction mixtures were stopped by addition of standard denaturing gel loading buffer (95% formamide, 10 mM EDTA, xylene cyanol and bromophenol blue), heated at 95 °C for 5 min and loaded on a 7-M urea 12% polyacrylamide (PA) gel. The reaction products were analysed by using Molecular Dynamics Phosphoimager (Typhoon Trio, GE Healthcare) and quantified by the program Image Quant.

DNA glycosylase assays. *hOGG1* was incubated with 5′-labelled ds 100-mer DNA with 8-oxo-G:dC or 8-oxo-G:rC mispairs. On incubation, the reaction products were treated with NaOH (2M), heated for 15 min at 75 °C and reactions analysed on a 7-M urea 10% polyacrylamide gel. The reactions were performed at 37 °C in final volume of 10 μl containing 20 fmol 5′-labelled ds 100-mer DNA with 8-oxo-G:dC or 8-oxo-G:rC, 20 mM Tris-HCl (pH 8), 1 mM DTT, 1 mM EDTA and 0.1 mg ml^{-1} BSA. hOGG1 concentration and incubation times varied and are indicated in figures. On incubation hOGG1 reaction products were treated with 1 μl NaOH (2 M), heated for 15 min at 75 °C and reactions stopped by the addition of denaturing gel loading buffer and heating at 95 °C for 5 min. The samples were separated on 7 M urea 10% PA gel, analysed by Phosphoimager and quantified by GelEval 1.35 scientific imaging software (FrogDance Software, UK).

MutYH assay[37] was performed in 10 μl reactions containing 25 mM Hepes–KOH pH 6.8, 5 mM EDTA, 1.5% glycerol, 50 μM $ZnCl_2$, 50 mM NaCl, 7.5 mM $MgCl_2$, 20 fmol 5′-labelled ds 100-mer DNA with dA:8-oxo-G or rA:8-oxo-G, 200 nM MutYH and varying amounts of APE1 as indicated in Supplementary Fig. 3. Reactions were stopped by the addition of denaturing gel-loading buffer, heating at 95 °C for 5 min and separated on 7 M urea 10% PA gel. The products were detected by Phosphoimager and quantified by GelEval 1.35 scientific imaging software (FrogDance Software, UK).

Kinetic analysis. Due to the highly distributive nature of the reaction and the relatively low efficiency of rNTPs incorporation, the enzymes and the DNA substrate were used at similar concentrations. This implies that, at equilibrium, the concentration of the binary enzyme–DNA complex does not approximate the total enzyme concentration, but there is always a fraction of enzyme not bound to the DNA substrate, that does not participate in catalysis. Thus, to account for the fraction of enzyme not bound to the DNA substrate at equilibrium, the variation of the nucleotide incorporation rates (v) as a function of the nucleotide substrate concentration was fitted to the modified Briggs–Haldane equation:

$$v = \frac{k_{cat} E_0 S}{(S \cdot a) + (K_m \cdot b)} \quad (1)$$

where k_{cat} is the apparent catalytic rate, E_0 is the input enzyme concentration, S is the variable nucleotide substrate concentration, K_m is the apparent equilibrium dissociation constant of the nucleotide substrate from the catalytically active ternary complex, a and b are two constants, whose values were kept fixed during the computer fitting and were calculated from the following expressions:

$$a = \frac{1}{\left(1 + \frac{K_m}{K'}\right)} \quad (2)$$

$$b = \frac{1}{\left(1 + \frac{K'}{S'}\right)} \quad (3)$$

where K_m is the same as in equation (1), K' is the apparent dissociation constant for binding to the DNA substrate and S' is the concentration of DNA use in each experiment. The values of K' used for the fitting process were for Pol β 22 nM (ref. 50) and for Pol λ 29 nM (ref. 51).

Under conditions of forced termination (single nucleotide incorporation), $K_m = K_s(k_{off}/(k_{pol} + k_{off}))$ and $k_{cat} = k_{pol}(k_{off}/(k_{pol} + k_{off}))$. Where K_s is the Michelis constant for nucleotide binding, k_{off} is the dissociation rate of the enzyme from the DNA substrate and k_{pol} is the polymerization rate. Hence $k_{cat}/K_m = k_{pol}/K_s$.

Nucleotide concentrations used were in the 0.005–5 μM range for dNTPs and 0.5–2,000 μM range for rNTPs.

Time-course experiments were fitted to the exponential equation:

$$[P]_t = A\left(1 - e^{-kt}\right) + k_{ss} t \quad (4)$$

where $[P]_t$ is the product concentrations at any given time point, t is time, k is the rate for the exponential phase, k_{ss} is the rate of the linear phase and A is a constant.

Fitting was obtained with the GraphPad Prism 3.0 computer program.

Electronic image manipulation. Linear transformations have been applied in some instance to the whole images using the exposure/brightness filters of Adobe Photoshop CS6 with the sole purpose of reducing excessive background. No masking/enhancement was applied to any specific feature of the images.

References

1. Nick McElhinny, S. A. *et al.* Abundant ribonucleotide incorporation into DNA by yeast replicative polymerases. *Proc. Natl Acad. Sci. USA* **107,** 4949–4954 (2010).
2. Yao, N. Y., Schroeder, J. W., Yurieva, O., Simmons, L. A. & O'Donnell, M. E. Cost of rNTP/dNTP pool imbalance at the replication fork. *Proc. Natl Acad. Sci. USA* **110,** 12942–12947 (2013).
3. Caldecott, K. W. Molecular biology. Ribose an internal threat to DNA. *Science* **343,** 260–261 (2014).
4. Ghodgaonkar, M. M. *et al.* Ribonucleotides misincorporated into DNA act as strand-discrimination signals in eukaryotic mismatch repair. *Mol. Cell* **50,** 323–332 (2013).
5. Lujan, S. A., Williams, J. S., Clausen, A. R., Clark, A. B. & Kunkel, T. A. Ribonucleotides are signals for mismatch repair of leading-strand replication errors. *Mol. Cell* **50,** 437–443 (2013).
6. Nick McElhinny, S. A. *et al.* Genome instability due to ribonucleotide incorporation into DNA. *Nat. Chem. Biol.* **6,** 774–781 (2010).
7. Reijns, M. A. *et al.* Enzymatic removal of ribonucleotides from DNA is essential for mammalian genome integrity and development. *Cell* **149,** 1008–1022 (2012).
8. Watt, D. L., Johansson, E., Burgers, P. M. & Kunkel, T. A. Replication of ribonucleotide-containing DNA templates by yeast replicative polymerases. *DNA Repair (Amst.)* **10,** 897–902 (2011).
9. Clausen, A. R., Zhang, S., Burgers, P. M., Lee, M. Y. & Kunkel, T. A. Ribonucleotide incorporation, proofreading and bypass by human DNA polymerase delta. *DNA Repair (Amst.)* **12,** 121–127 (2013).
10. Clausen, A. R., Murray, M. S., Passer, A. R., Pedersen, L. C. & Kunkel, T. A. Structure-function analysis of ribonucleotide bypass by B family DNA replicases. *Proc. Natl Acad. Sci. USA* **110,** 16802–16807 (2013).
11. Williams, J. S. *et al.* Proofreading of ribonucleotides inserted into DNA by yeast DNA polymerase varepsilon. *DNA Repair (Amst.)* **11,** 649–656 (2012).
12. Sparks, J. L. *et al.* RNase H2-initiated ribonucleotide excision repair. *Mol. Cell* **47,** 980–986 (2012).
13. Lazzaro, F. *et al.* RNase H and postreplication repair protect cells from ribonucleotides incorporated in DNA. *Mol. Cell* **45,** 99–110 (2012).
14. Rice, G. *et al.* Clinical and molecular phenotype of Aicardi-Goutieres syndrome. *Am. J. Hum. Genet.* **81,** 713–725 (2007).
15. van Loon, B., Woodgate, R. & Hübscher, U. DNA polymerases: biology, diseases and biomedical applications. *DNA Repair (Amst.)* **29,** 1–3 (2015).
16. Hubscher, U., Maga, G. & Spadari, S. Eukaryotic DNA polymerases. *Annu. Rev. Biochem.* **71,** 133–163 (2002).
17. Hubscher, U. & Maga, G. DNA replication and repair bypass machines. *Curr. Opin. Chem. Biol.* **15,** 627–635 (2011).
18. Brown, J. A. & Suo, Z. Unlocking the sugar "steric gate" of DNA polymerases. *Biochemistry* **50,** 1135–1142 (2011).
19. Nick McElhinny, S. A. & Ramsden, D. A. Polymerase mu is a DNA-directed DNA/RNA polymerase. *Mol. Cell. Biol.* **23,** 2309–2315.
20. Martin, M. J., Garcia-Ortiz, M. V., Esteban, V. & Blanco, L. Ribonucleotides and manganese ions improve non-homologous end joining by human Pol mu. *Nucleic Acids Res.* **41,** 2428–2436 (2013).
21. Brown, J. A. *et al.* A novel mechanism of sugar selection utilized by a human X-family DNA polymerase. *J. Mol. Biol.* **395,** 282–290 (2010).
22. Gosavi, R. A., Moon, A. F., Kunkel, T. A., Pedersen, L. C. & Bebenek, K. The catalytic cycle for ribonucleotide incorporation by human DNA Pol lambda. *Nucleic Acids Res.* **40,** 7518–7527 (2012).
23. Cavanaugh, N. A., Beard, W. A. & Wilson, S. H. DNA polymerase beta ribonucleotide discrimination: insertion, misinsertion, extension, and coding. *J. Biol. Chem.* **285,** 24457–24465 (2010).
24. Ruiz, J. F. *et al.* Lack of sugar discrimination by human Pol mu requires a single glycine residue. *Nucleic Acids Res.* **31,** 4441–4449 (2003).
25. Maga, G. *et al.* Replication protein A and proliferating cell nuclear antigen coordinate DNA polymerase selection in 8-oxo-guanine repair. *Proc. Natl Acad. Sci. USA* **105,** 20689–20694 (2008).
26. De Bont, R. & van Larebeke, N. Endogenous DNA damage in humans: a review of quantitative data. *Mutagenesis* **19,** 169–185 (2004).
27. Steitz, T. A. DNA and RNA polymerases: structural diversity and common mechanisms. *Harvey Lect.* **93,** 75–93 (1997).
28. Romani, A. M. & Scarpa, A. Regulation of cellular magnesium. *Front. Biosci.* **5,** D720–D734 (2000).
29. Romani, A. Regulation of magnesium homeostasis and transport in mammalian cells. *Arch. Biochem. Biophys.* **458,** 90–102 (2007).
30. Aschner, J. L. & Aschner, M. Nutritional aspects of manganese homeostasis. *Mol. Aspects Med.* **26,** 353–362 (2005).
31. Roth, J. A. Homeostatic and toxic mechanisms regulating manganese uptake, retention, and elimination. *Biol. Res.* **39,** 45–57 (2006).
32. Traut, T. W. Physiological concentrations of purines and pyrimidines. *Mol. Cell. Biochem.* **140,** 1–22 (1994).

33. Ferraro, P., Franzolin, E., Pontarin, G., Reichard, P. & Bianchi, V. Quantitation of cellular deoxynucleoside triphosphates. *Nucleic Acids Res.* **38,** e85 (2010).
34. Maga, G. *et al.* 8-oxo-guanine bypass by human DNA polymerases in the presence of auxiliary proteins. *Nature* **447,** 606–608 (2007).
35. Crespan, E., Maga, G. & Hubscher, U. A new proofreading mechanism for lesion bypass by DNA polymerase-lambda. *EMBO Rep.* **13,** 68–74 (2012).
36. van Loon, B., Markkanen, E. & Hubscher, U. Oxygen as a friend and enemy: how to combat the mutational potential of 8-oxo-guanine. *DNA Repair (Amst.)* **9,** 604–616 (2010).
37. van Loon, B. & Hubscher, U. An 8-oxo-guanine repair pathway coordinated by MUTYH glycosylase and DNA polymerase lambda. *Proc. Natl Acad. Sci. USA* **106,** 18201–18206 (2009).
38. Makarova, A. V., Nick McElhinny, S. A., Watts, B. E., Kunkel, T. A. & Burgers, P. M. Ribonucleotide incorporation by yeast DNA polymerase ζ. *DNA Repair (Amst.)* **18,** 63–67 (2014).
39. Donigan, K. A., McLenigan, M. P., Yang, W., Goodman, M. F. & Woodgate, R. The steric gate of DNA polymerase iota regulates ribonucleotide incorporation and deoxyribonucleotide fidelity. *J. Biol. Chem.* **289,** 9136–9145 (2014).
40. Batra, V. K., Shock, D. D., Beard, W. A., McKenna, C. E. & Wilson, S. H. Binary complex crystal structure of DNA polymerase beta reveals multiple conformations of the templating 8-oxoguanine lesion. *Proc. Natl Acad. Sci. USA* **109,** 113–118 (2012).
41. Cavanaugh, N. A. *et al.* Molecular insights into DNA polymerase deterrents for ribonucleotide insertion. *J. Biol. Chem.* **286,** 31650–31660 (2011).
42. Cilli, P., Minoprio, A., Bossa, C., Bignami, M. & Mazzei, F. Formation and repair of mismatches containing ribonucleotides and oxidized bases at repeated DNA sequences. *J. Biol. Chem.* **290,** 26259–26269 (2015).
43. Sastre-Moreno, G., Sánchez, A., Esteban, V. & Blanco, L. ATP insertion opposite 8-oxo-deoxyguanosine by Pol4 mediates error-free tolerance in Schizosaccharomyces pombe. *Nucleic Acids Res.* **42,** 9821–9837 (2014).
44. Iyama, T. & Wilson, 3rd D. M. DNA repair mechanisms in dividing and non-dividing cells. *DNA Repair (Amst.)* **12,** 620–636 (2013).
45. Meagher, M. & Lightowlers, R. N. The role of TDP1 and APTX in mitochondrial DNA repair. *Biochimie* **100C,** 121–124 (2014).
46. Simonelli, V. *et al.* Genotype-phenotype analysis of S326C OGG1 polymorphism: a risk factor for oxidative pathologies. *Free Radic. Biol. Med.* **63,** 401–409 (2013).
47. Bertocci, B., De Smet, A., Weill, J. C. & Reynaud, C. A. Nonoverlapping functions of DNA polymerases mu, lambda, and terminal deoxynucleotidyltransferase during immunoglobulin V(D)J recombination in vivo. *Immunity* **25,** 31–41 (2006).
48. Sobol, R. W. *et al.* Requirement of mammalian DNA polymerase-beta in base-excision repair. *Nature* **379,** 183–186 (1996).
49. Furrer, A. & van Loon, B. Handling the 3-methylcytosine lesion by six human DNA polymerases members of the B-, X- and Y-families. *Nucleic Acids Res.* **42,** 553–566 (2014).
50. Vande Berg, B. J., Beard, W. A. & Wilson, S. H. DNA structure and aspartate 276 influence nucleotide binding to human DNA polymerase beta. Implication for the identity of the rate-limiting conformational change. *J. Biol. Chem.* **276,** 3408–3416 (2001).
51. Maga, G. *et al.* Human DNA polymerase lambda functionally and physically interacts with proliferating cell nuclear antigen in normal and translesion DNA synthesis. *J. Biol. Chem.* **277,** 48434–48440 (2002).

Acknowledgements

This work has been partially supported by the Italian Association of Cancer Research AIRC Grants IG12084 and IG15868 to G.M., E.C. and F.B.; the University of Zurich to A.F., R.I. and B.v.L.; Wolfermann–Nägli Stiftung to M.R. and B.v.L.; SNSF to B.v.L. and S.J.S. and ERC to S.J.S. We thank E. Ferrari for purifying hOGG1.

Author contributions

G.M., B.v.L. and U.H. had the original idea and wrote the manuscript. G.M. and B.v.L. conceived and interpreted all the experiments. E.C., A.F. and G.M. performed most of the experiments. G.C. and E.M. contributed to the execution of DNA polymerase assays. F.B., R.I. and M.R. contributed to cell culture and to the preparation and analysis of the cell extracts. N.Z. and S.J.S. contributed reagents and chemical analyses.

Additional information

Supplementary Information accompanies this paper at http://www.nature.com/naturecommunications

Competing financial interests: The authors declare no competing financial interests.

Reprints and permission information is available online at http://npg.nature.com/reprintsandpermissions/

How to cite this article: Crespan, E. *et al.* Impact of ribonucleotide incorporation by DNA polymerases β and λ on oxidative base excision repair. *Nat. Commun.* 7:10805 doi: 10.1038/ncomms10805 (2016).